Chemical Investigation of Chytrid Fungi and Amphibian Skin Microbiome Bacteria

Dissertation

der Mathematisch-Naturwissenschaftlichen Fakultät
der Eberhard Karls Universität Tübingen
zur Erlangung des Grades eines
Doktors der Naturwissenschaften
(Dr. rer. nat.)

Vorgelegt von
Keshab Bhattarai
aus Syangja, Nepal

Tübingen
2023

Gedruckt mit Genehmigung der Mathematisch-Naturwissenschaftlichen Fakultät der Eberhard Karls Universität Tübingen.

Tag der mündlichen Qualifikation:	16.05.2023
Dekan:	Prof. Dr. Thilo Stehle
1. Berichterstatter	Prof. Dr. Harald Groß
2. Berichterstatter	PD Dr. Bertolt Gust

Dedicated to

My Parents

Ganesh Prasad Bhattarai and Indira Bhattarai

Joy is the key treasure of life, people often realize it at the end.

Statement on The Originality of This Thesis

I hereby declare that I alone wrote the doctoral work submitted here under the title ‘Chemical Investigation of Chytrid Fungi and Amphibian Skin Microbiome Bacteria’, that I only used the sources and materials cited in the work, and that all citations, whether word for word or paraphrased are given as such. I declare that I adhered to the guidelines set forth by the University of Tübingen to guarantee proper academic scholarship (Senate Resolution 25.05.2000). I declare that these statements are true and that I am concealing nothing. I understand that any false statements can be punished with a jail term of up to three years or a financial penalty.

Tuebingen, 18.04.2023

…….. ……..

Place, Date Signature

Scientific Publications, Posters and Workshops

Publications

Thomas Majer, **Keshab Bhattarai**, Jan Straetener, Justus Pohlmann, Patrick Cahill, Markus O. Zimmermann, Marc P. Hübner, Marcel Kaiser, Johan Svenson, Michael Schindler, Heike Brötz-Oesterhelt, Frank M. Boeckler, and Harald Gross. **(2022)**. Discovery of Ircinianin Lactones B and C - Two New Cyclic Sesterterpenes from the Marine Sponge *Ircinia wistarii*. Marine Drugs. 20, 8, 532.

Niraj Aryal, Junhong Chen, **Keshab Bhattarai**, Oliver Hennrich, Ira Handayani, Markus Kramer, Jan Straetener, Tatjana Wommer, Anne Berscheid, Silke Peter, Norbert Reiling, Heike Brötz-Oesterhelt, Christian Geibel, Michael Lämmerhofer, Yvonne Mast, and Harald Gross **(2022)**. High Plasticity of the Amicetin Biosynthetic Pathway in *Streptomyces* sp. SHP 22-7 Led to the Discovery of Streptcytosine P and Cytosaminomycins F and G and Facilitated the Production of 12F-Plicacetin. Journal of Natural Products. 85, 3, 530-539.

Posters/Workshops

Keshab Bhattarai, Harald Gross **(2023)**. A Single NRPS Gene Cluster but Two Products – The Case of *Pseudomonas* sp. RSB5.11. 35. Irseer Naturstofftage (Irsee, Germany), 26 – 27 April 2023.

Keshab Bhattarai (2022). Participant in a conference by Royal Society of Chemistry. Directing Biosynthesis VI (Edinburgh, United Kingdom), 27 – 29 June 2022.

Keshab Bhattarai (2022). Participant in a conference. HIPS Symposium 2022 (online conference). 12 May 2022.

Keshab Bhattarai (2022). Participant in a workshop by CMFI Cluster of Excellence and Aarhus University. 2nd International Summer School on Non-Targeted Metabolomics (Tuebingen, Germany), 22 – 26 August 2022.

Keshab Bhattarai (2019). Participant in the International VAAM Workshop 2019. Biology of Microorganisms Producing Natural Products (Jena, Germany), 15 – 17 September 2019.

Keshab Bhattarai, Harald Gross **(2020)**. Secondary Metabolites from the Endophytic Fungus *Plectosphaerella cucumerina* Isolated from the Plant *Urtica dioica* L. (Sisno). **3rd International Conference on Bioscience and Biotechnology** (Pokhara, Nepal), 28 – 31 January 2020.

Contributions of Other Scientists

High-Resolution Nuclear Magnetic Resonance

The collection of the 700 MHz NMR datasets was supported by Dr. Markus Kramer (Institute of Organic Chemistry, University of Tuebingen, Tuebingen, Germany).

High-Resolution Mass Spectrometry

HRMS/MS measurements were acquired by Dr. Dorothee Wistuba and Dr. Norbert Grzegorzek (Institute of Organic Chemistry, University of Tuebingen, Tuebingen, Germany).

X-Ray Crystallography

X-Ray Crystallographic measurements and analyses were done by Dr. Dieter Schollmeyer (Johannes Gutenberg-University Mainz, Mainz, Germany).

Stereochemical Study

Stereochemistry of the novel lipo-dipeptide was analysed by the group of Prof. Michael Lämmerhofer (Pharmaceutical Institute, University of Tuebingen, Tuebingen, Germany).

Microorganisms

B. dendrobatidis and salamander skin bacteria were kindly provided by Dr. Carly R. Muletz-Wolz (Smithsonian's National Zoo and Conservation Biology Institute, NW Washington, D.C., USA).

Abbreviations

$(NH_4)_2SO_4$	Ammonium Sulphate
^{o}C	Degree Celsius
1D	One Dimentional
2D	Two Dimentional
A	Adenylation domain
Å	Angstrom
antiSMASH	antibiotics and Secondary Metabolite Analysis Shell
Arg	Arginine
Asn	Asparagine
Asp	Aspartic acid
Bd	*Batrachochytrium dendrobatidis*
Bsal	*Batrachochytrium salamandrivorans*
C	Condensation domain
CLPs	Cyclic Lipopeptides
Cn	‘n’ number of Carbons
^{13}C-NMR	Carbon NMR
COSY	Correlation Spectroscopy
$C_{starter}$	Starter Condensation domain
D-	Latin, ‘dexter‘ configuration
Da	Dalton
Dab	Diaminobutyric acid
DAPG	Diacetylphloroglucinol
DEPT	Distortionless Enhancement by Polarization Transfer
Dhb	Dehydrobutyrine
DMB	Davis Minimal Broth
DMSO	Dimethylsulphoxide
d_n	‘n‘ Number of Deuterium
DNA	Deoxyribosenucleic acid
Dr.	Doctor
E	Epimerization domain
ESI	Electron Spray Ionization
FAS	Fatty Acid Synthase

FCS	Fetal Calf Serum
FT	Fourier Transform
g/L	Gram per Liter
Gln	Glutamine
Glu	Glutamic acid
GNPS	Global Natural Products Social Molecular Networking
HCl	Hydrochloric acid
His	Histidine
HMBC	Heteronuclear Multiple Bond Correlation
^{1}H-NMR	Proton NMR
HPLC	High-Performance Liquid Chromatography
Hse	Homoserine
HSQC	Heteronuclear Single Quantum Coherence
Ile	Isoleucine
IR	Infra Red
IUCN	International Union for Conservation of Nature
K	Kelvin
KH_2PO_4	Potassium Phosphate Monobasic
L-	Latin, ‘laevus‘ configuration
LC	Liquid Chromatography
LC_{50}	Lethal Concentration 50
LC-HRMS	Liquid Chromatography-High Resolution Mass Spectrometry
LCMS	Liquid Chromatography Mass Spectrometry
Leu	Leucine
LPs	Lipopeptides
Lys	Lysine
M	Molar
m/z	Mass to Charge Ratio
Mb	Megabase
mbar	Millibar
MF	Molecular Formula
MGF	Mascot Generic Format
$MgSO_4.7H_2O$	Magnesium Sulphate Heptahydrate
MHz	Megahertz

MIC	Minimum Inhibitory Concentration
Min	Minute
mL	Mililiter
mm	Millimeter
Mr.	Mister
MS/MS or MS^2	Tandem Mass Spectrometry
mult./m	Multiplet
NaOH	Sodium Hydroxide
NCBI	Nactional Center for Biotechnology Information
nm	Nanometer
NMR	Nuclear Magnetic Resonance
NOESY	Nuclear Overhauser Effect Spectroscopy
NRPS	Non-Ribosomal Peptide Synthetase
ODs	Optical Densities
OH	Hydroxyl
Orn	Ornithine
PCR	Polymerase Chain Reaction
pH	Potential Hydrogen
Phe	Phenylalanine
PKS	Polyketide Synthase
ppm	Parts per Million
Pro	Proline
Prof.	Professor
qPCR	Quantitative Polymerase Chain Reaction
RiPP	Ribosomally Synthesized and Post-Translationally Modified Peptide
rpm	Round per Minute
rRNA	Ribosomal Riboneuclic acid
S	Svedberg (unit of sedimentation rate)
Ser	Serine
T	Thiolation domain
TE	Thioesterase domain
TFA	Trifluoroacetic acid
TGhL	Tryptone, Gelatin hydrolysate, Lactose

Thr	Threonine
TOCSY	Total Correlation Spectroscopy
Tyr	Tyrosine
USA	United States of America
UV	Ultra Violet
Val	Valine
VLC	Vacuum Liquid Chromatography
Xle	Leucine/Isoleucine
µg	Microgram
µL	Microliter

Acknowledgment

I find the Ph.D. as a huge package of experiences with knowledge, emotions and challenges. This journey to obtain my Ph.D. has involved a number of people and institutions that I would like to sincerely thank.

First of all, I would like to express my heartful thanks to my supervisor, Prof. Dr. Harald Gross for trusting my strengths and providing me with this opportunity. He had always kept us going during the research with his unwavering intellectual and social support as well as his cutting-edge lab facilities. His well planned project design always directed me to the comfortable research practice. I would like to thank my second supervisor PD Dr. Bertolt Gust for providing me the recommendations and advices whenever they were needed. I would like to extend my thanks to Prof. Dr. Lisa Maier and JProf. Dr. Silja Mordhorst for accepting the offer to participate in my oral defence as the examiners.

I am grateful to the DAAD, which provided me with funding for 4 years during my research stay in Germany. My engagement with the science, culture, food and society of Germany was only possible through the DAAD scholarship. My academic career and experience with the DAAD are unforgettable.

I am grateful to my brother Prof. Dr. Hari Datta Bhattarai (Tribhuvan University, Nepal), who recommended and helped me through the entire process of the Ph.D. application. As a Humboldt fellow, he thoroughly helped me in the first few weeks to practice the research work in the laboratory. I am thankful to Dr. Bikash Baral (University of Turku, Finland) for his academic and moral support.

I would like to acknowledge all the recent and former members of the Gross group, who helped me understand the lab all the time. I am very thankful to Dr. Niraj Aryal, my compatriot in the lab, who motivated and guided me through the early period of my Ph.D. He was the biggest guardian in the laboratory and outside, during my Ph.D. stay in Germany. I would like to thank Mr. Wolfgang Kornberger for his friendly support and social knowledge that I admired. He helped me as a very good friend in my social life and technically (mass spectrometry instrument) in my Ph.D. research. Humbolt scientist Prof. Naheed Riaz was very inspiring, supportive and knowledgeful. I am

thankful to Thomas Majer as a good supportive friend who helped me through the spectroscopic techniques for research and German cultures for living. I would like to thank Dr. Hamada Saad for guiding me through metabolomic parts. Fred and Aziz were good-hearted and helpful colleagues in the lab. I thank Irina for taking good care of the NMR and helping me with the instrumentation in the early period. Likewise, Wolfgang, Patricia and recently Manuela facilitated the ordering process of research materials. Besides, I would like to thank Junjing, Tarik, Johanna, Mersida and Timur for their direct or indirect supports during my Ph.D. work.

Finally, I am grateful to my lovely and warm-hearted wife, Ms. Sushma Bhattarai for showing me with her unconditional love. I owe a debt of gratitute to all my family members; my brother (Chiranjibi Bhattarai) and my sisters (Gayatri, Ganga and Uma) for their enormous support. Additionally, I want to show my great respect to Hemraj Bhattarai, Jamuna Bhattarai, Khem Raj Neupane, Shankar Khanal and Sujan Upreti for their unconditional supports. I would like to thank my friendly brothers, Mr. Ram Prasad Pandey and Krishna Neupane for his moral support in my early period of life abroad. I would like to remember my close friends (Prabin, Gobinda, Ananta, Mani, Sudip, Basanta, Moti, Madhab, Shova, Krishna, Shishir, Ananta Raj, Bimal, Durga, Rabin, Keshari and others), who directly or indirectly supported me in my academic life so far to this point.

Keshab Bhattarai

Summary

Amphibians (kingdom: Animalia, phylum: Chordata) are ectothermic tetrapod vertebrates that can live both in water and on land. As an essential component of our ecosystem, they serve humanity ecologically, medically and culturally. Despite their importance, their population has declined dramatically over the past three decades. One of the main reasons for the alarming population decline is chytridiomycosis. The causative agents of such deadly mycosis are chytrid fungi, mainly *Batrachochytrium dendrobatidis* (*Bd*) and *Batrachochytrium salamandrivorans* (*Bsal*). However, some amphibians are not affected by the disease and this phenomenon is attributed to the presence of certain bacteria (anti-*Bd* bacteria) found in the skin microbiome of amphibians. Therefore, the present work deals with chemical aspects that could play a significant role during both the fungal infection and the bacterial defense processes.

To achieve this goal, the secondary metabolites produced by the attacking chytrid fungi, on the one hand, and by the defending bacteria of the skin microbiome, on the other hand, were intensively studied. These analyses were mainly performed by genomic-, mass spectroscopic- and NMR-spectroscopic-based methods. The chemical-physical experiments were further complemented with biological assays (of the strains, crude extracts and pure substances), in which the brine shrimp toxicity, antifungal and chitinase assays were decisive.

Genomic and metabolomic analyses of the fungus *Bd* revealed that it has a low potential to produce secondary metabolites. In agreement with this observation, the corresponding crude extract was also found to be inactive in the brine shrimp toxicity assay. These results indicate that secondary metabolites obviously play only a minor role in the infection process. In contrast, numerous secondary metabolites were successfully isolated from the four investigated anti-*Bd* bacteria. In total, six novel lipopeptides and four already known lipopeptides (pseudodesmin A, tensin, virginiafactin A and B) were fully characterized. In the bioassays, particularly pseudodesmin A, tensin and virginiafactin B showed moderate antifungal activity (MIC: 12.5 - 50 µg/mL) against both chytrid fungi. Seven other anti-*Bd* bacteria of the genera *Stenotrophomonas*, *Janthinobacterium*, *Duganella*, and *Paenibacillus* showed the ability to produce chitinases. This suggests that anti-*Bd* bacteria may use a

combination of enzymatic and chemical "weapons" for the defense against chytrid fungi.

Zusammenfassung

Amphibien (Reich: Animalia, Stamm: Chordata) sind wechselwarme Landwirbeltiere die sowohl im Wasser als auch an Land leben können. Als essentieller Bestandteil unseres Ökosystems dienen sie der Menschheit in ökologischer, medizinischer und kultureller Hinsicht. Trotz dieser Bedeutung hat der Bestand in den letzten drei Jahrzehnten dramatisch abgenommen. Einer der Hauptgründe für die alarmierende Bestandsabnahme ist die Chytridiomykose. Hierbei handelt es sich um eine tödliche Mykose. Erreger sind Chytridpilze, insbesondere *Batrachochytrium dendrobatidis* (*Bd*) und *Batrachochytrium salamandrivorans* (*Bsal*). Manche Amphibien werden jedoch nicht von der Krankheit erfasst und dieses Phänomen wird auf die Gegenwart von bestimmten Bakterien zurückgeführt (anti-*Bd*-Bakterien), die sich im Hautmikrobiom der Amphibien befinden. Die vorliegende Arbeit beschäftigt sich daher mit chemischen Aspekten, die sowohl während des fungalen Infektionsgeschehens als auch des bakteriellen Abwehrprozesses eine Rolle spielen könnten.

Zur Umsetzung dieses Ziels wurden einerseits die Sekundärmetabolite der angreifenden Chytridpilze, und andererseits auch die der verteidigenden Bakterien des Hautmikrobioms intensiv untersucht. Diese Analysen wurden hauptsächlich mittels genomisch-, massenspektroskopisch- und NMR-spektroskopisch-basierten Methoden durchgeführt. Die chemisch-physikalischen Experimenten wurden Des weiteren mit biologischen Assays (der Stämme, Rohextrakte und Reinsubstanzen) ergänzt, wobei hierbei der Salinenkrebs-Toxizitäts-, der antifungale und der Chitinase-Assay maßgeblich waren.

Sowohl die Analyse des Genoms, als auch des Metaboloms des Pilzes *Bd* ergab, dass dieser nur ein geringes Potential besitzt, Sekundärmetabolite zu produzieren. Übereinstimmend mit diesem Bild erwies sich der zugehörige Rohextrakt ebenfalls als inaktiv im Salinenkrebs-Toxizitäts-Assay. Diese Ergebnisse weisen darauf hin, dass Sekundärmetabolite nur eine untergeordnete Rolle beim Infektionsprozess spielen. Im Gegensatz dazu konnten zahlreiche Sekundärmetabolite aus den vier untersuchten anti-*Bd* Bakterien erfolgreich isoliert werden. Zusammenfassend wurden sechs neuartige Lipopeptide und vier bereits bekannte Lipopetide (Pseudodesmin A, Tensin, Virginiafactin A und B) vollständig charakterisiert. In den Bioassays zeigten

insbesondere Pseudodesmin A, Tensin und Virginiafactin B moderate antifungale Aktivität (MIC: 12.5 – 50 µg/mL) gegenüber beiden Chytridpilzen. Sieben weitere anti-*Bd* Bakterien der Gattungen *Stenotrophomonas*, *Janthinobacterium*, *Duganella* und *Paenibacillus* zeigten die Fähigkeit, Chitinasen zu produzieren. Dies legt den Schluss nahe, dass anti-*Bd* Bakterien eine Kombination aus enzymatischen und chemischen „Waffen“ zur Abwehr von Chytridpilzen einsetzen könnten.

1. Introduction

1.1 Amphibians and Chytridiomycosis

Amphibians are an extremely diverse vertebrate class of over 8,000 species worldwide comprising three orders: Anura (frogs and toads), Caudata (newts and salamanders) and Gymnophiona (caecilians). They represent an essential part of ecosystem (Figure 1 A). Ecosystems offer vital services to humankind such as provisioning, regulating and cultural aspects as well as environmental sectors. Amphibians also contribute to the provisioning aspect by offering food for human societies in Southeast Asia. In the medical sector, amphibians serve as model animals and deliver potential lead structures such as analgesic (epibatidine) and anti-viral compounds (dermaseptin S4, caerin 1.9/1.1 and maculatin 1.1) from their skin secretions. Some amphibians, such as fire salamanders, produce samandarin, a toxic alkaloid that causes strong muscle contraction and hypertension in all vertebrates (Figure 1 B).

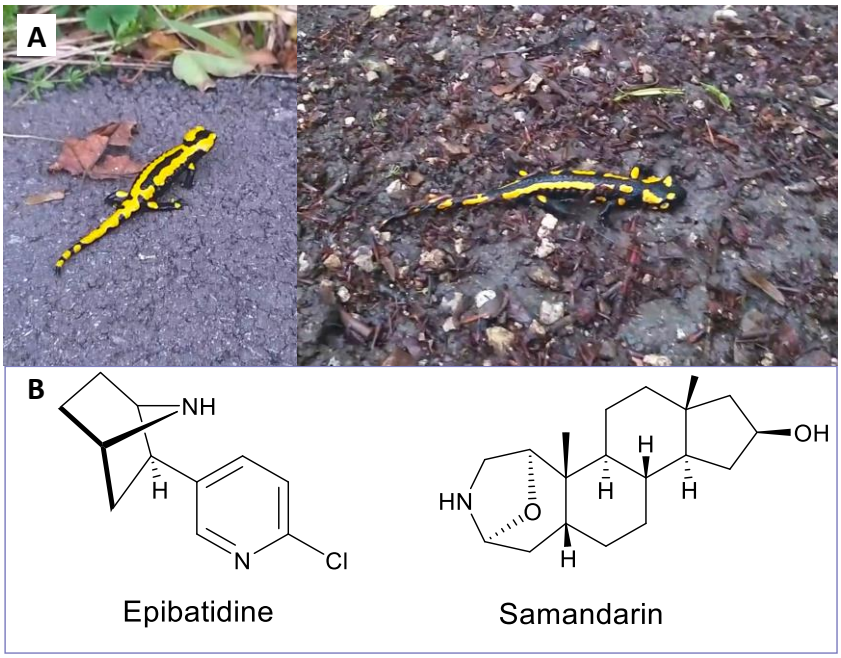

Figure 1: [A] Fire salamander observed on the campus Morgenstelle, University of Tuebingen (left) and at the forest of Bad Urach waterfall, Germany (right). [B] Structures of bioactive compounds isolated from amphibians' skin.

Furthermore, amphibians play a significant role in reducing mosquito population from ephemeral wetlands and other pest species. They can influence the structure of an ecosystem through aquatic bioturbation and soil burrowing. They also cover a huge sector of food web in the ecosystem. Besides, amphibians are a prominent part of the human culture such as art, literature and mythology.[4-8]

Unfortunately, amphibians are experiencing an intense decline in their population due to their overexploitation, habitat loss and enigmatic causes. According to the International Union for Conservation of Nature (IUCN) Red List data, 35 species of

amphibians are completely extinct, two species are extinct in the wild while 1085 species are endangered and 673 species are critically endangered. This extent of amphibians' decline represents one of the Earth's extreme mass extinction events. One of the enigmatic reasons against amphibians' decline has been revealed as fungal disease, called chytridiomycosis.[9-12]

Chytridiomycosis in amphibians is mainly caused by two fungal species, *Batrachochytrium dendrobatidis (Bd)* and *Batrachochytrium salamandrivorans (Bsal)* depending on the type of host organism. *Bd* is widely distributed throughout the world, mainly in Australia, East Asia, South Africa, Europe, South America and the United States of America whereas *Bsal* is detected so far only in Europe and East Asia (Figure 2). Several studies have claimed that Southeast Asia is the potential origin of both fungi. Later, they resulted in the global distribution by means of commercial trades of

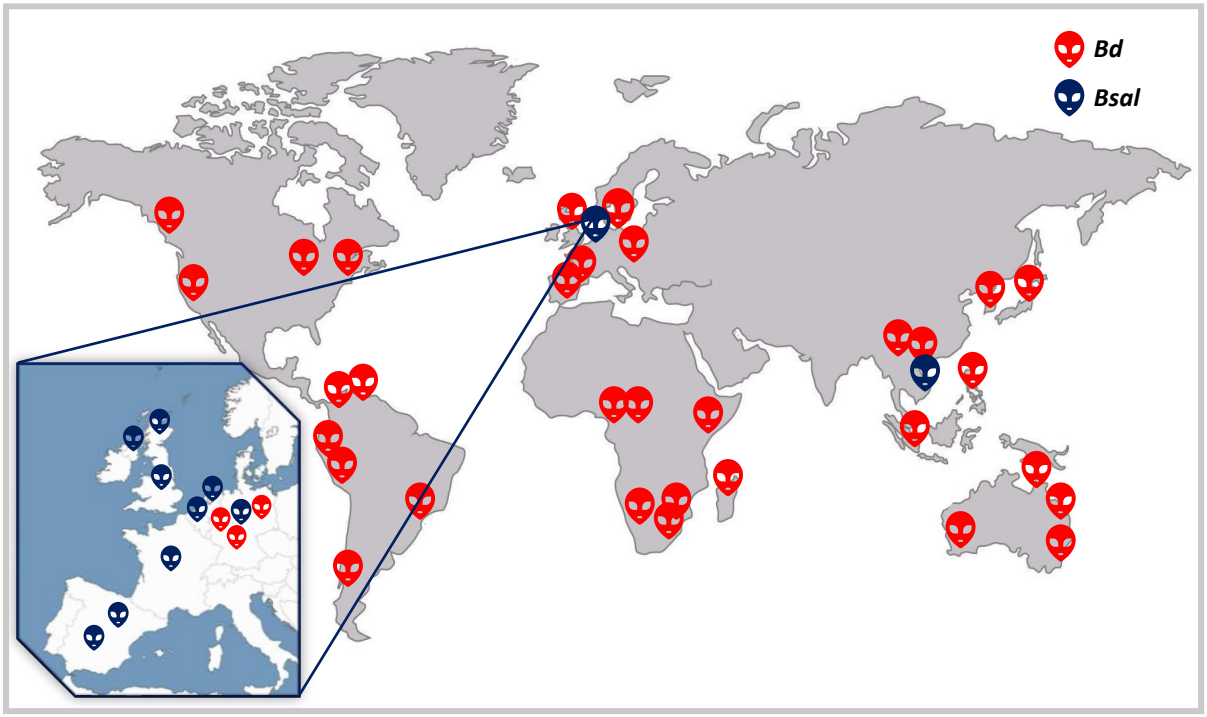

Figure 2: Global map of chytrid pathogens showing *B. dendrobatidis* (red) and *B. salamandrivorans* (dark blue) distributions throughout the world.

amphibians and/or aquatic birds. A previous study has suggested that *Bsal* was introduced into Europe by the transportation of Asian salamanders for pet trading purposes. The pathogen was even subsequently detected on commercially traded salamanders in the United Kingdom and Germany. Several waterfowls' feet swabs from Belgium and Bolivian high Andes showed that 15% and 42% of the tested birds found positive for *Bd* by quantitative PCR (qPCR). The researchers found that *Bd* is

attracted to, adheres and proliferates on keratinous toes of waterbirds, that may act as non-amphibian reservoirs of chytrids. Another study has revealed that *Bd* was detected in 11 indigenous frog species, 4 newt species and one salamander species in 64 different locations of Germany until 2011.[11, 13-17]

These fungal pathogens (Phylum; Chytridiomycota, Order; Chytridiales) are the only known parasites on vertebrates so far within the entire phylum of Chytridiomycota. They are characterized by their motile zoospores. The first case of chytridiomycosis was diagnosed in frogs, which was caused by *Bd*, while later on in salamanders it was found to be caused by *Bsal*. *Bd* was first discovered in 1998 and was isolated from the skin of ill and dead captive anurans found in Australia and western Panama. The optimum temperature range for the best *in-vitro* growth of *Bd* is 20°C to 23°C. The colonies of *Bd,* growing on solid media (1% tryptone agar), resemble like small buds of butter clumps when observed with naked eyes. However, an optical microscope visualizes the fully grown sporangia, spore sacs and a thallus surrounded by motile spores (Figure 3). The morphological features of *Bsal* also resemble that of *Bd* except some traits such as the formation of germ tubes and abundant colonial thalli in *in-vitro* cultures. In comparison with *Bd*, *Bsal* prefers to grow at a lower thermal temperature with an optimal range of 10°C to 15°C while it dies at ≥25°C. *Bsal* is known to cause lethal skin infections in salamanders, which led to the severe declines in salamander population in north-western Europe. At the beginning of the chytrid infection, both pathogens attack the epidermal tissue through the skin

Figure 3: Microscopic images of *Batrachochytrium dendrobatidis* showing fungal colonies, thalli, sporangia and spores.

surface of amphibians and cause a gradual development of symptoms. The clinical signs of infections are mainly excessive skin shedding, lethargy, anorexia, abnormal posture and death. *Bd* mainly causes epidermal hyperplasia and hyperkeratosis while *Bsal* typically causes erosive lesions, epidermal necrosis and skin ulcerations with significant destruction of the epidermis (Figure 4).[3, 18, 19]

In frogs and toads, the *Bd* infection mainly prefers initially toes, feet and the abdominal skin of the ventral body side. In salamanders, the infection of *Bsal* is highly susceptible to the fore and hind limbs, the pelvic region and the ventral side of the tail. Generally, the infection by chytrids comprises several steps such as attachment of chytrid zoospores to the host skin, germination of zoospores followed by germ tube formation and penetration into the skin cells, invasive growth of the chytrid and the loss of host cell functions. A study showed that, chytrid zoospores are attracted to the skin mucus (which is mainly composed of mucins and mucin glycoproteins) of amphibians which are rich in sugars such as L-fructose, N-acetylgalactosamine, N-acetylglucosamine, D-galactose and D-mannose as a mean of chemotaxis. However, the mucus also contains several interdependent host factors such as antimicrobial peptides, lysozymes, microbial metabolites and mucosal antibodies which will prevent the zoospores colonization. Although the zoospores are attractive to mucus, they must resist the mucosome defence factors to conduct a successful colonization on the host skin. Afterwards, germ tubes (tubular extensions) arise from the zoospore cysts which penetrate the cell membrane of the host tissue. The growing ends of germ tubes inside the cells are developed into the intracellular chytrid thalli. The thallus further develops sporangia which enclose several new zoospores upon maturity. The same phenomenon repeats after the dispersal of new zoospores from the sporangia which ultimately leads to the clinical symptoms of chytridiomycosis.[20]

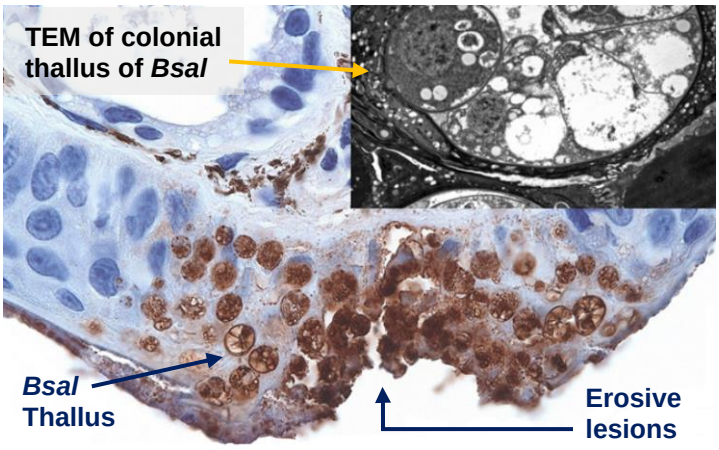

Figure 4: Salamander skin on microscopic view infected with *Batrachochytrium salamandrivorans* showing fungal thalli and skin rupture.[3]

The exact mechanism of infection to death of amphibians is still exclusive while some conclusions have been drawn. Amphibian skin is the vital permeable organ responsible for respiration (gaseous exchange), electrolytes exchange, temperature regulation, fluid balance, camouflage and deterrence against opportunistic pathogens. Disruption of the skin with chytrid infection causes therefore systemic diseases leading to a loss of essential physiological functions as well as bacterial infections and ultimately amphibian death. One of the studies in the infected frogs suggested that electrolyte transport across the infected epidermis was repressed by 50% while sodium and potassium concentration in blood plasma were reduced by 20% and 50%, respectively, resulting in asystolic cardiac attack and death. However, further studies have pointed out the important role of the skin as part of the innate immune system of amphibians. One of the major components of the host innate immune system is the skin microbiome that can contribute to chytrid resistance.[13, 21-23]

1.2 Survival of Amphibians Against Chytrids

In the regions of chytrid invasion, it has been observed that some of the amphibians are found intact and are resistant against the disease. This observation raised the interest of scientists to explore the fate of their survival against such a fatal disease. A wide range of defence mechanisms such as innate immune response, antimicrobial peptides and antibodies from mucus, microbial community along with their secretions (secondary metabolites and enzymes) on the host skin can be proposed to address this natural resistance of amphibians against the chytrids (Figure 5).

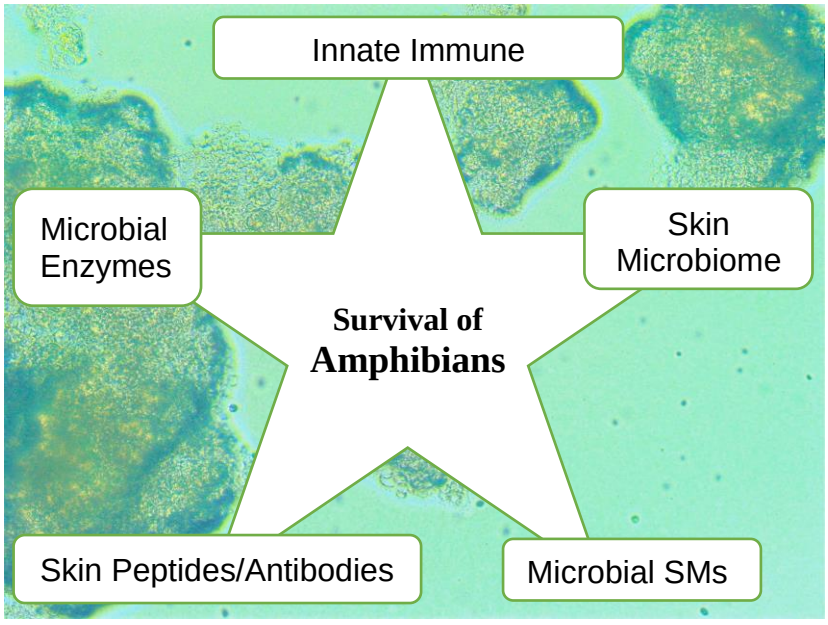

Figure 5: Different possible mechanisms of defense in amphibians against chytrid pathogens.

Lysozyme, lectins and phospholipases, present in the body fluid and mucosal linings of amphibians, are assumed to play a role in the defence against chytrids. Natural mucosal antibodies generated by innate-like B-cells may bind to and inhibit chytrid zoospores. Amphibians also produce a wide range of antimicrobial peptides which accumulate in their skin mucus. Depending on the type, number, concentration and sites of antimicrobial peptides secreted by the host organism, the extent of chytrid infection appears to vary substantially. The commensal microbial community inhabiting the skin of amphibians may provide an additional mechanism of constitutive innate immunity against chytrid pathogens. Numerous anti-chytrid bacterial species such as *Janthinobacterium lividum*, *Stenotrophomonas* sp. and *Pseudomonas* sp. from the skin of chytrid resistant *Plethodon* salamanders are reported for the antagonistic candidates against *Bd.* However, the exact mechanisms of their antifungal properties yet need to be discovered. Their anti-fungal action can be attributed either to enzymatic secretions (such as chitinase), antifungal metabolites, iron depleting siderophores or a combination of all.[24, 25]

1.3 Skin Bacteria from Chytrid Resistant Amphibians

The skin is an ecosystem, which represents a miscellaneous habitat of infoldings and unique niches, and shelters a wide assortment of microbes. Due to being an interface with the external environment, the skin gets colonized by the diverse microorganisms including bacteria, fungi, viruses and sometime mites. Many of these microbes are usually harmless and some also provide a protective function to the host organisms against pathogenic bugs. For instance, an actinomycetous bacterium protects the mutualism between a pine beetle, *Dendroctonus frontalis* and a fungus, *Entomocorticium* sp. against an antagonistic fungus, *Ophiostoma minus*. Similarly, a *Streptomyces* species located on a hunting wasp, called European beewolf protects the wasp cocoon from fungal infestation and enhances the survival of wasp larva. Another filamentous symbiotic species of the genus *Streptomyces* produces antibiotics to supress the growth of garden-parasite *Escovopsis* in fungus-growing ants. In humans also, skin microorganisms have important roles in enhancing the cutaneous immune system.[26-30]

A concept of interactions among pathogens, hosts and microbiomes may lead to management strategies to control disease outcomes. Cutaneous microbes and their

community structures are the essential parts of amphibians' innate immune system against chytridiomycosis. In amphibians, the skin microbes vary with species and population based on geographies, seasons and host ontogenies. Several previous reports are assuring that the skin bacteria can inhibit chytrid colonization and pathogenicity in amphibians. Some reports claim that the presence of chytrid inhibiting skin bacteria from the amphibians such as *Acinetobacter*, *Lysobacter*, *Janthinobacterium*, *Stenotrophomonas* and *Pseudomonas* can provide a protective function against chytrid pathogens. One previous report by Haris et al. (2009) shows, that adding the widely distributed antifungal skin bacterium *J. lividum* to the skin of *Rana muscosa,* protected the frog against the morbidity and mortality caused by *Bd*. One of the predicted mechanisms of preventing disease by skin bacteria could be the production of antifungal secondary metabolites such as violacein produced by *J. lividum*, but a recent study by Zimenez et al. (2022) confirmed that the secondary metabolites alone are not sufficient for the suppression of chytrids. However, further studies claimed that several cutaneous microbes from amphibians' skin are able to inhibit *Bd in-vitro*.[23, 31-33]

Muletz et al. (2017) reported 50 unique anti-*Bd* bacterial strains from chytrid resistant salamanders (*Plethodon cinereus, P. glutinosus and P. cylindraceus*) out of which, 5 strains were commonly detected in most of the salamander species. The majority in number of anti-chytrid skin bacteria were belonging to the genera *Pseudomonas* and *Stenotrophomonas*. The study also reveals the anti-chytrid potency of skin bacteria depending on the *Batrachochytrium* genotypes, bacterial strains and temperature. This, in one aspect, suggests the use of bioaugmentation of anti-*Bd* bacteria to prevent *Bd* infection and survival assurance of amphibian species.[25, 34]

1.4 *Pseudomonas*

Pseudomonas is the most dominant genus of bacteria that has been isolated from salamander skin. In general, they predominantly inhabit soil and aquatic environments. The genus belongs to the class of Gammaproteobacteria, and are gram negative rod-shaped motile bacteria. They are non-spore forming in nature. The genus, in general, includes currently more than 140 species of both pathogenic and beneficial traits. *P. aeruginosa* is considered a highly pathogenic strain to humans, causing nosocomial infections such as chronic lung infections, pneumonias, urinary tract infections and

bloodstream infections. Other organisms are also hampered with pathogenic *Pseudomonas* such as *P. fluorescens* (soft rot on plants), *P. anguilliseptica* (lethal hemorrages in marine fish) and *P. protegens or P. chlororaphis* (infections of insects). However, there are several beneficial *Pseudomonas* species which promote the growth of plants in agriculture while some play a protective role in animal infections. They are also considered to produce antibiotics and several other medicinally significant secondary metabolites and thus attracted the interest of pharmaceutical researchers in academia and industry.[35-38]

1.5 Secondary Metabolites

The organic compounds, produced by any forms of life such as bacteria, fungi, plants and animals, which have no direct involvement in their growth, development or reproduction are considered as secondary metabolites. They are classified in different categories based on their biosynthetic pathways or chemical scaffolds such as polyketides, non-ribosomal peptides, ribosomal peptides, alkaloids, terpenoids, glucosides, phenolic compounds and phenazines. Functionally, in nature, they serve as competitive weapons against foreign organisms, metal transporters, sexual hormones, and many more. Their selective functions such as antimicrobial, antitumor, anti-diabetic, cholesterol lowering, immunosuppressant, antiviral, antiprotozoal, antihelminthic and anti-ageing properties can be used for pharmaceutical applications. There are some bioactive metabolites with antifungal, antimicrobial, metal transporter and antiviral properties produced by the different species of *Pseudomonas* (Table 1). However, further studies are yet needed to explore their complete potential.[39]

Table 1: Bioactive secondary metabolites from Pseudomonads

Compounds	**Activities**	**Reference strains**
2,4-DAPG	antifungal	*P. fluorescens*[40]
Mupirocin	antibiotic	*P. fluorescens*[41]
Pyrrolnitrine	antifungal, antibiotic	*P. pyrrocinia*[42]
Pyocyanin	antifungal	*P. aeruginosa*[43]
Pyoverdine, Pyochelin	Iron transporter/siderophore	*P. aeruginosa*[44]
Rhamnolipid PS-17	antiviral	*Pseudomonas* sp. S-17[45]

1.5.1 *Pseudomonas* Derived Lipopeptides

Lipopeptides (LPs) are one of the predominant metabolites produced by *Pseudomonas*. They are amphiphilic molecules, formed by an oligopeptide chain acylated to a linear fatty acid. Structurally, the peptide chain in LPs is found either as linear head or a lactone ring (Figure 6). The lactone ring in the structure tags them as cyclic lipopeptides (CLPs). Cyclization of the peptide motif results in the absence of free C- and N- terminal and reduces proteolysis. This, therefore, enhances the *in-vivo* stability of the peptide unit compared to the linear counterpart. Additionally, cyclization also stabilizes the peptide conformation which may be relevant to biological functions. The lipid moiety is usually a β-hydroxy acid with a predominant *R*-configuration at the corresponding stereocenter. Furthermore, the lipid chain can be unsaturated (ferrocin A), bishydroxylated (pseudomycin A) or dicarboxylated (tolaasin A).[46, 47]

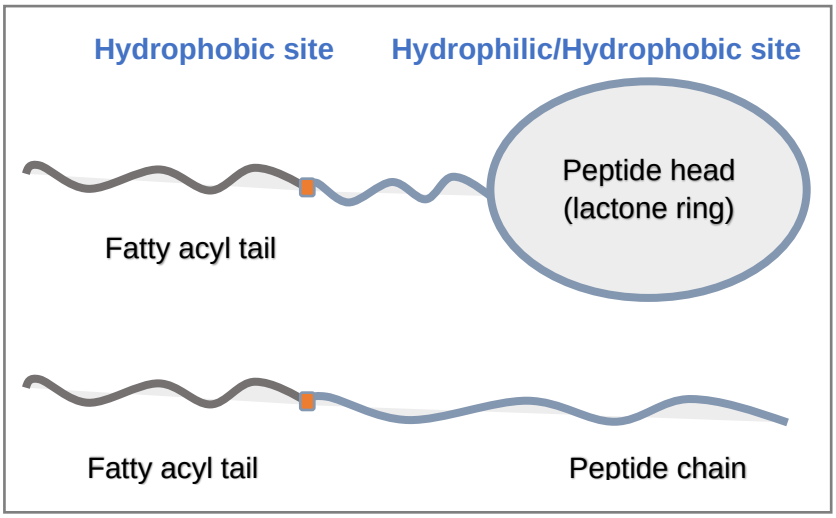

Figure 6: Schematic representation of *Pseudomonas* derived lipopeptides showing cyclic (top) and linear (bottom) forms of structures.

According to the Norine database until 2022, there are 13 families of *Pseudomonas* derived lipopeptides based on the structural prototype. These families are mainly differing in the number of amino acids (7 to 25), presence or absence of cyclization, ring size, lipid chain length (C_5 to C_{16}) and amino acids alignment (Table 2).[48]

Table 2: List of lipopeptide families produced by *Pseudomonas* showing different amino acid sequences and ring cyclization (blue line).

Name	Fatty acid	1	2	3	4	5	6	7	8	9	10	11	12	13	14	15	16	17	18	19	20	21	22	23	24	25
Syringafactin Family																										
Syringafactin A	C10OH	L-Leu	L-Leu	D-Gln	L-Leu	D-aThr	L-Val	D-Leu	L-Leu																	
Syringafactin B	C10OH	L-Leu	L-Leu	D-Gln	L-Leu	D-aThr	L-Leu	D-Leu	L-Leu																	
Syringafactin C	C10OH	L-Leu	L-Leu	D-Gln	L-Leu	D-aThr	L-Ile	D-Leu	L-Leu																	
Syringafactin D	C12OH	L-Leu	L-Leu	D-Gln	L-Leu	D-aThr	L-Val	D-Leu	L-Leu																	
Virginiafactin A	C10OH	L-Leu	L-Leu	D-Gln	L-Leu	D-Ser	L-Val	D-Leu	L-Leu																	
Virginiafactin B	C10OH	L-Leu	L-Leu	D-Gln	L-Leu	D-Ser	L-Ile	D-Leu	L-Leu																	
Cichofactin A	C10OH	L-Leu	L-Leu	D-Gln	L-Leu	D-Gln	L-Val	D-Leu	L-Leu																	
Cichofactin B	C12OH	L-Leu	L-Leu	D-Gln	L-Leu	D-Gln	L-Val	D-Leu	L-Leu																	
Bananamide family																										
Bananamide A	C12OH	Leu	Asp	Thr	Leu	Leu	Gln	Leu	Ile																	
Bananamide B	C12:1 (3-OH)	Leu	Asp	Thr	Leu	Leu	Gln	Leu	Ile																	
Bananamide E	C12OH	D-Leu	D-Asp	D-Thr	D-Leu	D-Leu	D-Ser	Leu	Ile																	
Viscosin Family																										
Viscosin	C10OH	L-Leu	D-Glu	D-aThr	D-Val	L-Leu	D-Ser	L-Leu	D-Ser	L-Ile																
Viscosinamide	C10OH	L-Leu	D-Gln	D-aThr	D-Val	L-Leu	D-Ser	L-Leu	D-Ser	L-Ile																
WLIP	C10OH	L-Leu	D-Glu	D-aThr	D-Val	D-Leu	D-Ser	L-Leu	D-Ser	L-Ile																
Massetolide A	C10OH	L-Leu	D-Glu	D-aThr	D-aIle	L-Leu	D-Ser	L-Leu	D-Ser	L-Ile																
Massetolide D	C10OH	L-Leu	D-Glu	D-aThr	D-aIle	L-Leu	D-Ser	L-Leu	D-Ser	L-Leu																
Massetolide E	C10OH	L-Leu	D-Glu	D-aThr	D-Val	L-Leu	D-Ser	L-Leu	D-Ser	L-Val																
Massetolide F	C10OH	L-Leu	D-Glu	D-aThr	D-Val	L-Leu	D-Ser	L-Leu	D-Ser	L-Leu																
Pseudophomin A	C10OH	L-Leu	D-Glu	D-aThr	D-Ile	D-Leu	D-Ser	L-Leu	D-Ser	L-Ile																
Pseudophomin B	C12OH	L-Leu	D-Glu	D-aThr	D-Ilel	D-Leu	D-Ser	L-Leu	D-Ser	L-Ile																
Pseudodesmin A	C10OH	L-Leu	D-Gln	D-aThr	D-Val	D-Leu	D-Ser	L-Leu	D-Ser	L-Ile																
Pseudodesmin B	C10OH	L-Leu	D-Gln	D-aThr	D-Val	D-Leu	D-Ser	L-Leu	D-Ser	L-Val																
Syringomycin Family																										
Syringomycin E	C12OH	L-Ser	D-Ser	D-Dab	L-Dab	L-Arg	L-Phe	Z-Dhb	L-Asp(3-OH)	L-Thr(4-Cl)																
Syringostatin A	C14OH	L-Ser	D-Dab	L-Dab	D-Hse	L-Orn	L-aThr	Z-Dhb	L-Asp(3-OH)	L-Thr(4-Cl)																

Syringostatin B	C14(OH)2	L-Ser	D-Dab	L-Dab	D-Hse	L-Orn	L-aThr	Z-Dhb	L-Asp(3-OH)	L-Thr(4-Cl)																		
Syringostatin D	C12OH	L-Ser	D-Dab	L-Dab	D-Hse	L-Orn	L-aThr	Z-Dhb	L-Asp(3-OH)	L-Thr(4-Cl)																		
Syringotoxin (B)	C14OH	L-Ser	D-Dab	Gly	D-Hse	L-Orn	L-aThr	Z-Dhb	L-Asp(3-OH)	L-Thr(4-Cl)																		
Pseudomycin A	C14(OH)2	L-Ser	D-Dab	L-Asp	L-Lys	L-Dab	L-aThr	Z-Dhb	L-Asp(3-OH)	L-Thr(4-Cl)																		
Cormycin A	C16(OH)2	L-Ser	D-Orn	L-Asn	D-Hse	L-His	L-aThr	Z-Dhb	L-Asp(3-OH)	L-Thr(4-Cl)																		
Orfamide Family																												
Orfamide A	C14OH	L-Leu	D-Glu	D-aThr	D-aIle	L-Leu	D-Ser	L-Leu	L-Leu	D-Ser	L-Val																	
Orfamide B	C14OH	L-Leu	D-Glu	D-aThr	D-Val	L-Leu	D-Ser	L-Leu	L-Leu	D-Ser	L-Val																	
	C12OH	L-Leu	D-Glu	D-aThr	D-aIle	L-Leu	D-Ser	L-Leu	L-Leu	D-Ser	L-Val																	
Amphisin Family																												
Amphisin	C10OH	D-Leu	D-Asp	D-aThr	D-Leu	D-Leu	D-Ser	L-Leu	D-Gln	L-Leu	L-Ile	L-Asp																
Tensin	C10OH	D-Leu	D-Asp	D-aThr	D-Leu	D-Leu	D-Ser	L-Leu	D-Gln	L-Leu	L-Ile	L-Glu																
Lokisin	C10OH	D-Leu	D-Asp	D-aThr	D-Leu	D-Leu	D-Ser	L-Leu	D-Ser	L-Leu	L-Ile	L-Asp																
Arthofactin	C10OH	D-Leu	D-Asp	D-Thr	D-Leu	D-Leu	D-Ser	L-Leu	D-Ser	L-Ile	L-Ile	L-Asp																
Milkisin A	C8OH	Leu	Asp	Thr	Leu	Leu	Ser	Leu	Gln	Leu	Ile	Glu																
Milkisin C	C10OH	Leu	Asp	Thr	Leu	Leu	Ser	Leu	Gln	Leu	Ile	Glu																
Pholipeptin	C10OH	D-Leu	L-Asp	L-Thr	D-Leu	D-Leu	D-Ser	D-Leu	D-Ser	D-Leu	L-Ile	D-Asp																
Putisolvin Family																												
Putisolvin I	C6	Leu	Glu	Leu	Ile	Gln	Ser	Val	Ile	Ser	Leu	Val	Ser															
Putisolvin II	C6	Leu	Glu	Leu	Ile	Gln	Ser	Val	Ile	Ser	Leu	Leu/Ile	Ser															
Tolaasin Family																												
Tolaasin A	C5OH	Dhb	Pro	Ser	Leu	Val	Ser	Leu	Val	Val	Gln	Leu	-	-	-	-	Val	Dhb	aThr	Ile	Hse	Dab	Lys					
Tolaasin B	C8OH	Dhb	Pro	Ser	Leu	Val	Ser	Leu	Val	Val	Gln	Leu	-	-	-	-	Val	Dhb	aThr	Val	Hse	Dab	Lys					
Tolaasin I	C8OH	Dhb	Pro	Ser	Leu	Val	Ser	Leu	Val	Val	Gln	Leu	-	-	-	-	Val	Dhb	aThr	Ile	Hse	Dab	Lys					
Tolaasin II	C8OH	Dhb	Pro	Ser	Leu	Val	Ser	Leu	Val	Val	Gln	Leu	-	-	-	-	Val	Dhb	aThr	Ile	Gly	Dab	Lys					
Corpeptin A	C10OH	Dhb	Pro	Ala	Ala	Ala	Val	Val	Dhb	Hse	Val	aIle	Dhb	Ala	Ala	Ala	Val	Dhb	aThr	Ala	Dab	Ser	Ile					
Syringopeptin Family																												
Syringopeptin 25A	C10OH	Dhb	Pro	Val	Ala	Ala	Val	Leu	Ala	Ala	Dhb	Val	Dhb	Ala	Val	Ala	Ala	Dhb	aThr	Ser	Ala	Val	Ala	Dab	Dab	Tyr		

1.5.2 Biological Functions of Lipopeptides

Lipopeptides are highly amphiphilic in nature and thus able to deplete surface tension. In this way, they can readily interact with cellular membranes of other organisms and exert biological activities. Furthermore, lipopeptides elevate the bacterial (producers') swarming mobility in both active and passive ways. This phenomenon promotes the expansion of colonies across the growing surfaces by lowering the surface tension. LPs can also increase the bioavailability of hydrophobic substrates, which enables the colonization of bacterial niche in a habitat of limited nutrients. The ecological roles of bacterial LPs remain highly unknown, however the yield and structural variation of LPs are quite intensive in some bacteria. This suggests the existence of vital roles of LPs in the natural environment, somehow developing the strategies which help the survival of microbes under unfavourable conditions.[47]

Some LPs are known for their versatile biofunctions such as biosurfactant, anti-microbial, antifungal and cytotoxic abilities. They are the second largest group of biosurfactants from natural products. Due to these characters attributed to LPs, they can be considered bifunctional, according to which they promote their own mobility and at the same time inhibit the growth and colonization of other microorganisms. Additionally, they might influence the biofilm formation and ligation with heavy metals for micronutrients or soil detoxification.[49, 50]

1.5.3 Biosynthesis and Bioinformatics

Every natural product compound is synthesized by a specific biomolecular mechanism called biosynthesis. The biosynthesis machinery of a compound is always encoded by the nucleotide sequences of the DNA, called gene cluster. The biosynthetic gene clusters of natural products are categorized into different groups depending on their corresponding biosynthetic origin such as the non-ribosomal peptide synthetase (NRPS), polyketide synthase (PKS), ribosomally synthesized and post-translationally modified peptide (RiPP), fatty acid synthase (FAS), terpene cyclase or shikimate.[51, 52]

Lipopeptides are formed mainly by NRPS enzyme complexes and are generally encoded by NRPS genes. The NRPS megaenzyme, which is primarily responsible for synthesizing the peptide chain of the LPs is comprised of different regions and each region further consists of different modules (Figure 7). Each module consists of three

domains called condensation domain (C), adenylation domain (A) and thiolation domain (T), which all together code for one amino acid. The final chain terminating thioesterase domain (TE) is responsible for the cyclization of peptide or/and release of the peptide from the biosynthesis machinery. An additional epimerization domain (E) can be adjacent to or be embedded within the C-domain in some modules of NRPs gene cluster, depending on the fate of compound structure, which will be responsible for determining the D - or L - configuration of amino acids in the peptide chain. In

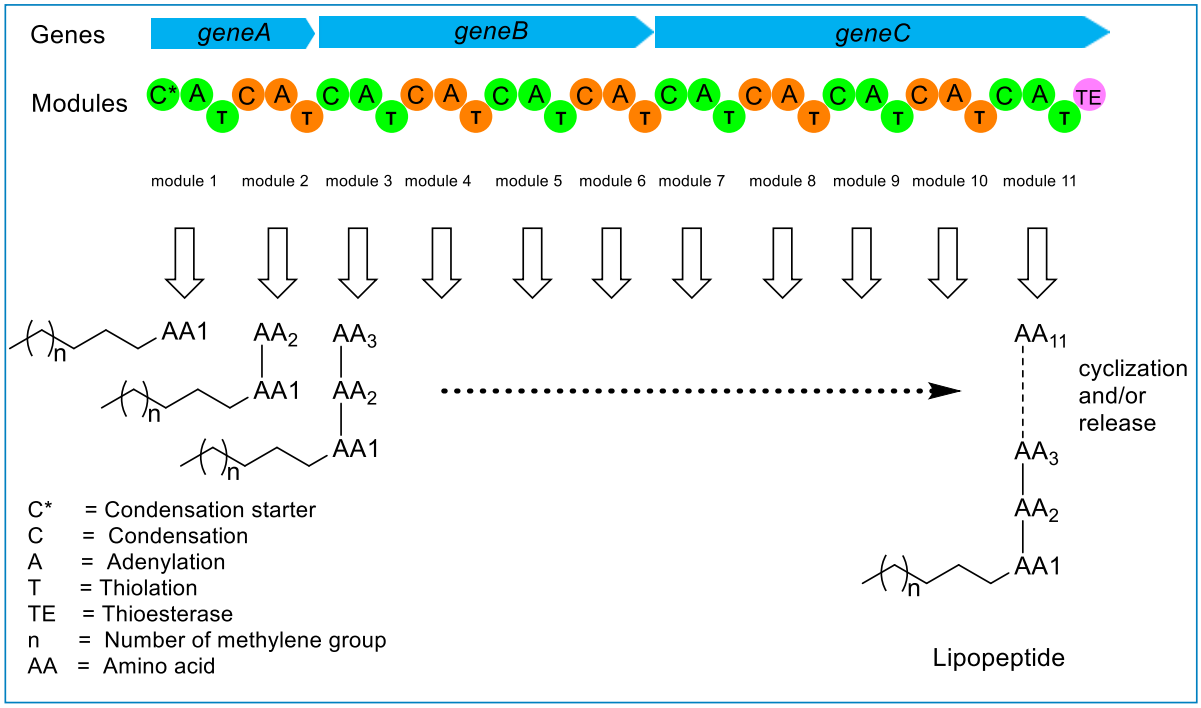

Figure 7: General biosynthesis scheme of lipo-undecapeptides by a NRPS enzyme complex system.

lipopeptides, there remains one of the C-domains as a lipo-initiation domain ($C_{starter}$) in a module, which is responsible for the attachment of the fatty acid chain. Nevertheless, the saturation degree and exact length of the fatty acid can currently not be predicted, because the fatty acid biosynthesis genes are not encoded in the NRPS gene cluster, but rather available as 3-OH fatty acid, produced by the primary metabolism.[53]

For a gene cluster analysis coding a secondary metabolite of interest, first a whole genome sequence of the bacterium is required. The sequenced genome data can be analysed with several bioinformatic tools such as antiSMASH, which permits the fast genome-wide identification and the analysis of biosynthetic gene clusters for secondary metabolites. Bioinformatic tools can be categorized as homology/similarity tool, protein function analysis tool, sequence analysis tool and structural analysis tool.

However, the last two tools help to identify the possible classes of secondary metabolites and their structural format such as amino acids alignment in peptides. This also helps to omit the efforts for isolation and identification of falsified artifacts (from fermentation media or other contaminations) during natural product investigations.[1, 54]

1.6 Metabolomics

Profiling of chemical and biochemical aspects of metabolites via several analytical tools is called a metabolomic study. The general metabolomics scheme consists of the extraction of biological resources using a suitable solvent, fractionation, purification, mass spectrometry, spectroscopic analysis and structure elucidation (Figure 8). In regard to the chemical identification of secondary metabolites, mass spectrometry has

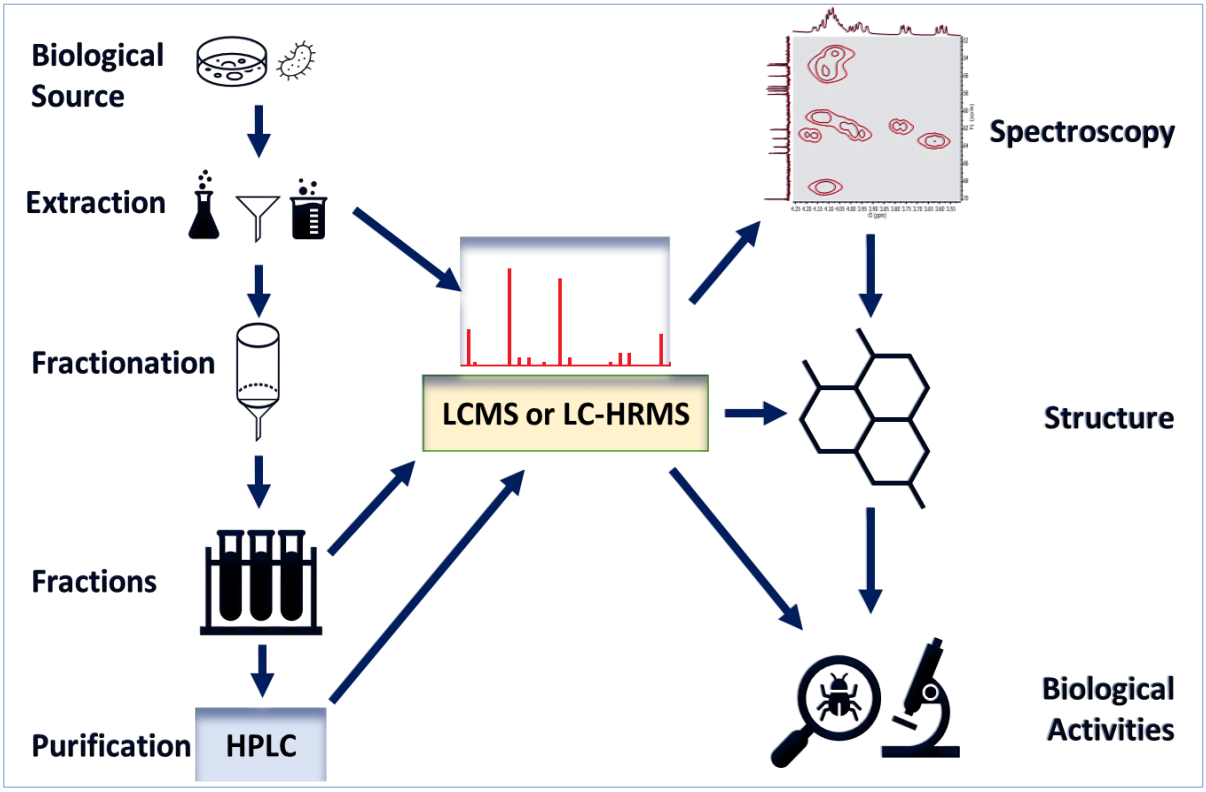

Figure 8: Overall scheme of metabolomics in natural product research

been a fast performing and widely used tool for the analysis of natural products. It has a broad range of application due to its higher sensitivity. Data, acquired with liquid chromatography in combination with high resolution mass spectrometry (LC-HR-MS), are utilized in various computational platforms to interpret and visualize the preliminary chemical and structural features of secondary metabolites from biological resources. This is applicable to identify untargeted metabolites as well as pre-known metabolites

throughout the biological system which facilitates the discovery of novel lead compounds for future drug development.[55]

In mass spectrometry-based metabolomics, the organisms are extracted and subjected to a LC-HR-MS measurement. The data acquisition of LC-HR-MS results in the separation of individual metabolites as a mean of retention times along with their molecular mass and corresponding fragments/-ions. In this regard, Global Natural Products Social Molecular Networking (GNPS), an online chemical analytic platform, has been used worldwide to analyse the mass spectrometry raw (and processed) data. With an increasing number of GNPS cited articles published each year, molecular networking based metabolomics has become a predominant tool for the identification of small molecules in a single attempt. Molecular networking works on the ethics of grouping structurally related metabolites having relatively similar fragments in mass spectrometry. The well generated network further visualizes the clumps of compound classes in each cluster consisting of identical molecules, derivatives and analogues. The GNPS platform further processes the fragmentation fingerprints of submitted data to match with the mass spectrometry database and finally reveals the best matched candidate compounds from the database. This leads to the tentative identification of metabolites and drugs in pharmaco-medicinal fields based on only HR-MS data. Besides, raw or processed MS-fragmentation data are widely analysed in another *in silico* platform called SIRIUS where the developers have claimed the annotation efficiency to be over 70% concerning the molecular formula (MF) and the compound structure. Additional chemoinformatic tools such as Cytoscape for network data visualization along with MetaboScape (Bruker) and MZmine for MS data featuring (or processing), XCMS, MetAlign, SIEVE (Thermo), Progenesis QI (Waters) are widely used in HR-MS based metabolomics. Each of these tools have unique advantages during pre-processing, data analysis, data interpretation and data visualization.[56-63]

HR-MS based metabolomics facilitate the search for target compounds, which are subsequently isolated for structural confirmation via spectroscopic techniques such as nuclear magnetic resonance (NMR), infrared (IR) spectroscopy and polarimetry. TopSpin (Bruker) and MestreNova are widely used software applications for the analysis of NMR spectra.[64]

1.7 HR-MS and NMR Spectroscopy

In metabolomics, natural product compounds were mainly characterized and identified by chemical analytics such as HR-MS and NMR. These tools with totally different principles analyse the compound structures in natural product research. All the compounds isolated in this study were discovered as LPs. Before outlining the results of this study, it shall be outlined briefly the key principles of structural interpretation based on HR-MS and NMR spectra. [65]

In HR-MS/MS data interpretation, there are mainly two spectral information of the analytes, referred to as MS^1 and MS^2 spectra. The spectra plot mainly consist of 'mass to charge' ratio (*m/z*) on the X-axis and ion intensities on the Y-axis. The sample injected to a mass spectrometer is first ionized, accelerated, detected, and is first observed in MS^1 spectra. The ions from MS^1 spectra are further fragmented and detected in MS^2 spectra as the second stage of mass spectrometry. This phenomenon is called tandem mass spectrometry (MS^2). In this way, MS^1 spectra reveal information on molecular ions, molecular masses and molecular formulae, whereas MS^2 spectra expose the chemical fragments of the molecular ions.[66-68]

LPs show a specific pattern of molecular ions and adducts in a positively ionized MS^1 spectrum. In the positively polarised ESI-HR-MS^1 spectrum, a LP is commonly observed as a pseudomolecular ion $[M+H]^+$, sodium adduct $[M+Na]^+$, potassium adduct $[M+K]^+$, water loss adduct $[M-H_2O+H]^+$, or as a doubly charged ion $[M+2H]^{2+}$. They further show some characteristic patterns of fragmentation in the MS^2 spectra. These fragments are called a, b, c and x, y, z, depending on the fragmentation sites and the fragmented motifs (Figure 9 A). The highly prominent fragments are mainly b and y fragments which appear due to the splitting of a peptide bond. The positively charged fragment with the carbonyl carbon is termed a b-fragment and the other a y-fragment. The b-fragment sometimes appears with a neutral loss of water in CLPs, called b^0-fragments.[69-71]

In NMR spectrometry, several 1D and 2D experiments are performed to elucidate the structures of the isolated LPs. ^{1}H-NMR, ^{13}C-NMR or DEPT135 spectra are obtained with 1D NMR experiments. ^{1}H-NMR spectra are analysed to determine the number and chemical environment of protons, while ^{13}C NMR spectra reveal the same features

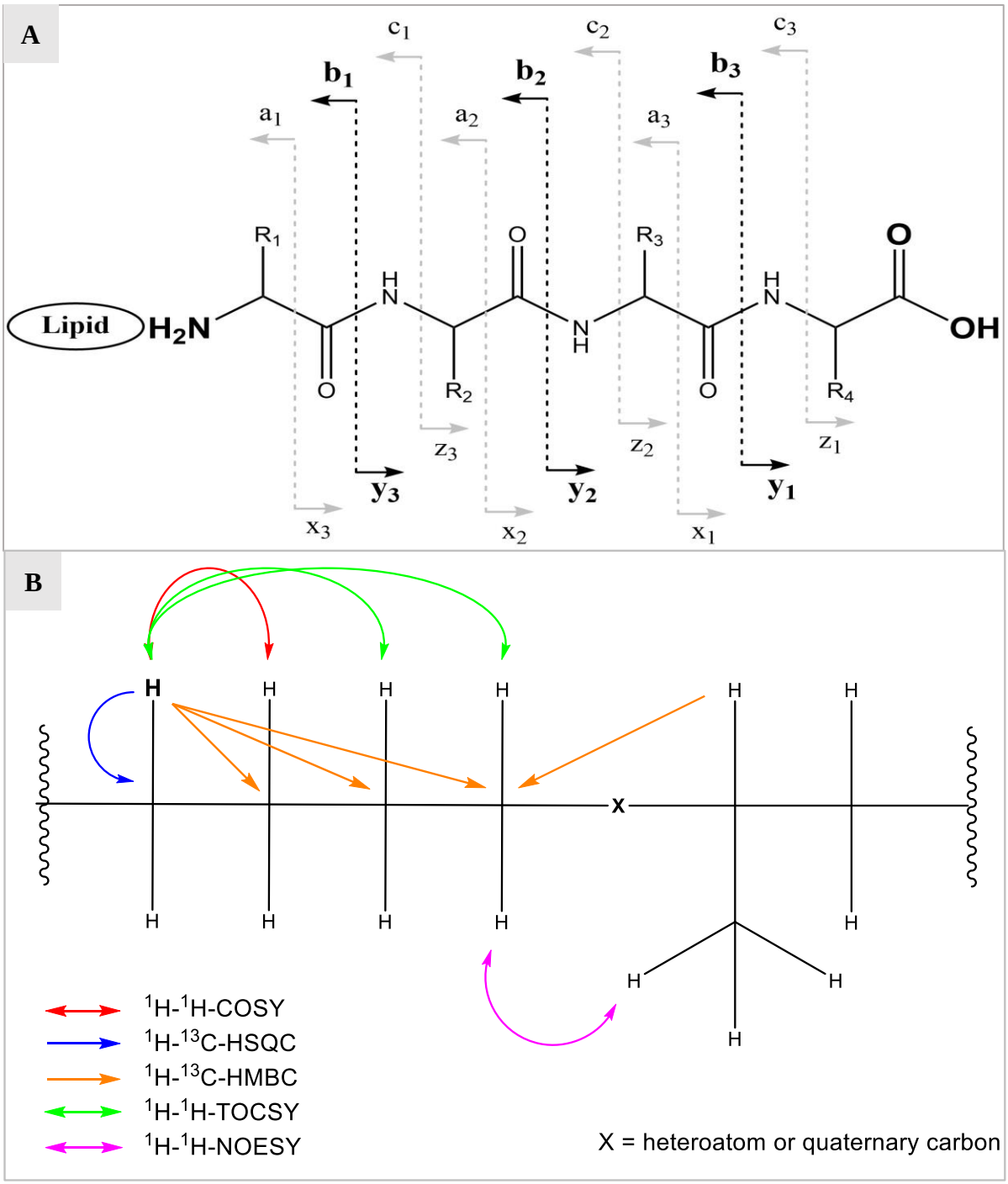

Figure 9: [A] General overview of fragmentation pattern in the MS^2 spectra of lipopeptides, and [B] a schematic diagram showing some of the spin interactions in different NMR experiments.

for carbons in the chemical structure. DEPT135 spectra are used to analyse the hydrogenated state of carbon, where the upright resonances denote -CH- or $-CH_3$ carbon atoms while the inverted peaks denote $-CH_2-$ carbons. The spectra of some protons are further split into smaller spectra (multiplicity), due to coupling interaction, depending on the number and nature of neighbouring protons in the chemical

structure. The coupling (spin-spin coupling) is induced due to a magnetic interaction between two nuclear spins transmitted through the bonding electrons. This phenomenon is useful to predict the number and nature of neighbouring protons.

2D NMR spectra represent the correlations (magnetic interaction) of protons within the different chemical environments (homonuclear) and with carbons (heteronuclear) as well (Figure 9 B). In heteronuclear 2D spectra, the proton spectrum is aligned in the X-axis (f2, ppm) while the carbon spectrum is aligned in the Y-axis (f1, ppm). The coupling interactions between proton and carbon nuclei appear as cross peaks in the plot. This interaction is specific for each 2D NMR experiment. Similarly, homonuclear 2D spectra reveal the coupling interactions between two proton types. For instance, each cross peak in the ^{1}H-^{13}C-HSQC spectrum appears due to the coupling interaction of a proton type with its directly attached carbon. The cross peaks in a ^{1}H-^{13}C-HMBC spectrum appears due to the coupling interactions between each proton type with its 2 to 4 bonds neighbouring carbons. The coupling interactions between each proton type, and its neighbouring carbon up to a heteroatom or a quaternary carbon, are observed in ^{1}H-^{13}C-HSQC-TOCSY spectra. The homonuclear coupling interactions from each proton type with 3 bonds proton types are observed in ^{1}H-^{1}H-COSY spectra, whereas with all neighbouring proton types up to a heteroatom or a quaternary carbon are observed in ^{1}H-^{1}H-TOCSY spectra.

The cross peaks in the ^{1}H-^{1}H-NOESY spectrum are observed between two spatially closer proton types due to the nuclear spins undergoing cross-relaxation. This unique observation reveals information on the spatial orientation of protons in the chemical structure, especially in the sequence of the amino acids in a peptide chain. ^{1}H-^{15}N-HSQC and ^{1}H-^{15}N-HMBC spectra show the coupling interactions of each -NH- proton to its adjacent nitrogen and neighbouring nitrogen, respectively. [72, 73]

1.8 Antifungal Metabolites and Enzymes

Several antifungal compounds are discovered from the natural resources such as bacteria (fungichromin), fungi (echinocandin) and plants (coumarin). There are additionally some highly recognized antifungal enzymes such as chitinases and β-1,3-glucanases which act strongly to inhibit the growth of fungi. Some well-known antifungal metabolites stemming from the genera, similar to that of salamander skin

bacteria, are violacein (from *Janthinobacterium*), maltophilin, pyrrolnitrin (from *Stenotrophomonas*), and 2,4-diacetylphloroglucinol (from *Pseudomonas*) (Figure 10). The modes of action of these metabolites differ strongly. Besides, chitinase as an

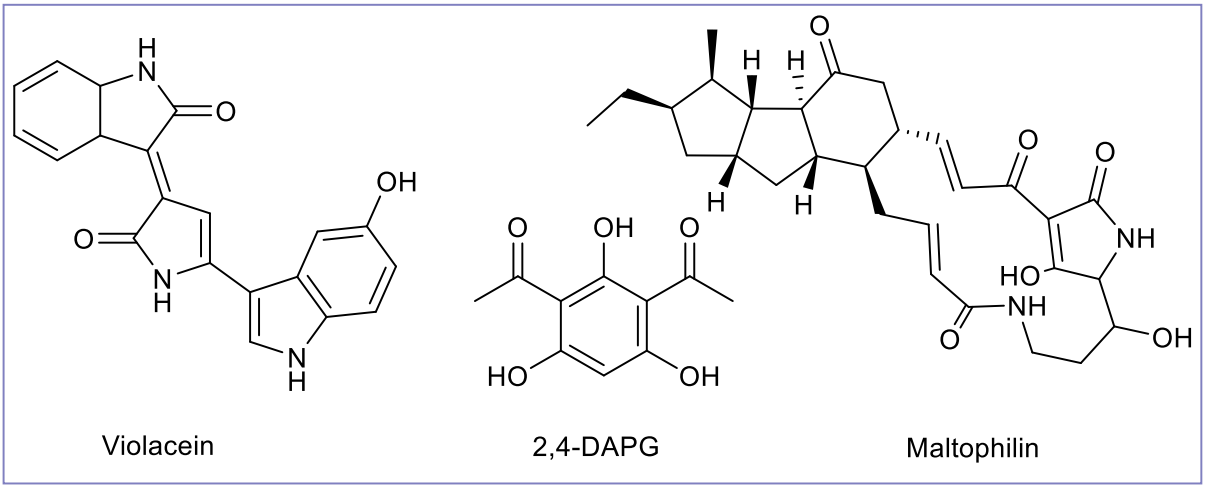

Figure 10: Structures of antifungal metabolites isolated from *Janthinobacterium* (violacein), *Pseudomonas* (2,4-DAPG) and *Stenotrophomonas* (maltophilin) species.

antifungal enzyme has the ability to digest chitin which is a vital component of fungal cell wall. Chitinase is selective to its potential activity with the temperature and pH at the site of action.[74-79]

A previous study has suggested that the inhibition of chytrid growth by *S. maltophilia* has been linked to its antifungal secondary metabolites and chitinolytic activity. Another study made on cutaneous bacteria isolated from different frog species has revealed *P. cichorii* as the greatest inhibitor against *Bd* in an *in-vitro* assay. Furthermore, they identified and isolated viscosin, from this strain and found it to be active against *Bd* with a minimum inhibitory concentration (MIC) value of 31.25 µg/mL. However, inhibition of *Bd* growth by viscosin at this concentration seems not sufficient to justify the complete antifungal potential of the producer strain. In this study, it has been hypothesized that anti-chytrid bacteria from salamander skin inhibit the chytrid infection either by producing antifungal secondary metabolites or chitinase enzymes or both.[80, 81]

2. Aim of the Research Project

The overall research project is conducted for exploring the chemical fundamentals of chytrid pathogens in amphibians and anti-chytrid microorganisms from salamander skin. The study mainly aims for the followings four aspects concerning chytridiomycosis:

2.1 Metabolic Screening of Chytrid Fungi in Amphibians

The study shall initially focus on the cultivation of *Bd* in laboratory environments in optimal media. The *Bd* culture is then extracted and further used in LC-HR-MS-based metabolomics and brine shrimp lethality assay. These sections aim for the identification of toxic metabolites, produced by the chytrid pathogen. Based on the results of these experiments, further experimental designs are made for the isolation and structural identification of toxic metabolites via chromatographic techniques and spectroscopic measurements respectively.

2.2 Metabolomics of anti-*Bd* Bacteria from Salamander Skin

The investigation of secondary metabolites produced by the anti-*Bd* bacteria isolated from salamander skin is one of the major focuses of this study. The study aims for the preliminary screening of secondary metabolites from all bacterial isolates using liquid chromatography mass spectrometry (LC-MS). The cultivation of these bacteria shall be conducted in complex media and minimal media. The resultant broth/supernatant shall then be extracted with two solvents: ethylacetate and n-butanol. The extracts examined by LC-MS go through further experimental measurements based on the observed number of UV peaks and novel masses in the individual chromatogram.

The selected bacteria after the LC-MS analysis will be cultivated on large-scale for the isolation and structural identification of targeted metabolites via chromatographic and spectroscopic tools, respectively. Some of the isolates are considered for genome sequencing, depending on the structural novelty of the isolated compounds, that predicts the possible biosynthetic pathways.

2.3 Chitinase Assay of anti-*Bd* Bacteria from Salamander Skin

In parallel, the chitinase enzyme activities of anti-*Bd* isolates on chitinase agar will be determined. The goal of this study is to provide the enzymatic aspects concerning the

antifungal properties of the bacterial strains.

2.4 Anti-chytrid Bioassay of Compounds Isolated from Salamander Skin Bacteria

The ultimate goal of this study is to determine the antifungal traits of secondary metabolites produced by salamander skin bacteria against chytrids. The selected bacteria produce different compounds including both known and unknown metabolites. All the isolated and structurally characterized compounds are considered to be tested for their antifungal activity against the chytrid pathogens *Bd* and *Bsal*.

In summary, this study will clarify the contribution of fungal secondary metabolites in chytrid infection. Furthermore, the study will illuminate the role of the salamander skin bacteria in the defense of chytrid fungi.

3. Materials and Methods

The methods used in this study are mainly centred on the fermentation of microorganisms, isolation and characterization of secondary metabolites, and biological activities.

3.1 Microorganisms

The microorganisms used in this study belong to two separate kingdoms, fungi and bacteria. Two chytrid fungi, *B. dendrobatidis* and *B. salamandrivorans* along with additional anti-*B. dendrobatidis* bacterial species isolated from the salamander skin were studied for their secondary metabolites profiling.

3.1.1 Chytrid Fungi

A chytrid strain, *B. dendrobatidis* JEL423 was kindly provided by Dr. Joyce E. Longcore (The University of Maine, USA). After the death of this strain during the laboratory storage (cryopreservation), *B. dendrobatidis* JEL404 was received from Dr. Carly Muletz-Wolz (Center for Conservation Genomics, Smithsonian's National Zoo and Conservation Biology Institute, USA). A further chytrid strain, *B. salamandrivorans* AMFP1 was kindly provided from Prof. Dr. An Martel (Faculty of Veterinary Medicine, Department of Pathobiology, Pharmacology and Zoological Medicine, Belgium).

3.1.2 Salamander Skin Bacteria

A total of 35 bacterial strains, isolated from the skin of chytrid-resistant salamanders, were received from Dr. Carly Muletz-Wolz. The initial identification of the isolates via 16S rRNA sequencing was conducted by Dr. Muletz-Wolz. The metadata of bacterial isolates comprising 16S rRNA sequences, identified names, host species, isolation sites and their anti-*B. dendrobatidis* strengths were received along with the isolates.

3.2 Cryopreservation of Microorganisms

3.2.1 Cryopreservation of Chytrid Strains

The following materials were prepared for the cryopreservation of *B. dendrobatidis* and *B. salamandrivorans* strains.

- Fresh TGhL broth (16 g tryptone, 4 g gelatin hydrolysate, 2 g lactose, 1 L milli-Q water) and fresh 1% tryptone broth.
- Sterile fetal calf serum (FCS).

- Sterile cell scrapers.
- 15 mL sterile falcon tubes for centrifugation,
- Centrifuge
- 1.8 mL sterile cryotubes with O-ring.
- Pipette and pipette tips (size; 1 mL)
- Sterile DMSO (light protected).
- Freezing container with isopropyl alcohol (Mr. Frosty).
- Laminar flow hood.
- Inverted optical microscope
- - 80ºC freezer.
- Styrofoam box filled with ice.

Then, fresh and healthy chytrid cultures were cryopreserved according to the protocol, provided by Prof. Dr. An Martel (personal communication) and the protocol reported by Boyle et al. (2003), as follows.[82]

1) The *B. dendrobatidis* and *B. salamandrivorans* were grown in 1% tryptone agar medium and TGhL agar medium, respectively, for 4 days at 17ºC.
2) The thalli of *B. dendrobatidis* and *B. salamandrivorans* were transferred after 4 days of incubation into 1% tryptone broth and TGhL broth, respectively, and incubated at 17ºC for 4 to 6 days until active spores were observed.
3) A stock solution of 5 mL cryo-medium was prepared in a falcon tube; 450 µL TGhL + 50 µL FCS for each cryo-tube.
4) A stock solution of 5 mL DMSO was prepared in a dark glass vial (350 µL TGhL + 100 µL DMSO + 50 µL FCS for each cryo-tube).
5) The spores and sporangia were collected with a cell scraper from the wall of each culture flask and aseptically transferred into a falcon tube with the help of a sterile pipette.
6) The culture solution was centrifuged at 2500 rpm for 10 minutes at 20ºC.
7) The supernatant was carefully discarded, and the pellets were suspended in 500 µL cryo-medium.
8) The cryo-medium with spores and sporangia was transferred into the cryotube at an ice-cold temperature and 500 µL DMSO solution added. In total, 8 cryotubes per strain were prepared and labelled accordingly.

9) The cryotubes were immediately placed into a freezing container (Mr. Frosty) and stored at -80ºC for 24 hours.
10) Finally, the cryotubes were preserved at - 80ºC out of the freezing container.

For the revival of cryopreserved chytrid strains, the whole material inside a cryotube was poured into a small culture flask containing 9 mL 1% tryptone medium or TGhL medium. The culture flask was then incubated, and the growth was monitored on a daily basis.

3.2.2 Cryopreservation of Salamander Skin Bacteria

After the arrival of 35 salamander skin bacteria on agar in petri dishes, they were cryopreserved in a glycerol assisted medium according to a slightly modified protocol provided by Muletz-Wolz et al. (2017).[25] The bacteria were first transferred to fresh 1% tryptone agar plates and incubated at 30ºC for 2 to 3 days. The colony morphology was examined for each strain. A pure single colony from each plate was then transferred to 15 mL 1% tryptone medium in a 50 mL falcon tube, which was then incubated at 30ºC and 220 rpm for 2 days. The turbid culture of grown bacteria was then mixed with 50% glycerol solution by 1:1 volume in a 1.8 mL cryotube to have a total volume of 1.6 mL each. The cryotubes were finally labelled and stored at -80ºC. Each strain was cryopreserved in triplicates.

For the revival of cryopreserved bacteria, a portion of the frozen culture from the cryotubes was thawed and poured into a 50 mL falcon tube containing 15 to 20 mL 1% tryptone medium and incubated at 30ºC and 220 rpm for 2 days. The revived pure culture was used for further experimental setups.

3.3 Fermentation and Extraction

3.3.1 Fermentation and extraction of *B. dendrobatidis*

At first, 1% tryptone agar (10 g tryptone [Bacto], 15 g agar [Sigma-Aldrich] and 1 L Milli-Q water) plates were prepared by pouring the 15 mL autoclaved (121ºC for 20 minutes) media solution into each 8.5 cm wide petri dish. Some big thalli of *B. dendrobatidis* were then placed at the middle of 1% tryptone agar plates. The thalli were then smashed gently with the sterile loop to break down and spread over the plates. The plates were then incubated for 3 to 7 days at 19ºC until active motile spores

appeared while observing under the optical microscope. These plates were then considered as seed cultures for the large-scale cultivation of *B. dendrobatidis*.

The culture of *B. dendrobatidis* was fermented under laboratory conditions in a total volume of 1 L fresh 1% tryptone broth (10 g tryptone, 1L Milli-Q water). For this, the seed culture plate with highly active spores was immersed with 2 mL 1% tryptone medium for 2 minutes and gently shaken to bring the spores into the floating medium. The liquid part was then transferred into a 50 mL falcon tube, as an inoculum for the batch culture. 2 mL inoculum of each strain was inoculated into 50 mL 1% tryptone medium in an Erlenmeyer flask (300 mL). The culture was then incubated at 19ºC for 1 to 3 weeks until an intense turbidity of maximum growth appeared. The growth cultures were then extracted two times with an equal volume of ethylacetate and evaporated using a rotary evaporator. The obtained extract was directly used to conduct the brine shrimp lethality assay.

3.3.2 Fermentation and Extraction of Salamander Skin Bacteria

Fermentation of bacteria was carried out in two phases depending on the purpose. The first fermentation of all the 35 bacteria was conducted in a small quantity (20 mL each) for the secondary metabolite screening, while the second fermentation was acquired on a large scale for the isolation, purification and characterization of the targeted secondary metabolites.

For metabolite screening, a pure colony of each strain was transferred from an agar plate into 5 mL 1% tryptone medium into a 15 mL falcon tube and incubated at 30ºC and 220 rpm for 1 to 2 days until a turbidity appeared. 0.2 mL of each preculture was then inoculated into 20 mL of two different culture media: 1% tryptone medium and Davis Minimal Broth-glycerol (DMBgly) medium (10.6 g DMB [CHEMSOLUTE], 1.8 mL glycerol [Roth], 1L Milli-Q water), in a 50 mL falcon tube. The cultures were then incubated at 30ºC and 220 rpm for 3 to 4 days. The fermentation of each culture was carried out in duplicates. One set of cultures was then extracted with a 1:1 volume of ethylacetate while another set was extracted with a 1:1 volume of n-butanol (Fischer Chemical). The organic phase of the solvent was then transferred to a 100 mL round bottom (RB) flask after filtration with Whatman filter paper. The extracted solution was evaporated using a rotary evaporator (Heidolph) until dryness. The dry extracts were

then stored at -20ºC until screening with LC-MS and LC-HR-MS.

For large-scale fermentation, only a few bacteria were selected based on their sufficient growth in minimal medium, their antagonistic potential against fungi and their metabolic profile unveiled by LC-MS or LC-HR-MS. The isolates selected for large-scale fermentation were *Pseudomonas tolaasii* RSB5.11, *Pseudomonas* sp. THA6.6, *Pseudomonas* sp. RSB5.7 and *Pseudomonas* sp. SFB8.6. During fermentation, 2 mL of a 1 to 2 days old inoculum was inoculated into 1 L of DMBgly medium in a 3 L Erlenmeyer flask and incubated at 28ºC and 140 rpm for 3 to 4 days. In total, a minimum volume of 21 L medium was fermented for each isolate. The fermented culture was then extracted twice with 1:1 volume of n-butanol. This was achieved each time by gently adding 1 L of n-butanol along the inner wall of the culture flask and shaking overnight at room temperature at 90 rpm. The upper layer of the organic phase in the flask was then decanted into an RB flask through Whatman filter paper and evaporated using a rotary evaporator until dryness. The dry extracts were then stored at -20ºC until the next experimental setup.

3.4 Fractionation of the Crude Extracts

The crude extracts of four prioritized bacterial isolates were fractionated via vacuum liquid chromatography (VLC) in an open glass column filled with reversed-phase silica gel (POLYGOPREP® 60-50, C_{18}). The dimensions of the column were 40 cm × 7.5 cm while the height of the packed resin was 30 cm. The RP material was filled into the column applying the wet packing method. At first, 1 L of methanol was eluted through the packed column and then followed by 1 L of 10 % methanol (initial gradient of the eluent) for equilibration just before loading the analytes (crude extract). The concentrated solution/sol of analytes was then loaded on the top of the RP material and allowed it just to completely soak on the surface. 500 mL of each methanol gradient with a 10 % successive stepwise gradient (from 10 % to 100 % methanol) was eluted through the column. During elution, a 950 mbar vacuum was applied and nine different fractions were obtained. Mostly, the eluent gradient interval was optimized irregularly with the successive difference of 20 % or 30 % depending on the predetermined desired fractions of the eluate. Subsequently, all eluted fractions were evaporated by a rotary evaporator until dryness and then stored at -20ºC for further experimental use.

3.5 Isolation and Purification of Secondary Metabolites

Depending on the bacterial strain and the class of secondary metabolites, different parameters of high-performance liquid chromatography (HPLC) were set up during the purification of compounds from the crude fractions. In general, a Waters HPLC system was used. The whole setup was comprised of a Waters 1525 pump integrated with a degasser, a Waters 2996 photodiode array detector and a Rheodyne 7725i injector. In the HPLC system, HPLC grade acetonitrile (Honeywell/Riedel-de Haen) and Milli-Q water (with 0.1% TFA) were used as mobile phase solvents. For the stationary phase, reversed-phase analytical HPLC columns (5 µm C18 100 Å 250 × 4.6 mm,) from Phenomenex and Waters were used. In some cases, further specialized columns were used which guaranteed an adapted selectivity and better separation of the compounds. During the HPLC run, the flow of the solvent was running at 1 mL/min while the injection volume of the compound mixture ranged from 10 µL to 100 µL, depending on the concentration of the injected fraction. The mobile phase was applied in a selective gradient manner for each bacterial strain and the sort of compounds for purification (Table 3).

Table 3. Solvent gradient for the mobile phases in HPLC system during purification of the targeted compounds.

Time [Min]	**Acetonitrile [%] (Solvent A)**	**0.1% TFA in Milli-Q water [%] (Solvent B)**
Target: lipo-dipeptide, produced by *P. tolaasii* RSB5.11, Flow: 1 mL/min; Waters 5 µm C18, 250 × 4.6 mm		
5	35	65
10	40	60
16	47	53
17	100	0
19	100	0
20	10	90
23	10	90
Target: compounds produced by *Pseudomonas* sp. THA6.6, Flow: 1 mL/min; Phenomenex Luna® 5 µm C18 (2) 250 × 4.6 mm		
0	10	90
2	20	80

4	67	33
16	70	30
16.5	100	0
18	100	0
19	10	90
20	10	90
Target: compounds produced by *Pseudomonas* sp. THA5.7, Flow: 1 mL/min; Phenomenex Luna® 5 µm C18 (2) 250 × 4.6 mm		
0	50	50
3	70	30
11	73	27
12	100	0
14	100	0
16	50	50
Target: compounds produced by *Pseudomonas* sp. SFB8.6, Flow: 1 mL/min; Phenomenex Kinetex® 5 µm EVO C18, 250 × 4.6 mm		
0	20	80
5	80	20
10	90	10
20	100	0
22	100	0
23	20	80
28	20	80

3.6 Basic Hydrolysis of Cyclic Peptides for Annotation in HR-MS Spectra

Hydrolysis of some samples (crude extracts or purified compounds) was conducted to open the ring cyclization in order to acquire simplified HR-MS dereplication of the compounds. For the hydrolysis, 1 mg crude extract of *Pseudomonas* sp. THA6.6 was treated with 400 µL of 1 M sodium hydroxide (NaOH) solution in a small pear-shaped flask and left standing for 18 hours. The mixture was then neutralized with 200 µL of 2 M hydrochloric acid (HCl) and shaken well for 10 minutes. The pH of the neutralized solution was adjusted to 7 by using 1 M solution of NaOH or HCl. The solution was

then evaporated using rotary evaporation until dryness and redissolved in methanol leaving the salt behind in the flask. The methanolic portion was then submitted to LC-HR-MS measurement for metabolomic analysis.

3.7 Genomics

The genome sequence of the chytrid fungus, *B. dendrobatidis* JEL423, was retrieved from the National Center for Biotechnology Information (NCBI) and analysed by antiSMASH (bacterial version). The selected strains of anti-chytrid bacteria after a preliminary metabolite screening were sequenced for their whole genomes. For this purpose, *Pseudomonas* sp. THA 6.6 and *P. tolaasii* RSB5.11 were grown in 1% tryptone agar medium and sent to the DNA sequencing company (BaseClear, Leiden, NL). The obtained genome data were analysed by antiSMASH bacterial version. The genomic study was mainly focused to the gene cluster analysis of lipo-peptides.[1]

3.8 Metabolomics and Molecular Networking

Every crude sample (around 0.2 mg/mL) from the cultures was dissolved in HPLC grade methanol and measured by liquid chromatography electrospray ionization tandem mass spectrometry (LC-ESI-MS/MS) at the Mass Spectrometry Department of the Institute of Organic Chemistry, University of Tuebingen. The measured LC-HR-MS data were first analysed with Bruker Compass DataAnalysis 4.0 software to assure the proper ionization of the compounds. Only the positively ionized LC-ESI-MS/MS data were further processed through Bruker MetaboScape 3.0 software for bucketing all molecular ions in a single file. Some specific parameters such as intensity threshold (counts); 4000, minimum peak length (spectra); 4, minimum peak length (recursive); 3, EIC correlation; 0.8 and mass calibration (true) were optimized during bucketing. The adduct ions were confirmed $[M+H]^+$ as primary ion, $[M+Na]^+$, $[M+K]^+$, $[2M+H]^+$, $[2M+Na]^+$, $[M+2H]^{2+}$, $[M+2Na]^{2+}$ as seed ions and $[M-H_2O+H]^+$, $[M+H_2O+H]^+$, $[2M+H_2O+H]^+$, $[2M-H_2O+H]^+$ as common ions during processing. From the raw LC-HR-MS chromatogram observed in DataAnalysis 4.0, the retention time ranging within 7 to 35 minutes and molecular masses ranging within *m/z* 150 to 1800 were considered for generating the bucket list. After bucketing, the software enlisted the molecular ions observed in the LC-HR-MS chromatogram into a column with their respective retention times, adduct ions or parent ions, molecular weights and abundance (relative ion intensity). The bucket list of these molecular ions was exported in the GNPS-mascot

generic format (MGF) files including the excel file type. The GNPS-MGF file was uploaded to the GNPS platform for molecular networking considering minimum matched fragment ions; 6 or 7 and minimum cosine score; 0.7. The network data retrieved from the GNPS platform were analysed and annotated via Cytoscape 3.8.1. Node and edge attributes were used to visualize the connection among different compounds. The isolated known as well as novel compounds were then manually labeled in the network.[56, 59]

3.9 Chemical Analytics

Different tools were used to track and elucidate the chemical structure of isolated compounds such as LC-MS, LC-HR-MS, NMR, IR and X-ray crystallography.

3.9.1 Low-Resolution Mass Spectrometry

After solvent extraction, fungal and bacterial crude extracts were first measured by LC-MS. The fractionated extracts from bacteria by VLC and all the purified samples via HPLC were measured by LC-MS to track down the compounds of interest in the fractions and to check the purity of purified compounds, respectively. Regarding the instrumentation, a 1100 Series HPLC system (Agilent Technologies; a G1312A binary pump, G1329A autosampler, G1315A diode array detector) fitted with Waters In-Line Degasser AF was connected with an ABSCIEX 3200 Q TRAP LC-MS/MS mass spectrometer (AB Sciex, Germany GmbH, Darmstadt, Germany). The experimental samples were prepared in small capped vials with inserts and run with the optimized gradients using LC-MS grade solvents (acetonitrile and water acidified with 0.1% TFA). A Phenomenex Luna 5 µm C18 (2) 250 × 2 mm analytical column was used as a reversed-phase LC column. The measured data were analysed with the software Analyst 1.6.3.

3.9.2 High-Resolution Mass Spectrometry

The extracted crude samples (which were screened via LC-MS), fractions and purified compounds were measured using a LC-ESI-TOF instrument in MS/MS mode. These analyses were conducted to identify the exact molecular masses, formulae and to deduce fragmentation-based tentative structures of the targeted compounds. The instrument used for LC-HR-MS was an Ultimate 3000 HPLC (Thermo Fisher Scientific) system connected with a MaXis-4G mass spectrometer (Bruker Daltonics, Bremen,

Germany). All measured data were analysed with the software Bruker DataAnalysis and used in LC-HR-MS based metabolomics.

3.9.3 Nuclear Magnetic Resonance

The purified compounds were dried employing a freeze-dryer (Christ, Alpha 3-4 LSCbasic) for at least 24 hours before preparing the samples for NMR measurement. At least 475 µL of NMR solvent (d_6-DMSO, d_3-methanol or d_6-acetone) was used to solubilize the dried samples and filled in a 5 mm NMR tube. For instrumentation, all NMR spectra were recorded on a Bruker Avance III HD spectrometer (400, 100 and 40.6 MHz for ^{1}H, ^{13}C and ^{15}N NMR, respectively) using a 5 mm SMART probe head. The measurements were performed at 298 K and the spectra were processed via MestReNova 12.0.4 with calibrated residual solvent signals at $\delta_{H/C}$ 3.31/49.00 for methanol, $\delta_{H/C}$ 2.50/39.52 for DMSO and $\delta_{H/C}$ 2.05/29.84,206.26 for acetone, respectively. Additional spectra were attained on a Bruker Avance III HDX spectrometer (700, 176 and 71 MHz for ^{1}H, ^{13}C and ^{15}N NMR, respectively) using a 5 mm Prodigy TCI CryoProbe head.

3.9.4 Infrared Spectroscopy

The isolated pure compounds, mostly with novel structures were measured by IR spectroscopy to assure the specific functional groups in their chemical scaffolds. To measure the IR spectra, 1 mg of the pure compound was dissolved in 100 µL of HPLC grade methanol and loaded to the sample platform dropwise to generate a thin layer of compound after drying. For the instrumentation, a Jasco FT/IR 4200 spectrometer, interfaced with a MIRacle ATR device (ZnSe crystal) was used.

3.9.5 Crystallization

The isolated pure compounds were dissolved in d_3-acetonitrile or d_6-acetone and stored in an NMR tube with an open lid for a few weeks. The obtained crystal samples were sent to Dr. Dieter Schollmeyer (Institute of Organic Chemistry, Johannes Gutenberg University, Mainz, Germany) for X-ray crystallography.

3.10 Biological Activities

3.10.1 Brine Shrimp Lethality Assay

The brine shrimp lethality assay was conducted to measure the tentative toxicity of the

ethylacetate extracts of *B. dendrobatidis* cultures. At first, brine shrimp eggs were hatched in a conical flask containing salty water (5 g/L NaCl). The larvae were then transferred to 96 well plates in the way of considering 5 to 21 larvae per well. The fungal extract was then added at different concentrations (5, 10, 20, 50, 100, 200, 500, 1000 µg/mL) to the larvae in each well. The number of surviving larvae was monitored by an optical microscope (Olympus) on a daily base for 3 days. One positive control of berberine chloride and a negative control of medium extract were also considered in the brine shrimp lethality assay.[83]

3.10.2 Chitinase Assay

To perform the chitinase assay of bacterial isolates, six chitin agar plates (diameter, 8.5 cm) were prepared by using a slightly modified protocol suggested by Hsu and Lockwood (1975).[84] The chitin agar medium was composed of 4 g/L chitin from shrimp shells (Sigma), 0.5 g/L yeast extract (Bacto), 1 g/L $(NH_4)_2SO_4$, 1.36 g/L KH_2PO_4, 0.3 g/L $MgSO_4.7H_2O$ and 15 g/L agar. During medium preparation, the pH was set to 8.5 by adding 1 M HCl or NaOH solution and autoclaved at 120ºC for 20 minutes. On each plate, 6 different bacterial isolates were inoculated as point spots in an equal distance from each other. In total, all 35 isolates were inoculated. The inoculated plates were then incubated at room temperature for 4 to 7 days and the growth observed on a daily basis.

3.10.3 Anti-chytrid Assay

All isolated compounds were tested for their anti-*B. dendrobatidis* and anti-*B. salamandrivorans* activities. During the procedure, 25 mL spore suspension of each chytrid fungus was prepared in a 50 mL falcon tube by washing the 3 to 5 days old actively grown chytrid agar plates with 2 % sterile tryptone medium. The spore concentration was set up to 5×10^4 by counting the spores with a Neubauer-improved bright line hemacytometer (MARIENFELD) and an optical microscope (Leica ICC50W). For the stock solution, 1 mg of each compound was dissolved in 1 mL of 10 % DMSO solution in a short thread bottle (32 ×11.6 mm). From the stock solution, 400 µL of the solution was transferred to a 1.5 mL Eppendorf tube (CHEMSOLUTE) under sterile conditions and diluted to 1 mL by adding sterile water to gain the concentration of 400 µg/mL. Each compound solution from the Eppendorf tube was serially diluted to a total of twelve dilutions subsequently from 400 µg/mL to 0.19 µg/mL which were

considered as the final test solutions. From each test compound solution, 50 µL was transferred into 96 well plate starting from the diluted to the concentrated solution. Afterwards, 50 µL of spore suspension in 2 % tryptone medium was added to the compound solution in each well. All the tests were set up in triplicates, including one negative control (spores only) and one positive control (spores + cycloheximide). The plates were then incubated at 17ºC for 15 days. On a daily basis, the well plates were then examined by an optical microscope and their optical densities (ODs) were measured with a 96-plate reader (Tecan) at a wavelength of 532 nm.[31, 85, 86]

4. Results

4.1 Genomics and Metabolomics of *B. dendrobatidis* JEL423

The genome sequence of *B. dendrobatidis* JEL423, retrieved from the National Center for Biotechnology Information (NCBI) with the accession number AATT00000000.1, was 23.9 Mb in size and was analysed by antiSMASH fungal version. While the fungal version returned no hits, the bacterial version unveiled the presence of four distinct BGCs coding for secondary metabolites (Figure 11). Among them, regions 7.1 and 19.1 encoded NRPS-like pathways whereas regions 15.1 and 21.1 coded for terpene biosynthetic pathways. However, further analysis of the regions 7.1 and 19.1 showed them to be mono-modular NRPS gene clusters, that are lacking a thioesterase (TE) or a reductive (R) domain to release the final product. Protein blast of the core genes of the regions 15.1 and 21.1 via NCBI revealed a hypothetical protein and a FDP-farnesyl transferase, respectively, which were responsible for terpene biosynthesis. A superficial analysis of other available genomes of the same species, such as *B. dendrobatidis* RTP6 and *B. dendrobatidis* JAM81, also showed similar gene regions.

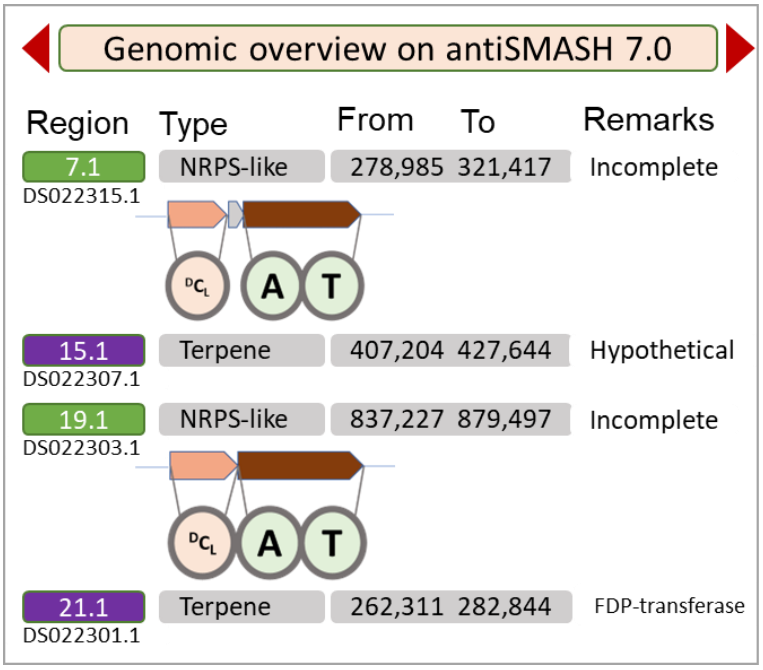

Figure 11: Genome analysis of *B. dendrobatidis* JEL423 by antiSMASH 7.0 showing four recognizable regions of biosynthesis gene clusters.[1]

After the *in-silico* analysis exploring the biosynthetic potential of the fungus, the metabolome was investigated.

Based on LC-HR-MS/MS data of a crude extract, obtained from a 21 days-culture, a molecular network was created using Metaboscape and the GNPS platform (Figure A1). The molecular network with 0.7 minimum pair cosine score, 6 minimum matched fragment ions, and 0.05 ionic mass tolerance showed several clusters consisting of

1,572 nodes (irregularly repeated masses). During the annotation of the network, each node was labelled with a molecular mass (PEPMASS) while the node's size represented the compound's ion intensity in the extracts. In the entire network, the highest sum ion intensity was 6971390 while the lowest was 4108. Each node was designated as a pie diagram comprising the ion intensities present in the *B. dendrobatidis* extract (red) and the medium extract (light blue). Most of the nodes with higher intensities belonged to medium components. A total of 197 irregularly repeated nodes belonged to only the *B. dendrobatidis* extract or both. The GNPS analysis showed the spectral matches of three molecular ions (highlighted in Figure A1) from the *B. dendrobatidis* extract with three different known compounds. They were D-*erythro*-sphingamine (*m/z* 302, Spectrum ID: CCMSLIB00003135250), an amino-fatty acid derivative (*m/z* 477, Spectrum ID: CCMSLIB00000845585) and an indole-acetamide analogue (*m/z* 203, Spectrum ID: CCMSLIB00000851993) with an error of 4.6, 12.2 and 0.9 ppm, respectively. D-*erythro*-sphingamine is considered a structural component in a large class of bioactive natural products.[56, 87]

Further annotation tools such as SIRIUS were not applied to dereplicate the other nodes due to their insignificant ion intensities in the crude extract. Most of these nodes were additionally observed in the medium extract (negative control), with small shifts in retention times when compared to those of the *B. dendrobatidis* extract.

4.2 Brine Shrimp Lethality Assay

The toxicity assay of brine shrimp larvae with *B. dendrobatidis* extract, medium extract and berberine chloride was successfully conducted in *in-vitro* experiment. In the assay, medium extract and berberine chloride were considered as negative and positive controls, respectively. According to Jha et al. (2017) the toxicity strength was categorized into strong (S), moderate (M), weak (W) and inactive (I), indicating the corresponding mortality rate of 80-100%, 50-80%, less than 50% and no death, respectively.[88] In this study, the culture extract of *B. dendrobatidis* and the medium extract showed a similar pattern of weak lethality at the concentration range of 0.02-1 mg/mL, while they were completely inactive below this this range (Table 4). This suggested the presence of either inactive or no secondary metabolites produced by *B. dendrobatidis* under laboratory culture conditions. Berberine chloride as a positive control had a LC_{50} value of 0.01 mg/mL.

Table 4: Results of the brine-shrimp lethality assay showing the mortality rate (%) of *B. dendrobatidis* extract, medium extract and the positive control after 24 hours of incubation.

Test samples → Concentration (µg/mL) ↓	***B. dendrobatidis* extract (dead/total), %**	**1% Tryptone extract (dead/total), %**	**Berberine chloride (dead /total), %**
1000	3/10 = 30 %	4/16 = 25 %	10/10 = 100 %
500	3/12 = 25 %	3/12 = 25 %	11/11 = 100 %
200	2/9 = 22 %	3/13 = 23 %	7/7 = 100 %
100	3/15 = 20 %	4/21 = 19 %	25/25 = 100 %
50	2/15 = 13 %	2/14 = 14 %	10/10 = 100 %
20	2/21 = 9 %	1/12 = 8 %	7/10 = 70 %
10	0/12 = 0 %	0/16 = 0 %	5/10 = 50 %
5	0/10 = 0 %	0/10 = 0 %	2/11 = 18 %

The results were drawn by observing the percentage mortality rates (dead/total) of brine larvae after 24 hours of incubation. Despite of the observed results, an alternative cultivation method or toxicity assay, or both was still needed to assure the production of toxic secondary metabolites by *B. dendrobatidis*.

In summary, the genome analysis and HR-MS-based metabolic profiles of the *B. dendrobatidis* culture unveiled a minor potential to produce secondary metabolites under laboratory conditions. The results of the brine-shrimp lethality assay showed a lack of toxic secondary metabolites (mycotoxins) in the culture extract of *B. dendrobatidis*.

4.3 Bacteria from Salamanders' Skin

In a preliminary study, 35 highly anti-chytrid active skin bacteria were isolated from chytrid-resistant salamanders (Table 5). Four species of *Pseudomonas* were selected for further in-depth studies to explore their secondary metabolites. The extent of bacterial growth in the minimal medium (DMB-glycerol) up to turbidity was considered for the primary selection of these four isolates. The number of ionisable masses (probably novel) and detectable UV absorption (210 to 450 nm), observed in a preliminary LC-MS screening, were considered as additional parameters for the selection of the strains.

Table 5: List of anti-chytrid bacteria, isolated from salamander skin.

S.N.	Isolate ID	Host	Phylum	Family	Genus
1	SFA2.2	*Plethodon cinereus*	Proteobacteria	Enterobacteriaceae	*Hafnia/Serratia*
2	THA2.2	*Plethodon cylindraceus*	Proteobacteria	Xanthomonadaceae	*Stenotrophomonas*
3	THA1.5	*Plethodon cinereus*	Proteobacteria	Enterobacteriaceae	*Hafnia*
4	SFA2.4	*Plethodon cinereus*	Proteobacteria	Sphingomonadaceae	*Novosphingobium*
5	THB1.5	*Plethodon cinereus*	Proteobacteria	Xanthomonadaceae	*Stenotrophomonas*
6	THA3.3	*Plethodon cinereus*	Proteobacteria	Enterobacteriaceae	--
7	SFA1.7	*Plethodon cinereus*	Proteobacteria	Enterobacteriaceae	--
8	THA5.13	*Plethodon cinereus*	Proteobacteria	Pseudomonadaceae	*Pseudomonas*
9	FDR44.12	*Plethodon cinereus*	Proteobacteria	Enterobacteriaceae	--
10	THA6.6	*Plethodon cinereus*	Proteobacteria	Pseudomonadaceae	*Pseudomonas*
11	THC2.2	*Plethodon cinereus*	Proteobacteria	Enterobacteriaceae	*Hafnia*
12	SFA1.6	*Plethodon cinereus*	Proteobacteria	Xanthomonadaceae	*Stenotrophomonas*
13	THB1.4	*Plethodon cinereus*	Proteobacteria	Pseudomonadaceae	*Pseudomonas*
14	LSB7.4	*Plethodon cylindraceus*	Proteobacteria	Xanthomonadaceae	*Stenotrophomonas*
15	RSB5.4	*Plethodon cinereus*	Proteobacteria	Pseudomonadaceae	*Pseudomonas*
16	RSB5.11	*Plethodon cinereus*	Proteobacteria	Pseudomonadaceae	*Pseudomonas*
17	THA14.10	*Plethodon cinereus*	Proteobacteria	Pseudomonadaceae	*Pseudomonas*
18	THC2.9	*Plethodon cinereus*	Actinobacteria	Microbacteriaceae	*Curtobacterium*
19	THC4.4	*Plethodon cinereus*	Proteobacteria	Alcaligenaceae	*Alcaligenes*
20	THA5.7	*Plethodon cinereus*	Proteobacteria	Pseudomonadaceae	*Pseudomonas*
21	NRA54B14	*Plethodon glutinosus*	Proteobacteria	Pseudomonadaceae	*Pseudomonas*
22	THA3.6	*Plethodon cinereus*	Proteobacteria	Pseudomonadaceae	*Pseudomonas*
23	THA1.4	*Plethodon cinereus*	Proteobacteria	Oxalobacteraceae	*Janthinobacterium*
24	THA14.9	*Plethodon cylindraceus*	Bacteroidetes	Sphingobacteriaceae	*Pedobacter*
25	FDR43.B61	*Plethodon glutinosus*	Proteobacteria	Enterobacteriaceae	--
26	FDR45.3	*Plethodon cinereus*	Actinobacteria	Microbacteriaceae	*Microbacterium*
27	RIM160B18	*Plethodon cinereus*	Proteobacteria	Pseudomonadaceae	*Pseudomonas*
28	RSB5.2	*Plethodon cinereus*	Proteobacteria	Pseudomonadaceae	*Pseudomonas*
29	SFA3.14	*Plethodon cinereus*	Bacteroidetes	Sphingobacteriaceae	*Pedobacter*
30	SFB1.B69	*Plethodon cinereus*	Proteobacteria	Oxalobacteraceae	*Duganella*
31	SFB8.6	*Plethodon cinereus*	Proteobacteria	Pseudomonadaceae	*Pseudomonas*
32	THA2.3	*Plethodon cinereus*	Firmicutes	Paenibacillaceae	*Paenibacillus*
33	THA6.5B68	*Plethodon cinereus*	Proteobacteria	Moraxellaceae	*Acinetobacter*
34	THA6.9	*Plethodon cinereus*	Actinobacteria	Microbacteriaceae	*Plantibacter*
35	THB1.1	*Plethodon cinereus*	Bacteroidetes	[Weeksellaceae]	*Chryseobacterium*

The remaining strains were either unable to grow in the preferred minimal medium or showed a reduced potential to produce novel secondary metabolites or remained unexplored due time constraints.

4.4. *Pseudomonas tolaasii* RSB5.11

4.4.1 Metabolomics and Genomics

The whole genome sequence of *P. tolaasii* RSB5.11, analysed by antiSMASH bacterial version 7.0, showed a genome size of 5.4 Mb consisting of 11 different regions of BGCs (Figure 12, Top). The antiSMASH software identified them as one redox-cofactor-, four NRPS-, two lipopolysaccharide-, one siderophore-, one betalactone-

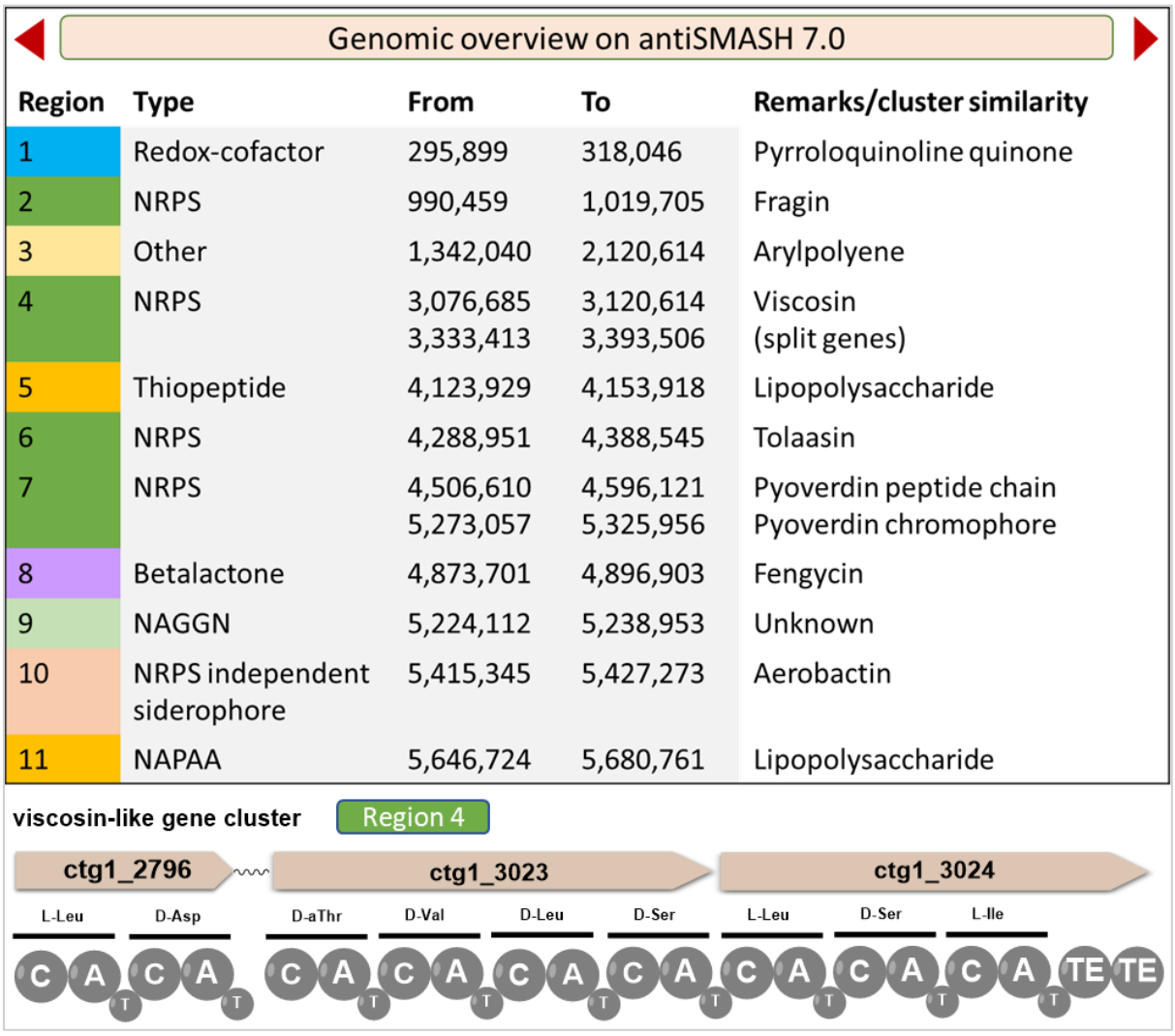

Figure 12: Bioinformatic analysis of the whole genome of *P. tolaasii* RSB5.11 through antiSMASH unveiled 11 regions comprising different biosynthesis pathways (Top) and the module- and domain-architecture of the viscosin-like biosynthetic gene cluster (Bottom).

and one NAGGN-gene clusters. Among the four NRPS gene clusters, two gene clusters were separately carrying 9 and 18 NRPS modules encoding for viscosin-like and tolaasin-like lipopeptides, respectively, both with 100% nucleotide similarity. The remaining NRPS gene clusters were mono-modular and trideca-modular, and could be recognised as fragin and pyoverdine gene clusters, respectively. The siderophore

and redox-cofactor gene clusters were blasted for corresponding nucleotides and were identified as genes responsible for aerobactin and quinone biosynthesis, respectively.

Further investigation of the viscosin-like gene cluster unveiled a split pattern of the gene cluster in two different regions, separated by 251 kbp (Figure 12, Bottom). The first split region was bimodular, and the first module consisted of a $C_{starter}$ domain. The second split region contained two successive genes with tetra-modular and tri-modular systems. The latter hold a tandem TE domain. The antiSMASH software predicted the amino acid sequence of this complete gene cluster as Leu1-Asp2-Thr3-Val4-Leu5-Ser6-Leu7-Ser8-Ile9. Similarly, the tolaasin-like gene cluster appeared with three distinct gene regions, each with a hexa-modular system. In this gene cluster, the first module also consisted of a $C_{starter}$ domain, and the last module consisted of a tandem TE domain. The antiSMASH software predicted the amino acid sequence as Thr1-Pro2-Ser3-Leu4-Val5-Ser6-Leu7-Val8-Val9-Gln10-Leu11-Val12-Thr13-Thr14-Ile15-X16-Dab17-Lys18.

A HR-MS-based molecular network was created from the n-butanol extract of the bacteria, which was fermented for 4 days. The created network employing the GNPS platform with 0.7 minimum cosine score, 6 minimum matched fragment ions, and 0.05 ionic mass tolerance, showed 669 unequally repeated nodes. These nodes represented 75 molecular clusters of different sizes and other self-looped nodes. As predicted, using genome mining, a nonapeptide was allocated in a peptide cluster along with an unexpected dipeptide, labelled with the PEPMASS 1124.70 Da and 429.28 Da, respectively (Figure 13). The HR-MS data verified these compounds as lipopeptides. This observation further supported the predicted biosynthetic pathway for the viscosin-like peptide. Besides, a cluster of tolaasins was observed in the network, which were also showing their spectral matches with the GNPS database.

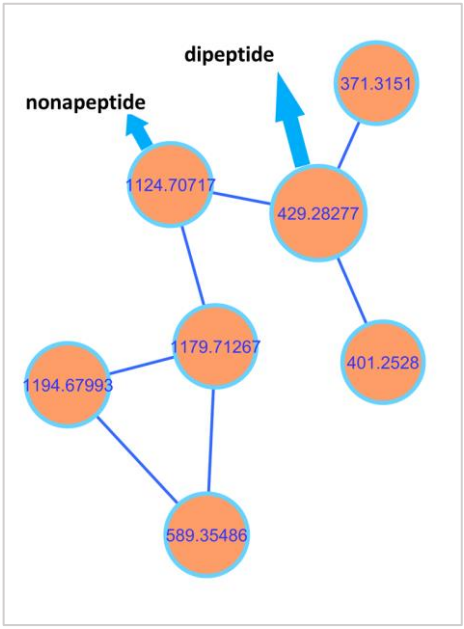

Figure 13: A peptide cluster in the molecular network of *P. tolaasii* extract revealing a nonapeptide clustering with a dipeptide.

4.4.2 Isolation and Structural Identification of a Lipo-dipeptide

The VLC fraction of 40% methanol showed the presence of the lipo-dipeptide upon LC-MS analysis. The compound was then purified using RP-HPLC (Figure 14, Top). A total of 6 mg of the lipo-dipeptide was isolated.

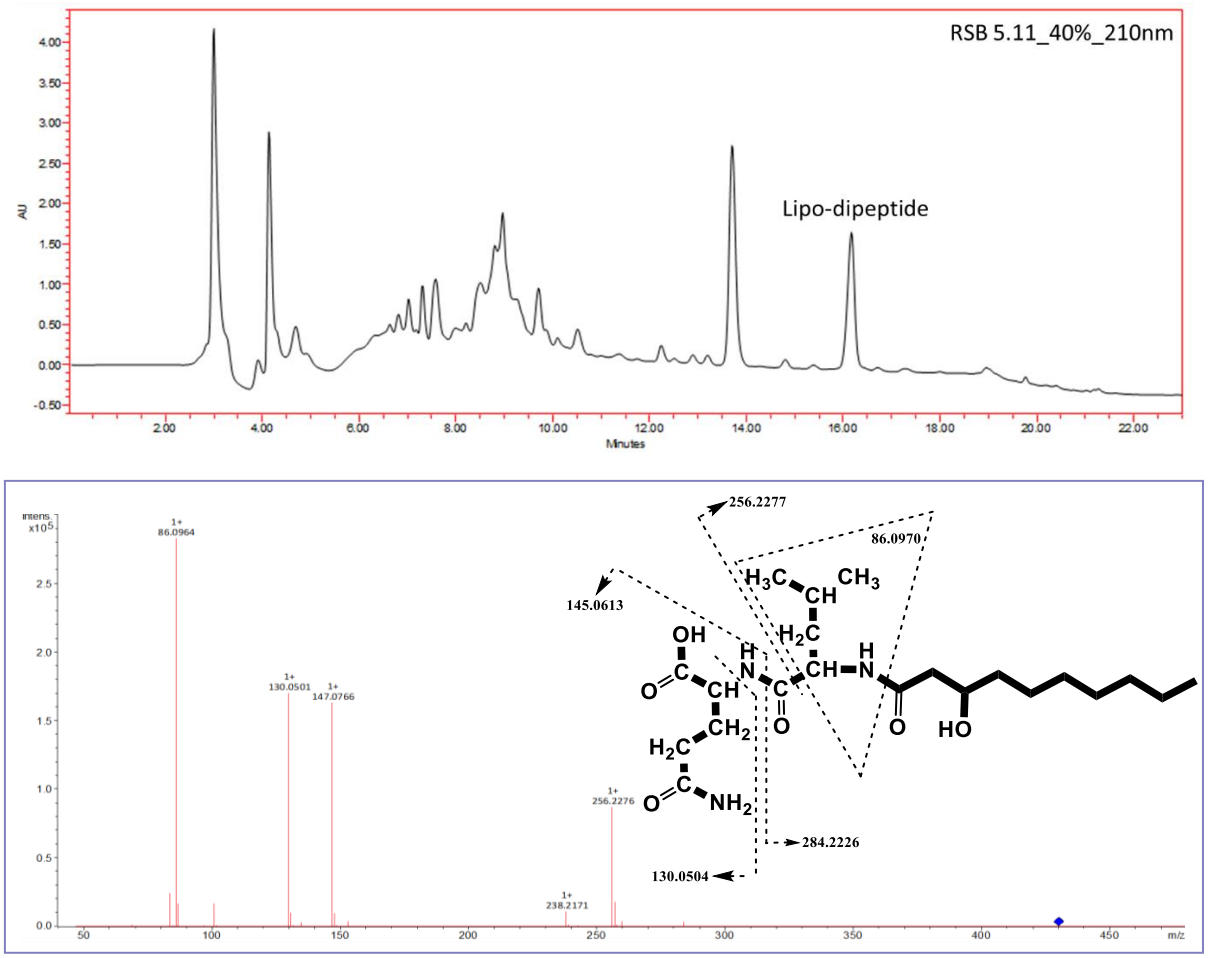

Figure 14: UV-HPLC chromatogram (210 nm) of the 40% VLC fraction (Top) and the MS^2 spectrum of lipo-dipeptide isolated from *P. tolaasii* RSB5.11 showing the structural annotation of fragment ions (Bottom).

The HR-MS results of the sample showed a pseudomolecular ion for the lipo-dipeptide at *m/z* 430.2914 $[M+H]^+$ (MF; $C_{21}H_{39}N_3O_6$), a sodium adduct at *m/z* 452.2736 $[M+Na]^+$ and a potassium adduct at *m/z* 468.2470 $[M+K]^+$. The tandem mass spectrum (MS^2) of the pseudomolecular ion $[M+H]^+$ showed clear fragments of a C-terminal glutamine, leucine and a C_{10} (3-hydroxy) fatty acid chain. The fragment at *m/z* 256.22 represented the a_1 ion, at *m/z* 147.07 referred to the y_1 ion with [+2H] adduct and at *m/z* 130.05 referred to the z_1 ion. Another fragment at *m/z* 86.09 referred to a general fragment ion resulting from leucine moiety (Figure 14, Bottom). In the MS^2 spectrum, the *m/z* values for all the y-type fragments of peptides are indeed after the addition of $2[H]^+$ to the negatively charged original y-fragments. This is because, y-types are the fragments

with negatively charged nitrogen (-CO^+···/···**-NH^-**) at the cleaving site. For the detection of these fragments in the positive ionisation mode of HR-MS, they need to be positively ionised so as by adding 2 protons to each fragment.[89]

During the NMR spectral analysis, the chemical shifts of protons and their directly bonded carbons were listed by analysing the ^{1}H-NMR, ^{13}C-NMR and edited ^{1}H-^{13}C-HSQC spectra (Table 6). This revealed the chemical shifts for two amide (-NH-) protons for leucine and glutamine at 7.88 ppm and 8.14 ppm, respectively. The side chain of leucine and glutamine were elucidated with ^{1}H-^{1}H-TOCSY and ^{1}H-^{13}C-HSQC-TOCSY assisted by ^{1}H-^{1}H-COSY spectra (Figure A2). The lipid chain was also confirmed with the same NMR spectra. The unique chemical shift values of amide protons in the glutamine side chain were observed at 6.76 (s) ppm and 7.24 (s) ppm for *-cis* and *-trans* configurations, respectively. The peptide linkage (-CONH-) between leucine and glutamine was confirmed with ^{1}H-^{13}C-HMBC correlation from $\delta_{NH,\ Glu}$ 8.14 to $\delta_{CO,\ Leu}$ 172.3. The fatty acid linkage with the peptide sequence was confirmed with a HMBC correlation between the -NH-proton (δ_{NH} 7.88) of leucine and the carbonyl carbon (δ_{CO} 170.79) of the lipid chain.[90]

Table 6: NMR table of the isolated lipo-dipeptide showing the chemical shift values (δ in ppm) for ^{1}H, ^{13}C and ^{15}N (d_6-DMSO).

Residue	**Position**	**δ_H, mult. (*J* in Hz)**	**δ_C, type**	**δ_N, type**	**comment**
Leucine	NH	7.88; d (8.3)		123.8; NH	
	α	4.34; dt (6.2, 8.4)	50.55; CH		
	β	1.44; m	40.85; CH_2		
	γ	1.63; m (6.6)	24.01; CH		
	δ	0.85; m	21.59; CH_3		^{1}H overlap
		0.88; m	23.12; CH_3		^{1}H overlap
	C=O		172.3, C		
Glutamine	NH	8.14; d (7.5)		117.4; NH	
	α	4.12; dt (5.5, 8.0)	51.53; CH		
	β	1.94, 1.78; m	26.73; CH_2		
	γ	2.13; m	31.26; CH_2		
	NH_2 (*cis*)	6.76; s		108.5; NH_2	
	(*trans*)	7.24; s		108.5; NH_2	
	COOH		173.18; C		
	$CONH_2$		173.48; C		

3-OH-C_{10}	C=O		170.79; C	
-fatty acid	2’	2.21; m	43.46; CH_2	
	3’	3.77; m	67.49; CH	
	4’	1.34; m	36.86; CH_2	
	5’	1.24; m	25.10; CH_2	
	6’	1.24; m	29.05; CH_2	
	7’	1.24; m	28.71; CH_2	
	8’	1.24; m	31.32; CH_2	
	9’	1.26; m	22.08; CH_2	
	10’	0.87; m	13.95; CH_3	^{1}H overlap
	OH	4.58; d (3.2)		

The FT-IR spectrum of the isolated pure compound showed absorbance at the maximum frequencies of 3287 cm^{-1}(-**OH**, -CO**NH**), 2925 cm^{-1} (**CH**/**CH_2**/**CH_3**) and 1650 cm^{-1} (-**CO**-) (Figure 15). This justified the confirmation of the key functional groups present in the compound. Finally, the verified skeleton of the isolated lipo-peptide was found to have a novel structure with no previous records in the literature.

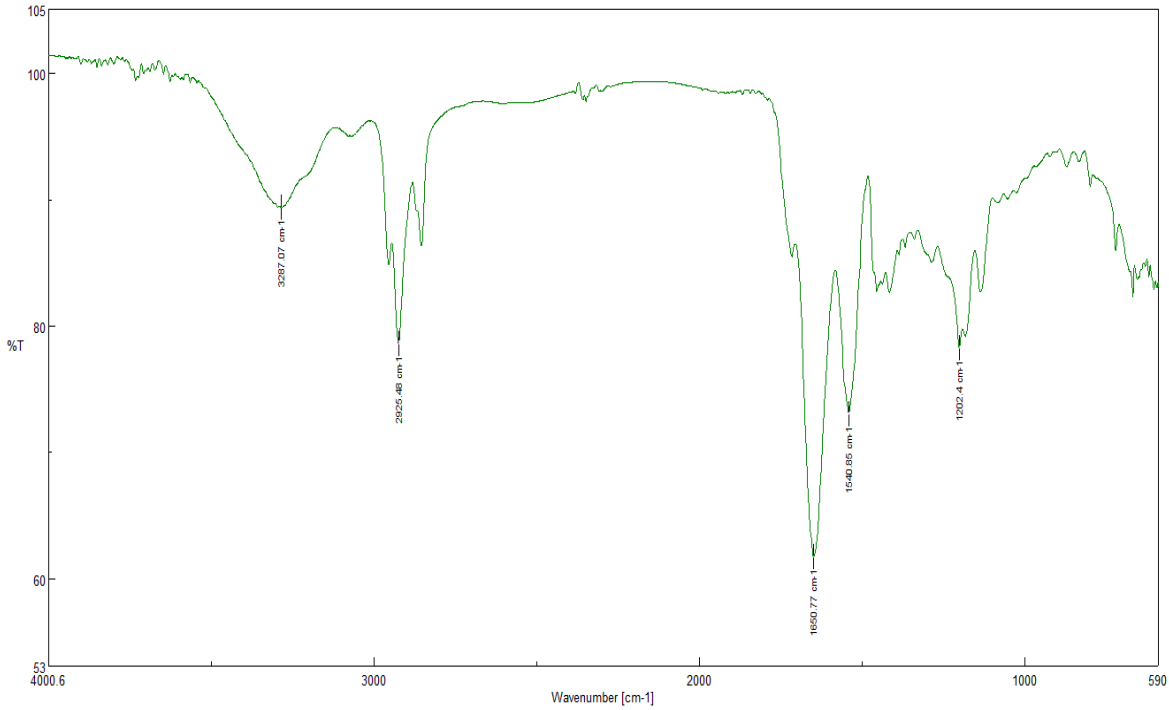

Figure 15: FT-IR spectrum of the lipo-dipeptide isolated from *P. tolaasii* RSB5.11.

The stereochemical investigation of the lipo-dipeptide was carried out by Prof. Michael Lämmerhofer, Pharmaceutical Institute, University of Tuebingen. The obtained results of the study showed L-configurations of both amino acids as L-Leu1 and L-Glu2.

4.4.3 Isolation and Structural Elucidation of a Lipo-nonapeptide

A lipo-nonapeptide was tracked in the VLC fractions based on LC-MS screening of those fractions. The compound was observed in the 100% methanol fraction after VLC. A total amount of 120 mg was isolated and purified by HPLC (Figure A3). The LC-MS chromatogram of the targeted fraction revealed a pseudomolecular ion of the compound at *m/z* 1126 $[M+H]^+$ (Figure 16).

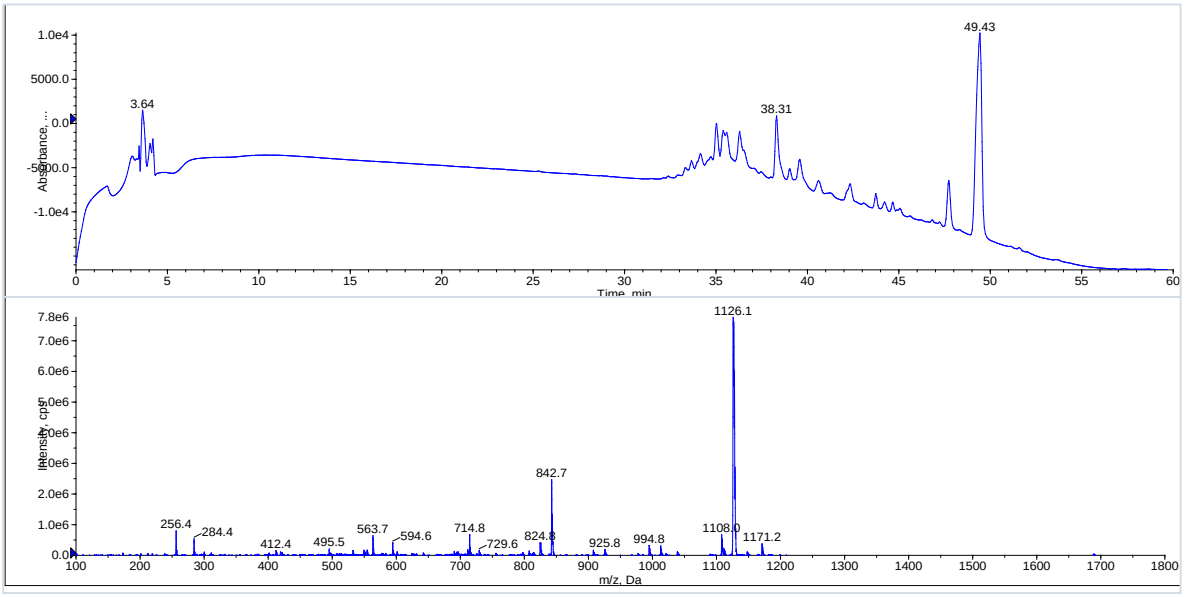

Figure 16: LC-MS chromatogram of 100% methanolic VLC fraction showing DAD spectral data (top) and MS^1 spectra (bottom) of the lipo-nonapeptide.

In the HR-MS results, the compound appeared as a pseudomolecular ion at *m/z* 1125.7129 $[M+H]^+$ (MF; $C_{54}H_{96}N_{10}O_{15}$), a sodium adduct at *m/z* 1147.6947 $[M+Na]^+$ and a potassium adduct at *m/z* 1163.6687 $[M+K]^+$. The MS^2 spectra of the pseudomolecular ion showed clear fragments at *m/z* 284.22 and *m/z* 412.28, which indicated the b_1 and b_2 fragments of the fatty acid moiety including leucine and glutamine, successively. The former b_1 fragment ion included the lipid moiety with leucine while the latter b_2 included an additional glutamine moiety. At the same time, the complementary fragments (fragments on the other side), y_8 and y_7 appeared at *m/z* 842.49 and *m/z* 714.44, respectively. Due to the cyclic skeleton of the remaining amino acids, the further fragmentation was observed with the successive b^0 fragments (water loss) after the annotation of Gln2.[71] Thus, the annotation of the amino acid sequence inside the cyclic ring was assigned as Thr3-Val4-Xle5-Ser6-Xle7-Ser8-Xle9 in the MS^2 spectra (Figure 17).

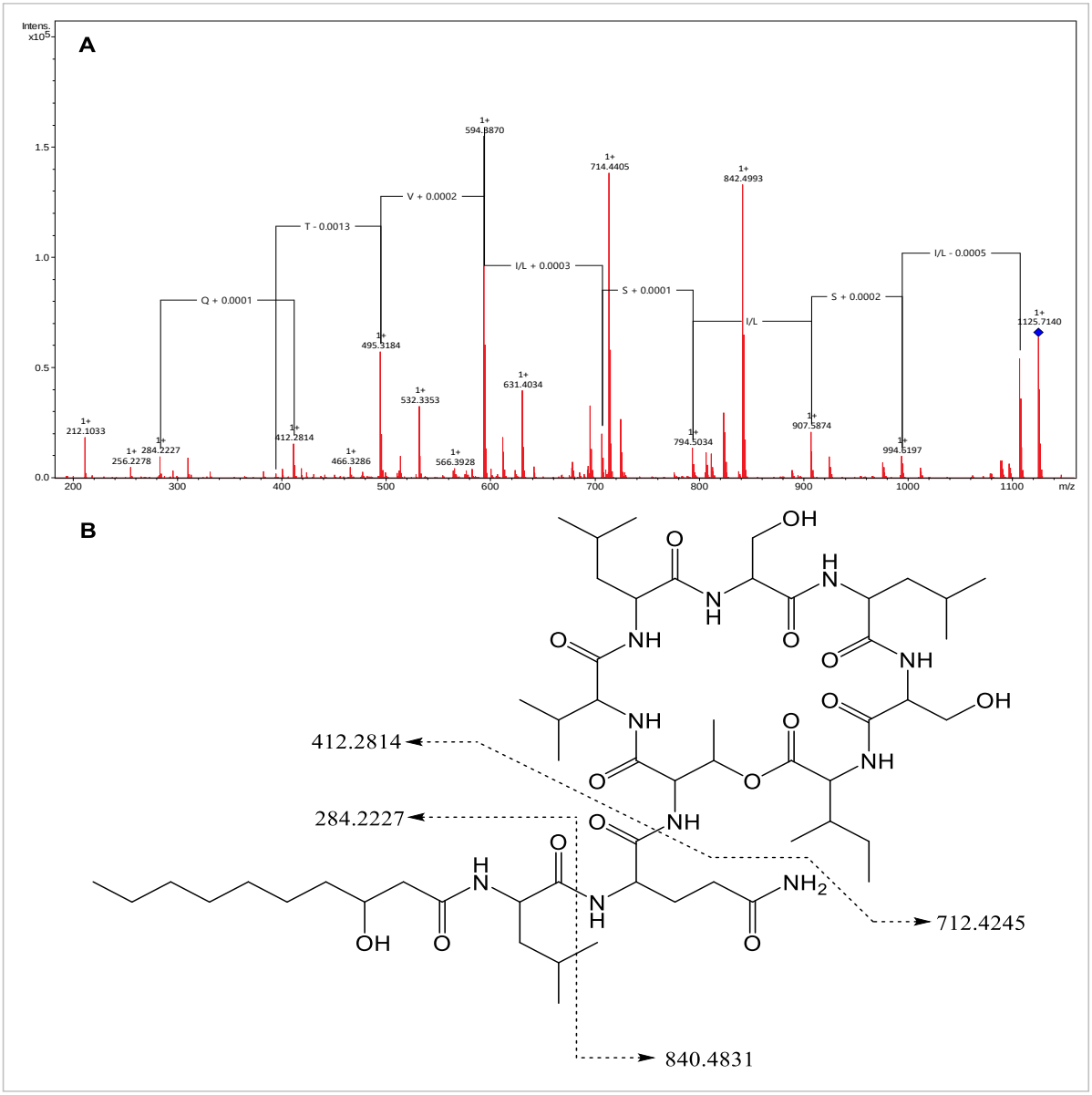

Figure 17: Mass spectrometry of the lipo-nonapeptide isolated from *P. tolaasii* RSB5.11 showing a MS^2 spectrum, [A] and the fragmentation pattern annotated in the chemical structure [B].

In the NMR spectral analysis, the chemical shift values of protons and carbons measured in d_3-acetonitrile were found to be identical to the literature data of pseudodesmin A (Figure A4).[91] However, a complete set of NMR spectra (1D and 2D) measured in d_3-methanol were analysed to further assure the compound structure (Figure A5). Just in a similar way to the lipo-dipeptide, the chemical shifts values of all the protons and their hosting carbons were assigned with ^{1}H-NMR, ^{13}C-NMR and edited ^{1}H-^{13}C-HSQC spectra (Table A1). This revealed the chemical shifts for eleven amide (-NH-) protons (6.8 ppm - 9.3 ppm) and eleven carbonyl (-CO-) carbons (169.8 ppm - 176.9 ppm). The lipidic moiety and the amino acid side chains were elucidated by analysing ^{1}H-^{1}H-TOCSY, ^{1}H-^{13}C-HSQC-TOCSY and ^{1}H-^{1}H-COSY spectra. In the

^{1}H-^{1}H-TOCSY spectrum, the spin systems from nine -NH- protons and nine α-protons to all their subsequent -CH$_n$- protons (α, β, ϒ and δ) were assigned, while in the ^{1}H-^{13}C-HSQC-TOCSY spectrum the same spin systems with all their subsequent -CH$_n$- carbons (α, β, ϒ and δ) were assigned. The ^{1}H-^{1}H-COSY spectrum was employed particularly to find the adjacent -CH$_n$- group from each proton by observing the spin systems between them. The peptide linkages to connect the amino acids were elucidated by using the ^{1}H-^{13}C-HMBC spectrum where the amide (-NH-) proton showed a cross peak (correlation) with the adjacent carbonyl (-CO-) carbon. These peptide bonds were further confirmed by the ^{1}H-^{1}H-NOESY correlations from each amide (-NH-) proton of one amino acid to the nearest α-proton of the adjacent amino acid. In this way, the amino acid sequence was depicted as Leu1-Gln2-Thr3-Val4-Leu5-Ser6-Leu7-Ser8-Ile9. The ester link between the terminal isoleucine residue and threonine was confirmed with the ^{1}H-^{13}C-HMBC correlation from the β-proton (5.46 ppm) of threonine to the carbonyl (-CO-) carbon of isoleucine at 169.8 ppm (Figure 18).

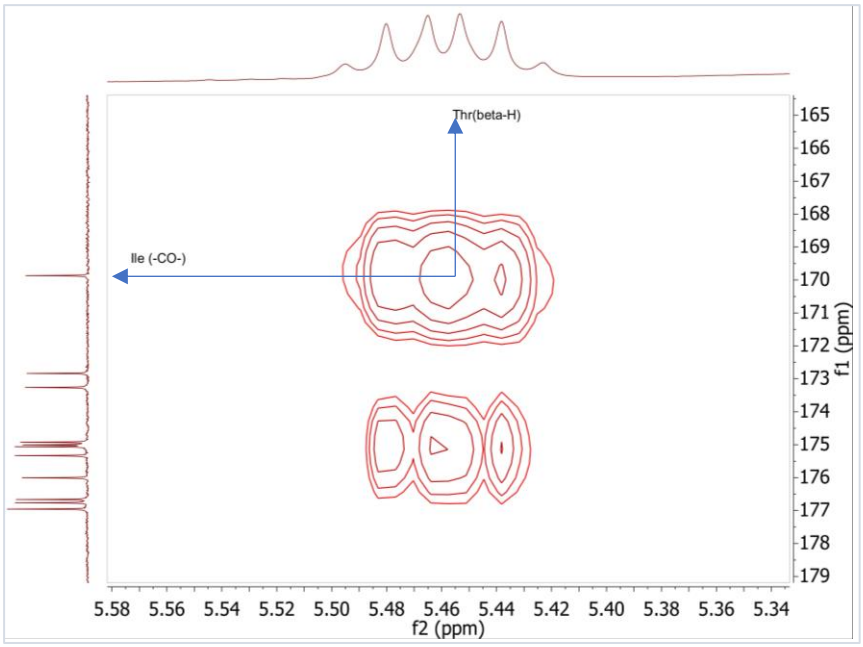

Figure 18: ^{1}H-^{13}C-HMBC correlation showing the cross peak of the ester linkage for the ring cyclization.

However, the structure of pseudodesmin A and viscosinamide A are almost similar, except for the amino acid configuration at the 5th position in the peptide chain. In viscosinamide A, the amino acid at the 5th position is L-leucine while it is D-leucine in the case of pseudodesmin A. In this study, the configuration of leucine was confirmed by comparing its chemical shift values from ^{1}H-NMR and ^{1}H-^{13}C-HSQC-TOCSY spectra, measured in *d*$_3$-acetonitrile, with the literature data (Table 7). In this way, the chemical shift of α-proton of leucine at 5th position was observed at 3.97 ppm. Similarly,

the β-protons were observed at 1.66 ppm and 1.51 ppm. These spectral data were in excellent agreement with the literature data of pseudodesmin A, and not with those of viscosinamide A.[2]

Table 7: Comparison of the NMR data of the isolated compound with pseudodesmin A,and viscosinamide A from literature showing the chemical shifts for Leu5 (bottom).[2]

Isolated compound	**δ ^{1}H**	**δ ^{13}C**	**Pseudodesmin A (literature)**	**δ ^{1}H**	**δ ^{13}C**	**Viscosinamide A (literature)**	**δ ^{1}H**	**δ ^{13}C**
Leu5			**Leu5**			**Leu5**		
NH $^{3}J_{HNH\alpha}$ 3.9 Hz	7.73	-	NH $^{3}J_{HNH\alpha}$ n.d.	7.94	-	NH $^{3}J_{HNH\alpha}$ 6.3 Hz	8.45	-
CHα	3.97	55.68	CHα	3.97	55.68	CHα	3.68	53.81
CO	-	n.d.	CO	-	173.77	CO	-	n.d.
$CH_2\beta1$	1.66	40.63	$CH_2\beta1$	1.67	40.63	$CH_2\beta1$	1.94	37.35
$CH_2\beta1$	1.51	40.63	$CH_2\beta1$	1.51	40.63	$CH_2\beta1$	1.73	37.35
CHϒ	1.75	25.48	CHϒ	1.77	25.49	CHϒ	1.61	25.50
$CH_3\delta1$	0.88	21.29	$CH_3\delta1$	0.88	21.29	$CH_3\delta1$	0.83	23.92
$CH_3\delta2$	0.86	23.48	$CH_3\delta1$	0.86	23.33	$CH_3\delta1$	0.86	21.28

In this way, the configuration of leucine at the 5th position was determined as D-configuration. Hence, the isolated compound was confirmed as pseudodesmin A.

4.4.4 X-Ray Crystallography

Colourless blocks of crystals were obtained from a long-standing solution of the isolated nonapeptide in *d_3*-acetonitrile. The experimental results of x-ray crystallography were obtained from Dr. Dieter Schollmeyer, Institute of Organic Chemistry, Johannes Gutenberg University Mainz, Germany. The crystallography data showed an orthorhombic crystal structure of the compound in a monohydrated form,

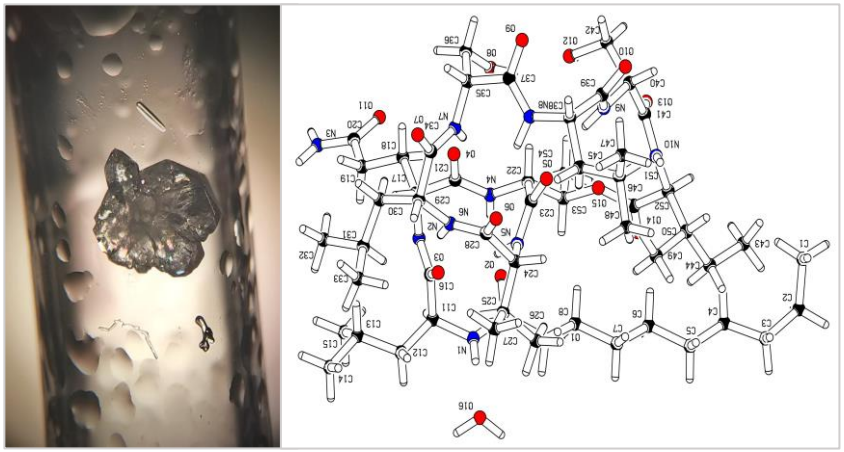

Figure 19: Image of the crystal under an optical microscope (left) and graphical representation of crystal structure of the isolated compound (right).

$C_{54}H_{96}N_{10}O_{15}.H_2O$ (Figure 19). The structure showed an amino acid sequence of the peptide chain along with absolute configurations as C_{10}(3-OH)-L-Leu1-D-Gln2-D-*allo*-Thr3-D-Val4-D-Leu5-D-Ser6-L-Leu7-D-Ser8-L-Ile9. The amino acid sequence, their absolute configurations and the lipidic moiety were in agreement with the structure of pseudodesmin A.

4.4.5 Characterization of Lipo-dipeptides Produced by Other Homologous Gene Clusters

The homologous gene cluster analysis of other viscosin-class producers (*Pseudomonas* sp. COR52, *Pseudomonas* sp. A2W4.9, *Pseudomonas* sp. U2W1.5 and *Pseudomonas* sp. SS101) also showed a similar or the same lipo-dipeptide upon the preliminary screening under LC-MS. They were further verified with LC-HR-MS spectral annotation.

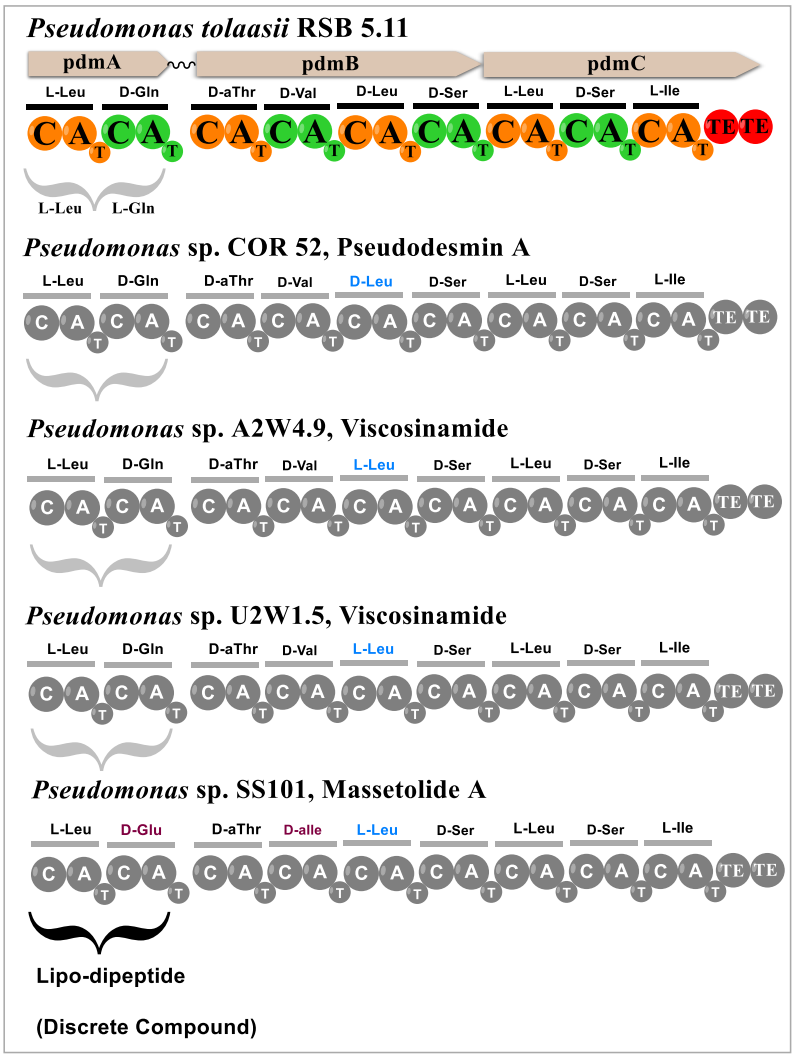

Figure 20: Module scheme for the pseudodesmin A biosynthetic gene cluster from *P. tolaasii* RSB5.11 and other homologous gene clusters from other viscosin-like producers.

Genome mining of *P. tolaasii* along with other viscosin-class producers such as *Pseudomonas* sp. SS101 (massetolide producer), *Pseudomonas* sp. A2W4.9 (viscosinamide producer), *Pseudomonas* sp. UZW1.5 (viscosinamide producer) and *Pseudomonas* sp. COR52 (pseudodesmin producer) revealed the fact that there remained a first separated gene of the viscosin-like BGC, that could be responsible for independently producing the corresponding lipo-

dipeptide (Figure 20).

The HR-MS analysis of the culture extracts from all these strains except *Pseudomonas* sp. SS101 showed the presence of the characteristic lipo-dipeptide pseudomolecular ion at *m/z* 430.2914 $[M+H]^+$ (MF; $C_{21}H_{39}N_3O_6$) along with a corresponding sodium adduct. The HR-MS data from *Pseudomonas* sp. SS101 showed a pseudomolecular ion of a different lipo-dipeptide at *m/z* 431.2761 $[M+H]^+$ (MF; $C_{21}H_{38}N_2O_7$) along with a corresponding sodium adduct at *m/z* 453.2574 $[M+Na]^+$ and a potassium adduct at *m/z* 469.2244 $[M+K]^+$. The MS^2 spectra of these pseudomolecular ions produced by all these strains showed a clear fragmentation pattern, typical to the expected lipo-dipeptide. The annotated fragmentation pattern in the MS^2 spectra confirmed that all the strains except *Pseudomonas* sp. SS101 produced the same lipo-dipeptide as produced by *P. tolaasii* RSB5.11. *Pseudomonas* sp. SS101 produced another novel lipo-dipeptide differing by glutamic acid instead of glutamine at the terminal position (Figure 21). This was because *Pseudomonas* sp. SS101 is the massetolide producer which comprises glutamic acid at the second position of the peptide sequence while the other strains produce 9AA-lipopeptides, that contain glutamine at the same position.[2, 92]

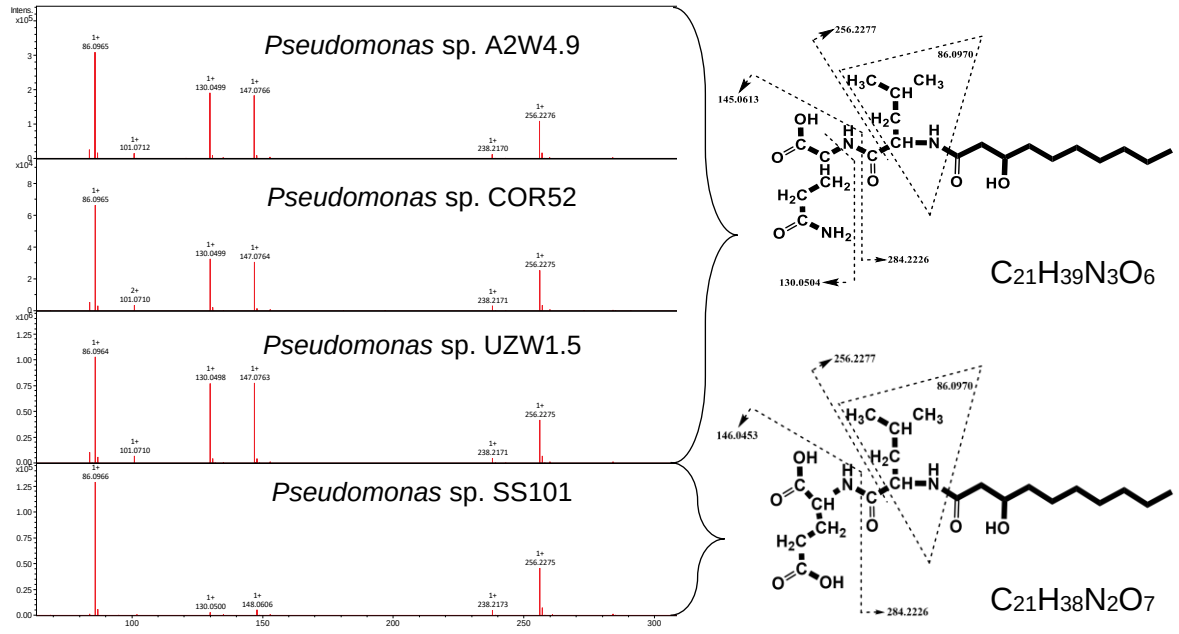

Figure 21: MS^2 spectra of the novel lipo-dipeptides produced by different *Pseudomonas* strains.

4.5 *Pseudomonas* sp. THA6.6

4.5.1 Metabolomics and Genomics

The whole genome sequence of *Pseudomonas* sp. THA6.6 analysed by antiSMASH bacterial version 7.0 and showed a genome of 6.3 Mb, comprising 8 different BGCs (Figure 22, Top). The antiSMASH software identified them as two NRPSs, one redox-

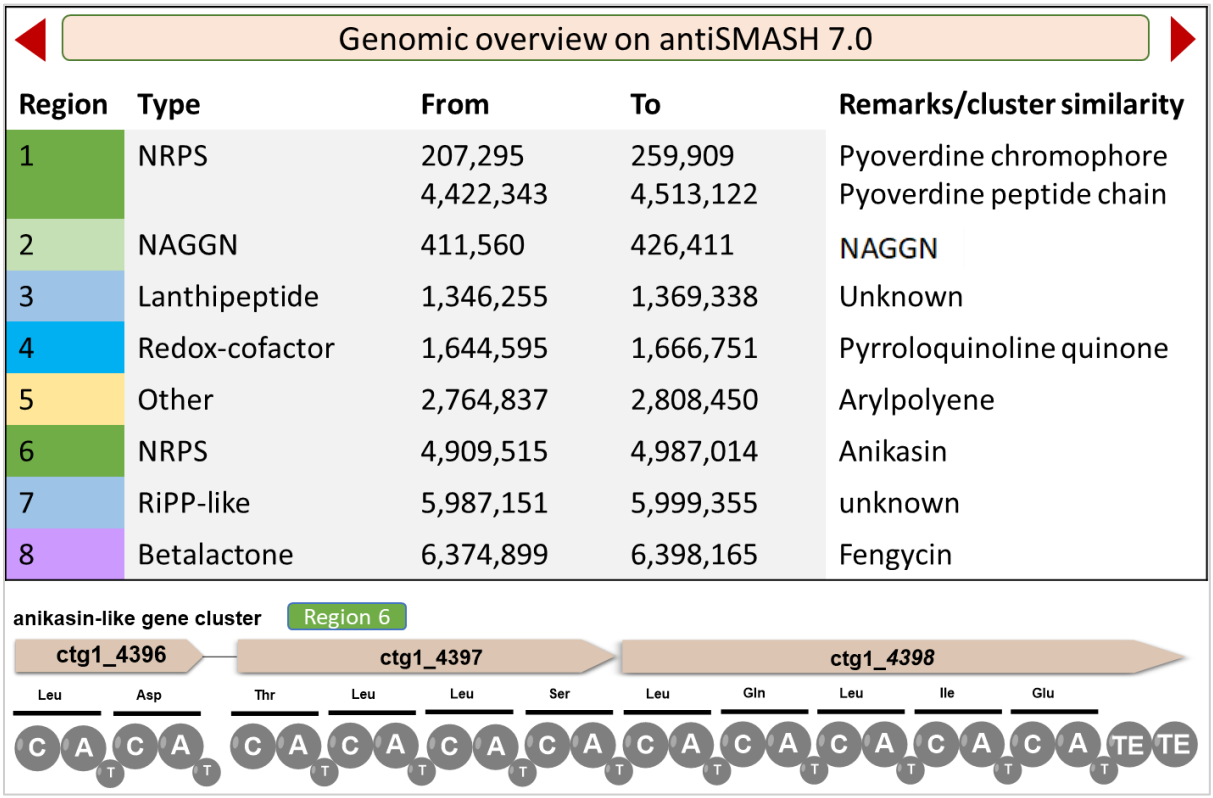

Figure 22: Bioinformatic analysis of the genome of *Pseudomonas* sp. THA6.6 through antiSMASH which unveiled 8 regions comprising different biosynthesis pathways (Top) and module- and domain-achritecture of the anikasin-like biosynthetic gene cluster (Bottom).

cofactor, one betalactone, one NAGGN and two RiPP-like gene clusters. One of the NRPS gene clusters was carrying a 11 NRPS modules encoding an anikasin-like compound with 100% nucleotide similarity. The encoded compound resembled a lipopeptide belonging to the amphisin class. The other NRPS gene cluster was split into two regions with tri-modular and hepta-modular patterns, encoding a pyoverdine-like compound. The RiPP-like gene cluster appeared without any metabolomic hits in the antiSMASH software.

The anikasin-like gene cluster consisted of three core genes: ctg1_4396, ctg1_4397 and ctg1_4398. They were comprised of two, four and five successive NRPS modules (Figure 22, Bottom). The first module of the first gene coded for leucine and comprised a $C_{starter}$ domain. This domain could initiate the assembly of the peptide chain by linking

the first amino acid (Leu1) to the carbonyl motif of a fatty acid. The second NRPS module of the first gene catalyses the fusion of an aspartic acid (Asp2). The four modules of the second gene successively encoded the sequence Thr3-Leu4-Leu5-Ser6. The third gene contained five NRPS modules, that sequentially encoded Leu7-Gln8-Leu9-Ile10-Glu11 and comprised a tandem TE domain. The amino acids sequence in the peptide chain was further clarified by HR-MS-based annotation.

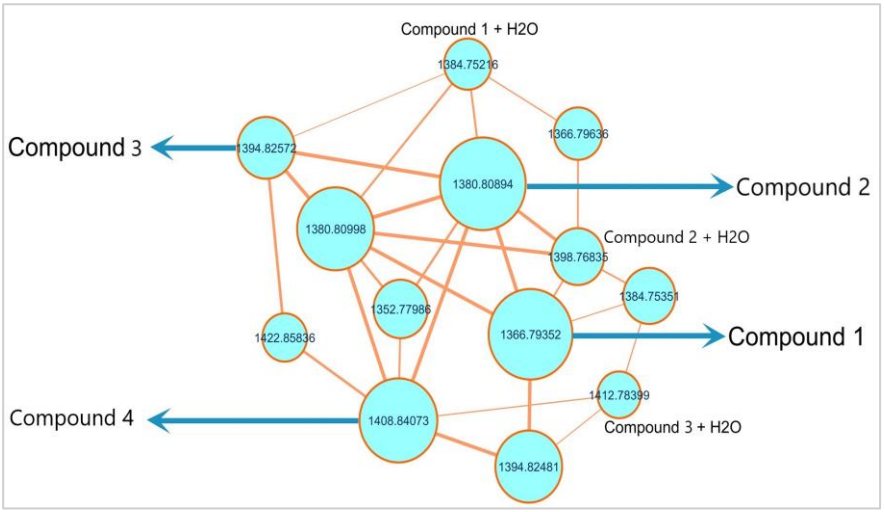

Figure 23: An amphisin cluster in the molecular network of the *Pseudomonas* sp. THA6.6 extract revealing compounds **1**, **2**, **3** and **4**.

A HR-MS-based molecular network was created from the n-butanol extract of the bacterium, which was fermented for 4 days in a DMB-glycerol medium. The created network, employing GNPS with 0.7 minimum cosine score, revealed 874 inconsistently repeated nodes. As predicted, using genome mining, an amphisin cluster was observed in the network. The cluster was annotated with the four major compounds which were isolated using HPLC system (Figure 23). The water adducts or the hydrolysed forms (M+18) of these compounds also appeared in the cluster and represent most likely the ring-opened-versions of the targeted lipopeptide. The label in each node represented PEPMASS (molecular mass) of the corresponding compound. The target compounds were labelled with the corresponding PEPMASS as 1366.7935 (**1**), 1380.8089 (**2**), 1394.8257 (**3**) and 1408.8407 (**4**). Based on HR-MS/MS spectral analysis, these compounds were differing by 14 Dalton (methylene, -CH_2- units) either on the fatty acyl chain or at the side chain of 10th amino acid. The size of the node and the width of the edge in the network indicated the molecular ion intensity and cosine score in between the bridged compounds, respectively.

4.5.2 Isolation and Structural Identification of New Lipopeptides of the Amphisin Family

The LC-MS profiling of the crude extract, from a fermented culture for 4 days, showed the presence of compounds **1**, **2**, **3** and **4** in different amounts. While cultivating in a

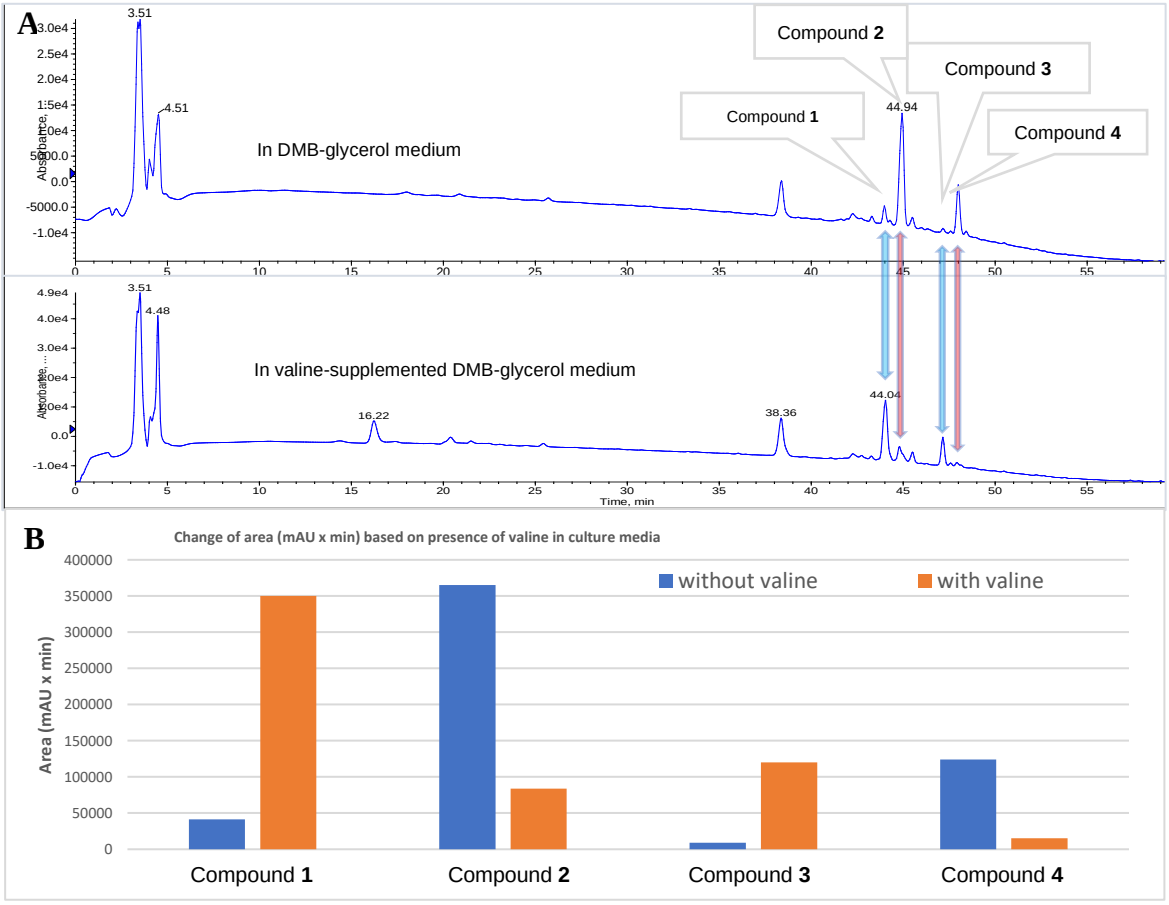

Figure 24: [A] Total wavelength chromatogram of LC-MS runs comparing the production yield of compounds in DMB-glycerol medium (top) and valine-supplemented medium (bottom). [B] Bar diagram showing the average area under the UV peak of each compound.

normal DMB-glycerol medium, compound **2** and compound **4** were produced abundantly while compounds **1** and **3** represented minor compounds. However, the yield pattern of the compounds was reversed after the cultivation in a valine-supplemented DMB-glycerol medium (Figure 24A). This phenomenon was observed by measuring the area underneath the compound peaks in LC chromatograms of both culture extracts (Figure 24B). This observation provided a hint of valine incorporation in the structures of compounds **1** and **3**. All the compounds were further detected in the 70% methanol fraction after VLC while profiling upon LC-MS analysis. Via RP-HPLC purification, all four compounds were successively isolated in pure forms with

the yield of 33.8 mg (**1**), 50.0 mg (**2**), 13.8 mg (**3**) and 15.0 mg (**4**). The structures of these compounds were elucidated with HR-MS and NMR spectroscopy.

The HR-MS data showed a pseudomolecular ion of compound **1** at *m/z* 1367.8021 $[M+H]^+$ (MF; $C_{64}H_{110}N_{12}O_{20}$), of compound **2** at *m/z* 1381.8165 $[M+H]^+$ (MF; $C_{65}H_{112}N_{12}O_{20}$), of compound **3** at *m/z* 1395.8344 $[M+H]^+$ (MF; $C_{66}H_{114}N_{12}O_{20}$) and of compound **4** at *m/z* 1409.8501 $[M+H]^+$ (MF; $C_{67}H_{116}N_{12}O_{20}$) along with their corresponding sodium adducts at *m/z* 1389.7843 $[M+Na]^+$, *m/z* 1403.7981 $[M+Na]^+$, *m/z* 1417.8154 $[M+Na]^+$ and *m/z* 1431.8324 $[M+Na]^+$, respectively (Table 8).

Table 8: Chemical features and yields of the isolated compounds.

Compounds	**Precursor mass (*m/z*)**	**Molecular formula**	**Yield (mg)**	***m/z* error**
Compound **1**	1367.8021	$C_{64}H_{110}N_{12}O_{20}$	33.8	0.9
Compound **2**	1381.8165	$C_{65}H_{113}N_{12}O_{20}$	50.0	1.8
Compound **3**	1395.8344	$C_{66}H_{114}N_{12}O_{20}$	13.8	0.7
Compound **4**	1409.8501	$C_{67}H_{116}N_{12}O_{20}$	15.0	0.1

In the annotation of MS^2 spectra, compound **1** and **2** revealed the a_1 and b_1 fragments at *m/z* 228.1963 and *m/z* 256.1909, respectively. This indicated a hydroxylated C_8 fatty acyl moiety extended with leucine, the first amino acid of the peptide chain. Nonetheless, compound **3** and **4** exerted a_1 and b_1 fragments at *m/z* 256.2276 and *m/z* 284.2226 respectively, indicating a hydroxylated C_{10} fatty acyl chain fused to a leucine residue. Additionally, compound **1** and **2** showed b_2 fragments at *m/z* 371.2179 whereas compound **3** and **4** showed b_2 fragments at *m/z* 399.2495. This indicated aspartic acid as the second amino acid in all four peptides. The fatty acyl part along with leucine and aspartic acid were exocyclic to the compound structure. The remaining sequence of nine amino acids was structurally involved in the cyclic ring, which was completely annotated with the MS^2 spectra of the hydrolysed forms of the compounds. After basic hydrolysis, the ring opening of the cyclic peptides through the ester link was observed with an increase of 18 Da (water, H^+ and OH^-) in the corresponding hydrolysed pseudomolecular ions. The hydrolysis was successfully applied only for compounds **1**, **2** and **4** (Figure 25). Compound **3** could not be hydrolysed and hence its hydrolysed pseudomolecular ion was not observed in the HR-MS spectrum.

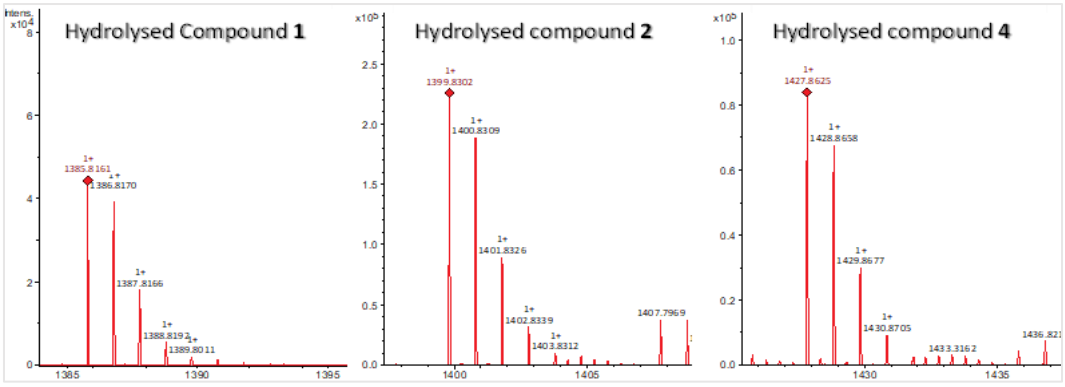

Figure 25: HR-MS spectra showing *m/z* values for the hydrolysed compounds.

With the MS^2 spectra, the alignment of amino acids in all four compounds was annotated as Leu1-Asp2-Thr3-Leu4-Leu5-Ser6-Leu7-Gln8-Leu9-Ile10 (**2** and **4**) or -Val10 (**1** and **3**)-Glu11 (Figure 26 to 29). During annotation, all b- and y- type fragments from b_1 to b_{10} and y_1 to y_{10} could be assigned, except fragment y_1 for **1**, y_9 for **2** and y_1/y_8 for **4**. Regarding compound **3**, the annotation of the amino acid sequence was annotated in the MS^2 spectrum of the intact compound, where successive b^0 fragments (water loss) were observed after the annotation of Thr3 (Figure 28).

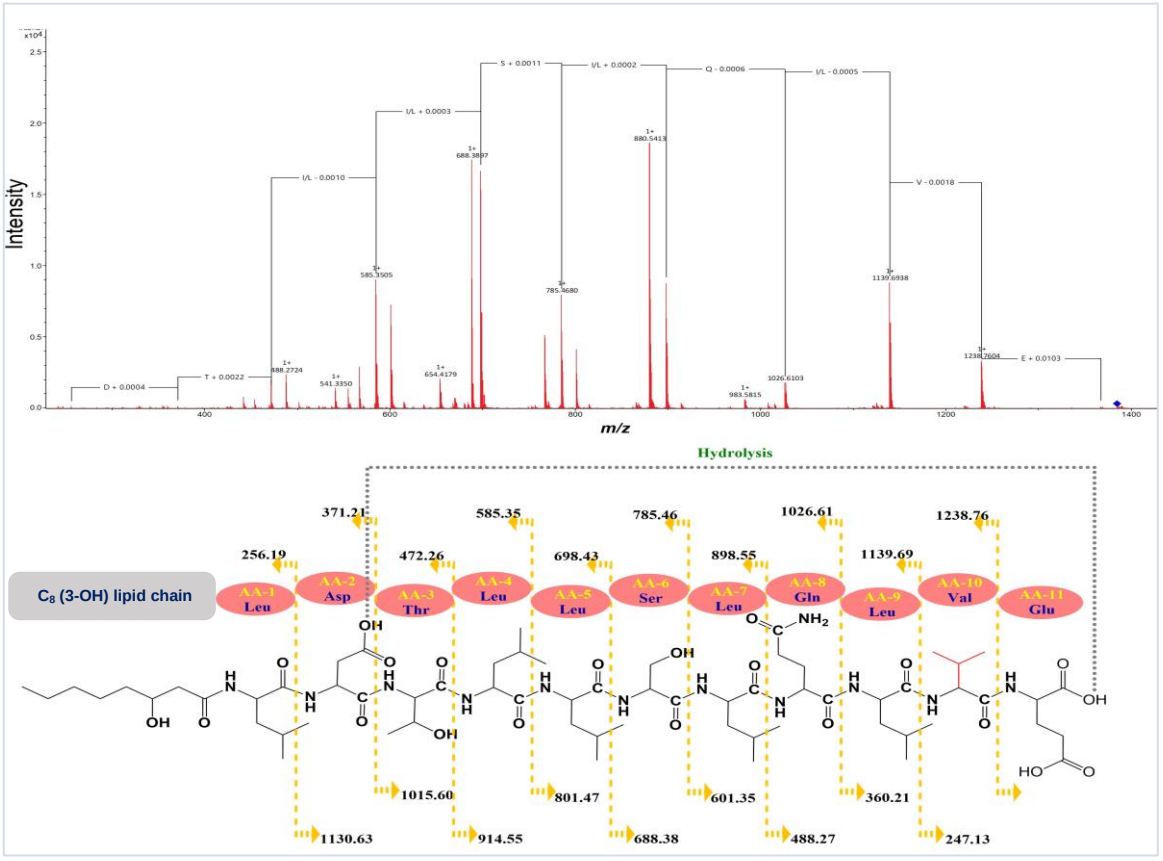

Figure 26: Annotation of the fragments of compound **1** in the MS^2 spectrum of its hydrolysed pseudomolecular ion.

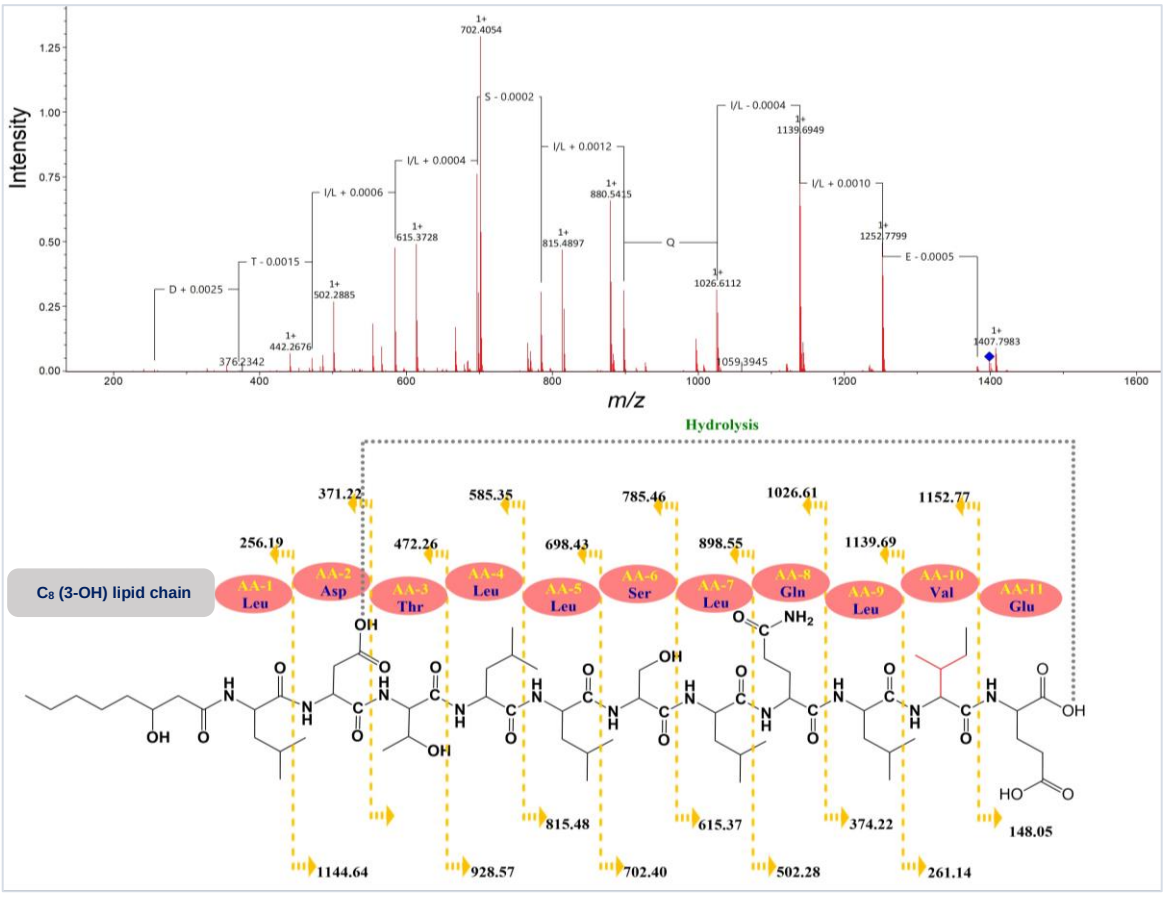

Figure 27: Annotation of the fragments of compound **2** in the MS^2 spectrum of its hydrolysed pseudomolecular ion.

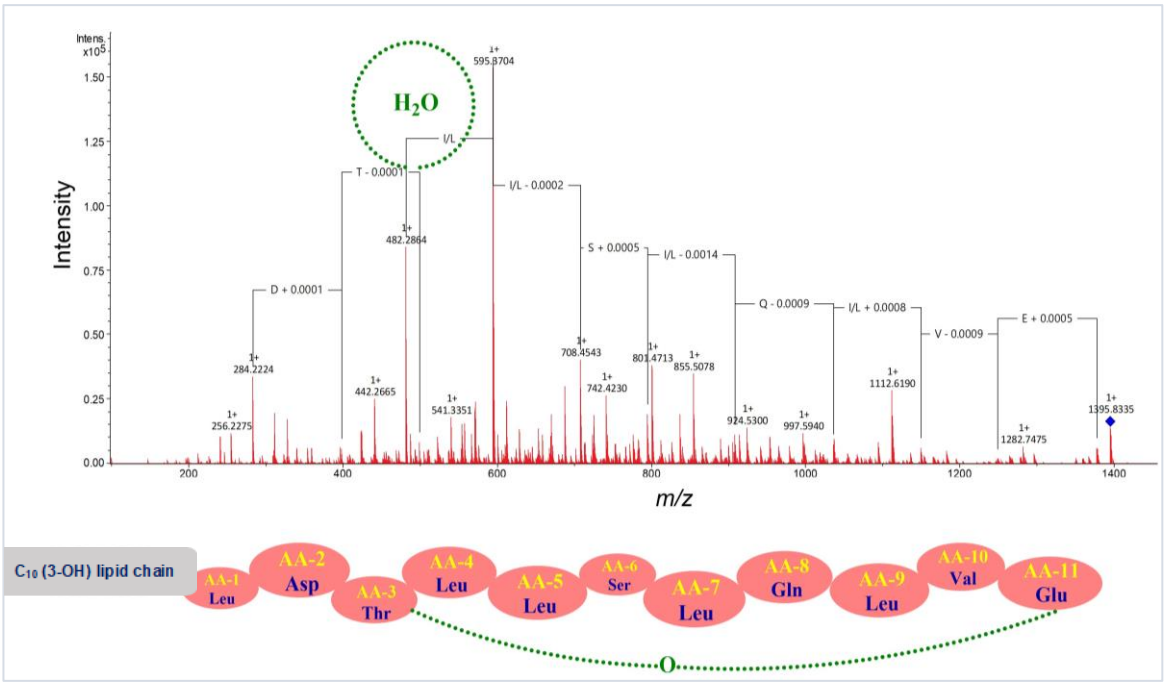

Figure 28: Annotation of the fragments of compound **3** in the MS^2 spectrum of its intact pseudomolecular ion.

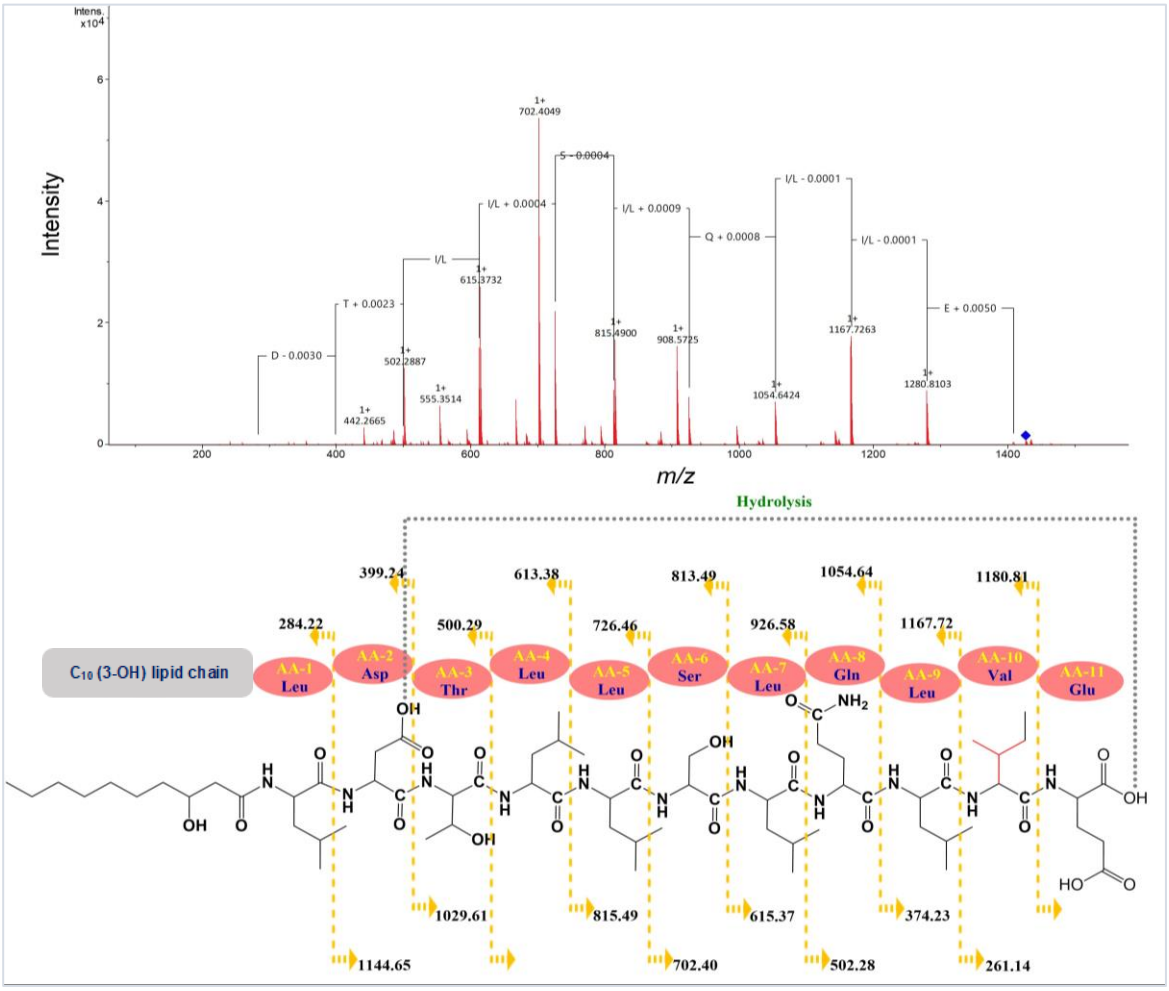

Figure 29: Annotation of the fragments of compound **4** in the MS^2 spectrum of its hydrolysed pseudomolecular ion.

During NMR spectral analysis, the structures of all the compounds except compound **4** were analysed from 1D and 2D NMR spectra measured in d_3-methanol. Due to solubility issues, the NMR spectra of **4** were measured in d_6-acetone. The chemical shift values of protons and their adjacent carbons were assigned and listed using ^{1}H-NMR, ^{13}C-NMR and edited ^{1}H-^{13}C-HSQC spectra. This revealed the chemical shifts for thirteen amide (-NH-) protons (6.8 ppm – 8.5 ppm) and fifteen carbonyl (-CO-) carbons (170 ppm - 178 ppm) in all four compounds. The fatty acyl moiety and amino acid side chain were elucidated by the interpretation of ^{1}H-^{1}H-TOCSY, ^{1}H-^{13}C-HSQC-TOCSY and ^{1}H-^{1}H-COSY spectra. In the ^{1}H-^{1}H-TOCSY spectrum, the spin systems from eleven -NH- protons and eleven α-protons to all their subsequent -CH_n- protons (α, β, ϒ and δ) were assigned while in ^{1}H-^{13}C-HSQC-TOCSY, the same spin systems with all their subsequent -CH_n- carbons (α, β, ϒ and δ) were assigned. ^{1}H-^{1}H-COSY cross

peaks were used particularly to assign the adjacent -CH_n- group from each proton by observing the spin systems between them.

The peptide bonds between two adjacent amino acids were assigned with the help of ^{1}H-^{13}C-HMBC spectrum where each amide (-NH-) proton showed cross peaks with the adjacent carbonyl (-CO-) carbon. These linkages were further confirmed by assigning ^{1}H-^{1}H-NOESY correlations from amide (-NH-) proton of one amino acid to the nearest α-proton of the adjacent amino acid (Figure 30 and 31). The ester link for ring cyclization between the terminal glutamic acid and threonine residue was confirmed by assigning the ^{1}H-^{13}C-HMBC correlations from the β-proton of threonine (5.4 ppm) to the α-carbonyl (-CO-) carbon (170.6 ppm) of the terminal glutamic acid (Figure A6 to A11). The presence of one glutamine was further confirmed with the assignment of characteristic two chemical shift values of the side-chain amide protons (-NH_2-). Which were observed at $\delta_{H/N}$ 6.8$_{(s)}$ ppm and $\delta_{H/N}$ 7.5$_{(s)}$ ppm as *cis*- and *trans*- configurations, respectively.

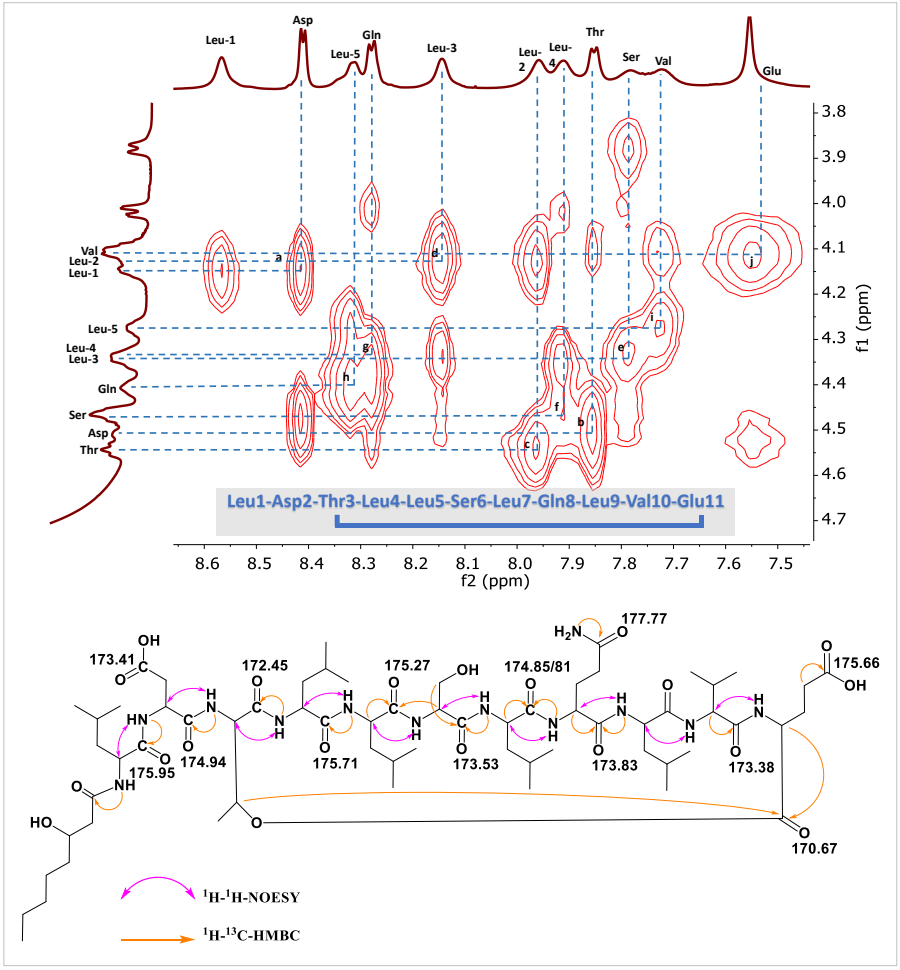

Figure 30: Annotation of spin system in ^{1}H-^{1}H-NOESY spectra of compound **1** and it's structural overview along with key ^{1}H-^{13}C-HMBC correlations.

During the spectral inspection of each individual compound, compound **1** and

compound **3** were assigned with the same set of amino acids along with the same sequence. There was a valine in both compounds at the 10th position of the peptide chain, where the amide proton of the 10th amino acid showed a spin system with α, β and two unequal Ɣ-protons in the ^{1}H-^{1}H-TOCSY spectrum and with the corresponding carbons in ^{1}H-^{13}C-HSQC-TOCSY spectrum. This justified the presence of valine at the 10th position of the peptide chain, which was for the first time observed in the amphisin class.

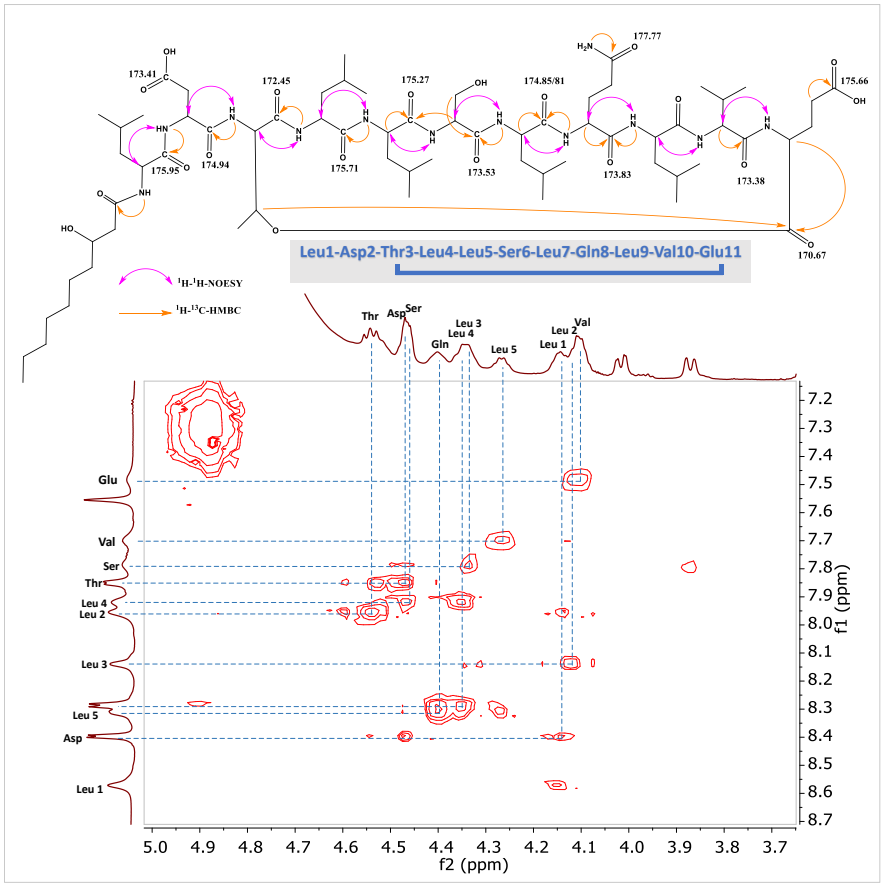

Figure 31: Annotation of spin systems in the ^{1}H-^{1}H-NOESY spectrum of compound **3** and its structural overview along with key ^{1}H-^{13}C-HMBC correlations.

In total, the structural motifs of five leucine, one aspartic acid, one threonine, one serine, one glutamine, one valine and one glutamic acid were assigned in both of these compounds. While analysing the lipidic moiety, some spectral overlapping was observed in the chemical shifts values of methylene (-CH_2-) groups. This hindered the clear elucidation of fatty acyl chain length by NMR, however HR-MS data could readily confirm the chain size. In a combined analysis of NMR spectra and HR-MS data, the lipidic chain was found to be 8 and 10 carbons in length for **1** and **3**, respectively. In both compounds, there was a hydroxyl (-OH) group at the 3rd position of the lipid chain, which was confirmed with chemical shift values of adjacent carbons (-CH(OH)-) at 70.1 ppm and 2D spectral correlations. All assigned NMR data of compound **1** and compound **3** were summarized in Table 9 and Table 10, respectively.

Table 9: Chemical shifts for protons and carbons of **1** along with diagrammatic representation of ^{1}H-^{13}C-HSQC-TOCSY correlations (bold) and key ^{1}H-^{13}C-HMBC (red) correlations.

Amino acid	Site	δ ^{1}H [ppm]	δ ^{13}C [ppm]	HSQC- TOCSY and key HMBC correlation
Leu^{1}	α	4.15	55.58	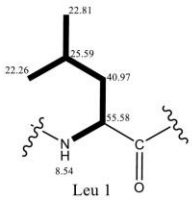
	β	1.63	40.97	
	β	1.74		
	ϒ	1.74	25.59	
	δ	0.95	22.81	
	δ′	0.95	22.26	
	NH	8.54		
	C=O		overlap	
Asp^{2}	α	4.50	53.53	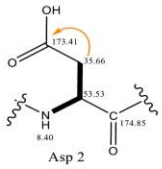
	β	2.84	35.66	
	β′	2.75		
	NH	8.40		
	C=O		174.85	
	C=O		173.41	
Thr^{3}	α	4.54	59.97	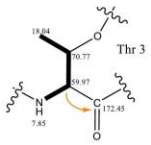
	β	5.44	70.77	
	ϒ	1.31	18.04	
	NH		7.85	
	C=O		172.45	
Leu^{4}	α	4.13	55.18	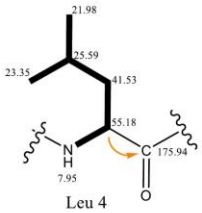
	β	1.56	41.53	
	β′	1.73		
	ϒ	1.60	25.59	
	δ	0.90	21.98	
	δ′	0.94	23.35	
	NH	7.95		
	C=O		175.94	
Leu^{5}	α	4.35	54.53	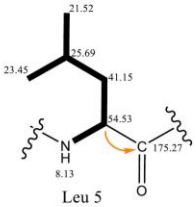
	β	1.56	41.15	
	β′	1.73		
	ϒ	1.74	25.69	
	δ	0.88	21.52	
	δ′	0.92	23.45	
	NH	8.13		
	C=O		175.27	
Ser^{6}	α	4.47	57.69	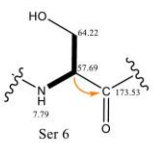
	β	3.87	64.22	
	β′	4.01		
	NH	7.79		
	C=O		173.53	
Leu^{7}	α	4.34	54.00	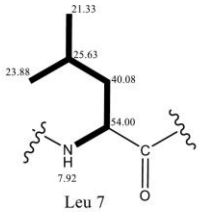
	β	1.63	40.08	
	β′	1.86		
	ϒ	1.74	25.63	
	δ	0.88	21.33	
	δ′	0.95	23.88	
	NH	7.92		
	C=O		overlap	

Amino acid	Site	δ ^{1}H [ppm]	δ ^{13}C [ppm]		HSQC- TOCSY and key HMBC correlation
Gln^{8}	α	4.40	54.61		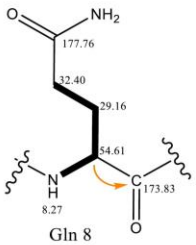
	β	1.92	29.16		
	β′	2.08			
	ϒ	2.29	32.40		
	NH	8.27			
	C=O		173.83		
	NH_2^{1}	6.85			
	NH_2^{2}	7.54			
	C=O		177.76		
Leu^{9}	α	4.28	54.12		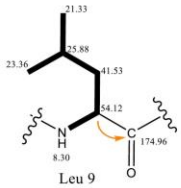
	β	1.63	41.53		
	β′	1.73			
	ϒ	1.73	25.88		
	δ	0.88	21.33		
	δ′	0.95	23.36		
	NH	8.30			
	C=O		174.96		
Val^{10}	A	4.12	61.39		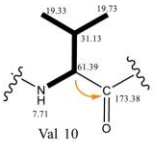
	B	2.15	31.13		
	ϒ	0.98	19.33		
	ϒ′	0.98	19.73		
	NH	7.71			
	C=O		173.38		
Glu^{11}	A	4.53	53.43		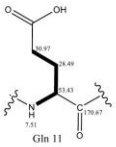
	B	1.79	28.49		
	β′	1.93			
	ϒ	2.30	30.97		
	NH	7.51			
	C=O		170.67		
3-OH-C_{10} -fatty acid	C=O		175.82		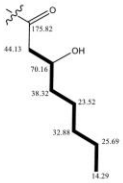
	2′	2.45	44.13	CH_2	
	3′	4.10	70.16	CH	
	4′	1.52	38.32	CH_2	
	5′	1.33	23.52	CH_2	
	6′	1.32	32.88	CH_2	
	7′	1.74	25.69	CH_2	
	8′	0.91	14.29	CH_3	

Table 10: Chemical shifts for protons and carbons of compound **3.**

Amino acid	Site	δ ^{1}H [ppm]	δ ^{13}C [ppm]	Amino acid	Site	δ ^{1}H [ppm]	δ ^{13}C [ppm]	
Leu[1]	α	4.15	55.58	Gln[8]	α	4.40	54.61	
	β	1.74	40.97		β	1.92	29.16	
	ϒ	1.62	25.59		β′	2.08		
	δ	0.95	22.81		ϒ	2.29	32.40	
	δ′	0.95	22.26		NH	8.27		
	NH	8.54			C=O		173.83	
	C=O				NH_2^1	6.85		
					NH_2^2	7.49		
Asp[2]	α	4.50	53.53		C=O		177.76	
	β	2.84	35.66					
	β′	2.75		Leu[9]	α	4.28	54.12	
	NH	8.40			β	1.56	41.53	
	C=O		174.85		β′	1.73		
	C=O		173.41		ϒ	1.64	25.88	
					δ	0.88	21.33	
Thr[3]	α	4.54	59.97		δ′	0.95	23.36	
	β	5.44	70.77		NH	8.30		
	ϒ	1.31	18.04		C=O		174.96	
	NH		7.85					
	C=O		172.45	Val[10]	A	4.12	61.39	
					B	2.15	31.13	
Leu[4]	α	4.13	55.18		ϒ	0.98	19.33	
	β	1.56	41.53		ϒ′	0.98	19.73	
	β′	1.73			NH	7.71		
	ϒ	1.60	25.59		C=O		173.41	
	δ	0.90	21.98					
	δ′	0.94	23.35	Glu[11]	A	4.53	53.43	
	NH	7.95			B	1.79	28.49	
	C=O		175.94		β′	1.93		
					ϒ	2.30	30.97	
Leu[5]	α	4.35	54.53		NH	7.51		
	β	1.56	41.15		C=O		170.67	
	β′	1.73			C=O			
	ϒ	1.74	25.69					
	δ	0.88	21.52		C=O		175.82	
	δ′	0.92	23.45	3-OH-C_{10} -fatty acid	2′	2.45	44.13	CH_2
	NH	8.13			3′	4.10	70.16	CH
	C=O		175.27		4′	1.52	38.32	CH_2
					5′	1.33	23.52	CH_2
Ser[6]	α	4.47	57.69		6′	1.32	32.88	CH_2
	β	3.87	64.22		7′	1.74	25.69	CH_2
	β′	4.01			8′	overlap	overlap	CH_2
	NH	7.79			9′	overlap	overlap	CH_2
	C=O		173.53		10′	0.91	14.29	CH_3
Leu[7]	α	4.34	54.00					
	β	1.63	40.08					
	β′	1.86						
	ϒ	1.74	25.63					
	δ	0.88	21.33					
	δ′	0.95	23.88					
	NH	7.92						
	C=O							

In compound **2** and **4**, Ile10 was assigned instead of Val10, while the rest of the spectral features were identical with that of compound **1**. In compound **2**, the assignment of isoleucine was deduced by the observed spin system of the α-proton with a single β-proton (sp^3-hybridized) via the ^1H-^1H-COSY spectrum and with β, ϒ and δ-protons via the ^1H-^1H-TOCSY spectrum. Furthermore, there was an absence of correlations in the ^1H-^1H-COSY spectrum from methylene (-CH_2) ϒ-protons with one of the two terminal methyls (-CH_3). This suggested the two methyl groups of isoleucine in unequal distance/environment from the ϒ-protons (-CH_2) as it was meant to be. The NMR data of compound **2** are provided in Table A2, and Figure A8 and A9. The NMR data of compound **4** measured in d_6-acetone are provided in Figure A12. With key features of NMR spectra along with the MS^2 spectral analysis, the structure of compound **4** was confirmed as tensin while the rest represented novel analogues.

4.6 *Pseudomonas* sp. THA 5.7

4.6.1 Metabolomics

The initial screening of n-butanol extract of the bacterium, fermented for 4 days, upon LC-MS revealed two distinct pseudomolecular ions at *m/z* 1068 $[M+H]^+$ (**5**) and 1082 $[M+H]^+$ (**6**) as major compounds. They were observed as intense peaks in UV chromatograms and were feasible to be isolated using a RP-HPLC system. The preliminary search of the secondary metabolites considering these molecular masses showed the candidates virginiafactin A and B in the norine database, a database for NRPS metabolites. They are well known compounds as linear lipo-octapeptides from the genus *Pseudomonas*. Upon further investigation, the LC-HR-MS data, measured for the same extract, unveiled two additional pseudomolecular ions at *m/z* 1040 $[M+H]^+$ (**7**) and 1054 $[M+H]^+$ (**8**) in a very low abundance. For the complete identification of these compounds, the two trivial compounds were not produced in a sufficient amount for structure elucidation by NMR and hence were characterized only with the annotation of MS^2 fragments. The structures of the major compounds were elucidated with HR-MS and NMR spectroscopy.

4.6.2 Isolation and Characterization of Virginiafactins

The VLC fraction of 80% methanol showed the presence of two major compounds upon LC-MS analysis (Figure 32). They were further purified using HPLC with the yield of 37.5 mg for **5** and 42.0 mg for **6**.

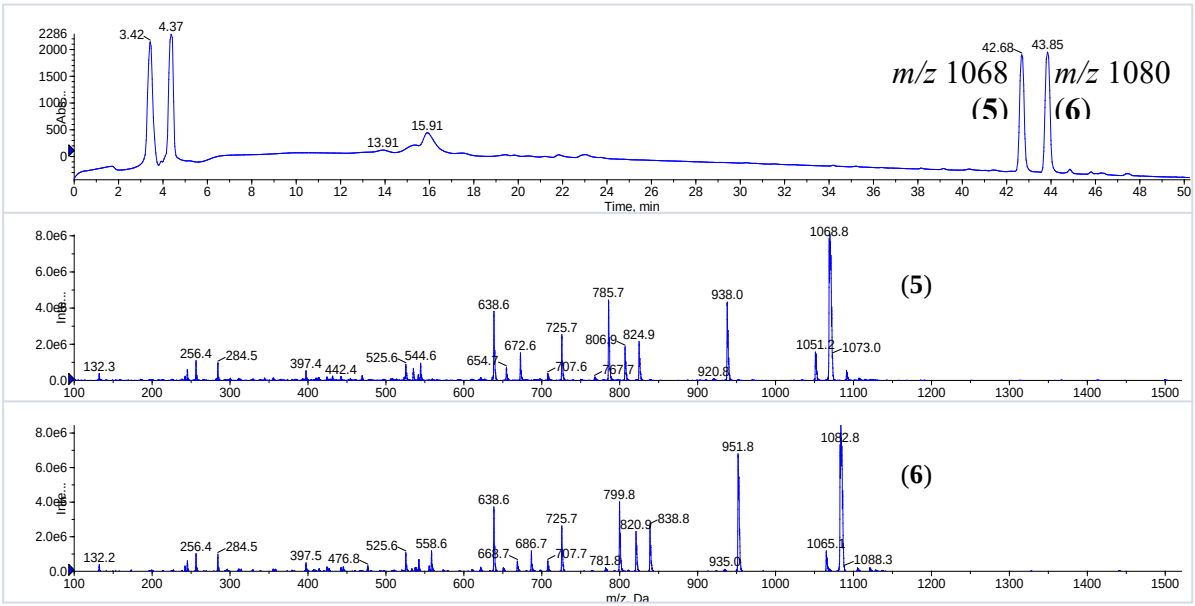

Figure 32: LC-MS measurement of the 80% VLC fraction, showing the UV chromatogram at 208 nm (top), MS^1 spectrum of **5** (middle) and MS^1 spectrum of **6** (bottom).

In the HR-MS spectral analysis, **5** showed a pseudomolecular ion at *m/z* 1068.7294 $[M+H]^+$ ($C_{53}H_{97}N_9O_{13}$) and a sodium adduct at *m/z* 1090.7115 $[M+Na]^+$ while **6** showed a pseudomolecular ion at *m/z* 1082.7443 $[M+H]^+$ ($C_{54}H_{99}N_9O_{13}$) and a sodium adduct at *m/z* 1104.7262 $[M+Na]^+$. The other two minor compounds, **7** and **8**, were allocated with pseudomolecular ions at *m/z* 1040.6955 $[M+H]^+$ ($C_{51}H_{93}N_9O_{13}$) and *m/z* 1054.7102 $[M+H]^+$ ($C_{52}H_{95}N_9O_{13}$) along with their corresponding sodium adducts at *m/z* 1062.6774 $[M+Na]^+$ and *m/z* 1076.6920 $[M+Na]^+$, respectively (Figure 33).

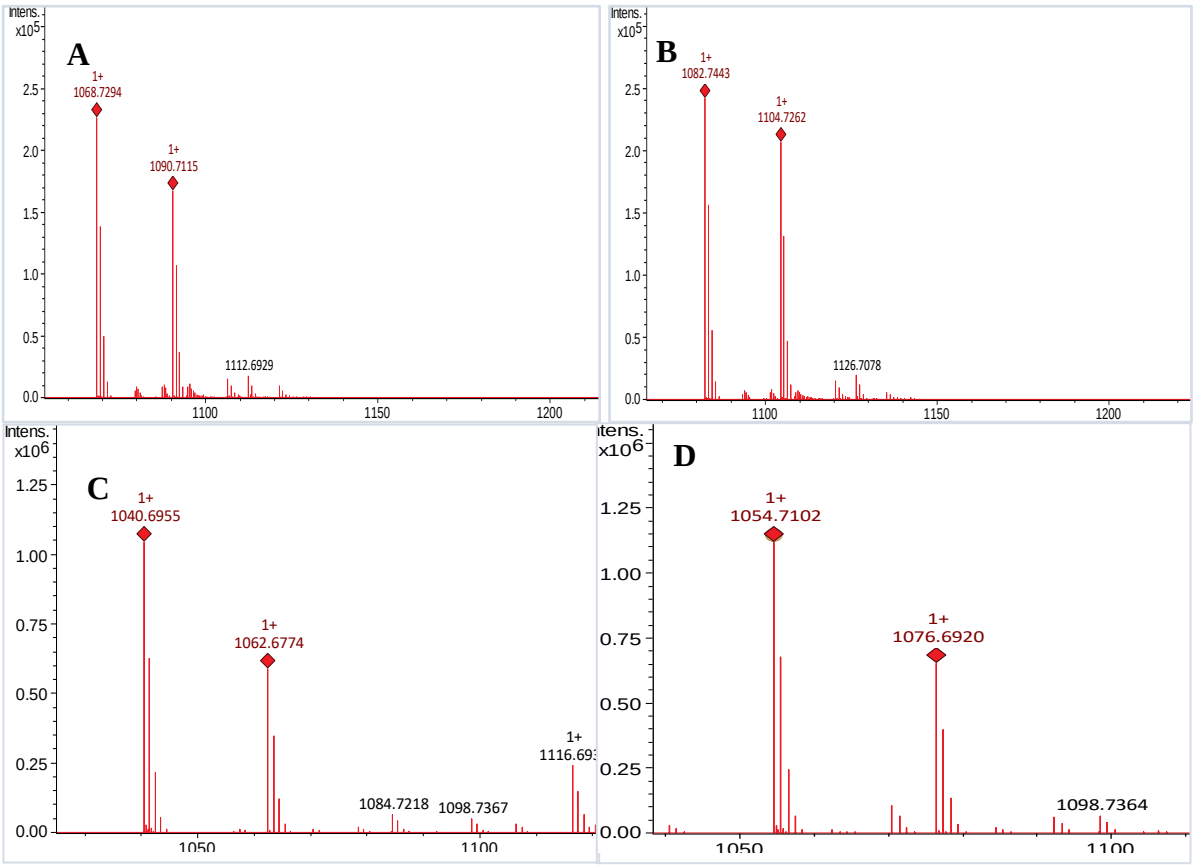

Figure 33: HR-MS spectra (MS^1) showing pseudomolecular ions and sodium adducts of four compounds: [A] **5**, [B] **6**, [C] **7** and [D] **8**.

In the MS^2 specctra of the compounds **5** and **6** (Figure 34 A and B), b_1 fragments were observed at *m/z* 284.2230 (*m/z* ±0.0005) that indicated a C_{10} hydroxy fatty acyl moiety fused to a leucine as the first amino acid of the peptide chain. In both compounds, b-type fragments up to the 5th amino acid were identical (with *m/z* ±0.0005). They were identified as Xle1-Xle2-Gln3-Xle4-Ser5 by assigning their corresponding b_1, b_2 (*m/z* 397.3071), b_3 (*m/z 525.3661*), b_4 (*m/z* 638.4503) and b_5 (*m/z* 725.4822) fragments, respectively. The next subsequent observed fragments were significantly different in

both compounds. In compound **5**, the b_6, b_7 and b_8 fragments appeared at *m/z* 824.5506, *m/z* 937.6353 and *m/z* 1050.7248, respectively, indicating the sequential addition of Val6-Xle7-Xle8 (Figure 34 A). But in the compound **6**, the b_6, b_7 and b_8 fragments appeared at *m/z* 838.5664, *m/z* 951.6499 and *m/z* 1064.7319, respectively, indicating the sequential addition of Xle6-Xle7-Xle8 (Figure 34 B). This pointed out the structural differentiation of two major compounds by valine and iso-/leucine (Xle) at the

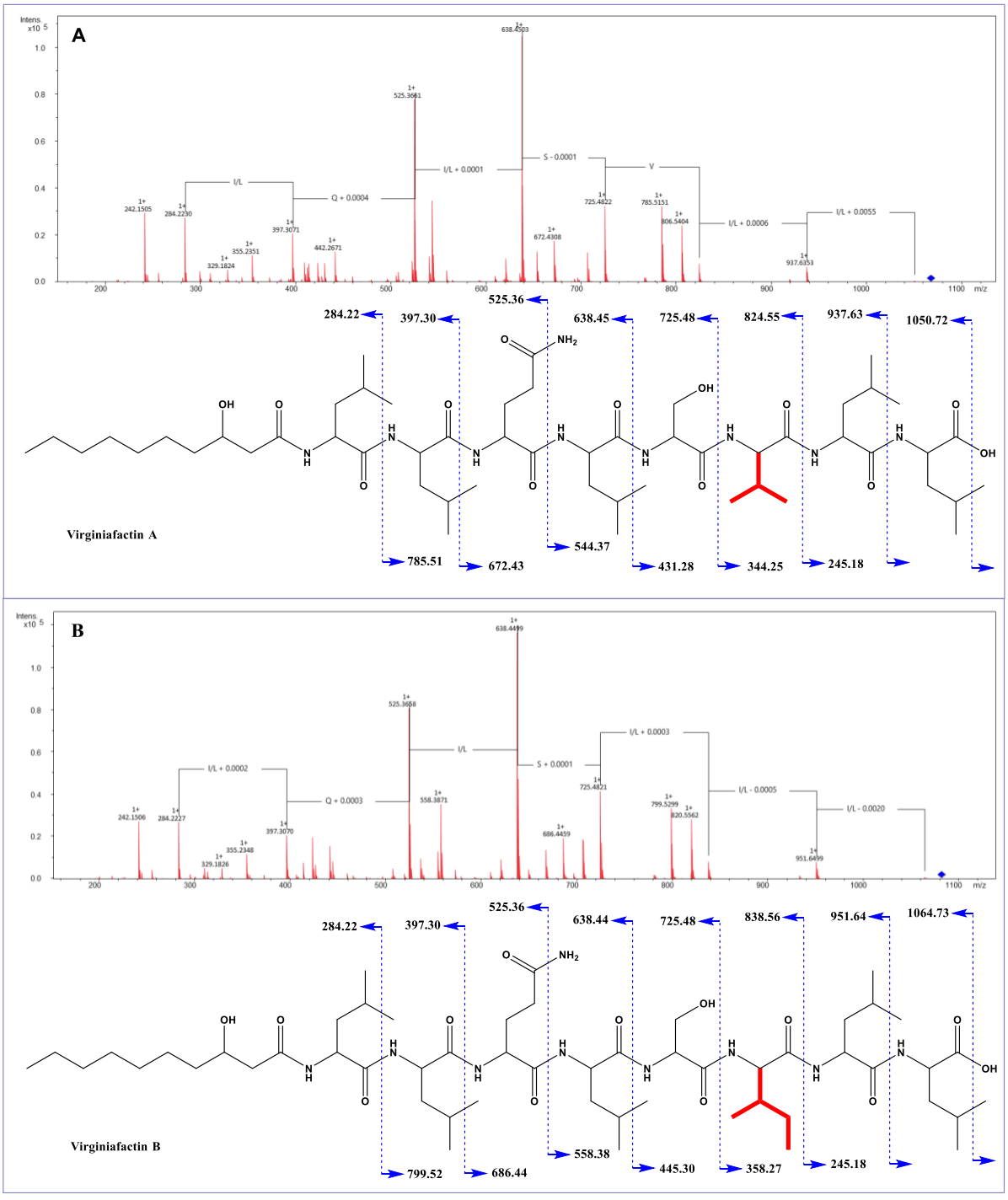

Figure 34: MS^2 spectra showing the sequential annotation of the amino acid sequences of [A] **5** and [B] **6**.

6th amino acid in the peptide chain which was verified by the NMR data.

During the NMR spectral analysis of the compound **5**, measured in d_3-methanol, the chemical shift values for protons and their adjacent carbons were assigned from ^{1}H-NMR, ^{13}C-NMR and edited ^{1}H-^{13}C-HSQC spectra. This revealed the chemical shifts for ten amide (-NH-) protons (6.8 ppm - 8.3 ppm) and ten carbonyl (-CO-) carbons (172.5 ppm - 177.6 ppm). The skeleton of fatty acyl moiety and amino acid side chain were elucidated by assigning the spin systems in ^{1}H-^{1}H-TOCSY, ^{1}H-^{13}C-HSQC-TOCSY and ^{1}H-^{1}H-COSY spectra. In the ^{1}H-^{1}H-TOCSY spectrum, the spin systems from each -NH-proton and each α-proton to all their subsequent -CH$_n$- protons (α, β, ϒ and δ) were assigned, while in the ^{1}H-^{13}C-HSQC-TOCSY spectrum, the same spin systems with all their subsequent -CH$_n$- carbons (α, β, ϒ and δ) were observed. The ^{1}H-^{1}H-COSY spectrum was assigned particularly to find the adjacent -CH$_n$- group from each proton by allocating the spin systems between them. The peptide bonds between two adjacent amino acids were determined with the ^{1}H-^{13}C-HMBC spectrum, where each amide (-NH-) proton showed a cross peak with the adjacent carbonyl (-CO-) carbon (Figure 35). The presence of one glutamine was further confirmed with characteristic two chemical shift values of the side-chain amide (-NH$_2$-) protons at 6.8 (s) and 7.5 (s), indicating the *cis*- and *trans*- configurations, respectively. The ^{1}H-^{15}N-HSQC spectrum was assigned to characterize all nine amide groups (Table A3). The analysis confirmed the structure of the compound as virginiafactin A, revealing the C$_{10}$ fatty acyl chain fused to a peptide sequence of Leu1-Leu2-Gln3-Leu4-Ser5-Val6-Leu7-Leu8.

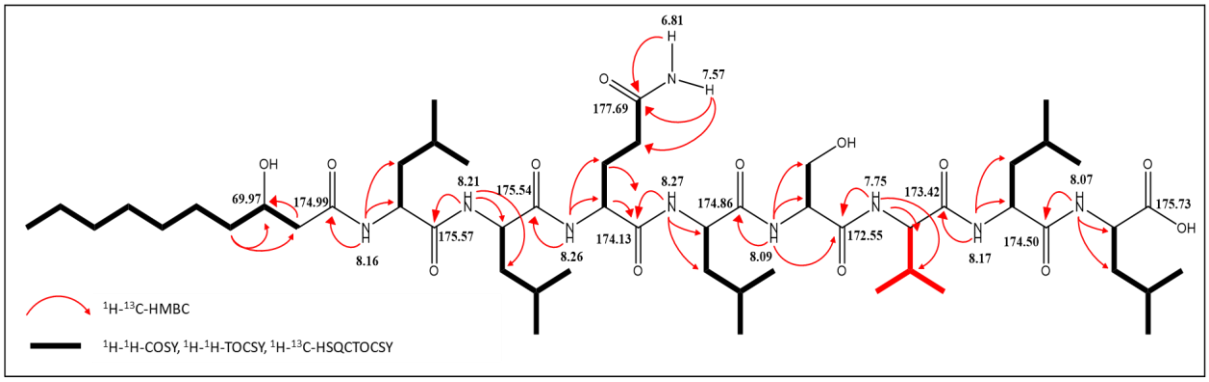

Figure 35: Structure of **5** (virginiafactin A) showing ^{1}H-^{13}C-HMBC, ^{1}H-^{1}H-COSY, ^{1}H-^{1}H-TOCSY and ^{1}H-^{13}C-HSQC-TOCSY correlations.

During the spectral assignment of compound **6**, measured in d_4-methanol, all the chemical shift values of protons and carbons were identical to the literature data of

virginiafactin B. In virginiafactin A, there was a valine as 6th amino acid in the peptide chain, where its α-proton (4.20 ppm) showed the spin systems with one β-proton (-CH-) and ϒ-protons of two methyl (-CH_3) groups in the ^{1}H-^{1}H-TOCSY spectrum, and with corresponding carbons in ^{1}H-^{13}C-HSQC-TOCSY spectrum. This verified the valine moiety embedded in the structure. In virginiafactin B, there was a correlation from the α-proton (4.25 ppm) to one β-proton (-CH-), two times ϒ-protons (-CH_2-, -CH_3) and δ-protons of a methyl (-CH_3) group in the ^{1}H-^{1}H-TOCSY spectrum, and with corresponding carbons in the ^{1}H-^{13}C-HSQC-TOCSY spectrum. This indicated the presence of an isoleucine moiety. In this way, virginiafactin A and virginiafactin B differed by the type of the 6th amino acid in the peptide chain (Figure 36).[93]

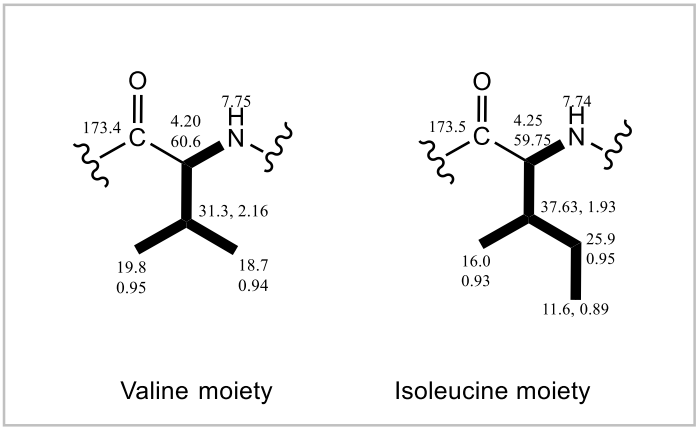

Figure 36: NMR assignment of valine moiety from virginiafactin A and isoleucine moiety from virginiafactin B, showing ^{1}H-^{1}H-TOCSY correlations.

All NMR spectral data of virginiafactin A and B were provided in Figure A13 and A14, respectively. Though virginiafactin A was measured in *d*$_3$-methanol and virginiafactin B was measured in *d*$_4$-methanol, both had no significant effects from the solvent types except some reduced signal intensities of amide protons in *d*$_4$-methanol.

In the MS^2 spectra of **7** and **8** (Figure 37 A and B), b_1 fragments were observed at *m/z* 256.1911 (±0.0005), indicating a C_8 hydroxy fatty acyl moiety connected to leucine as the first amino acid. In both compounds, b-type fragments up to the 5th amino acid were identical (with *m/z* ±0.0009). They were sequentially identified as Xle1-Xle2-Gln3-Xle4-Ser5 by assigning their corresponding b_1, b_2 (*m/z* 369.2751), b_3 (*m/z* 497.3338), b_4 (*m/z* 610.4178) and b_5 (*m/z* 697.4500) fragments, respectively. The next subsequent fragments were observed significantly different in both compounds. In compound **7**, the b_6, b_7 and b_8 fragments appeared at *m/z* 796.5183, *m/z* 909.6024 and *m/z* 1022.6866, respectively, indicating the sequential addition of Val6-Xle7-Xle8. But in the compound **8**, the b_6, b_7, and b_8 fragments appeared at *m/z* 810.5333, m/z 923.6170 and *m/z* 1036.6998, respectively, indicating the sequential addition of Xle6-Xle7-Xle8.

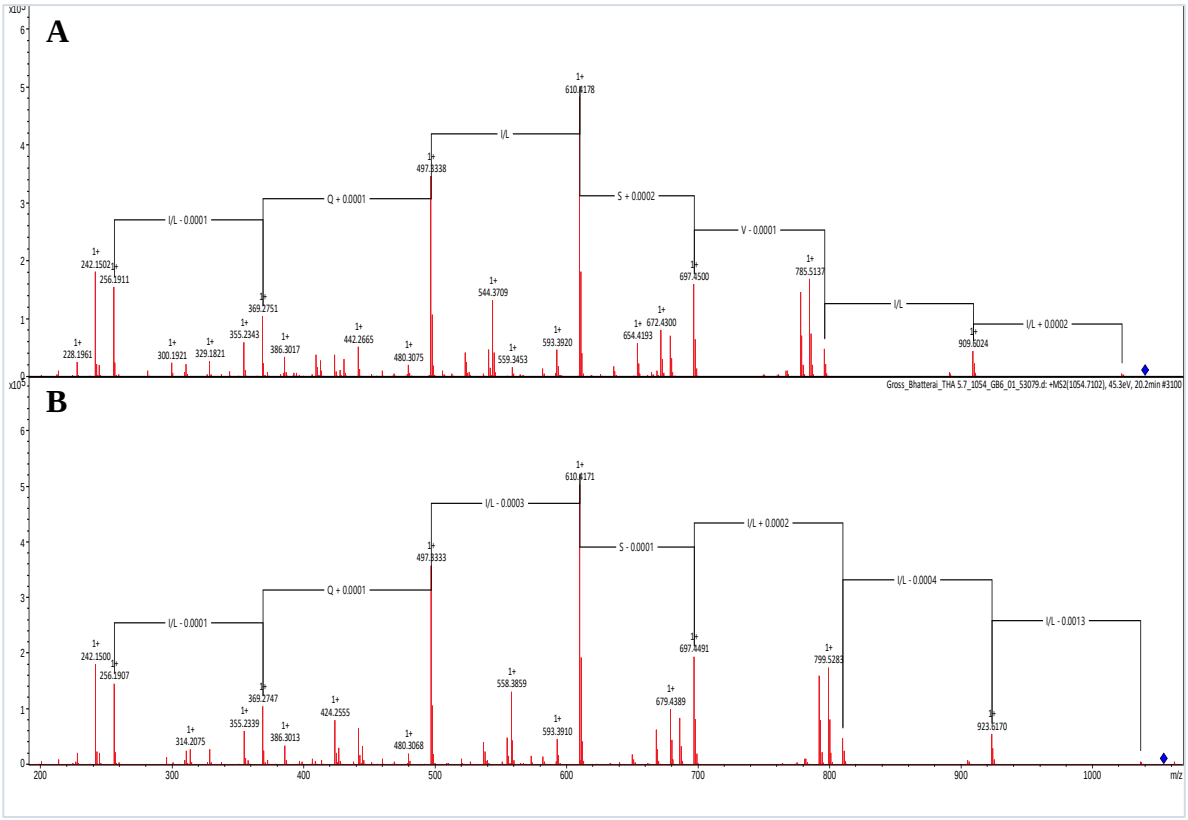

Figure 37: MS^2 spectra showing sequential annotation of amino acids of [A] **7** and [B] **8**.

This pointed out the structural differentiation of **7** and **8** by valine and iso-/leucine (Xle) at the 6th amino acid of the peptide chain. However, considering the structural skeletons of virginiafactin A and B, the minors were analogues. The analogues **7** and **8** differed by shortening the fatty acyl chain with one biosynthetic acetate unit from

Compound	MF	*m/z*	3-OH (Lipid)	AA1	AA2	AA3	AA4	AA5	AA6	AA7	AA8
Compound **7**	$C_{51}H_{93}N_9O_{13}$	1040.6955	-C_8	Leu	Leu	Gln	Leu	Ser	Val	Leu	Leu
Compound **8**	$C_{52}H_{95}N_9O_{13}$	1054.7102	-C_8	Leu	Leu	Gln	Leu	Ser	Ile	Leu	Leu
Virginiafactin A	$C_{53}H_{97}N_9O_{13}$	1168.7294	-C_{10}	Leu	Leu	Leu	Leu	Ser	Val	Leu	Leu
Virginiafactin B	$C_{54}H_{100}N_9O_{13}$	1182.7443	-C_{10}	Leu	Leu	Leu	Leu	Ser	Ile	Leu	Leu

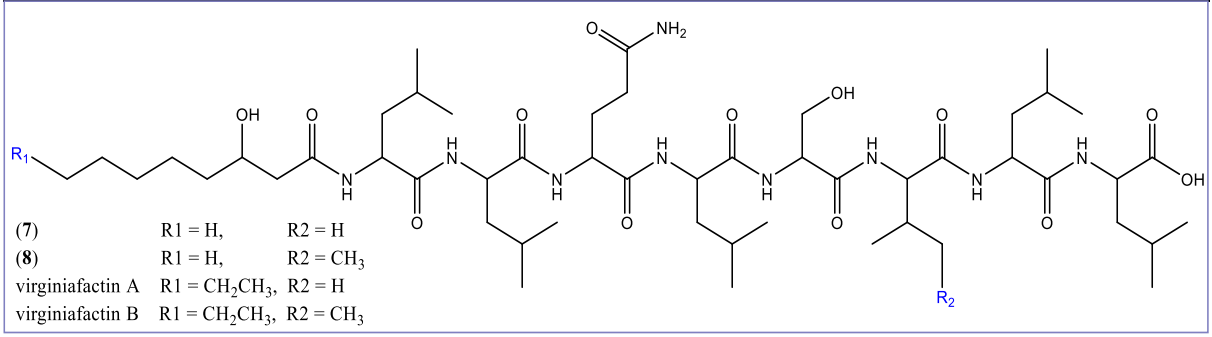

Figure 38: Chemical and structural features of the isolated virginiafactins A and B and their novel analogues

virginiafactin A and B, respectively. The two annotated structures of **7** and **8** as virginiafactin analogues are reported for the first time ever.

To summarize the structures of these compounds, they mainly differed by either the type of the 6th amino acid or the different size of the lipid chain (Figure 38). Virginiafactin A and virginiafactin B were different from the analogues **7** and **8** with respect to the length of the fatty acyl chain. Virginiafactin A and virginiafactin B were differentiated by the 6th amino acid, which was valine for virginiafactin A and isoleucine for virginiafactin B. It seemed possibly the same case for the analogues **7** and **8**.

4.7 *Pseudomonas* sp. SFB8.6

4.7.1 Metabolomics

The initial screening of the n-butanol extract of the bacterium, fermented for 4 days, upon LC-MS revealed two distinct pseudomolecular ions at *m/z* 1113 $[M+H]^+$ (**9**) and 1127 $[M+H]^+$ (**10**). They were observed as intense peaks in UV chromatograms and it was feasible to isolate them using a RP-HPLC system. Upon further investigation, the LC-HR-MS data measured for the same extract unveiled more accurate pseudomolecular ions at *m/z* 1112.6788 $[M+H]^+$ (**9**) and 1126.6606 $[M+H]^+$ (**10**). The preliminary search of the secondary metabolites considering these molecular masses showed the candidates of **9** as massetolide E and that of **10** as massetolide F or viscosin. They are known cyclic lipodepsipeptides from the genus *Pseudomonas*. Furthermore, the structures of these compounds were characterized with HR-MS, NMR spectroscopy and X-ray crystallography.

4.7.2 Isolation and Structural Identification of New Massetolide-Stereoisomers

The VLC fraction of 80% methanol showed two of the target compounds upon LC-MS analysis. The compounds were then isolated using HPLC employing the wavelength of 210 nm (Figure 39). The yields of **9** and **10** were 22 mg and 15 mg, respectively. Further structures of these compounds were determined with the annotation of HR-MS/MS data along with NMR and X-ray crystallography.

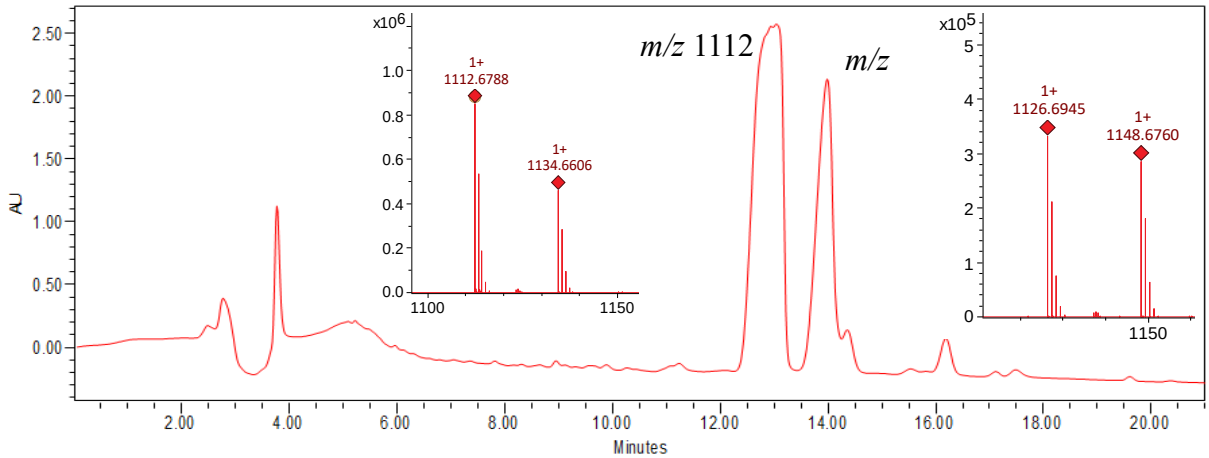

Figure 39: RP-HPLC chromatogram of the 80% VLC fraction of the bacterial extract, showing two major compounds, along with their HR-MS spectra.

In the LC-HR-MS data, **9** showed a pseudomolecular ion at *m/z* 1112.6788 $[M+H]^+$ ($C_{53}H_{94}N_9O_{16}$), and a sodium adduct at *m/z* 1134.6606 $[M+Na]^+$ while **10** showed a

pseudomolecular ion at *m/z* 1126.6945 $[M+H]^+$ ($C_{54}H_{96}N_9O_{16}$) and a sodium adduct at *m/z* 1148.6760 [M+Na]+ (Figure 39).

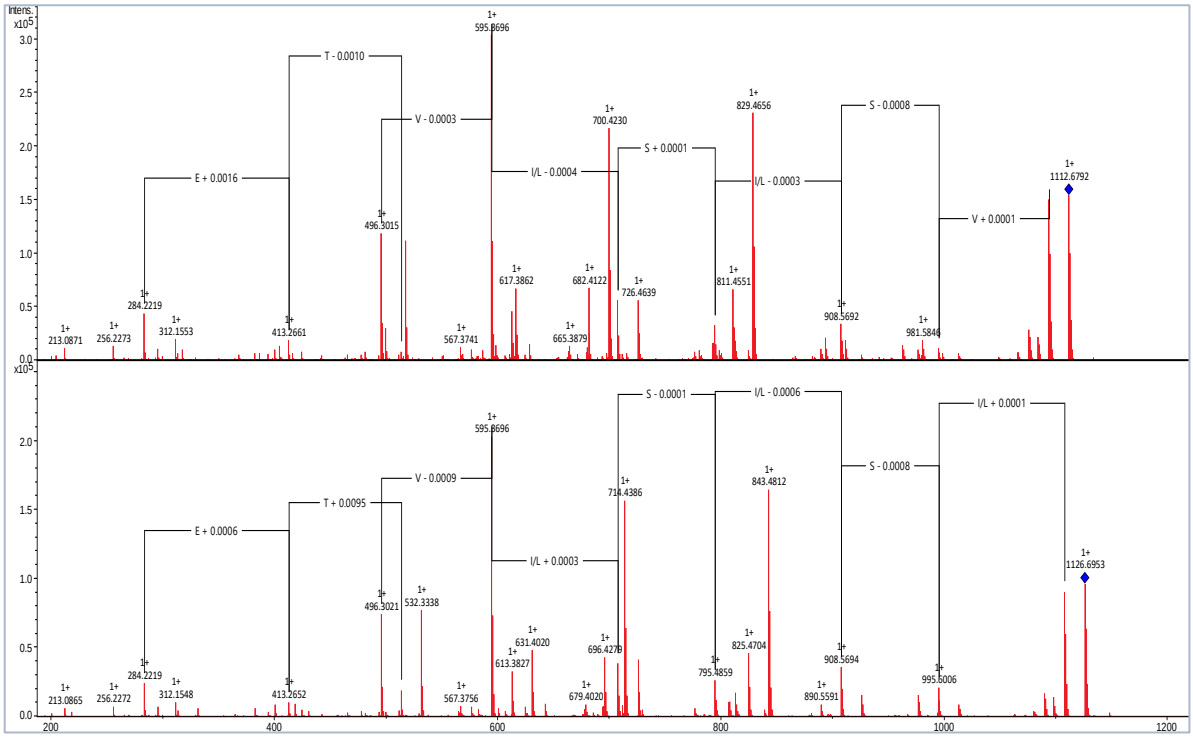

Figure 40: MS^2 spectra showing sequential annotation of amino acids of **9** (top) and **10** (bottom).

In the MS^2 spectra of both compounds (Figure 40), b_1 fragments appeared at *m/z* 284.2219, indicating the C_{10} hydroxy fatty acyl moiety fused to leucine, the first amino acid of the peptide chain. This was further verified with a_1 fragments at *m/z* 256.2263 (±0.0001), referring one less carbonyl (28 Da) from b_1 fragments. In both compounds, b-type fragments up to the 8th amino acid were identical (with m/z ±0.0009), which verified the sequence of Xle1-Glu2-Thr3-Val4-Xle5-Ser6-Xle7-Ser8 as b_1, b_2 (*m/z* 413.2261), b_3 (*m/z* 514.3129), b^0_4 (*m/z* 595.3696), b^0_5 (*m/z* 708.4533), b^0_6 (*m/z* 795.4855), b^0_7 (*m/z* 908.5692) and b^0_8 (*m/z* 995.6005) fragments, respectively. Here, the b^0_4 and afterward fragments in the spectra were assigned with the loss of 18 Da (a water mass) due to the ring cyclization in the structures. The b^0_9 fragment of the **9** and **10** appeared differently at *m/z* 1094.6690 and *m/z* 1108.6848, respectively, indicating the sequential addition of corresponding Val9 and Xle9 in the peptide chain. It was difficult to confirm the leucine or isoleucine in the chemical structure, e.g. by side chain loss, only via HR-MS data. To resolve this, NMR spectra of **9** and **10** were measured and analysed. However, the MS^2 spectra also revealed the differentiation of these

isolated compounds by Val (for **9**) or Xle (for **10**) at the 9th amino acid of the peptide chain.

Coincidently, the strain additionally produced the novel lipo-dipeptide which was detected in the HR-MS/MS data of the crude extract (Figure 41). The MS^2 spectrum of the lipo-dipeptide showed an identical fragmentation pattern to the one produced by *Pseudomonas* sp. SS101 (another massetolides producer, already mentioned in 'section 4.2').

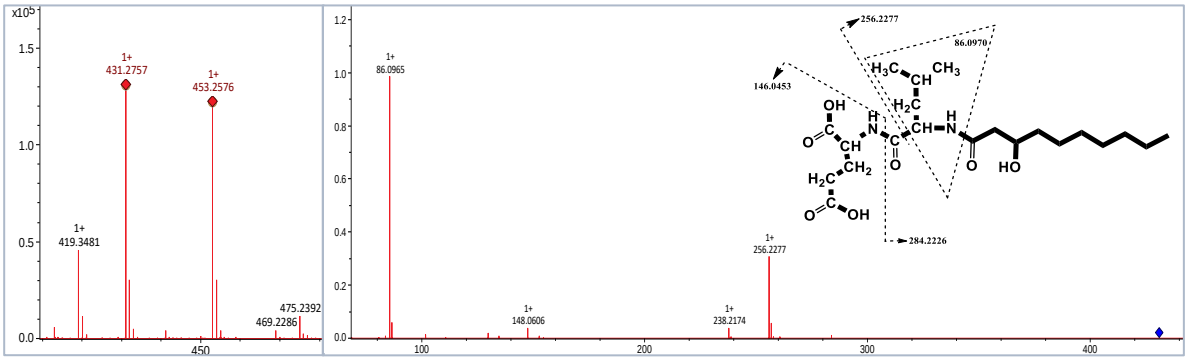

Figure 41: MS^1 spectrum of the lipo-dipeptide, produced by *Pseudomonas* sp. SFB8.6 (left) and MS^2 spectra along with structural fragmentation (right).

In the NMR spectral analysis of **9**, measured in d_3-methanol, the chemical shift values of protons and their adjacent carbons were assigned with ^{1}H-NMR, ^{13}C-NMR and edited ^{1}H-^{13}C-HSQC spectra (Figure A15). This revealed the chemical shifts for nine amide (-NH-) protons (7.15 ppm - 9.22 ppm) and eleven carbonyl (-CO-) carbons (169.9 ppm - 177.0 ppm). In the ^{1}H-^{1}H-TOCSY spectrum, the spin systems from each -NH- proton and each α-proton to their subsequent -CH$_n$- protons (α, β, ϒ and δ) were assigned, while the in ^{1}H-^{13}C-HSQC-TOCSY spectrum, the same spin systems with their subsequent -CH$_n$- carbons (α, β, ϒ and δ) were assigned. The spin systems in the ^{1}H-^{1}H-COSY spectrum were assigned, particularly to allocate the adjacent -CH$_n$- group from each proton. The spectral analysis showed the amino acid sequence as Leu1-Glu2-Thr3-Val4-Leu5-Ser6-Leu7-Ser8-Val9. Two valine moieties in the peptide chain were assigned with α-protons at δ_{AA4} 3.61 (dd, 7.0, 9.8) and δ_{AA9} 4.58 (dd, 3.3, 9.7), each of them had the couplings with their corresponding β-proton (-CH-) and two sets of ϒ-protons (-CH$_3$) in the ^{1}H-^{1}H-TOCSY spectrum. The ester link for the ring cyclization was confirmed with a ^{1}H-^{13}C-HMBC correlation from the β-proton of threonine at δ_{AA3} 5.49 to the carbonyl carbon (-CO-) of the terminal leucine at 169.9 ppm. The sequence of amino acids was assigned with ^{1}H-^{1}H-NOESY correlations from

the α-proton of each amino acid to the nearest amide (-NH-) proton of the adjacent amino acid (Figure 42).

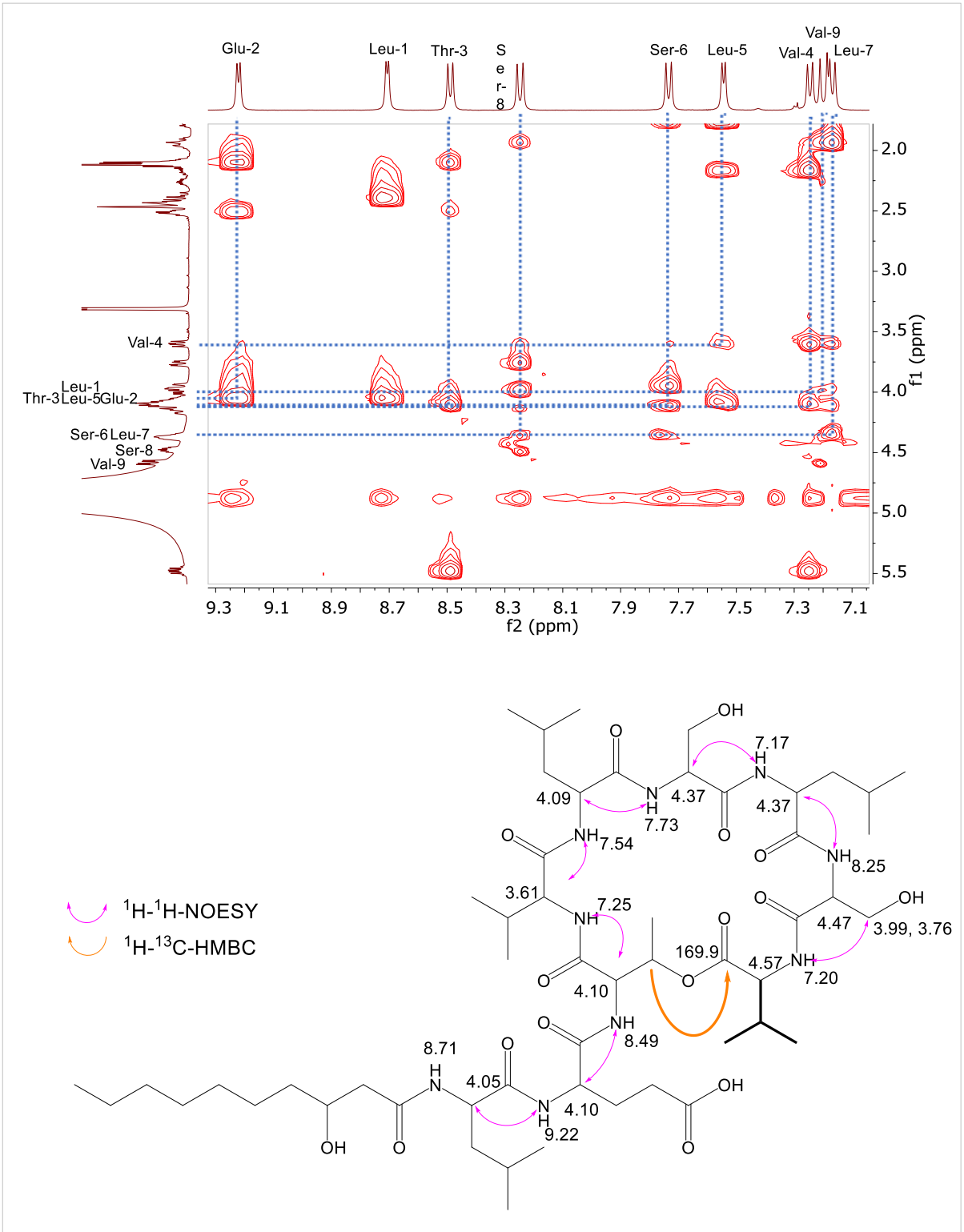

Figure 42: NMR spectroscopic analysis of **9** (d_3-methanol), showing the ^{1}H-^{1}H-NOESY spectrum along with the structural annotation with ^{1}H-^{1}H-NOESY (pink) and ^{1}H-^{13}C-HMBC (orange) correlations.

All the assigned NMR data of compound **9** is summarized in Table 11.

Table 11: Chemical shifts for protons, carbons and nitrogens of compound **9.**

Residue	Position	δ ^{1}H [ppm]	δ ^{13}C [ppm]	δ ^{15}N [ppm]	Residue	Position	δ ^{1}H [ppm]	δ ^{13}C [ppm]	δ ^{15}N [ppm]
Leu[1]	α	4.05	54.62		Ser[6]	α	4.37	57.55	
	B	1.75	40.60			β	4.16, 3.95	63.93	
	Ɣ	1.64	25.64			NH	7.73		107.0
	δ	0.99	22.85			C=O			
	δ’	0.96	22.63						
	NH	8.71		128.2	Leu[7]	α	4.37	54.59	
	C=O					β	1.93, 1.63	41.96	
						Ɣ	1.65	25.66	
Glu[2]	α	4.10	57.05			δ	0.99	23.42	
	β	2.11	26.75			δ’	0.93	21.02	
	Ɣ	2.52	30.79			NH	7.16		120.7
	NH	9.22		122.4		C=O			
	C=O								
	C=O		176.02		Ser[8]	α	4.47	57.94	
						β	3.99, 3.76	62.98	
Thr[3]	α	4.10	61.94			NH	8.25		110.5
	β	5.49	70.30			C=O			
	Ɣ	1.40	18.43						
	NH	8.49		113.2	Val[9]	α	4.57	57.31	
	C=O		175.04			β	2.26	30.68	
						Ɣ	0.88	19.44	
Val[4]	α	3.61	64.66			Ɣ’	0.76	17.23	
	β	2.17	30.28			NH	7.20		112.8
	Ɣ	0.97 overlap	21.41			C=O			
	Ɣ	0.97 overlap	19.44						
	NH	7.25		120.0	3-OH-C_{10}	C=O		175.34	
	C=O				fatty acid	2’	2.40	44.52	CH_2
						3’	4.10	69.89	CH
Leu[5]	α	4.09	55.85			4’	1.51	38.44	CH_2
	β	1.75	40.52			5’	-	-	CH_2
	Ɣ	1.65	25.62			6’	1.29	30.53	CH_2
	δ	0.90	23.40			7’	-	-	CH_2
	δ’	0.87	21.03			8’	-	-	CH_2
	NH	7.54		114.6		9’	-	-	CH_2
	C=O					10’	0.89	14.31	CH_3

The NMR spectra of compound **10** measured in d_3-methanol showed an isoleucine as the terminal amino acid of the peptide chain while the rest of the amino acids remained identical with compound **9** (Figure A16). This was verified by comparing the ^{1}H- and ^{13}C-NMR spectra of **10** with that of **9** and peseudodesmin A which contained a terminal

isoleucine). In this way, the amino acid sequence of **10** was identified as Leu1-Glu2-Thr3-Val4-Leu5-Ser6-Leu7-Ser8-Ile9.

The amino acid sequence of **9** was verified by NMR spectral analysis (measured in d_3-methanol) and was identical with that of massetolide E, however the NMR data of massetolide E were measured in d_6-acetone (Gerard et al., 1997).[94] Hence, compound **9** was also measured in d_6-acetone. However, the chemical shifts of α-protons for Glu2 (4.26 ppm), Val4 (3.47 ppm), Leu5 (3.69 ppm) and Leu7 (4.20 ppm) from the literature data of massetolide E did not match with the compound **9**. The chemical shift values for all α-protons in compound **9** were extracted from the ^{1}H-^{13}C-HSQC spectrum (Figure 43). This hinted the possibility, that one or more amino acids possess a different configuration in compound **9**.

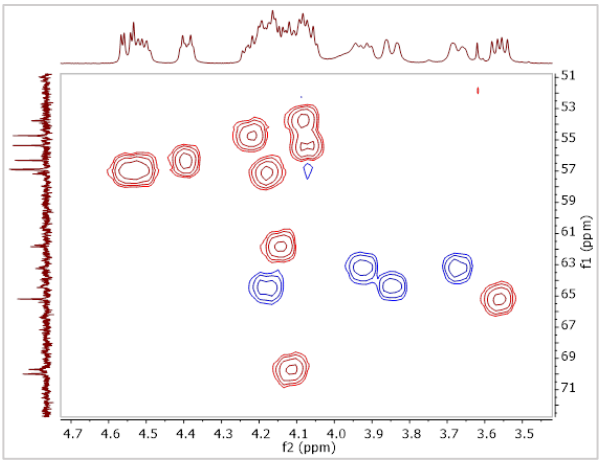

Figure 43: ^{1}H-^{13}C-HSQC spectrum of **9** (d_6-acetone), showing cross peaks for α-protons (red)

4.7.3 X-Ray Crystallography

Colourless blocks of crystals were obtained from a long-standing solution of compound **9** in d_6-acetone and moist methanol (4:6). The experimental results of x-ray crystallography were obtained from Dr. Dieter Schollmeyer, Institute of Organic Chemistry, Johannes Gutenberg University Mainz, Germany. The crystallography data showed an orthorhombic crystal structure of compound **9** in a monohydrated form, $C_{53}H_{93}N_9O_{16}.H_2O$ (Figure 44). The structure showed an amino acid sequence of the peptide

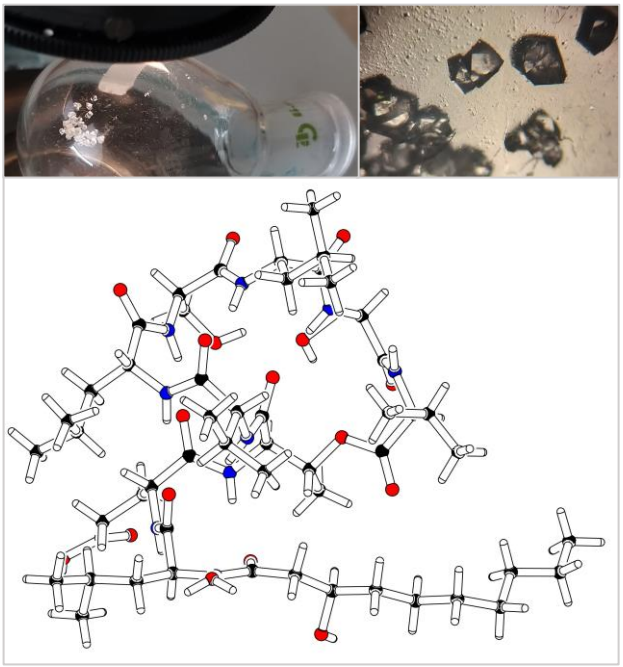

Figure 44: Images of crystal in the flask and under an optical microscope (top) and graphical representation of crystal structure of compound **9** isolated from *Pseudomonas* sp. SFB8.6.

chain along with absolute configurations as C_{10}(3-OH)-L-Leu1-D-Glu2-D-Thr3-D-Val4-D-Leu5-D-Ser6-L-Leu7-D-Ser8-L-Val9. The amino acid sequence and the lipidic moiety were almost identical with the structure of massetolide E, except the absolute configuration of Leu5. Massetolide E has a L-configuration of leucine at position 5 (L-Leu5), which was D-configuration (D-Leu5) in the case of compound **9**. This verified the compound, with a novel structure, an epimer of massetolide E.

Compound **10** did not crystallise, possibly due to lower amount of the compound compared with **9**. Nevertheless, it was very likely that compound **10** might also have the identical configurations of amino acids along with a terminal L-Ile9 instead of L-Val9. In such case, the amino acid sequence of compound **10** remained as Leu1-D-Glu2-D-Thr3-D-Val4-D-Leu5-D-Ser6-L-Leu7-D-Ser8-L-Ile9, which represents the epimer of massetolide F.

4.8 Biological Activities of the Isolated Compounds

4.8.1 Chitinase Assay

All the available salamander skin bacteria were pre-screened anti-*B. dendrobatidis* strains. On this basis, their antifungal mechanism was hypothesized to be based either on the production of antifungal secondary metabolites or some enzymatic activities to inhibit the fungal growth. Considering the latter case, a qualitative chitinase assay was performed on all the available strains. Chitinase is an enzyme that is supposed to degrade chitin, a major cell wall component of all fungi. The main ethics behind this assay was whether the bacteria produce chitinase so that it could degrade the chitin of fungal cell walls, and inhibit in this way the fungal growth. The *in-vitro* chitinase assay conducted in the chitin agar plates demonstrated that seven bacterial isolates among the tested strains produced a chitinase enzyme. The extent of enzyme production was considered with the relative size of the clear zone in the agar plates. (Figure 45).

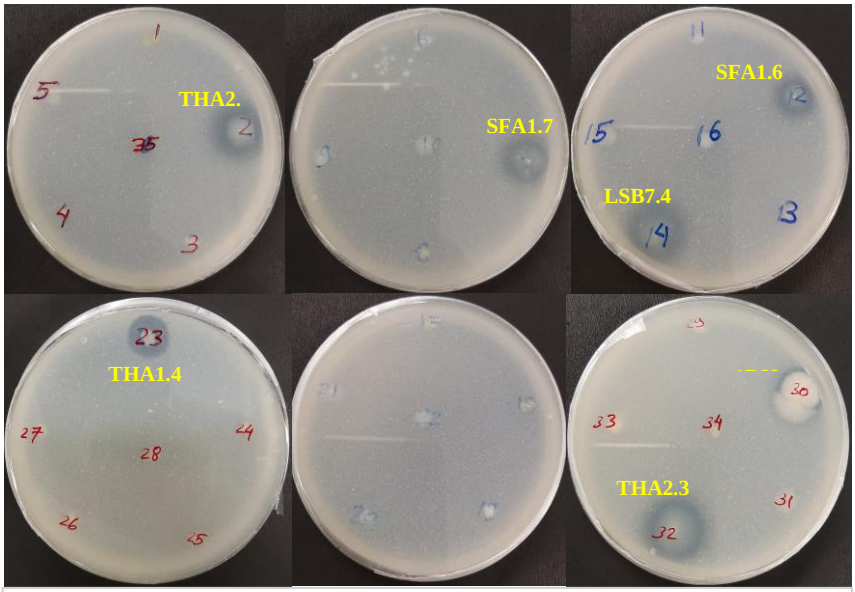

Isolates	Inhibition zone (diameter)	Activity
***Stenotrophomonas* sp. THA2.2**	15 mm	Strong
Isolate SFA1.7	12 mm	Mild
***Stenotrophomonas* sp. SFA1.6**	11 mm	Mild
***Stenotrophomonas* sp. LSB7.4**	15 mm	Strong
***Janthinobacterium lividum* THA1.4**	13 mm	Strong
***Duganella* sp. SFB1B69**	12 mm	Mild
***Paenibacillus* sp. THA2.3**	16 mm	Strong

Figure 45: Agar plates showing the chitinase assay of 35 salamander skin bacteria labelled with serial numbers mentioned in Table 5. The clear zone around the bacterial colony represented the degradation of chitin by the secreted chitinase enzyme.

Based on this assay; the chitinase-producing strains were *Stenotrophomonas* sp. THA2.2, unknown isolate SFA1.7, *Stenotrophomonas* sp. SFA1.6, *Stenotrophomonas*

sp. LSB7.4, *Janthinobacterium lividum* THA1.4, *Duganella* sp. SFB1B69 and *Paenibacillus* sp. THA2.3. The genus *Stenotrophomonas* was found here as a major representative that produced chitinase enzyme. *Stenotrophomonas* was one of the abundant bacterial genera found on the skin surface of chytrid-resistant amphibians. Among the observed chitinase producers, *Stenotrophomonas* sp. LSB7.4 and *Janthinobacterium lividum* THA1.4 showed the strongest chitinolytic activity while the rest remained mildly active. The other tested strains stayed inactive for the chitinolytic activity under the laboratory conditions.

4.8.2 Anti-chytrid Assay

In this study, there was a total of ten compounds isolated from four different salamander skin bacteria. Among them, three compounds were found to have novel structures while the rest were known compounds. All these compounds were tested for antifungal activity against the chytrid fungi, *B. dendrobatidis* and *B. salamandrivorans*. Cycloheximide was used as a positive control in the assay. During the anti-chytrid assay, the results were concluded from the 9th day of the incubation period, although they were inspected daily for 15 successive days.

The assay results revealed pseudodesmin A as the strongest anti-chytrid compound with a minimum inhibitory concentration (MIC) of 12.5 µg/mL. Virginiafactin B was found as the second strongest candidate for anti-chytrid activity with an MIC of 25 µg/mL. Virginiafactin B and **4** were showing partial inhibition against both chytrid fungi at the concentration of 12.5 µg/mL and 25 µg/mL, respectively. This was considered a partial inhibition because, at these concentrations, there was neither proper growth of chytrid spores nor complete inhibition of the growth. This partial inhibition was observed by the visual inspection via an optical microscope (Figure A17-d, h and A18-d, h). Compound **4** was showing complete inhibition of both chytrids growth at a MIC of 50 µg/mL. Virginiafactin A showed a complete inhibition against *B. dendrobatidis* at a MIC of 50 µg/mL and against *B. salamandrivorans* at a MIC of 100 µg/mL (partially at 50 µg/mL). The rest of the compounds were almost inactive below the concentration of 100 µg/mL. The positive control of cycloheximide showed complete inhibition against *B. dendrobatidis* at a MIC of 0.39 µg/mL, while against *B. salamandrivorans* at a MIC of 1.56 µg/mL (partially at 0.78 µg/mL). All the assay results were examined and calculated by measuring the optical density of 96 well plates with assay sample at 532

nm wavelength. They were additionally examined under an optical microscope and their images recorded for further confirmation (Figure A17 and A18). The overall results were concluded with the measured optical density data and optical images of the assay samples (Table 12).

Table 12: Minimum inhibitory concentration (MIC) of all isolated compounds against two amphibian pathogenic fungi, *B. dendrobatidis* and *B. salamandrivorans* (*moderate inhibition)

Strain → **Compound ↓**	***B. dendrobatidis*** (µg/mL)	***B. salamandrivorans*** (µg/mL)
Lipo-dipeptide (*P. tolaasii* RSB5.11)	100	200
Pseudodesmin A (*P. tolaasii* RSB5.11)	12.5	12.5
Virginiafactin A (*Pseudomonas* sp. THA5.7)	50	100 (50*)
Virginiafactin B (*Pseudomonas* sp. THA5.7)	25 (12.5*)	25 (12.5*)
Compound **1** (*Pseudomonas* sp. THA6.6)	200	100
Compound **2** (*Pseudomonas* sp. THA 6.6)	100	100
Compound **3** (*Pseudomonas* sp. THA6.6)	200 (100*)	100
Compound **4** (*Pseudomonas* sp. THA6.6)	50 (25*)	50 (25*)
Compound **9** (*Pseudomonas* sp. SFB8.6)	200	100
Compound **10** (*Pseudomonas* sp. SFB8.6)	200	100
Cycloheximide (positive control)	0.39	1.56 (0.78*)

In the observed assay results, the images showed that pseudodesmin A and **4** were precipitated at the highest concentration. Additionally, **9** and **10** were a bit insoluble and appeared like dumbbell-shaped particles in the assay solution. In this case, the MIC values against chytrid fungi can also be false positive or true negative results for these compounds.

All the assay results were plotted in the graphs with an optical density at the y-axis versus sample concentration at the x-axis (Figure 46). The x-axis was labelled with the highest concentration (200 µg/mL) to the lowest concentration (0.09 µg/mL). Each unit of the x-axis referred to half of the concentration from the previous concentration. Thus, each unit represented the serially diluted concentration which was placed at an equal distance from its adjacent concentrations.

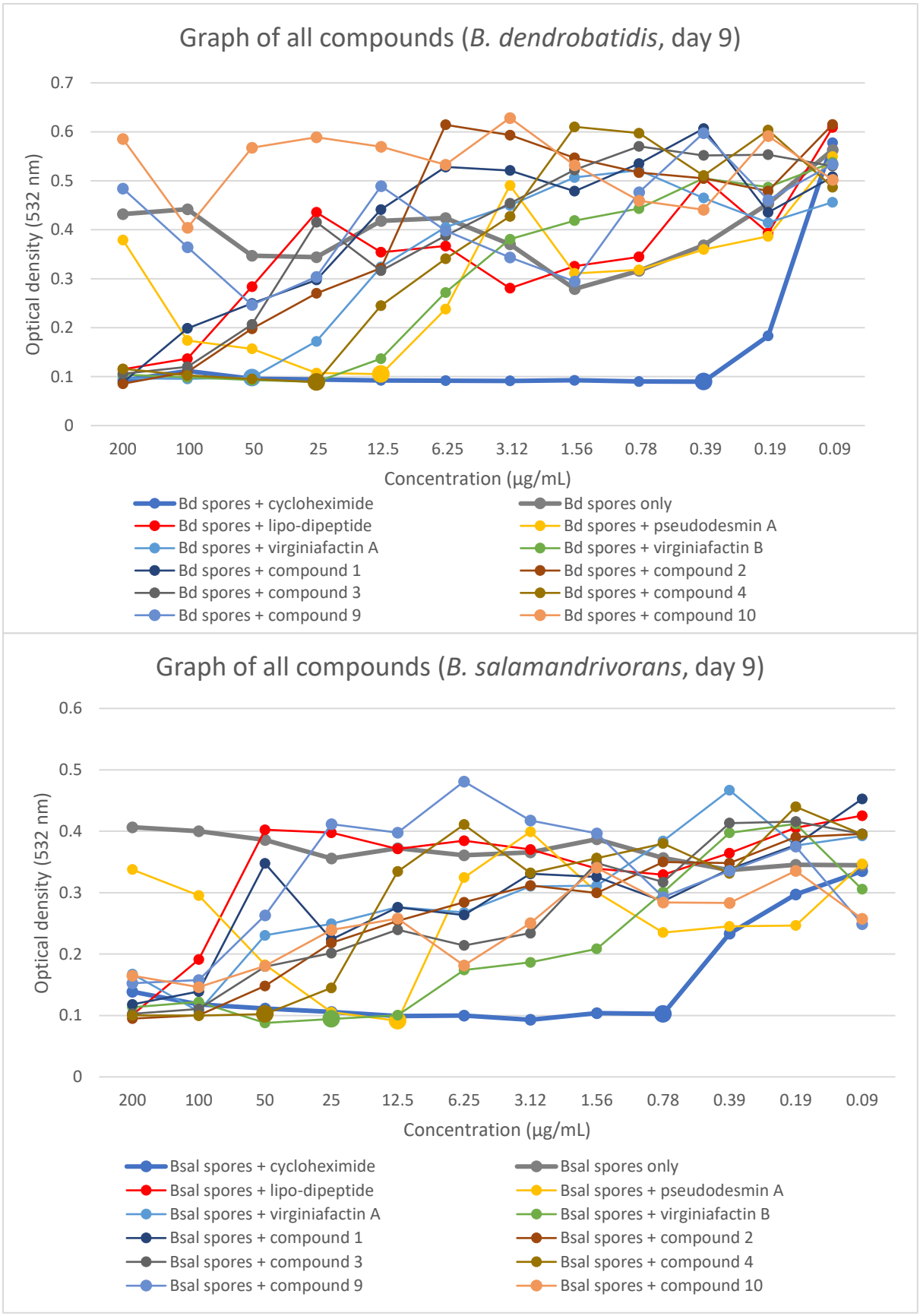

Figure 46: Graphs summarizing the results of the antifungal assay of all isolated compounds against *B. dendrobatidis* (top) and *B. salamandrivorans* (bottom) on day 9.

The results concluded only with optical densities in the graphs showed pseusodesmin A and virginiafactin B as the most active compounds against *B. salamandrivorans* with the MIC of 12.5 µg/mL, while merely pseudodesmin A was the most active agent against *B. dendrobatidis* with the same MIC value. The inhibition phenomenon of cycloheximide and virginiafactin A revealed the fact that both chytrid fungi responded differently against some antifungal compounds. As per this basis, *B. salamandrivorans* was found a bit more resistant to antifungal compounds in comparison to *B. dendrobatidis*.

5. Discussion

5.1 Analysis of the Chytrid Fungus *B. dendrobatidis*

Initially, we hypothesized that the virulence can be mediated or at least assisted by secondary metabolites which is why we sought to analyse the fungus – on the genetic as well as on the metabolic level for the production of secondary metabolites. The origin of this thought is supported by several examples reported in the literature (Figure 47). The phytopathogenic fungus *Botrytis cinerea* for example secretes the toxic sesquiterpene botrydial and oxalic acid.[95] Further examples represent the immunosuppressive gliotoxin or the fungal siderophores triacetylfusarinine C and desferriferricrocin, produced by *Aspergillus nidulans*.[96]

However, neither the genomic, nor the metabolomic analysis unveiled a significant capacity to produce secondary metabolites. While the fungal antiSMASH analysis returned no hits, the bacterial version of this program suggested at least four putative BGCs. This represents a comparatively low count of putative BGCs in contrast with filamentous fungi, which contains a range of ~15-50 BGCs, and sometime up to more than 80 BGCs.[97, 98] Possibly, there is a lack of understanding of chytrid-specific BGCs and the true number of BGCs could be greater than four.

The NRPS-like mono modular gene clusters detected in our study are split, which are usual for coding the secondary metabolites, just like in the case of fragin BGC.[99] However in our case, the terminal domain such as TE, R or TD is missing and therefore could represent an incomplete module for the release of biosynthetic products. The FDP-farnesyl transferase, detected with NCBI protein blast of the core gene from one of the terpene BGC, could enhance the pathogenicity in fungi by developing the filamentous structures (germ tubes and hyphae).[100]

The absence of secondary metabolites during the metabolomic analysis of *B. dendrobatidis* could also be influenced by the biological aspects such as growth conditions. Possibly the cultivation of chytrid fungi in a special medium, which mimics more closely the amphibians' skin-environment, may be required to activate possible silent gene clusters which might be hidden in the fungal genome.

The absence of compounds can be also explained by technical aspects such as

choosing an inappropriate extraction procedure which does not address the correct polarity or affinity of the metabolome. Furthermore, it can reasons can be found in the choice of the analytical tools. Examples in this context can be non-ionizable metabolites in the HR-MS experiments or the absence of chromophores concerning UV detection. Additionally, several metabolites have been identified as nodes in the molecular network which were not annotated due to low intensities in the HR-MS measurement, possibly caused by either weak ionization or by insufficient amounts.

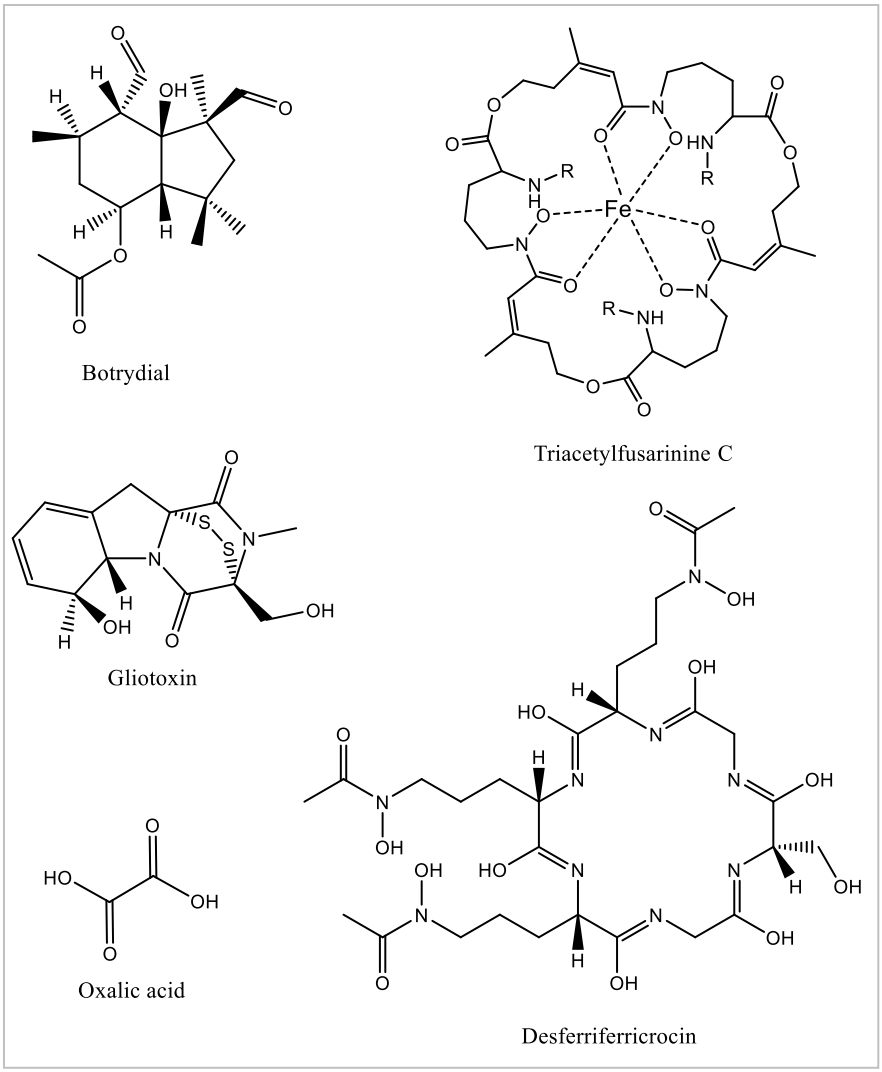

Figure 47: Structures of secondary metabolites produced by pathogenic fungi such as *Botrytis cinerea* and *Aspergillus nidulans*.

Thus, in summary the initial hypothesis that secondary metabolites are decisive in the infection process could not be supported by our genomic and chemical analyses. Due to the lack of chytrid mycotoxins, also depicted by the brine-shrimp lethality assay, this study opens the vision of alternative mode of actions in the fate of chytridiomycosis, such as enzymatic or physical mechanisms. This new hypothesis would be also in line with a recent study that reported *B. dendrobatidis*-specific genes, that in significant numbers, encode proteases (aspartyl proteases, serine type proteases and

metalloproteases) and play an important role in the attachment, penetration and growth through the host cells.[101, 102]

5.2 Anti-chytrid Bacteria from Salamander Skin

Muletz et al. reported that the extent of chytrid inhibition was independent to the phylogenetic relationship of the anti-chytrid bacteria.[25] However, five major anti-chytrid bacterial species (two *Pseudomonas* species, *Stenotrophomonas* sp., *Acinetobacter rhizosphaerae* and *Leteibacter rhizovicinus*) were found in multiple amphibian species including salamanders, globally.[103] The understanding of anti-chytrid mechanism of such bacteria could contribute to the fighting of chytridiomycosis and survival of the amphibians. The metabolomic and genomic screening of all 35 bacterial isolates from the salamander skin were not possible in this study due to time constraints. However, potent producers of secondary metabolites were selected for further study. The predominantly produced secondary metabolites were isolated, characterized and tested for their antifungal activity.

5.3 Secondary Metabolites Produced by *P. tolaasii* RSB5.11

P. tolaasii RSB5.11 produced a number of NRPS-based compounds such as pseudodesmins, a lipo-dipeptide and tolaasins. The structures of pseudodesmin A and the lipo-dipeptide were fully characterized in this study. Surprisingly, both of these compounds shared a single NRPS-BGC, which primarily encodes a nona-peptide (pseudodesmin) and a part of it independently encodes a lipo-dipeptide. There are only few literature reports for multiple NRPS-like genes encoding the same natural product produced by some fungi. For an example, aspulvinone E is encoded by two NRPS-like genes *atmelA* and *apvA*.[104] However, the reverse phenomenon of a single gene cluster with multiple products is not so far reported particularly from the genus *Pseudomonas*. In case of *P. tolaasii* RSB5.11, the first gene *ctg1_2796* of the bimodular module system, could independently encode Leu1-Gln2 sequence of the dipeptide.

The evidence of the dipeptide as an independent metabolite, not being a degradation product of pseudodesmin, is clarified by the amino acid configurations of the dipeptide. The stereochemical results of the discrete dipeptide molecule shows L-Leu1 and L-Gln2, while pseudodesmin A reveals L-Leu1 and D-Gln2 for the first two amino acids in the peptide chain. In such a case, Gln2 of pseudodesmin A could be epimerised to

D-configuration by the catalytic activity of the C-domain of the following module from the second gene *ctg1_2797*. In the case of the dipeptide, the configuration of Gln2 remained unaffected (i.e., L-configuration). This depicts the absence of roles by second and third genes in the biosynthesis of the dipeptide. Intriguingly, the analyses of further splitted NRPS-lipopeptide BGCs unveiled that this appears to be a common mechanism, but the in the amphibian *Pseudomonas* strain it was pronounced and detectable, while the plant-associated *Pseudomonas* strains produce only minute amounts of their corresponding di-lipopeptides.

Tolaasins were not isolated and hence not characterized via NMR. Nevertheless, they were observed predominantly in the bacterial genome as well as in the crude extract with pseudomolecular ions at *m/z* 994.1145, *m/z* 1001.1211, *m/z* 1003.1180 and *m/z* 1010.1257 $[M+2H]^{2+}$. Tolaasins, consisted of 18 amino acid units, are known for their biological importance of fungal growth inhibitions.[105, 106] Similarly, another NRPS biosynthetic product, pseudodesmin A, is also known for its antifungal property. Both tolaasins and pseudodesmins represented the major peaks in the HPLC chromatogram and therefore the dominant lipopeptides. The lipo-dipeptide remained inactive against chytrid fungi. Its biological role is still elusive and remains to be investigated. Furthermore, tolaasins are pseudodesmins and are well known for their surfactant characters.[107, 108] This surfactant characters help the bacteria to spread rapidly over the growing surface and occupying a niche, which could repel the growth of other surrounding microorganisms.

Tolaasins and pseudodesmins possibly could play in combination a strong role in of chytrid fungi. To completely conclude this statement, tolaasins still need to be isolated and tested in combination with pseudodesmins against the chytrid fungi.

5.4 Secondary Metabolites Produced by *Pseudomonas* sp. THA6.6

Pseudomonas sp. THA6.6 produced a lipopeptide of the amphisin family. Tensin and its three novel analogues were fully characterized as cyclic depsipeptides in this study. These analogues differ from each other either by an interchange of valine and isoleucine at the 9th position of the peptide chain or by an extension or shortening of an acetate unit in the fatty acyl chain. Biosynthetically, some adenylation domains of the NRPS biosynthesis pathway are promiscuous and can bind and activate multiple

amino acids such as leucine, isoleucine and valine.[109] The outcomes from the valine supplemented cultivation of this strain showed that the binding and activation of the amino acid could also be shifted based on the available amino acid concentration in the cultivation medium. Similarly, the different sizes of fatty acyl chain, fused to the N-terminal amino acid, can be explained by an unspecific $C_{starter}$ domain.[110] The size of fatty acid is controlled by a primary metabolism (more specifically by the involved fatty acyl synthase) where the chain extends successively by a C_2-acetate moiety.[111] In this way, compound **1** and **2** contained a C_8-fatty acyl chain while the compounds **3** and **4** contained a C_{10}-fatty acyl chain. However, the extent of the metabolites' yield based on the size of fatty acyl moiety remains still unclear.

Tensin is known as an antifungal agent that is able to reduce the radial mycelial growth of filamentous fungi.[112] In this study, tensin was also moderately active against both of the chytrid fungi, while its analogues remained inactive. Besides, tensin and its analogues, being a surfactantant, could facilitate the spreading of the bacterium on the growing surface of the amphibians' skin and hence could prevent the chytrid colonization.

5.5 Secondary Metabolites Produced by *Pseudomonas* sp. THA5.7

Pseudomonas sp. THA5.7 produced NRPS-based lipopeptides belonging to the family of linear lipo-octapeptides. They were identified as virginiafactin A, virginiafactin B and two new analogues (**7** and **8**). Again, virginiafactin A and B differs by the interchange of valine and isoleucine at the 6th position of the peptide chain, that could be attributed to the speciality of adenylation domain of the 6th NRPS module of the virginiafactin BGC. The same mechanism can explain the production of compounds **7** and **8**. These new analogues, only characterized by HR-MS, differ from virginiafactin A and B by a shortening of lipidic moiety by an acetate unit, just like the above-mentioned analogues of tensin.

Considering the bioactivity of these metabolites, the surfactant nature of virginiafactins is not yet clarified. However, virginiafactin B (AA6 as isoleucine) was found to be moderately active against chytrid fungi. Virginiafactin A (AA6 as valine) is 2 to 4 times less active against chytrid fungi than virginiafactin B. This result reveals the structure-activity relation of virginiafactins influenced by a valine and isoleucine moiety. The new

analogues were not isolated during the study due to insignificant production in the culture medium, and hence their anti-chytrid activity remained unknown.

5.6 Secondary Metabolites Produced by *Pseudomonas* sp. SFB8.6

Pseudomonas sp. SFB8.6 produced two new members of the viscosin family (**9** and **10**), through a NRPS biosynthetic pathway. They were identified as epimers of massetolide E and F, and again differ from each other by an interchange of valine and isoleucine moieties at 9th position, the terminal amino acid, of the peptide chain. The results of X-ray crystallography of compound **9** reveals the configuration of 5th amino acid as D-Leu5, which is L-Leu5 in the case of massetolide E. Other members of this family also show a similar phenomenon, which are already explained biosynthetically. For an example, WLIP differs from viscosin by a different absolute configuration of the amino acid at position 5. WLIP contains D-Leu5 whereas viscosin contains L-Leu5. The catalytic activity (epimerization) of the C-domain of the following 6th module is considered to cause this different stereochemistry.[113] In the same way, pseudophomin A and B are the epimers (D-Leu5) of massetolide A and C (L-Leu5), respectively, by a different stereochemistry at position 5.[114] A massetolide producing strain, *P. fluorescens* SS101 has been already reported to have a combined C/E domain in its BGC.[111] The similar biosynthetic route could also apply to the isolated compounds **9** and **10**. The D-configuration of the compound **9** could be accomplished due to an additional epimerization activity of a condensation domain of the following module (6th module), even though the genome sequence of this strain is not yet determined.

In this study, compound **9** and **10** remained inactive against chytrid fungi. However other massetolides and their epimers such as massetolide A and pseudophomin B have been reported to have strong antifungal activities.[92, 115] Additionally, massetolides are known to have a strong biosurfactant character.[92] In this way, compound **9** and **10** could help the spreading of bacteria on the growing surface of the amphibians' skin and hence could repel the chytrid colonisations.

5.7 Chytrid Inhibitions

The salamander skin bacteria, investigated in this study, produced a large number and quantity of lipopeptides. Most of these lipopeptides are known for their surfactant character, which help themselves to spread rapidly over the growing surface. Up on the anti-chytrid assay of these isolated lipopeptides, only four showed chytrid inhibition

in the MIC range of 12.5 to 50 µg/mL. The observed MIC values represent a rather feeble antifungal activity. However, the chytrid inhibition could be significantly influenced by a combined function of these lipopeptides. Our findings are in lines with results of other researchers. Martin et al. discovered the anti-*Bd* activity of viscosin at the MIC of 31.25 µg/mL.[116] Similarly, Guiterez et al., in some extent, determined the ecologic role of LPs. The study demonstrated the primary functions of LPs as motility, metals detoxification, biofilm formation and antimicrobial activity.[117]

There must be a reason behind the ability of these bacteria to produce such an extent of lipopeptides. A further *in-vivo* assay of these metabolites against chytrid infection can reveal the validation of their role in chytrid inhibition.

In this study, in the genome of two of the bacterial isolates, RSB5.11 and THA6.6, a pyoverdin and/or other siderophore gene clusters are present. The genus *Pseudomonas* is foremost known for their potential to produce pyoverdins, which are considered the strongest natural siderophores ever observed. A separate cultivation (iron deficient medium) and an adapted extraction protocol could be applied to isolate these metabolites. These metabolites are known to strongly chelate (and therefore trap) iron from the surrounding, and hence left nearly no iron for other microorganisms to grow. In this way, they are known to have a significant antagonistic activity.[118] This principle of iron depletion from the surrounding could also apply to the salamander skin bacteria while growing on the surface of the skin, and act as an antimicrobial factor.

Besides the roles of antifungal secondary metabolites, antifungal enzymes produced by the salamander skin bacteria could also contribute to the chytrid defence. The study showed seven strains (Figure 45) out of 35 strains produce chitinase. These enzymes possess a chitinolytic function and act on the chytrid fungi, possibly by disrupting the fungal cell wall and inhibiting their growth. The total sum of chitinase production by these amphibians' skin microbiome can reinforce the chytrid defence mechanism. However, a more precise quantitative chitinase assay is needed to explore the full effect of the chitinolytic activity. Other antifungal enzymes such as glucanase and protease may assist in the role of chytrid defence. Therefore, a further study of the bacterial isolates is needed to screen these for the presence of antifungal enzymes.[119]

Out of 35 anti-chytrid bacterial isolates, only four were extensively investigated in this study. The remaining strains, including some strong antifungal genera such as *Janthinobacterium* and *Stenotrophomonas*, deserve to be studied for a greater overview of amphibian protection against chytrids. So far, these two antifungal genera

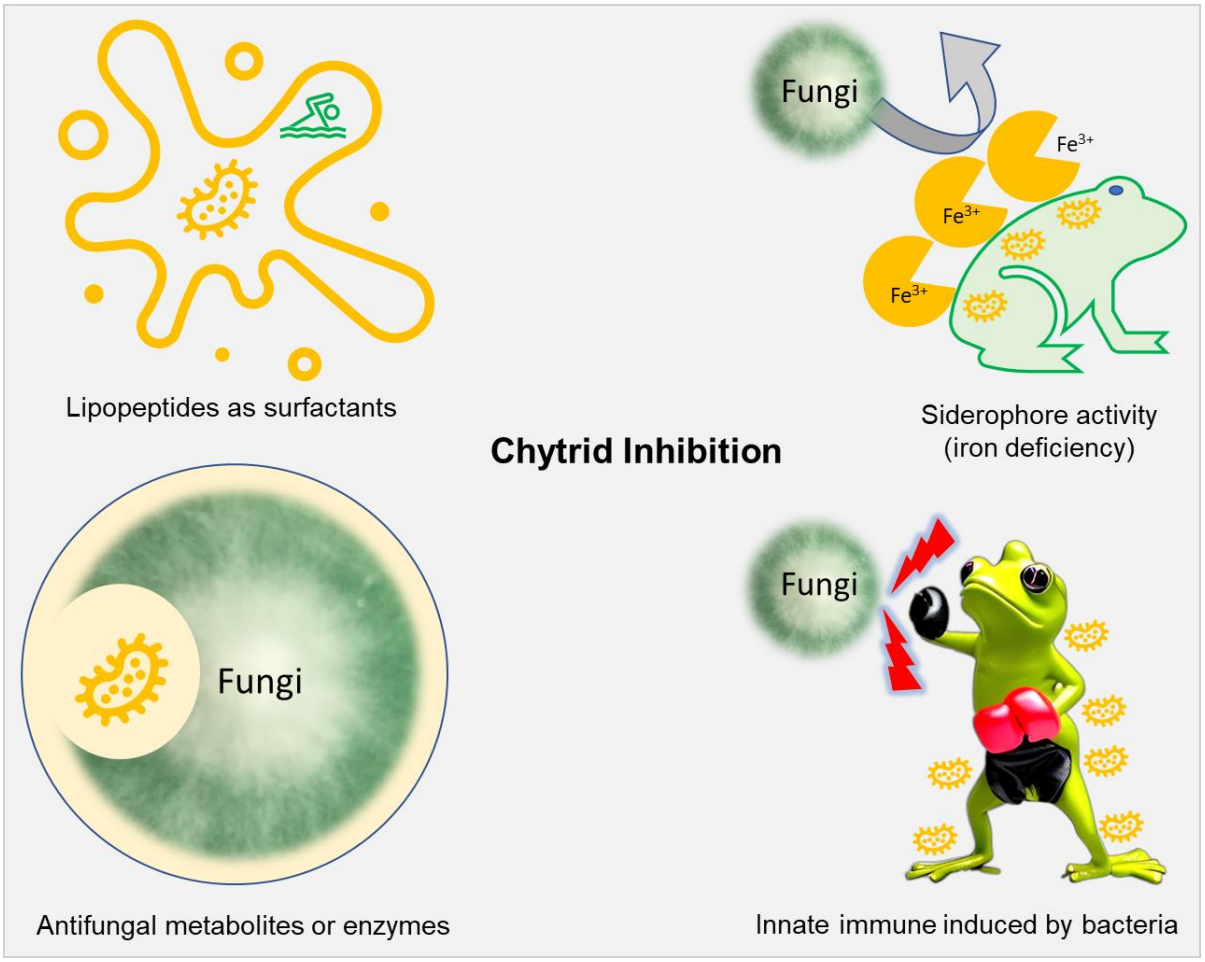

Figure 48: Schematic diagram showing chytrid inhibitions by different possible mechanisms.

are already known to produce antifungal compounds such as violacein, indole-3-carboxaldehyde and maltophillin.[85, 120] Besides, some study reported that the amphibians-symbiotic bacteria could also contribute to the innate immune defences of the amphibian species.[121]

To summarize all in one message, this study opens a ground platform to study a role of the microbiome of the amphibians' skin, for the protection against a life-threatening disease, chytridiomycosis (Figure 48). The study also opens several questions and responsibilities to future researchers regarding the welfare of ecosystems.

References

1. Blin, K.; Shaw, S.; Kloosterman, A. M.; Charlop-Powers, Z.; van Wezel, G. P.; Medema, Marnix H.; Weber, T., antiSMASH 6.0: improving cluster detection and comparison capabilities. *Nucleic Acids Research* **2021,** *49* (W1), W29-W35.
2. Oni, F. E.; Geudens, N.; Adiobo, A.; Omoboye, O. O.; Enow, E. A.; Onyeka, J. T.; Salami, A. E.; De Mot, R.; Martins, J. C.; Höfte, M., Biosynthesis and Antimicrobial Activity of Pseudodesmin and Viscosinamide Cyclic Lipopeptides Produced by Pseudomonads Associated with the Cocoyam Rhizosphere. *Microorganisms* **2020,** *8* (7), 1079.
3. Martel, A.; Spitzen-van der Sluijs, A.; Blooi, M.; Bert, W.; Ducatelle, R.; Fisher, M. C.; Woeltjes, A.; Bosman, W.; Chiers, K.; Bossuyt, F.; Pasmans, F., *Batrachochytrium salamandrivorans* sp. nov. causes lethal chytridiomycosis in amphibians. *Proceedings of the National Academy of Sciences* **2013,** *110* (38), 15325-15329. (Thesis page 4, Figure 4 - PNAS is not responsible for the accuracy of this tranlsation.)
4. Frost, D. Amphibians Species of the World 6.1, an Online Reference. American Museum of National History, 2022.
5. Hocking, D.; Babbitt, K., Amphibian contributions to ecosystem services. *Herpetological Conservation and Biology* **2014,** *9*, 1-17.
6. VanCompernolle, S. E.; Taylor, R. J.; Oswald-Richter, K.; Jiang, J.; Youree, B. E.; Bowie, J. H.; Tyler, M. J.; Conlon, J. M.; Wade, D.; Aiken, C.; Dermody, T. S.; KewalRamani, V. N.; Rollins-Smith, L. A.; Unutmaz, D., Antimicrobial Peptides from Amphibian Skin Potently Inhibit Human Immunodeficiency Virus Infection and Transfer of Virus from Dendritic Cells to T Cells. *Journal of Virology* **2005,** *79* (18), 11598-11606.
7. Bergaoui, I.; Zairi, A.; Tangy, F.; Aouni, M.; Selmi, B.; Hani, K., In vitro antiviral activity of dermaseptin S4 and derivatives from amphibian skin against herpes simplex virus type 2. *Journal of Medical Virology* **2013,** *85* (2), 272-281.
8. Daly, J. W.; Martin Garraffo, H.; Spande, T. F.; Decker, M. W.; Sullivan, J. P.; Williams, M., Alkaloids from frog skin: the discovery of epibatidine and the potential for developing novel non-opioid analgesics. *Natural Product Reports* **2000,** *17* (2), 131-135.
9. Stuart, S. N.; Chanson, J. S.; Cox, N. A.; Young, B. E.; Rodrigues, A. S. L.; Fischman, D. L.; Waller, R. W., Status and Trends of Amphibian Declines and Extinctions Worldwide. *Science* **2004,** *306* (5702), 1783-1786.
10. IUCN The IUCN Red List of Threatened Species. Version 2021-3. https://www.iucnredlist.org.
11. Fisher, M. C.; Henk, D. A.; Briggs, C. J.; Brownstein, J. S.; Madoff, L. C.; McCraw, S. L.; Gurr, S. J., Emerging fungal threats to animal, plant and ecosystem health. *Nature* **2012,** *484* (7393), 186-194.
12. Lips, K. R., Overview of chytrid emergence and impacts on amphibians. *Philos Trans R Soc Lond B Biol Sci* **2016,** *371* (1709).
13. Martel, A.; Blooi, M.; Adriaensen, C.; Van Rooij, P.; Beukema, W.; Fisher, M. C.; Farrer, R. A.; Schmidt, B. R.; Tobler, U.; Goka, K.; Lips, K. R.; Muletz, C.; Zamudio, K. R.; Bosch, J.; Lötters, S.; Wombwell, E.; Garner, T. W. J.; Cunningham, A. A.; Spitzen-van der Sluijs, A.; Salvidio, S.; Ducatelle, R.; Nishikawa, K.; Nguyen, T. T.; Kolby, J. E.; Van Bocxlaer, I.; Bossuyt, F.; Pasmans, F., Recent introduction of a chytrid fungus endangers Western Palearctic salamanders. *Science* **2014,** *346* (6209), 630-631.
14. Ohst, T.; Graeser, Y.; Plötner, J., *Batrachochytrium dendrobatidis* in Germany: Distribution, prevalences, and prediction of high risk areas. *Diseases of aquatic organisms* **2013,** *107*, 49-59.

15. Olson, D. H.; Ronnenberg, K. L.; Glidden, C. K.; Christiansen, K. R.; Blaustein, A. R., Global Patterns of the Fungal Pathogen *Batrachochytrium dendrobatidis* Support Conservation Urgency. *Frontiers in Veterinary Science* **2021,** *8*.
16. Burrowes, P. A.; De la Riva, I., Detection of the Amphibian Chytrid Fungus *Batrachochytrium dendrobatidis* in Museum Specimens of Andean Aquatic Birds: Implications for Pathogen Dispersal. *J Wildl Dis* **2017,** *53* (2), 349-355.
17. Garmyn, A.; Van Rooij, P.; Pasmans, F.; Hellebuyck, T.; Van Den Broeck, W.; Haesebrouck, F.; Martel, A., Waterfowl: Potential Environmental Reservoirs of the Chytrid Fungus *Batrachochytrium dendrobatidis*. *PLOS ONE* **2012,** *7* (4), e35038.
18. Berger, L.; Speare, R.; Daszak, P.; Green, D. E.; Cunningham, A. A.; Goggin, C. L.; Slocombe, R.; Ragan, M. A.; Hyatt, A. D.; McDonald, K. R.; Hines, H. B.; Lips, K. R.; Marantelli, G.; Parkes, H., Chytridiomycosis causes amphibian mortality associated with population declines in the rain forests of Australia and Central America. *Proceedings of the National Academy of Sciences* **1998,** *95* (15), 9031-9036.
19. Longcore, J. E.; Pessier, A. P.; Nichols, D. K., *Batrachochytrium dendrobatidis* gen. et sp. nov., a chytrid pathogenic to amphibians. *Mycologia* **1999,** *91* (2), 219-227.
20. Van Rooij, P.; Martel, A.; Haesebrouck, F.; Pasmans, F., Amphibian chytridiomycosis: a review with focus on fungus-host interactions. *Veterinary Research* **2015,** *46* (1), 137.
21. Gray, M. J.; Lewis, J. P.; Nanjappa, P.; Klocke, B.; Pasmans, F.; Martel, A.; Stephen, C.; Parra Olea, G.; Smith, S. A.; Sacerdote-Velat, A.; Christman, M. R.; Williams, J. M.; Olson, D. H., *Batrachochytrium salamandrivorans*: The North American Response and a Call for Action. *PLOS Pathogens* **2015,** *11* (12), e1005251.
22. Voyles, J.; Young, S.; Berger, L.; Campbell, C.; Voyles, W. F.; Dinudom, A.; Cook, D.; Webb, R.; Alford, R. A.; Skerratt, L. F.; Speare, R., Pathogenesis of Chytridiomycosis, a Cause of Catastrophic Amphibian Declines. *Science* **2009,** *326* (5952), 582-585.
23. Jiménez, R. R.; Alvarado, G.; Estrella, J.; Sommer, S., Moving Beyond the Host: Unraveling the Skin Microbiome of Endangered Costa Rican Amphibians. *Front Microbiol* **2019,** *10*, 2060.
24. Grogan, L. F.; Robert, J.; Berger, L.; Skerratt, L. F.; Scheele, B. C.; Castley, J. G.; Newell, D. A.; McCallum, H. I., Review of the Amphibian Immune Response to Chytridiomycosis, and Future Directions. *Frontiers in Immunology* **2018,** *9*.
25. Muletz-Wolz, C. R.; DiRenzo, G. V.; Yarwood, S. A.; Grant, E. H. C.; Fleischer, R. C.; Lips, K. R., Antifungal Bacteria on Woodland Salamander Skin Exhibit High Taxonomic Diversity and Geographic Variability. *Applied and Environmental Microbiology* **2017,** *83* (9), e00186-17.
26. Grice, E. A.; Segre, J. A., The skin microbiome. *Nature Reviews Microbiology* **2011,** *9* (4), 244-253.
27. Scott, J. J.; Oh, D.-C.; Yuceer, M. C.; Klepzig, K. D.; Clardy, J.; Currie, C. R., Bacterial Protection of Beetle-Fungus Mutualism. *Science* **2008,** *322* (5898), 63-63.
28. Kaltenpoth, M.; Göttler, W.; Herzner, G.; Strohm, E., Symbiotic Bacteria Protect Wasp Larvae from Fungal Infestation. *Current Biology* **2005,** *15* (5), 475-479.
29. Currie, C. R.; Scott, J. A.; Summerbell, R. C.; Malloch, D., Fungus-growing ants use antibiotic-producing bacteria to control garden parasites. *Nature* **1999,** *398* (6729), 701-704.
30. Byrd, A. L.; Belkaid, Y.; Segre, J. A., The human skin microbiome. *Nature Reviews Microbiology* **2018,** *16* (3), 143-155.
31. Harris, R. N.; Brucker, R. M.; Walke, J. B.; Becker, M. H.; Schwantes, C. R.; Flaherty, D. C.; Lam, B. A.; Woodhams, D. C.; Briggs, C. J.; Vredenburg, V. T.; Minbiole, K. P. C., Skin microbes on frogs prevent morbidity and mortality caused by a lethal skin fungus. *The ISME Journal* **2009,** *3* (7), 818-824.
32. Becker, M. H.; Brophy, J. A. N.; Barrett, K.; Bronikowski, E.; Evans, M.; Glassey, E.; Kaganer, A. W.; Klocke, B.; Lassiter, E.; Meyer, A. J.; Muletz-Wolz, C. R.; Fleischer,

R. C.; Voigt, C. A.; Gratwicke, B., Genetically modifying skin microbe to produce violacein and augmenting microbiome did not defend Panamanian golden frogs from disease. *ISME Communications* **2021,** *1* (1), 57.
33. Jiménez, R. R.; Carfagno, A.; Linhoff, L.; Gratwicke, B.; Woodhams, D. C.; Chafran, L. S.; Bletz, M. C.; Bishop, B.; Muletz-Wolz, C. R., Inhibitory Bacterial Diversity and Mucosome Function Differentiate Susceptibility of Appalachian Salamanders to Chytrid Fungal Infection. *Appl Environ Microbiol* **2022,** *88* (8), e0181821.
34. Muletz-Wolz, C. R.; Almario, J. G.; Barnett, S. E.; DiRenzo, G. V.; Martel, A.; Pasmans, F.; Zamudio, K. R.; Toledo, L. F.; Lips, K. R., Inhibition of Fungal Pathogens across Genotypes and Temperatures by Amphibian Skin Bacteria. *Front Microbiol* **2017,** *8*, 1551.
35. Driscoll, J. A.; Brody, S. L.; Kollef, M. H., The Epidemiology, Pathogenesis and Treatment of *Pseudomonas aeruginosa* Infections. *Drugs* **2007,** *67* (3), 351-368.
36. Vesga, P.; Flury, P.; Vacheron, J.; Keel, C.; Croll, D.; Maurhofer, M., Transcriptome plasticity underlying plant root colonization and insect invasion by *Pseudomonas protegens*. *The ISME Journal* **2020,** *14* (11), 2766-2782.
37. Wiklund, T., *Pseudomonas anguilliseptica* infection as a threat to wild and farmed fish in the Baltic Sea. *Microbiology Australia* **2016,** *37* (3), 135-136.
38. Sah, S.; Krishnani, S.; Singh, R., Pseudomonas mediated nutritional and growth promotional activities for sustainable food security. *Curr Res Microb Sci* **2021,** *2*, 100084.
39. Demain, A. L.; Fang, A., The natural functions of secondary metabolites. *Adv Biochem Eng Biotechnol* **2000,** *69*, 1-39.
40. Picard, C.; Bosco, M., Heterozygosis drives maize hybrids to select elite 2,4-diacethylphloroglucinol-producing Pseudomonas strains among resident soil populations. *FEMS Microbiol Ecol* **2006,** *58* (2), 193-204.
41. Gao, S.-S.; Hothersall, J.; Wu, J. e.; Murphy, A. C.; Song, Z.; Stephens, E. R.; Thomas, C. M.; Crump, M. P.; Cox, R. J.; Simpson, T. J.; Willis, C. L., Biosynthesis of Mupirocin by *Pseudomonas fluorescens* NCIMB 10586 Involves Parallel Pathways. *Journal of the American Chemical Society* **2014,** *136* (14), 5501-5507.
42. Wiesner, W.; van Pee, K. H.; Lingens, F., Detection of a new chloroperoxidase in *Pseudomonas pyrrocinia*. *FEBS Lett* **1986,** *209* (2), 321-4.
43. Kerr, J. R.; Taylor, G. W.; Rutman, A.; Høiby, N.; Cole, P. J.; Wilson, R., *Pseudomonas aeruginosa* pyocyanin and 1-hydroxyphenazine inhibit fungal growth. *J Clin Pathol* **1999,** *52* (5), 385-7.
44. Takase, H.; Nitanai, H.; Hoshino, K.; Otani, T., Impact of siderophore production on *Pseudomonas aeruginosa* infections in immunosuppressed mice. *Infect Immun* **2000,** *68* (4), 1834-9.
45. Remichkova, M.; Galabova, D.; Roeva, I.; Karpenko, E.; Shulga, A.; Galabov, A. S., Anti-herpesvirus activities of *Pseudomonas* sp. S-17 rhamnolipid and its complex with alginate. *Z Naturforsch C J Biosci* **2008,** *63* (1-2), 75-81.
46. Hamley, I. W., Lipopeptides: from self-assembly to bioactivity. *Chemical Communications* **2015,** *51* (41), 8574-8583.
47. Götze, S.; Stallforth, P., Structure elucidation of bacterial nonribosomal lipopeptides. *Organic & Biomolecular Chemistry* **2020,** *18* (9), 1710-1727.
48. Flissi, A.; Ricart, E.; Campart, C.; Chevalier, M.; Dufresne, Y.; Michalik, J.; Jacques, P.; Flahaut, C.; Lisacek, F.; Leclère, V.; Pupin, M., Norine: update of the nonribosomal peptide resource. *Nucleic Acids Research* **2019,** *48* (D1), D465-D469.
49. Schneider, T.; Müller, A.; Miess, H.; Gross, H., Cyclic lipopeptides as antibacterial agents - potent antibiotic activity mediated by intriguing mode of actions. *Int J Med Microbiol* **2014,** *304* (1), 37-43.
50. Baltz, R. H.; Miao, V.; Wrigley, S. K., Natural products to drugs: daptomycin and related lipopeptide antibiotics. *Nat Prod Rep* **2005,** *22* (6), 717-41.

51. Winter, J. M.; Tang, Y., Synthetic biological approaches to natural product biosynthesis. *Current Opinion in Biotechnology* **2012,** *23* (5), 736-743.
52. Wenski, S. L.; Thiengmag, S.; Helfrich, E. J. N., Complex peptide natural products: Biosynthetic principles, challenges and opportunities for pathway engineering. *Synthetic and Systems Biotechnology* **2022,** *7* (1), 631-647.
53. Jahanshah, G.; Yan, Q.; Gerhardt, H.; Pataj, Z.; Lämmerhofer, M.; Pianet, I.; Josten, M.; Sahl, H.-G.; Silby, M. W.; Loper, J. E.; Gross, H., Discovery of the Cyclic Lipopeptide Gacamide A by Genome Mining and Repair of the Defective GacA Regulator in *Pseudomonas fluorescens* Pf0-1. *Journal of Natural Products* **2019,** *82* (2), 301-308.
54. Albarano, L.; Esposito, R. T.; Ruocco, N.; Costantini, M., Genome Mining as New Challenge in Natural Products Discovery. *Marine Drugs* **2020,** *18*.
55. Hautbergue, T.; Jamin, E. L.; Costantino, R.; Tadrist, S.; Meneghetti, L.; Tabet, J.-C.; Debrauwer, L.; Oswald, I. P.; Puel, O., Combination of Isotope Labeling and Molecular Networking of Tandem Mass Spectrometry Data To Reveal 69 Unknown Metabolites Produced by *Penicillium nordicum*. *Analytical Chemistry* **2019,** *91* (19), 12191-12202.
56. Wang, M.; Carver, J. J.; Phelan, V. V.; Sanchez, L. M.; Garg, N.; Peng, Y.; Nguyen, D. D.; Watrous, J.; Kapono, C. A.; Luzzatto-Knaan, T.; Porto, C.; Bouslimani, A.; Melnik, A. V.; Meehan, M. J.; Liu, W. T.; Crüsemann, M.; Boudreau, P. D.; Esquenazi, E.; Sandoval-Calderón, M.; Kersten, R. D.; Pace, L. A.; Quinn, R. A.; Duncan, K. R.; Hsu, C. C.; Floros, D. J.; Gavilan, R. G.; Kleigrewe, K.; Northen, T.; Dutton, R. J.; Parrot, D.; Carlson, E. E.; Aigle, B.; Michelsen, C. F.; Jelsbak, L.; Sohlenkamp, C.; Pevzner, P.; Edlund, A.; McLean, J.; Piel, J.; Murphy, B. T.; Gerwick, L.; Liaw, C. C.; Yang, Y. L.; Humpf, H. U.; Maansson, M.; Keyzers, R. A.; Sims, A. C.; Johnson, A. R.; Sidebottom, A. M.; Sedio, B. E.; Klitgaard, A.; Larson, C. B.; P, C. A. B.; Torres-Mendoza, D.; Gonzalez, D. J.; Silva, D. B.; Marques, L. M.; Demarque, D. P.; Pociute, E.; O'Neill, E. C.; Briand, E.; Helfrich, E. J. N.; Granatosky, E. A.; Glukhov, E.; Ryffel, F.; Houson, H.; Mohimani, H.; Kharbush, J. J.; Zeng, Y.; Vorholt, J. A.; Kurita, K. L.; Charusanti, P.; McPhail, K. L.; Nielsen, K. F.; Vuong, L.; Elfeki, M.; Traxler, M. F.; Engene, N.; Koyama, N.; Vining, O. B.; Baric, R.; Silva, R. R.; Mascuch, S. J.; Tomasi, S.; Jenkins, S.; Macherla, V.; Hoffman, T.; Agarwal, V.; Williams, P. G.; Dai, J.; Neupane, R.; Gurr, J.; Rodríguez, A. M. C.; Lamsa, A.; Zhang, C.; Dorrestein, K.; Duggan, B. M.; Almaliti, J.; Allard, P. M.; Phapale, P.; Nothias, L. F.; Alexandrov, T.; Litaudon, M.; Wolfender, J. L.; Kyle, J. E.; Metz, T. O.; Peryea, T.; Nguyen, D. T.; VanLeer, D.; Shinn, P.; Jadhav, A.; Müller, R.; Waters, K. M.; Shi, W.; Liu, X.; Zhang, L.; Knight, R.; Jensen, P. R.; Palsson, B. O.; Pogliano, K.; Linington, R. G.; Gutiérrez, M.; Lopes, N. P.; Gerwick, W. H.; Moore, B. S.; Dorrestein, P. C.; Bandeira, N., Sharing and community curation of mass spectrometry data with Global Natural Products Social Molecular Networking. *Nat Biotechnol* **2016,** *34* (8), 828-837.
57. Quinn, R. A.; Nothias, L.-F.; Vining, O.; Meehan, M.; Esquenazi, E.; Dorrestein, P. C., Molecular Networking As a Drug Discovery, Drug Metabolism, and Precision Medicine Strategy. *Trends in Pharmacological Sciences* **2017,** *38* (2), 143-154.
58. Dührkop, K.; Fleischauer, M.; Ludwig, M.; Aksenov, A. A.; Melnik, A. V.; Meusel, M.; Dorrestein, P. C.; Rousu, J.; Böcker, S., SIRIUS 4: a rapid tool for turning tandem mass spectra into metabolite structure information. *Nature Methods* **2019,** *16* (4), 299-302.
59. Shannon, P.; Markiel, A.; Ozier, O.; Baliga, N. S.; Wang, J. T.; Ramage, D.; Amin, N.; Schwikowski, B.; Ideker, T., Cytoscape: a software environment for integrated models of biomolecular interaction networks. *Genome Res* **2003,** *13* (11), 2498-504.
60. Pluskal, T.; Castillo, S.; Villar-Briones, A.; Oresic, M., MZmine 2: modular framework for processing, visualizing, and analyzing mass spectrometry-based molecular profile data. *BMC Bioinformatics* **2010,** *11*, 395.

61. Smith, C. A.; Want, E. J.; O'Maille, G.; Abagyan, R.; Siuzdak, G., XCMS: processing mass spectrometry data for metabolite profiling using nonlinear peak alignment, matching, and identification. *Anal Chem* **2006,** *78* (3), 779-87.
62. Lommen, A., MetAlign: interface-driven, versatile metabolomics tool for hyphenated full-scan mass spectrometry data preprocessing. *Anal Chem* **2009,** *81* (8), 3079-86.
63. Hao, L.; Wang, J.; Page, D.; Asthana, S.; Zetterberg, H.; Carlsson, C.; Okonkwo, O. C.; Li, L., Comparative Evaluation of MS-based Metabolomics Software and Its Application to Preclinical Alzheimer's Disease. *Sci Rep* **2018,** *8* (1), 9291.
64. Emwas, A. H.; Roy, R.; McKay, R. T.; Tenori, L.; Saccenti, E.; Gowda, G. A. N.; Raftery, D.; Alahmari, F.; Jaremko, L.; Jaremko, M.; Wishart, D. S., NMR Spectroscopy for Metabolomics Research. *Metabolites* **2019,** *9* (7).
65. Wolfender, J.-L.; Nuzillard, J.-M.; van der Hooft, J. J. J.; Renault, J.-H.; Bertrand, S., Accelerating Metabolite Identification in Natural Product Research: Toward an Ideal Combination of Liquid Chromatography–High-Resolution Tandem Mass Spectrometry and NMR Profiling, in Silico Databases, and Chemometrics. *Analytical Chemistry* **2019,** *91* (1), 704-742.
66. He, Z.; Yu, W., Improving peptide identification with single-stage mass spectrum peaks. *Bioinformatics* **2009,** *25* (22), 2969-2974.
67. Wilding-McBride, D.; Dagley, L. F.; Spall, S. K.; Infusini, G.; Webb, A. I., Simplifying MS1 and MS2 spectra to achieve lower mass error, more dynamic range, and higher peptide identification confidence on the Bruker timsTOF Pro. *PLOS ONE* **2022,** *17* (7), e0271025.
68. Giné, R.; Capellades, J.; Badia, J. M.; Vughs, D.; Schwaiger-Haber, M.; Alexandrov, T.; Vinaixa, M.; Brunner, A. M.; Patti, G. J.; Yanes, O., HERMES: a molecular-formula-oriented method to target the metabolome. *Nature Methods* **2021,** *18* (11), 1370-1376.
69. María-Concepción, A.; Miguel, A. S.; Fidel, T., Peptides. In *Handbook of Muscle Foods Analysis*, CRC Press: 2008.
70. Amoresano, A.; Carpentieri, A.; Giangrande, C.; Palmese, A.; Chiappetta, G.; Marino, G.; Pucci, P., Technical advances in proteomics mass spectrometry: identification of post-translational modifications. *Clinical Chemistry and Laboratory Medicine* **2009,** *47* (6), 647-665.
71. Liu, W. T.; Ng, J.; Meluzzi, D.; Bandeira, N.; Gutierrez, M.; Simmons, T. L.; Schultz, A. W.; Linington, R. G.; Moore, B. S.; Gerwick, W. H.; Pevzner, P. A.; Dorrestein, P. C., Interpretation of tandem mass spectra obtained from cyclic nonribosomal peptides. *Anal Chem* **2009,** *81* (11), 4200-9.
72. Ma, Z.; Hu, J.; Wang, X.; Wang, S., NMR spectroscopic and MS/MS spectrometric characterization of a new lipopeptide antibiotic bacillopeptin B1 produced by a marine sediment-derived *Bacillus amyloliquefaciens* SH-B74. *The Journal of Antibiotics* **2014,** *67* (2), 175-178.
73. Baumgart, F.; Kluge, B.; Ullrich, C.; Vater, J.; Ziessow, D., Identification of amino acid substitutions in the lipopeptide surfactin using 2D NMR spectroscopy. *Biochemical and Biophysical Research Communications* **1991,** *177* (3), 998-1005.
74. Zaas, A. K.; Alexander, B. D., Echinocandins: role in antifungal therapy, 2005. *Expert Opinion on Pharmacotherapy* **2005,** *6* (10), 1657-1668.
75. Shih, H.-D.; Liu, Y.-C.; Hsu, F.-L.; Mulabagal, V.; Dodda, R.; Huang, J.-W., Fungichromin: A Substance from *Streptomyces padanus* with Inhibitory Effects on Rhizoctonia solani. *Journal of Agricultural and Food Chemistry* **2003,** *51* (1), 95-99.
76. Kuc, J., Antifungal Compounds from Plants. In *Phytochemical Resources for Medicine and Agriculture*, Nigg, H. N.; Seigler, D., Eds. Springer US: Boston, MA, 1992; pp 159-184.
77. Choi, S. Y.; Yoon, K. H.; Lee, J. I.; Mitchell, R. J., Violacein: Properties and Production of a Versatile Bacterial Pigment. *Biomed Res Int* **2015,** *2015*, 465056.

78. Jakobi, M.; Winkelmann, G.; Kaiser, D.; Kempler, C.; Jung, G.; Berg, G.; Bahl, H., Maltophilin: a new antifungal compound produced by *Stenotrophomonas maltophilia* R3089. *J Antibiot (Tokyo)* **1996,** *49* (11), 1101-4.
79. Gleeson, O.; O'Gara, F.; Morrissey, J. P., The *Pseudomonas fluorescens* secondary metabolite 2,4 diacetylphloroglucinol impairs mitochondrial function in *Saccharomyces cerevisiae*. *Antonie Van Leeuwenhoek* **2010,** *97* (3), 261-73.
80. Robak, M. J.; Richards-Zawacki, C. L., Temperature-Dependent Effects of Cutaneous Bacteria on a Frog's Tolerance of Fungal Infection. *Frontiers in Microbiology* **2018,** *9*.
81. Martin, H. C.; Ibáñez, R.; Nothias, L. F.; Boya, P. C.; Reinert, L. K.; Rollins-Smith, L. A.; Dorrestein, P. C.; Gutiérrez, M., Viscosin-like lipopeptides from frog skin bacteria inhibit *Aspergillus fumigatus* and *Batrachochytrium dendrobatidis* detected by imaging mass spectrometry and molecular networking. *Sci Rep* **2019,** *9* (1), 3019.
82. Boyle, D. G.; Hyatt, A. D.; Daszak, P.; Berger, L.; Longcore, J. E.; Porter, D.; Hengstberger, S. G.; Olsen, V., Cryo-archiving of *Batrachochytrium dendrobatidis* and other chytridiomycetes. *Dis Aquat Organ* **2003,** *56* (1), 59-64.
83. Paudel, B.; Bhattarai, K.; Bhattarai, H. D., Antimicrobial and antioxidant activities of two polyketides from lichen-endophytic fungus *Preussia* sp. *Z Naturforsch C J Biosci* **2018,** *73* (3-4), 161-163.
84. Hsu, S. C.; Lockwood, J. L., Powdered Chitin Agar as a Selective Medium for Enumeration of Actinomycetes in Water and Soil. *Applied Microbiology* **1975,** *29*, 422 - 426.
85. Brucker, R. M.; Harris, R. N.; Schwantes, C. R.; Gallaher, T. N.; Flaherty, D. C.; Lam, B. A.; Minbiole, K. P. C., Amphibian Chemical Defense: Antifungal Metabolites of the Microsymbiont *Janthinobacterium lividum* on the Salamander Plethodon cinereus. *Journal of Chemical Ecology* **2008,** *34* (11), 1422-1429.
86. Lindauer, A.; May, T.; Rios-Sotelo, G.; Sheets, C.; Voyles, J., Quantifying *Batrachochytrium dendrobatidis* and *Batrachochytrium salamandrivorans* Viability. *Ecohealth* **2019,** *16* (2), 346-350.
87. Siciliano, C.; Barattucci, A.; Bonaccorsi, P.; Di Gioia, M. L.; Leggio, A.; Minuti, L.; Romio, E.; Temperini, A., Synthesis of d-erythro-Sphinganine through Serine-Derived α-Amino Epoxides. *The Journal of Organic Chemistry* **2014,** *79* (11), 5320-5326.
88. Jha, B. N.; Shrestha, M.; Pandey, D. P.; Bhattarai, T.; Bhattarai, H. D.; Paudel, B., Investigation of antioxidant, antimicrobial and toxicity activities of lichens from high altitude regions of Nepal. *BMC Complementary and Alternative Medicine* **2017,** *17* (1), 282.
89. Harrison, A. G.; Young, A. B., Fragmentation of protonated oligoalanines: Amide bond cleavage and beyond. *Journal of the American Society for Mass Spectrometry* **2004,** *15* (12), 1810-1819.
90. Harsch, T.; Schneider, P.; Kieninger, B.; Donaubauer, H.; Kalbitzer, H. R., Stereospecific assignment of the asparagine and glutamine sidechain amide protons in proteins from chemical shift analysis. *J Biomol NMR* **2017,** *67* (2), 157-164.
91. Sinnaeve, D.; Michaux, C.; Van hemel, J.; Vandenkerckhove, J.; Peys, E.; Borremans, F. A. M.; Sas, B.; Wouters, J.; Martins, J. C., Structure and X-ray conformation of pseudodesmins A and B, two new cyclic lipodepsipeptides from *Pseudomonas* bacteria. *Tetrahedron* **2009,** *65* (21), 4173-4181.
92. de Bruijn, I.; de Kock, M. J.; de Waard, P.; van Beek, T. A.; Raaijmakers, J. M., Massetolide A biosynthesis in *Pseudomonas fluorescens*. *J Bacteriol* **2008,** *190* (8), 2777-89.
93. Götze, S.; Arp, J.; Lackner, G.; Zhang, S.; Kries, H.; Klapper, M.; García-Altares, M.; Willing, K.; Günther, M.; Stallforth, P., Structure elucidation of the syringafactin lipopeptides provides insight in the evolution of nonribosomal peptide synthetases. *Chemical Science* **2019,** *10* (48), 10979-10990.

94. Gerard, J.; Lloyd, R.; Barsby, T.; Haden, P.; Kelly, M. T.; Andersen, R. J., Massetolides A−H, Antimycobacterial Cyclic Depsipeptides Produced by Two Pseudomonads Isolated from Marine Habitats. *Journal of Natural Products* **1997,** *60* (3), 223-229.
95. González, C.; Brito, N.; Sharon, A., Infection Process and Fungal Virulence Factors. In *Botrytis – the Fungus, the Pathogen and its Management in Agricultural Systems*, Fillinger, S.; Elad, Y., Eds. Springer International Publishing: Cham, 2016; pp 229-246.
96. Eisendle, M.; Oberegger, H.; Zadra, I.; Haas, H., The siderophore system is essential for viability of *Aspergillus nidulans*: functional analysis of two genes encoding l-ornithine N 5-monooxygenase (sidA) and a non-ribosomal peptide synthetase (sidC). *Molecular Microbiology* **2003,** *49* (2), 359-375.
97. Robey, M. T.; Caesar, L. K.; Drott, M. T.; Keller, N. P.; Kelleher, N. L., An interpreted atlas of biosynthetic gene clusters from 1,000 fungal genomes. *Proceedings of the National Academy of Sciences* **2021,** *118* (19), e2020230118.
98. Schüller, A.; Studt-Reinhold, L.; Strauss, J., How to Completely Squeeze a Fungus—Advanced Genome Mining Tools for Novel Bioactive Substances. *Pharmaceutics* **2022,** *14* (9), 1837.
99. Jenul, C.; Sieber, S.; Daeppen, C.; Mathew, A.; Lardi, M.; Pessi, G.; Hoepfner, D.; Neuburger, M.; Linden, A.; Gademann, K.; Eberl, L., Biosynthesis of fragin is controlled by a novel quorum sensing signal. *Nature Communications* **2018,** *9* (1), 1297.
100. McGeady, P.; Logan, D. A.; Wansley, D. L., A protein-farnesyl transferase inhibitor interferes with the serum-induced conversion of *Candida albicans* from a cellular yeast form to a filamentous form. *FEMS Microbiology Letters* **2002,** *213* (1), 41-44.
101. Joneson, S.; Stajich, J. E.; Shiu, S.-H.; Rosenblum, E. B., Genomic Transition to Pathogenicity in Chytrid Fungi. *PLOS Pathogens* **2011,** *7* (11), e1002338.
102. Monod, M.; Capoccia, S.; Léchenne, B.; Zaugg, C.; Holdom, M.; Jousson, O., Secreted proteases from pathogenic fungi. *International Journal of Medical Microbiology* **2002,** *292* (5), 405-419.
103. Woodhams, D. C.; Alford, R. A.; Antwis, R. E.; Archer, H.; Becker, M. H.; Belden, L. K.; Bell, S. C.; Bletz, M.; Daskin, J. H.; Davis, L. R.; Flechas, S. V.; Lauer, A.; Gonzalez, A.; Harris, R. N.; Holden, W. M.; Hughey, M. C.; Ibáñez, R.; Knight, R.; Kueneman, J.; Rabemananjara, F.; Reinert, L. K.; Rollins-Smith, L. A.; Roman-Rodriguez, F.; Shaw, S. D.; Walke, J. B.; McKenzie, V., Antifungal isolates database of amphibian skin-associated bacteria and function against emerging fungal pathogens. *Ecology* **2015,** *96* (2), 595-595.
104. Guo, C.-J.; Sun, W.-W.; Bruno, K. S.; Oakley, B. R.; Keller, N. P.; Wang, C. C. C., Spatial regulation of a common precursor from two distinct genes generates metabolite diversity. *Chemical Science* **2015,** *6* (10), 5913-5921.
105. Bassarello, C.; Lazzaroni, S.; Bifulco, G.; Lo Cantore, P.; Iacobellis, N. S.; Riccio, R.; Gomez-Paloma, L.; Evidente, A., Tolaasins A−E, Five New Lipodepsipeptides Produced by *Pseudomonas tolaasii*. *Journal of Natural Products* **2004,** *67* (5), 811-816.
106. Lo Cantore, P.; Lazzaroni, S.; Evidente, A.; Cafarchia, C.; Iacobellis, N. S. In Production of Tolaasin I and WLIP by *Pseudomonas tolaasii* and *P. "reactans",* their Antimicrobial Activity and Possible Role in the Virulence of the Pathogens, *Pseudomonas syringae* and related pathogens, Dordrecht, 2003//; Iacobellis, N. S.; Collmer, A.; Hutcheson, S. W.; Mansfield, J. W.; Morris, C. E.; Murillo, J.; Schaad, N. W.; Stead, D. E.; Surico, G.; Ullrich, M. S., Eds. Springer Netherlands: Dordrecht, 2003; pp 255-262.
107. Cho, K.-H.; Kim, Y.-K., Two types of ion channel formation of tolaasin, a *Pseudomonas* peptide toxin. *FEMS Microbiology Letters* **2003,** *221* (2), 221-226.
108. Hermenau, R.; Kugel, S.; Komor, A. J.; Hertweck, C., Helper bacteria halt and disarm mushroom pathogens by linearizing structurally diverse cyclolipopeptides. *Proceedings of the National Academy of Sciences* **2020,** *117* (38), 23802-23806.

109. Izoré, T.; Cryle, M. J., The many faces and important roles of protein–protein interactions during non-ribosomal peptide synthesis. *Natural Product Reports* **2018,** *35* (11), 1120-1139.
110. Baltz, H. R., Biosynthesis and Genetic Engineering of Lipopeptide Antibiotics Related to Daptomycin. *Current Topics in Medicinal Chemistry* **2008,** *8* (8), 618-638.
111. Gross, H.; Loper, J. E., Genomics of secondary metabolite production by *Pseudomonas* spp. *Natural Product Reports* **2009,** *26* (11), 1408-1446.
112. Nielsen, T. H.; Thrane, C.; Christophersen, C.; Anthoni, U.; Sørensen, J., Structure, production characteristics and fungal antagonism of tensin – a new antifungal cyclic lipopeptide from *Pseudomonas fluorescens* strain 96.578. *Journal of Applied Microbiology* **2000,** *89* (6), 992-1001.
113. Rokni-Zadeh, H.; Li, W.; Yilma, E.; Sanchez-Rodriguez, A.; De Mot, R., Distinct lipopeptide production systems for WLIP (white line-inducing principle) in *Pseudomonas fluorescens* and *Pseudomonas putida*. *Environmental Microbiology Reports* **2013,** *5* (1), 160-169.
114. Gross, H.; Stockwell, V. O.; Henkels, M. D.; Nowak-Thompson, B.; Loper, J. E.; Gerwick, W. H., The Genomisotopic Approach: A Systematic Method to Isolate Products of Orphan Biosynthetic Gene Clusters. *Chemistry & Biology* **2007,** *14* (1), 53-63.
115. Pedras, M. S.; Ismail, N.; Quail, J. W.; Boyetchko, S. M., Structure, chemistry, and biological activity of pseudophomins A and B, new cyclic lipodepsipeptides isolated from the biocontrol bacterium *Pseudomonas fluorescens*. *Phytochemistry* **2003,** *62* (7), 1105-14.
116. Martin H, C.; Ibáñez, R.; Nothias, L.-F.; Boya P, C. A.; Reinert, L. K.; Rollins-Smith, L. A.; Dorrestein, P. C.; Gutiérrez, M., Viscosin-like lipopeptides from frog skin bacteria inhibit *Aspergillus fumigatus* and *Batrachochytrium dendrobatidis* detected by imaging mass spectrometry and molecular networking. *Scientific Reports* **2019,** *9* (1), 3019.
117. Gutiérrez-Chávez, C.; Benaud, N.; Ferrari, B. C., The ecological roles of microbial lipopeptides: Where are we going? *Computational and Structural Biotechnology Journal* **2021,** *19*, 1400-1413.
118. Deveau, A.; Gross, H.; Palin, B.; Mehnaz, S.; Schnepf, M.; Leblond, P.; Dorrestein, P. C.; Aigle, B., Role of secondary metabolites in the interaction between *Pseudomonas fluorescens* and soil microorganisms under iron-limited conditions. *FEMS Microbiol Ecol* **2016,** *92* (8).
119. Qingzhi, W.; Zou, S.; Wang, Q.; Chen, L.; Yan, X.; Gao, L., Catalytic defense against fungal pathogens using nanozymes. *Nanotechnology Reviews* **2021,** *10* (1), 1277-1292.
120. Jakobi, M.; Winkelmann, G.; Kaiser, D.; Kempter, C.; Jung, G.; Berg, G.; Bahl, H., Maltophilin: A New Antifungal Compound Produced by *Stenotrophomonas maltophilia* R3089. *The Journal of Antibiotics* **1996,** *49* (11), 1101-1104.
121. Woodhams, D. C.; Vredenburg, V. T.; Simon, M.-A.; Billheimer, D.; Shakhtour, B.; Shyr, Y.; Briggs, C. J.; Rollins-Smith, L. A.; Harris, R. N., Symbiotic bacteria contribute to innate immune defenses of the threatened mountain yellow-legged frog, *Rana muscosa*. *Biological Conservation* **2007,** *138* (3), 390-398.

Appendix

Table A1: ^{1}H, ^{13}C and ^{15}N NMR assignment for pseudodesmin A [d_3-MeOH, 300 K, 400 MHz]

Residue	Position	δ ^{1}H	δ ^{13}C	δ^{15}N	
Leu[1]	α	4.01	54.52		
	B	1.63, 1.75	40.45		
	Ɣ	1.65	25.67		
	δ	0.99	22.80		
	δ’	0.95	22.66		
	NH	8.76		127.93	
	C=O		176.76		
Gln[2]	α	3.99	57.62		
	β	2.10	27.07		
	Ɣ	2.43	32.20		
	NH	9.28		122.08	
	C=O		176.66		
	C=O		176.95		
	NH_2	6.90, 7.60		107.22	
Thr[3]	α	4.13	61.89		
	β	5.46	70.40		
	Ɣ	1.37	18.44		
	NH	8.40		112.84	
	C=O		175.06		
Val[4]	α	3.58	64.83		
	β	2.19	30.19		
	Ɣ	0.99	21.25		
	Ɣ	0.94	19.50		
	NH	7.34		120.08	
	C=O		174.92		
Leu[5]	α	4.10	55.85		
	β	1.75, 1.52	40.58		
	Ɣ	1.65	25.67		
	δ	0.89	23.43		
	δ’	0.88	20.96		
	NH	7.61		114.46	
	C=O		176.00		
Ser[6]	α	4.39	57.62		
	β	4.15, 3.94	63.89		
	NH	7.71		107.36	
	C=O		173.26		
Leu[7]	α	4.35	54.59		
	β	1.93, 1.64	42.06		
	Ɣ	1.97	25.63		
	δ	1.00	23.62		
	δ’	0.92	21.03		
	NH	7.22		120.72	
	C=O		175.00		
Ser[8]	α	4.48	57.68		
	β	4.00, 3.74	62.89		
	NH	8.24		110.34	
	C=O		172.82		
Ile[9]	α	4.61	57.54		
	β	1.99	37.46		
	Ɣ	1.21, 0.99	25.46		
	Ɣ’	0.87	16.06		
	δ	0.88	12.21		
	NH	7.08		113.36	

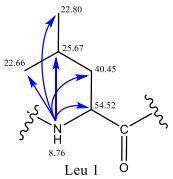

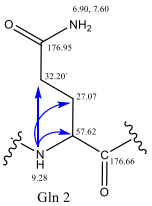

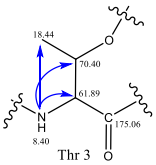

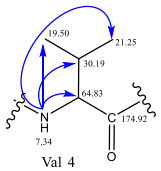

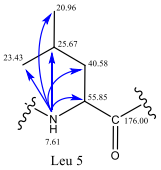

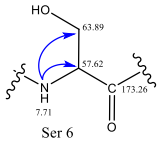

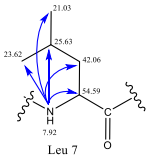

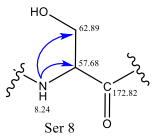

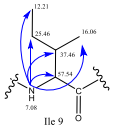

	C=O		169.86	
Lipid chain	C=O		175.34	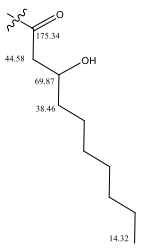
	CH_2	2.44	44.58	
	CH	4.10	69.87	
	CH_2	1.51	38.46	
	CH_2	-	-	
	CH_2	-	-	
	CH_2	-	-	
	CH_2	-	-	
	CH_2	-	-	
	CH_3	0.89	14.32	

Table A2: ^{1}H and ^{13}C-NMR assignment for compound **2** [d_3-MeOH, 300 K, 400 MHz]

Residue	**Site**	**δ^{1}H**	**δ^{13}C**	**Residue**	**Site**	**δ^{1}H**	**δ^{13}C**
Leu^{1}	α	4.16	55.10	Gln^{8}	α	4.39	54.68
	β	1.64	41.58		β	2.07, 1.91	29.14
	γ	1.73	25.56		γ	2.29	32.39
	δ	0.89	22.00		NH	8.29	
	δ´	0.92	23.45		C=O		-
	NH	7.95			NH_2^1	6.86	
	C=O		-		NH_2^2	7.55	
Asp^{2}	α	4.49	53.53		C=O		177.73
	β	2.86, 2.77	35.65				
	NH	8.38		Leu^{9}	α	4.37	54.54
	C=O		173.74		β	1.62, 1.56	41.16
	C=O		174.88		γ	1.74	25.68
					δ	0.92	23.45
Thr^{3}	α	4.57	59.81		δ´	0.88	21.58
	β	5.43	70.81		NH	8.14	
	γ	1.31	17.99		C=O		-
	NH	7.85					
	C=O		172.36	Ile^{10}	α	4.17	60.20
					β	1.96	36.99
Leu^{4}	α	4.36	53.87		γ	0.96	15.87
	β	1.85	40.08		γ`	1.20	26.35
	β´	/			δ	0.91	10.94
	γ	1.74	25.61		NH	7.73	
	δ	0.88	21.33		C=O		-
	δ´	0.95	23.90				
	NH	7.91		Glu^{11}	α	4.54	53.40
	C=O		-		β	1.79. 1.93	28.51
					γ	2.30	30.98
Leu^{5}	α	4.27	54.06		NH	7.47	
	β	1.71	41.49		C=O		170.62
	γ	1.74	25.88		C=O		175.71
	δ	0.88	21.32				
	δ´	0.92	23.45	Lipid chain	C=O		175.76

	NH	8.31			CH_2	2.46	44.12
	C=O		-		CH	4.10	70.15
					CH_2	1.53	38.32
Ser[6]	α	4.48	57.63		CH_2	-	-
	β	4.02, 3.85	64.27		CH_2	-	-
	NH	7.81			CH_2	-	-
	C=O		173.52		CH_2	-	-
					CH_2	-	-
Leu[7]	α	4.16	55.48		CH_3	0.91	14.29
	β	1.62	40.97				
	γ	1.74	25.61				
	δ	0.93	22.25				
	δ´	0.98	22.82				
	NH	8.53					
	C=O		-				

Table A3: ^{1}H, ^{13}C and ^{15}N NMR assignment for virginiafactin A [d_3-MeOH, 300 K, 400 MHz]

Residue	**Site**	**δ ^{1}H**	**δ ^{13}C**	**δ^{15}N**	**Residue**	**Site**	**δ ^{1}H**	**δ ^{13}C**	**δ^{15}N**
					Val[7]	α	4.20	60.63	
Leu[1]	α	4.37	53.74			β	2.16	31.38	
	β	1.64	41.53			Ɣ	0.95	19.81	
	Ɣ	1.70	25.97			Ɣ’	0.94	18.76	
	δ	0.96	23.58			NH	7.75		116.38
	δ’	0.92	21.84			C=O		173.42	
	NH	8.16		124.98					
	C=O		175.57		Leu[8]	α	4.49	53.06	
						β	1.64	41.93	
Leu[2]	α	4.31	53.80			Ɣ	1.65	25.87	
	β	1.64	41.00			δ	0.96	23.54	
	Ɣ	1.70	25.96			δ’	0.92	21.76	
	δ	0.96	23.36			NH	8.17		123.30
	δ’	0.92	22.01			C=O		174.50	
	NH	8.21		118.44	Leu[9]	α	4.45	52.01	
	C=O		175.54			β	1.64	41.53	
						Ɣ	1.70	25.96	
Gln[3]	α	4.25	55.10			δ	0.96	23.58	
	β	2.16, 2.04	28.08			δ’	0.92	21.86	
	Ɣ	2.33	32.76			NH	8.07		119.26
	NH	8.26		119.31		C=O		175.73	
	NH_2^1 NH_2^2	6.81, 7.57		107.20					
	C=O		177.69		Lipid chain	C=O		174.99	
	C=O		174.13			CH_2	2.35 2.48	44.64	
						CH	3.99	69.97	
Leu[4]	α	4.37	53.67			CH_2	1.49	38.49	
	β	1.64	41.33			CH_2	-	-	

	Ɣ	1.70	25.96		CH_2	-	-
	δ	0.96	23.36		CH_2	-	-
	δ’	0.92	22.01		CH_2	-	-
	NH	8.27		119.51	CH_2	-	-
	C=O		174.86		CH_3	0.90	14.44
Ser[5]	α	4.39	57.40				
	β	3.85	62.96				
	NH	8.09		113.16			
	C=O		172.55				

Figure A1: Molecular network of *B. dendrobatidis* culture extract and medium extract showing several clusters with nodes and edges (In each node, red = *B. dendrobatidis* culture extract and blue = media extract).

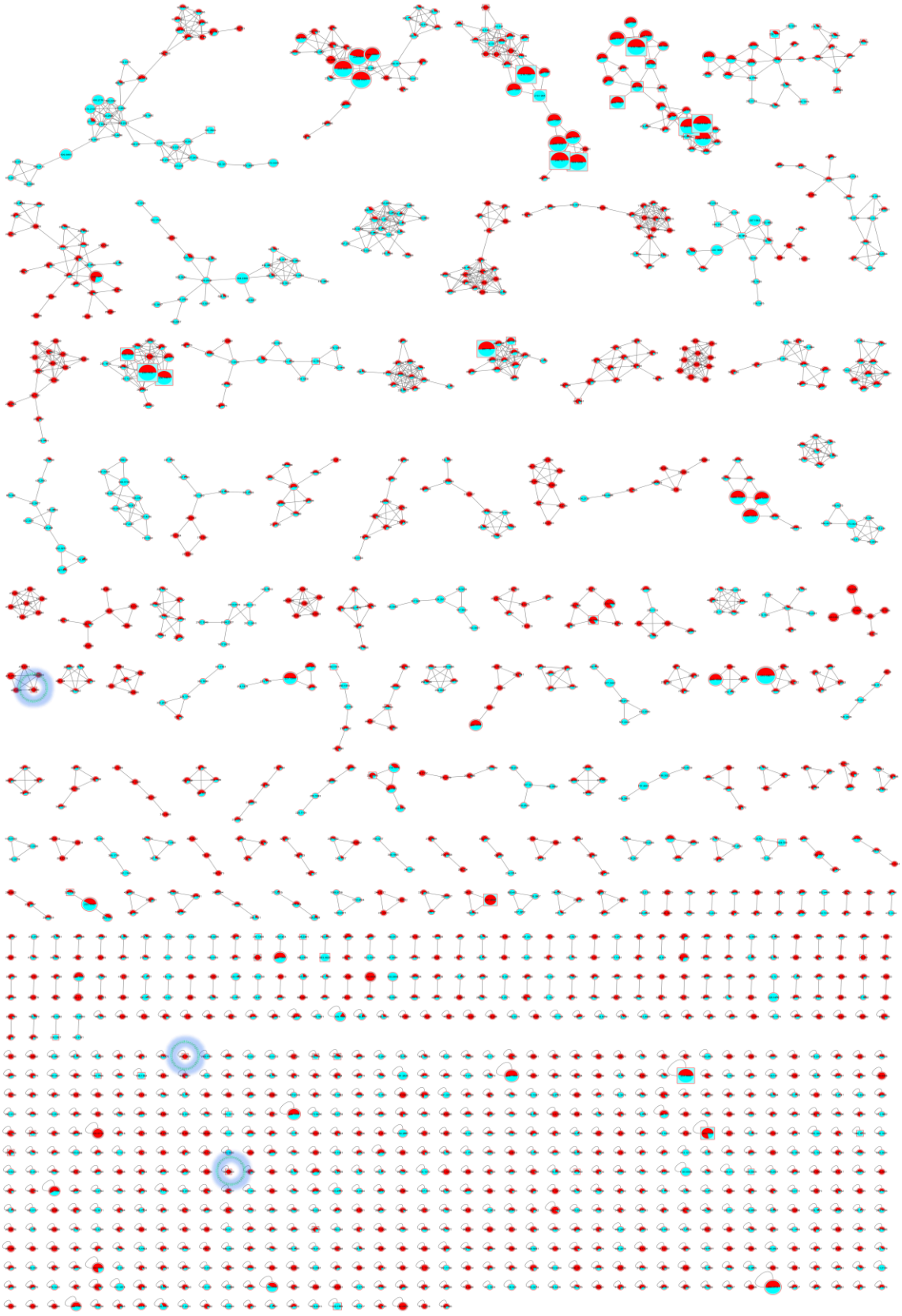

Figure A2: NMR spectra of lipo-dipeptide (solvent: d_6-DMSO, 400 MHz)

a. ^{1}H-NMR

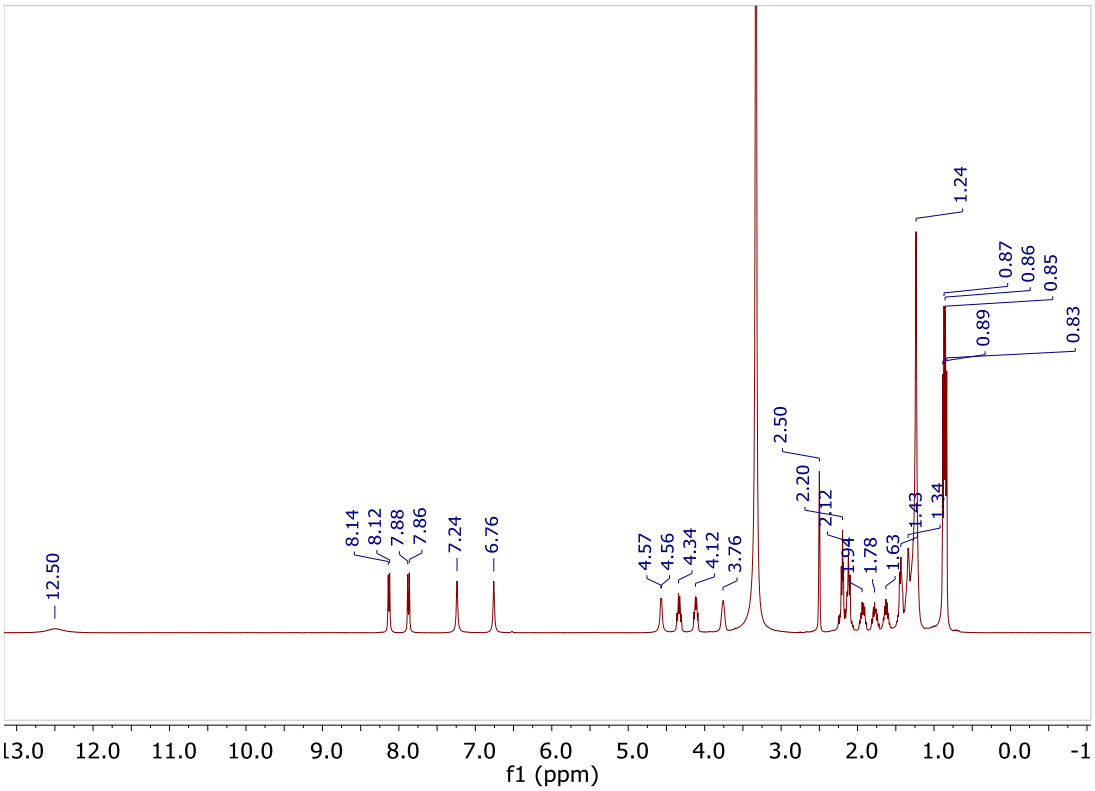

b. ^{13}C-NMR (100 MHz)

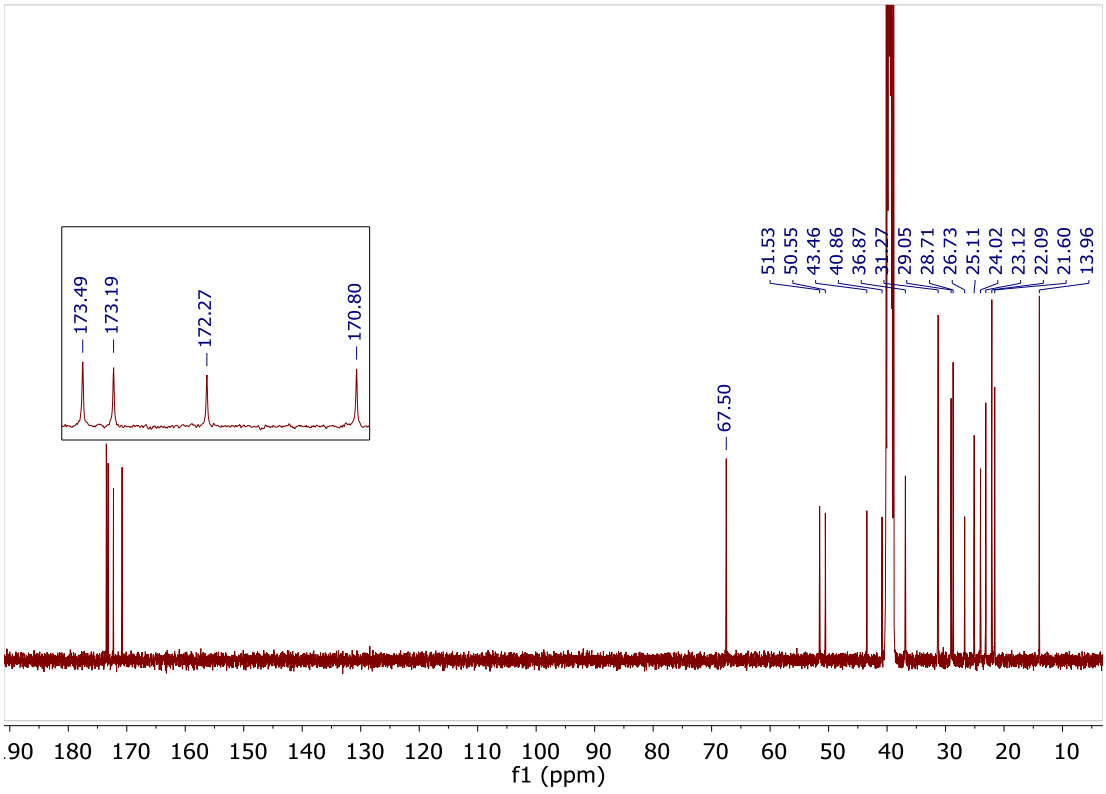

c. ^{13}C-DEPT_135

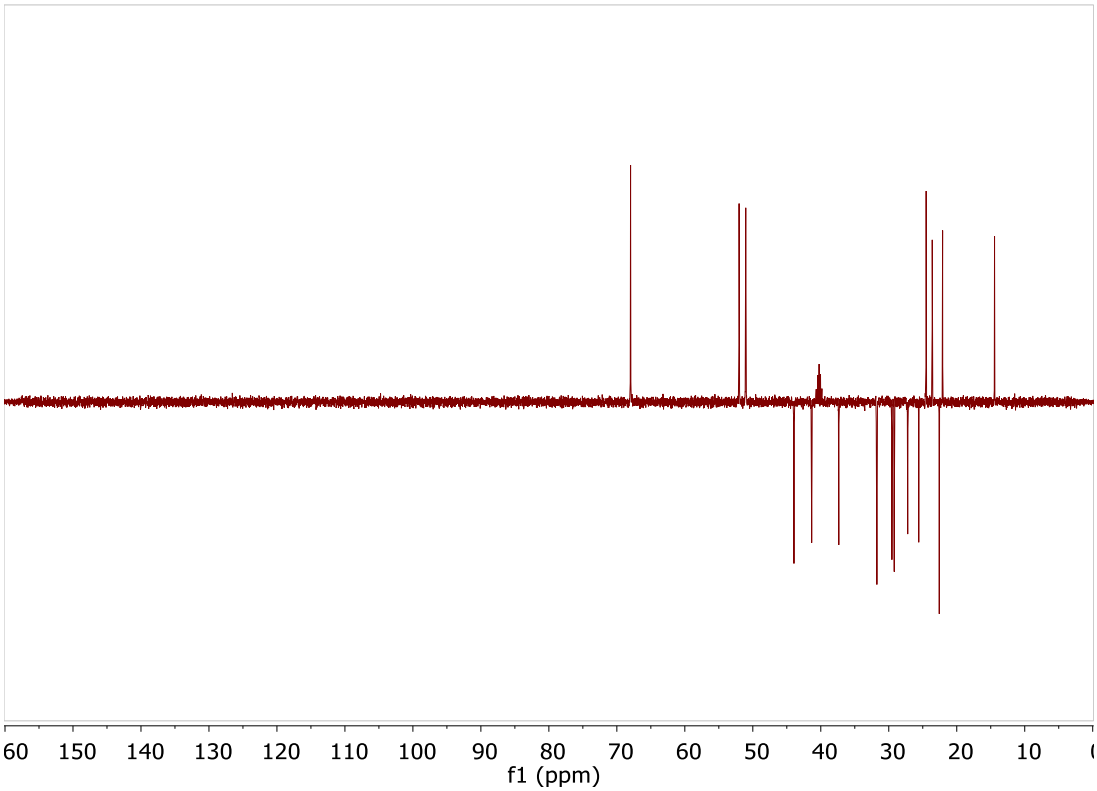

d. Comparison of spectra between ^{13}C-NMR and ^{13}C-DEPT-135 (100 MHz)

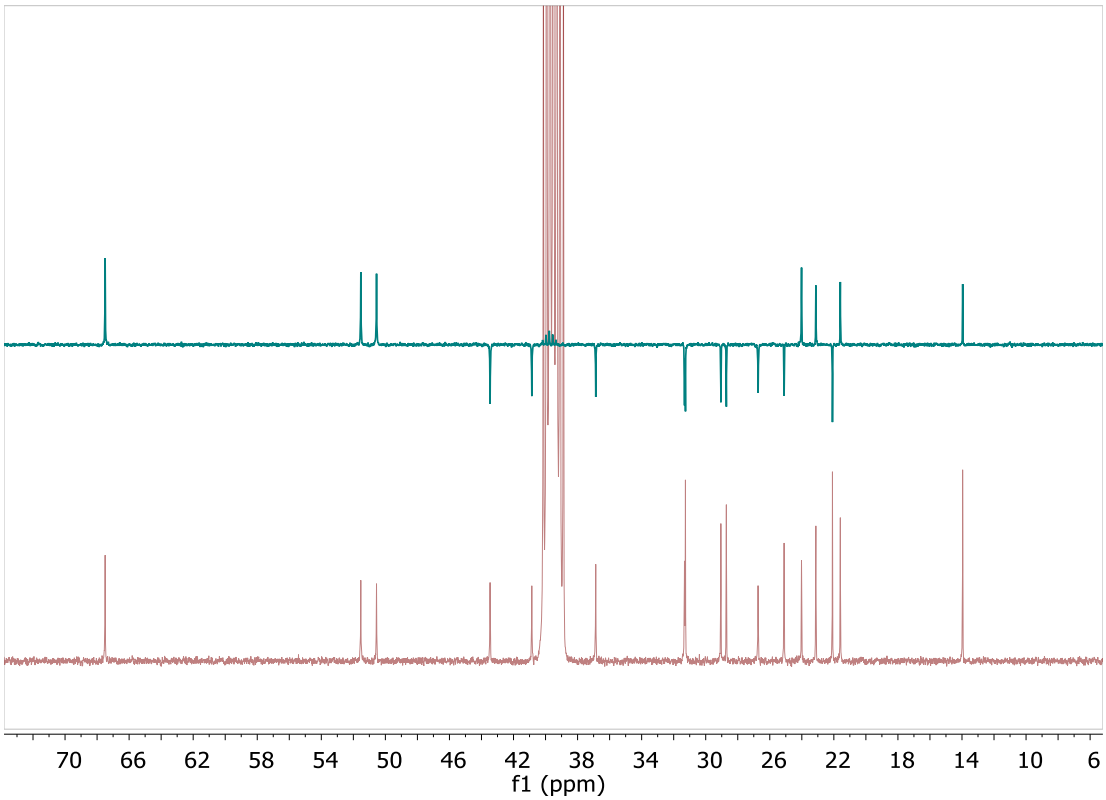

e. ^{1}H-^{1}H-COSY

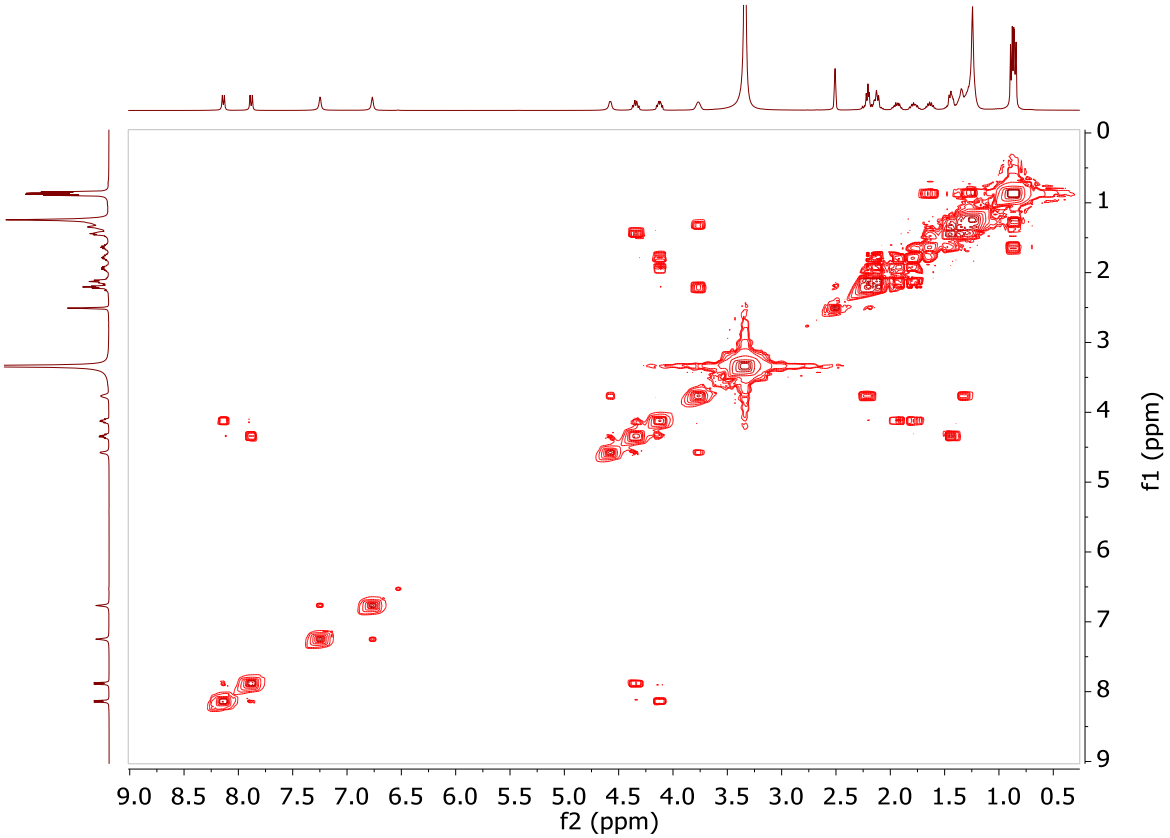

f. ^{1}H-^{13}C_HSQC

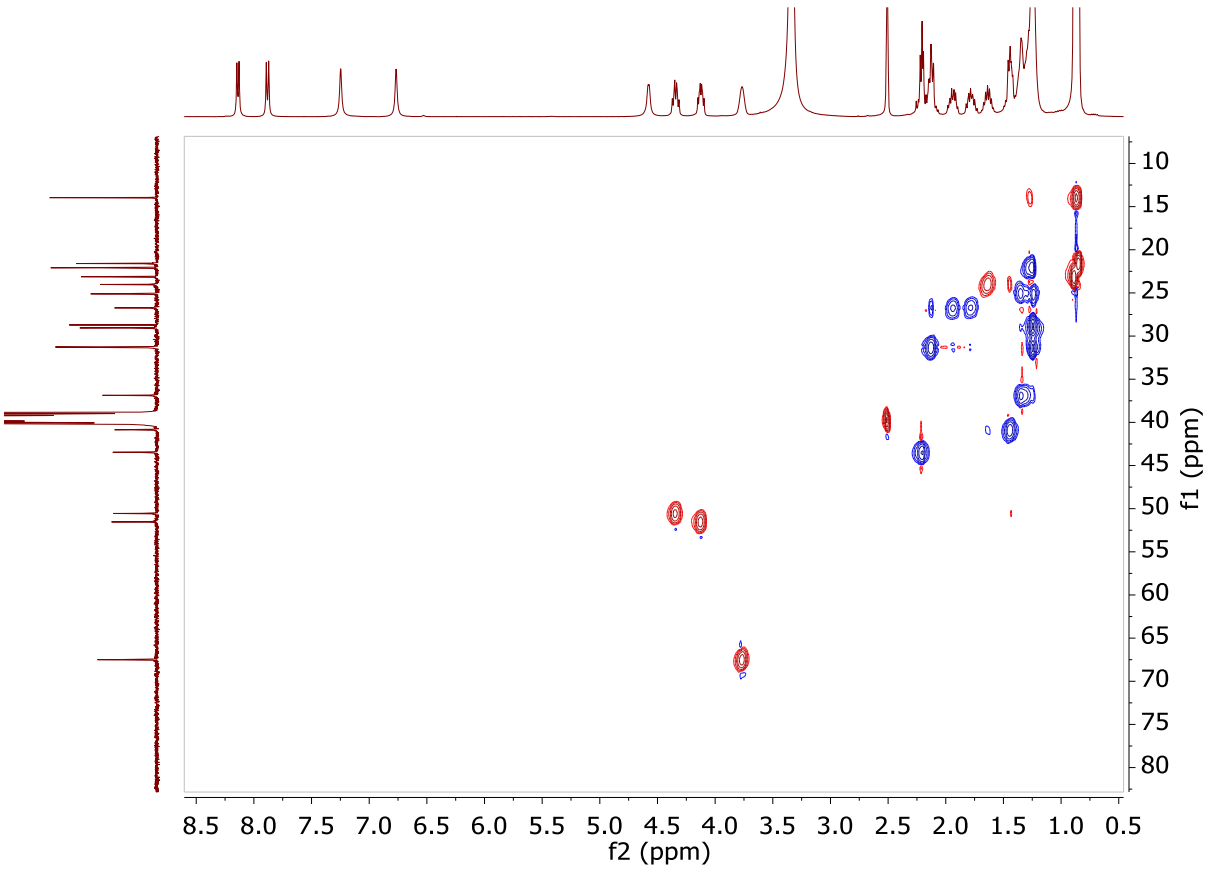

g. ^{1}H-^{13}C-HMBC

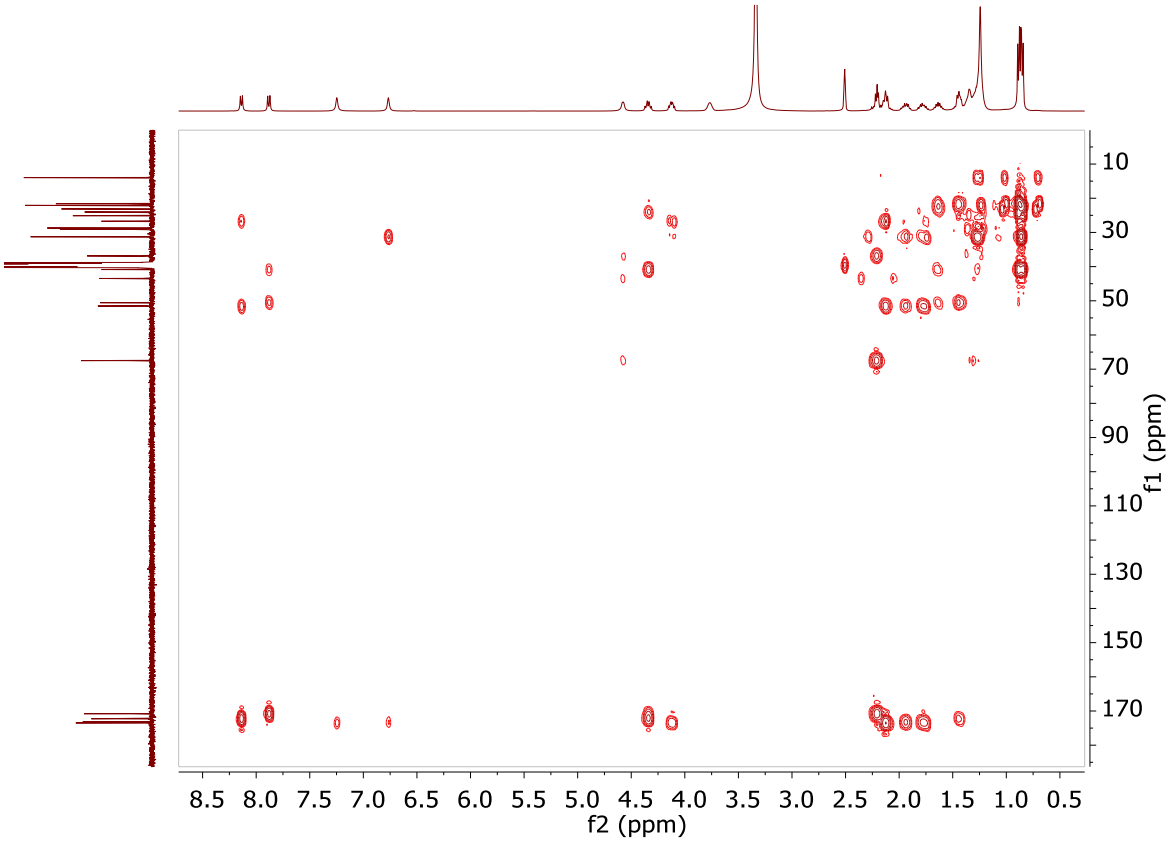

h. ^{1}H-^{13}C-HSQC-TOCSY

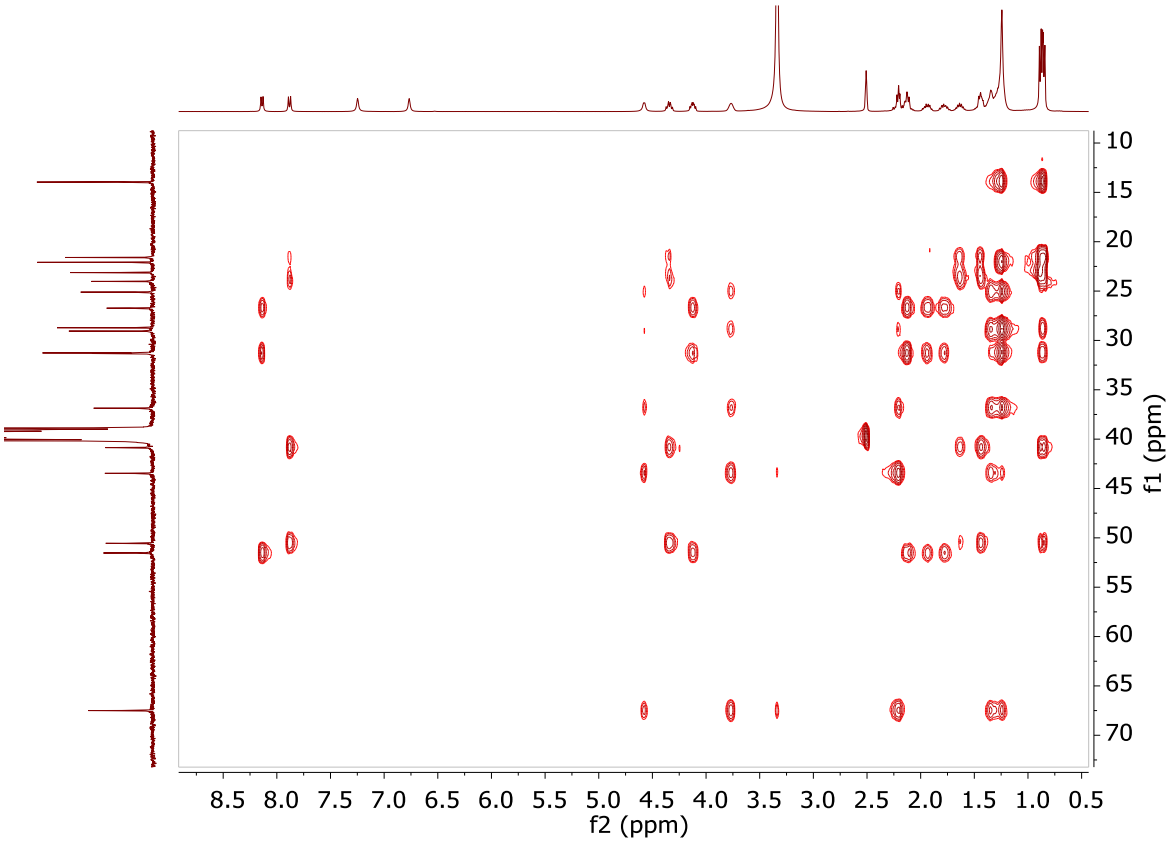

Appendix

i. ^{1}H-^{1}H-NOESY

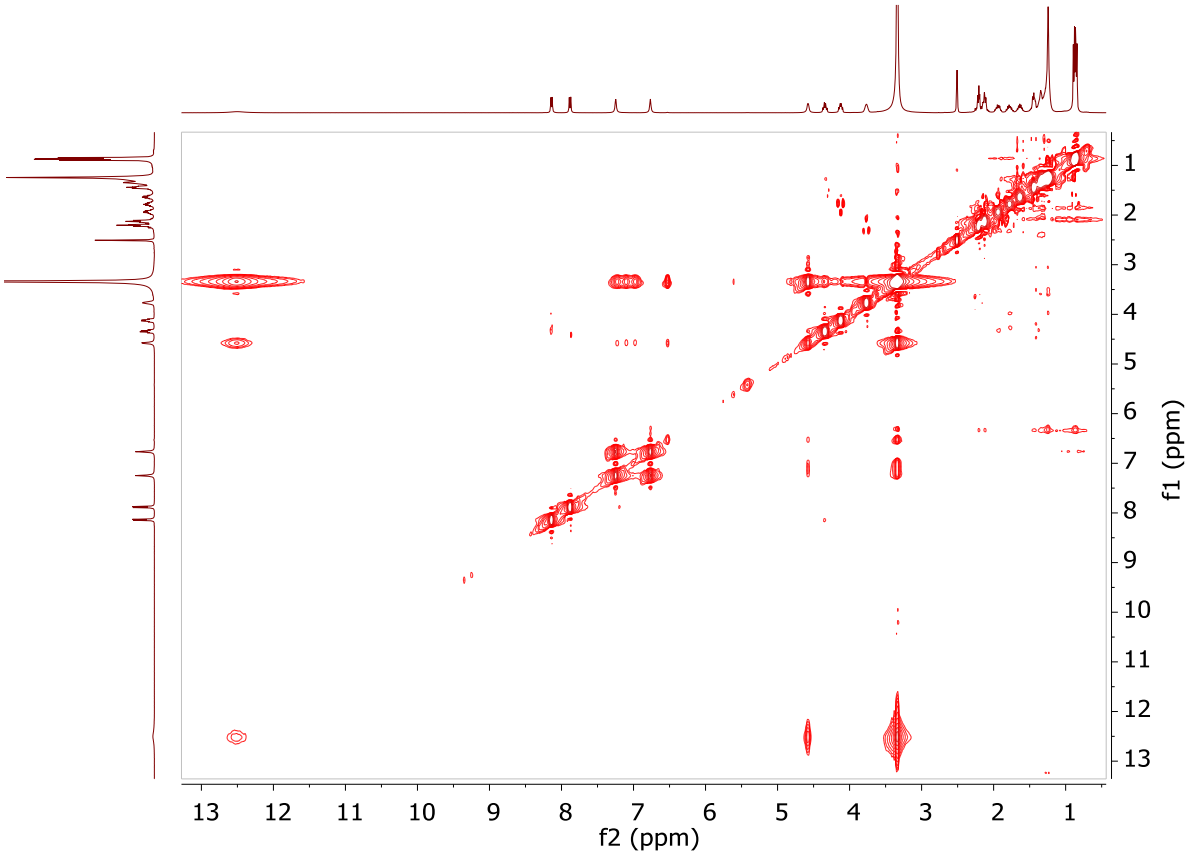

j. ^{1}H-^{13}C-HMBC-band selective

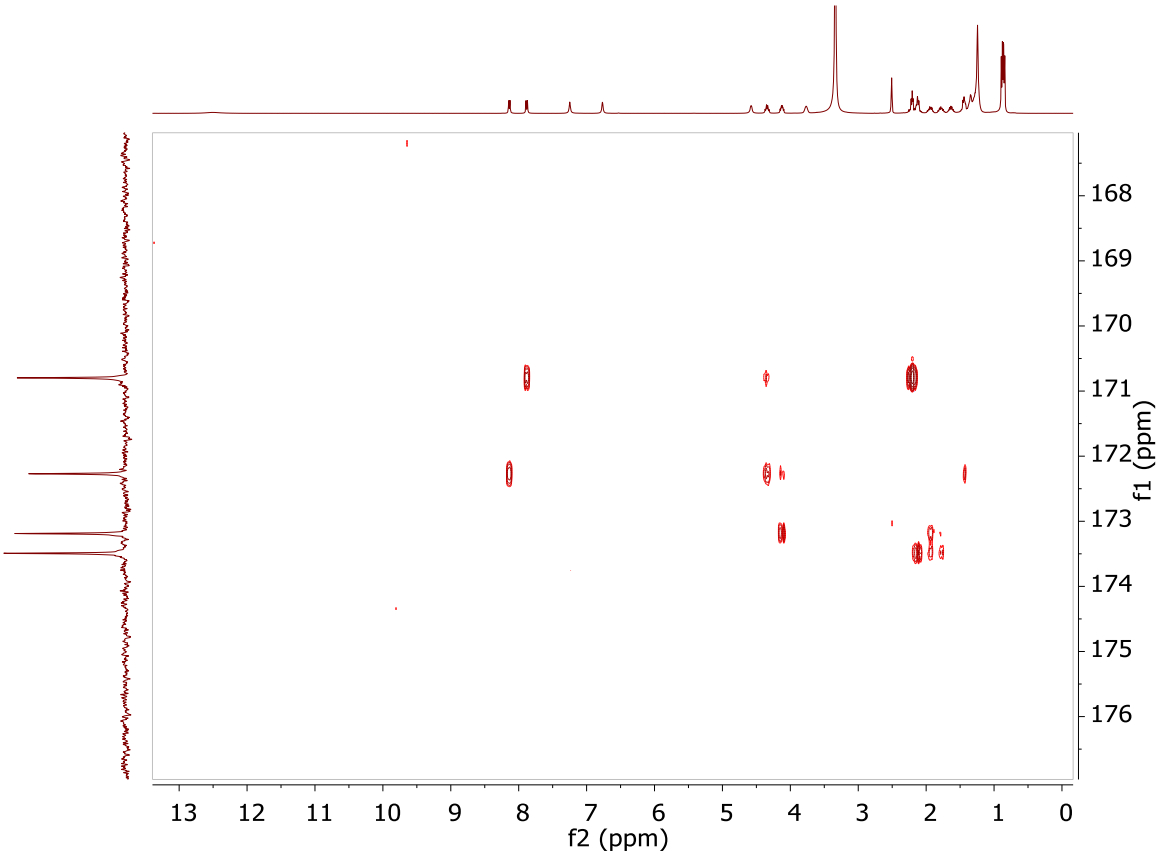

k. ^{1}H-^{13}C-HMBC-band selective

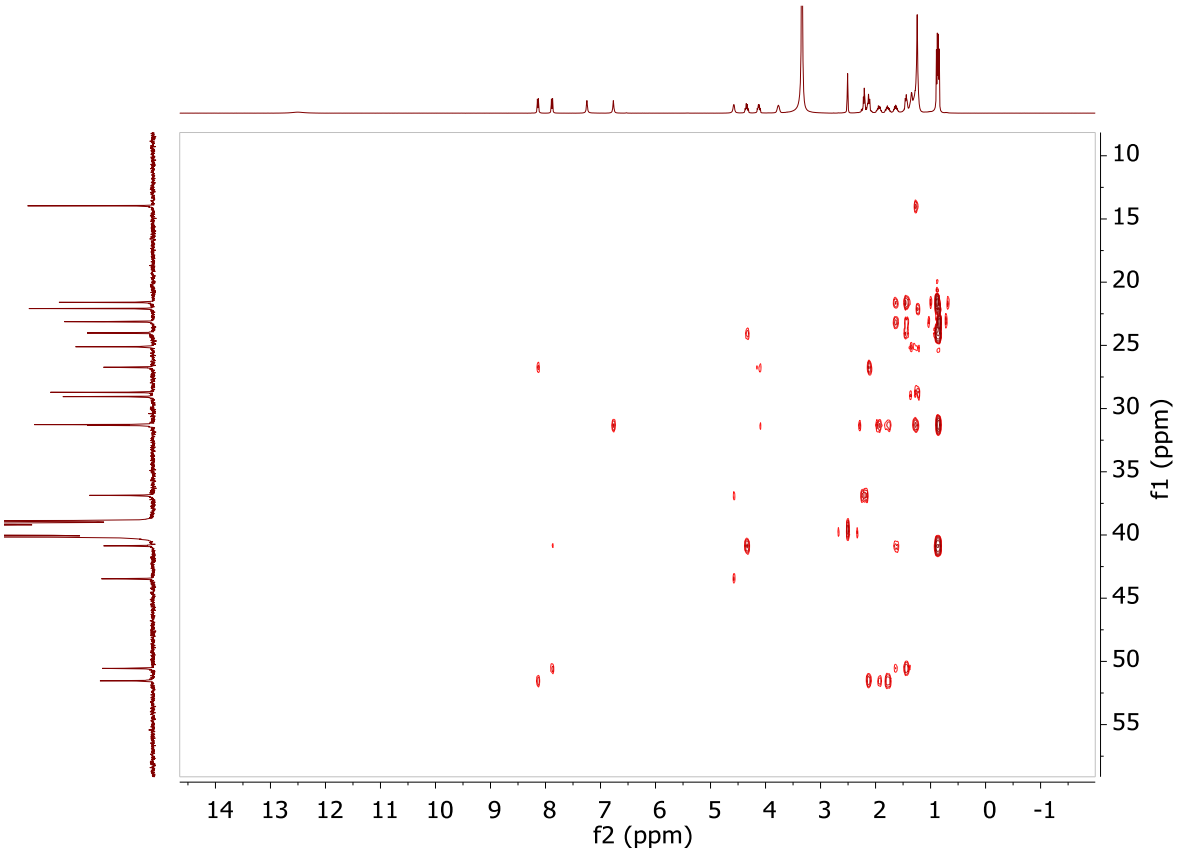

l. ^{1}H-^{15}N-HSQC

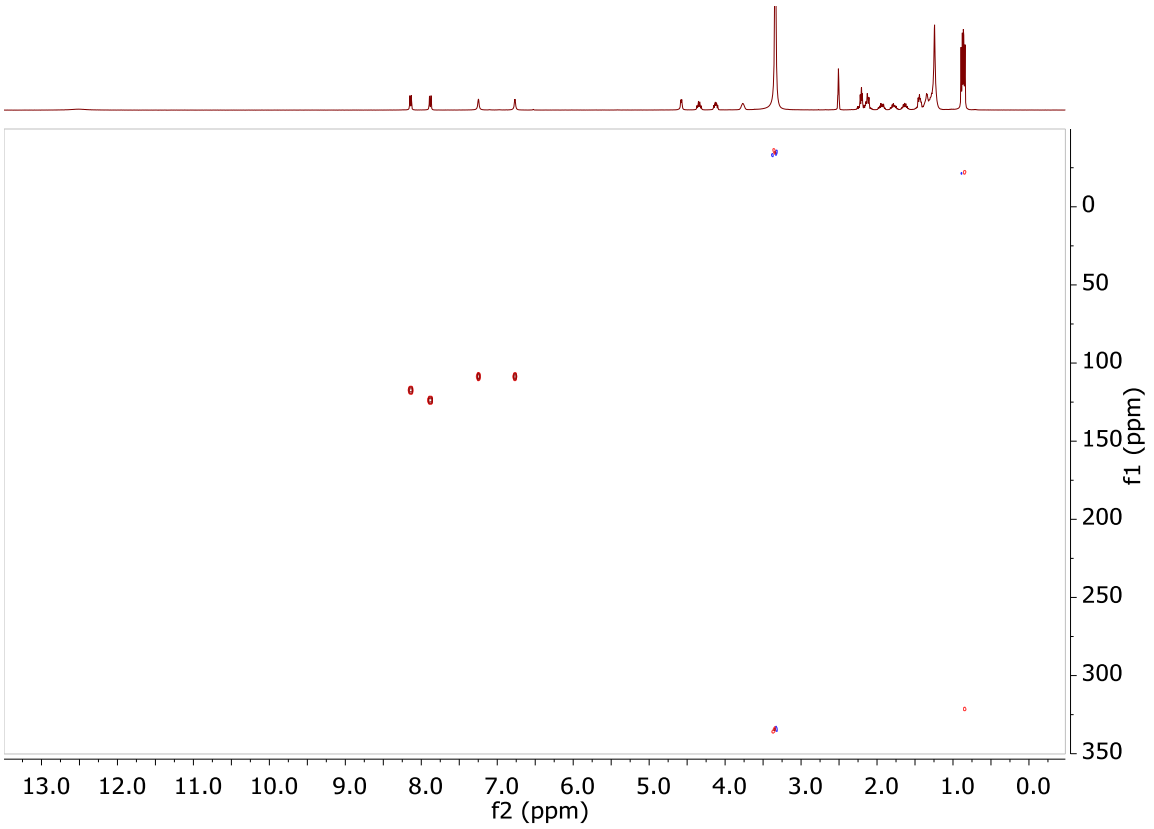

m. ^{1}H-^{15}N-HMBC

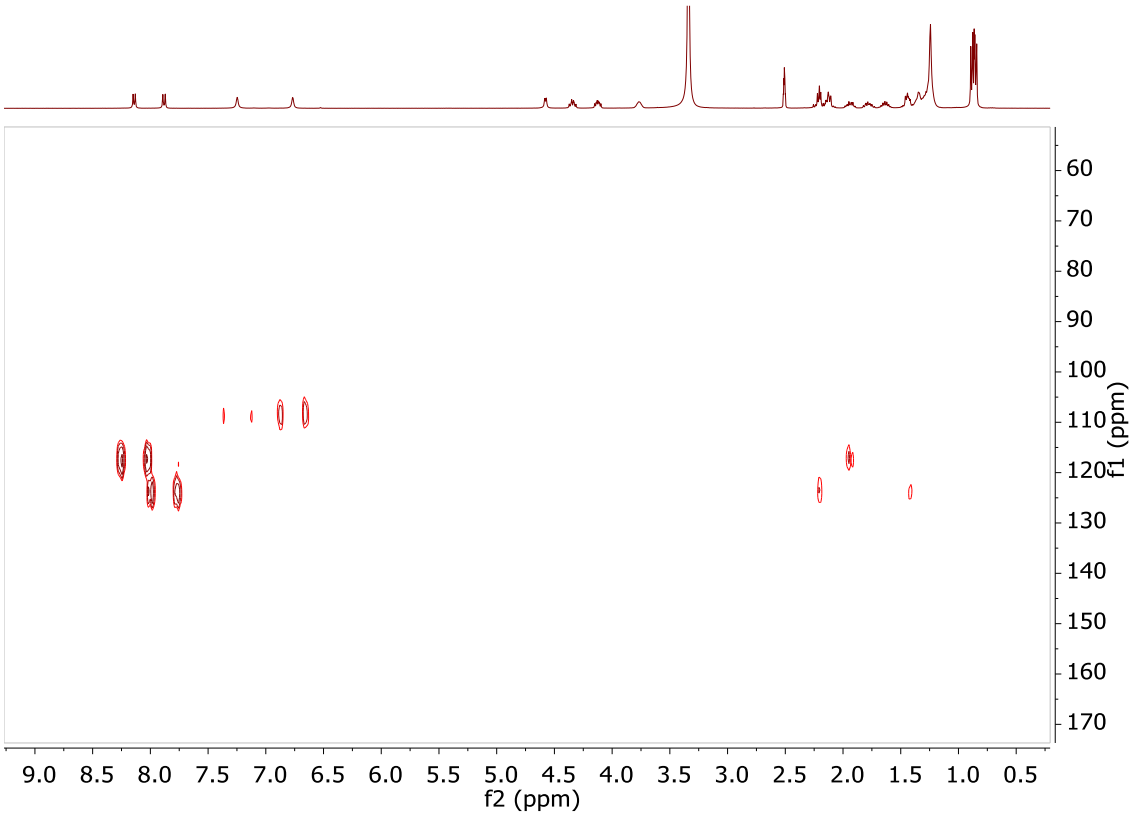

n. ^{1}H-^{1}H-TOCSY

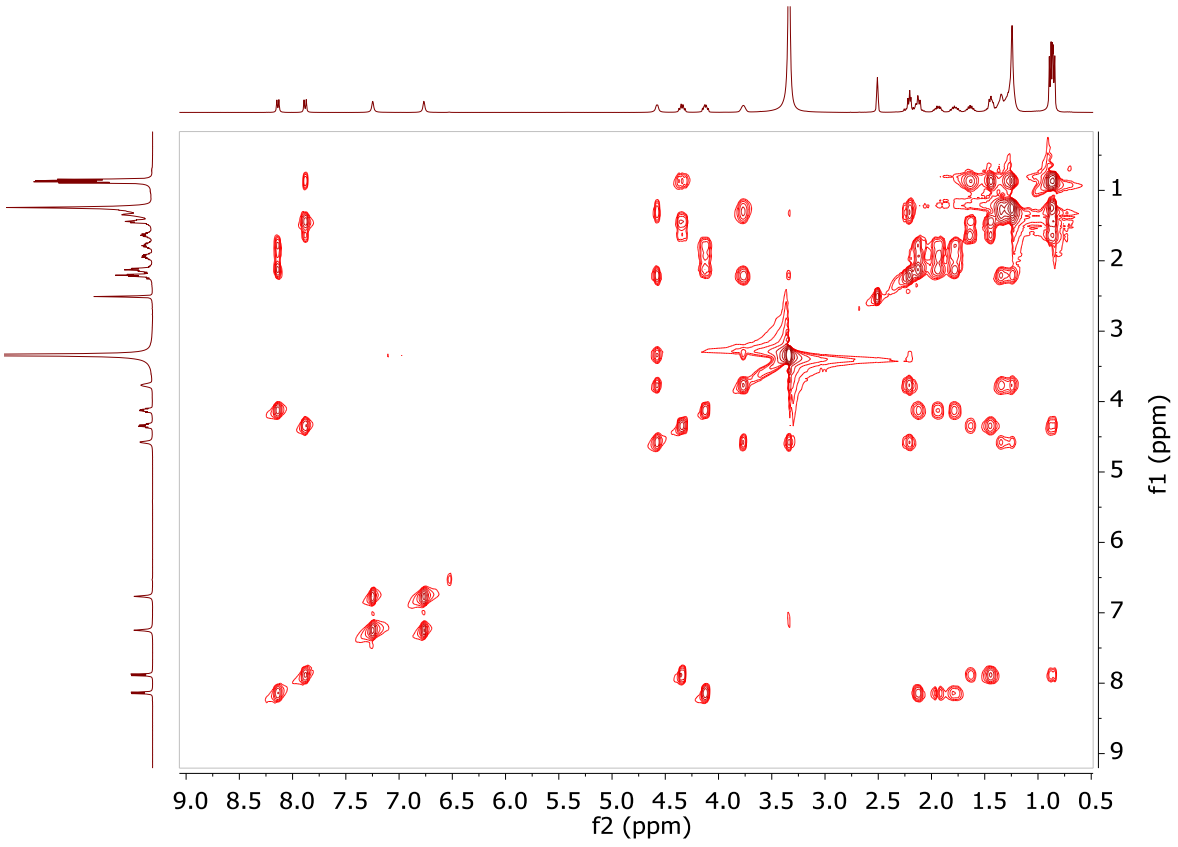

Figure A3: HPLC chromatogram of pseudodesmin A in 100% methanol fraction at 220 nm.

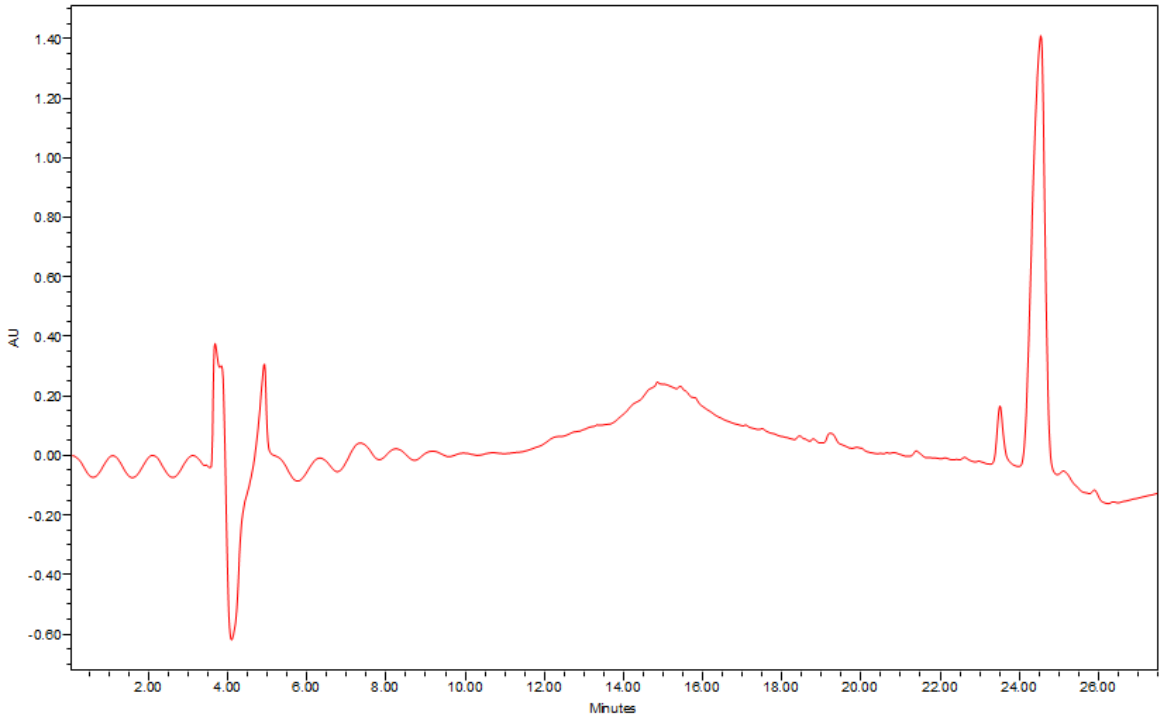

Figure A4: NMR spectra of pseudodesmin A (solvent: d_3-acetonitrile, 400 MHz)

a. ^{1}H-NMR

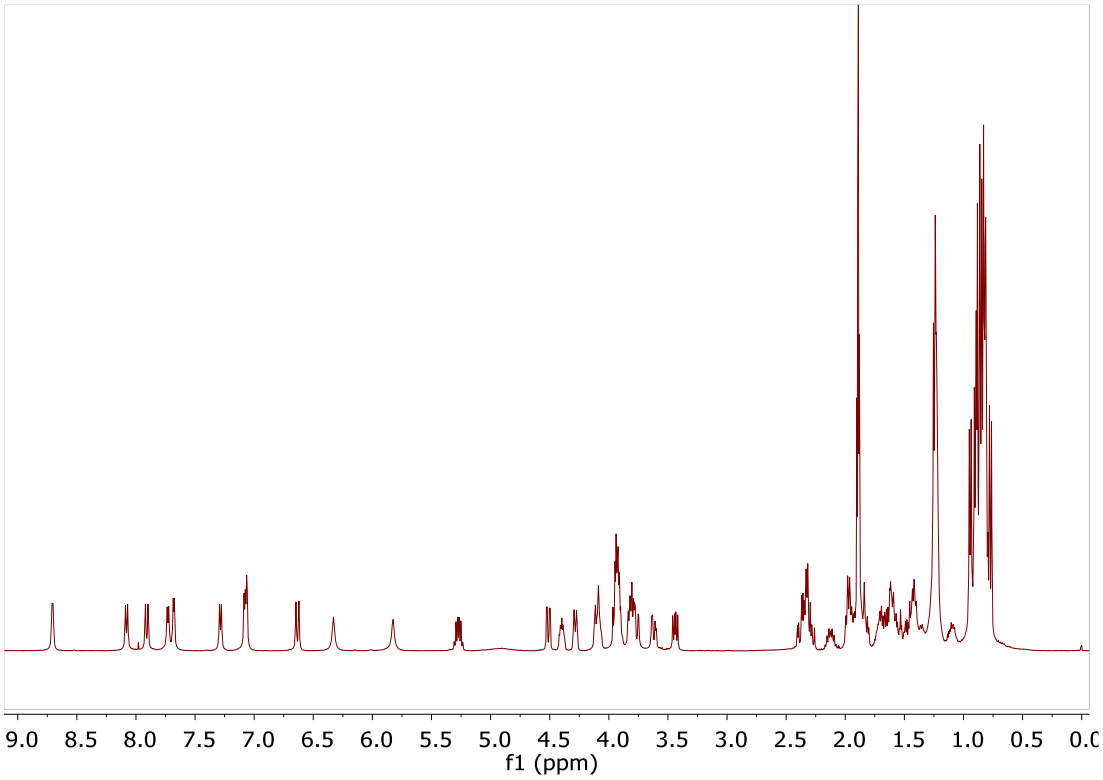

b. ^{13}C-NMR (100 MHz)

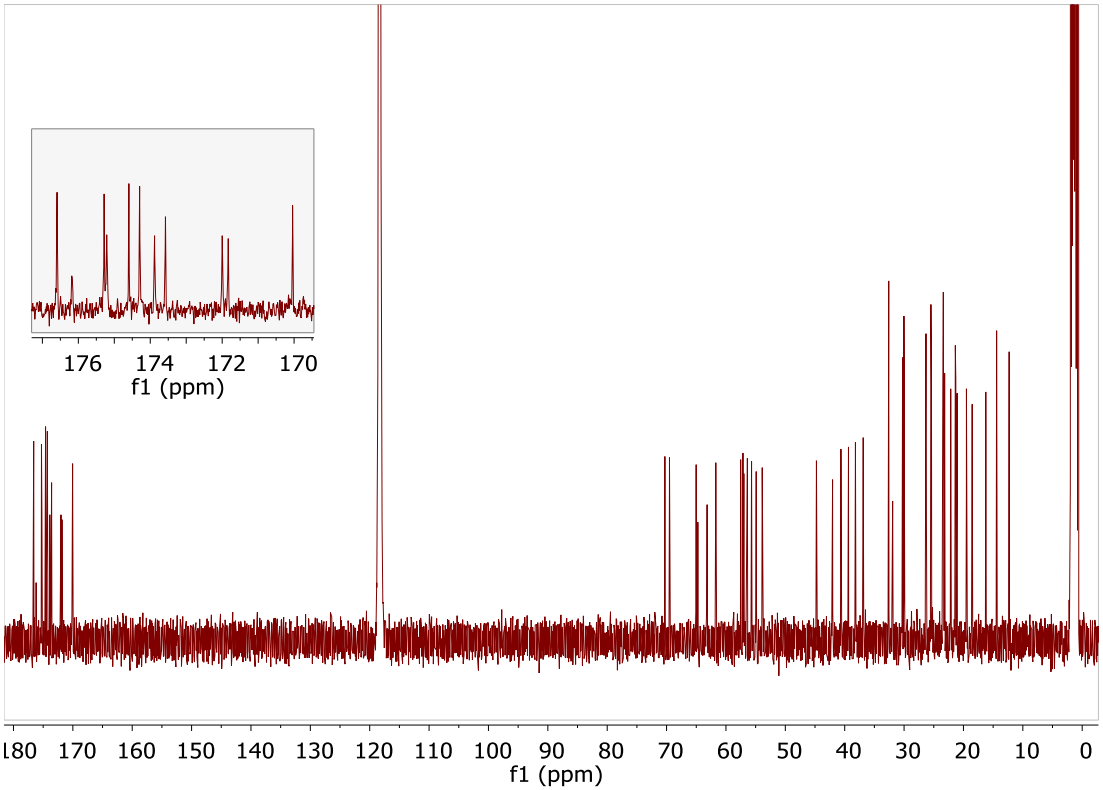

c. ^{1}H-^{1}H-TOCSY

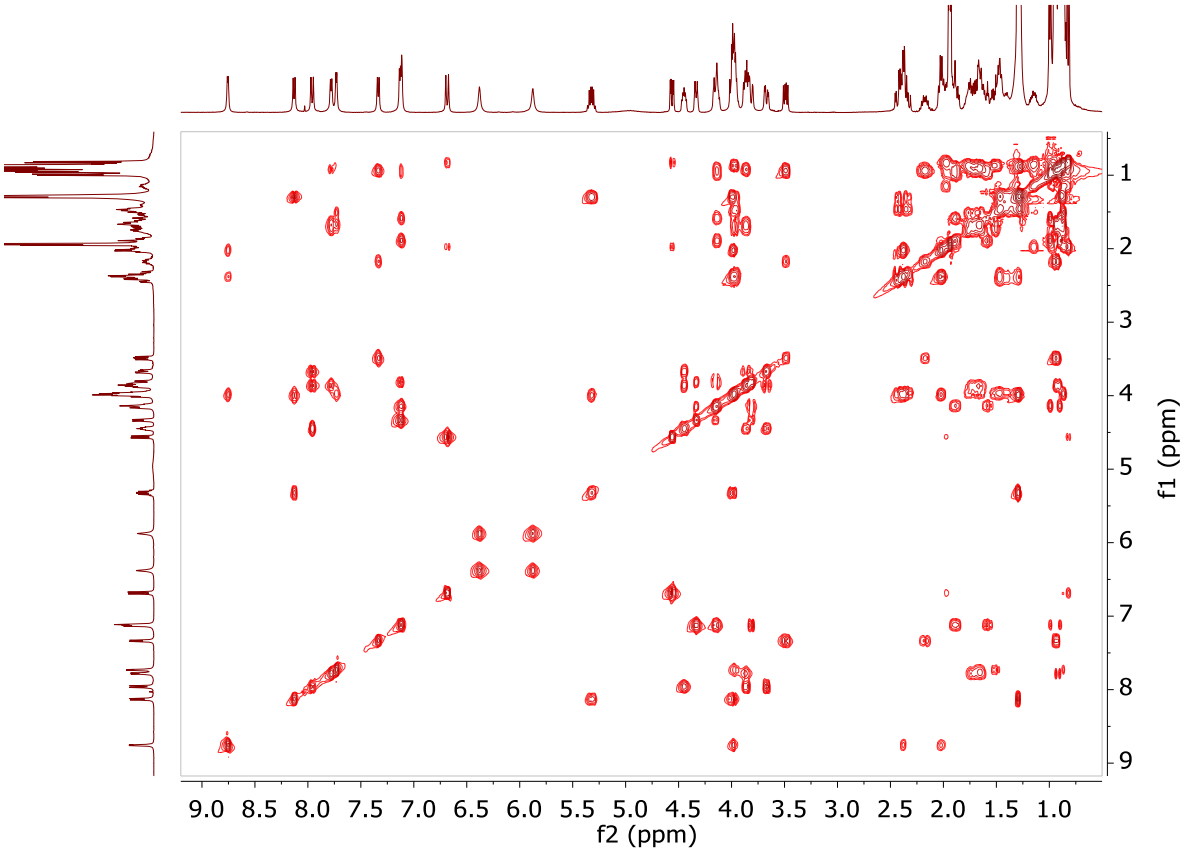

d. ^{1}H-^{13}C-HSQC-TOCSY

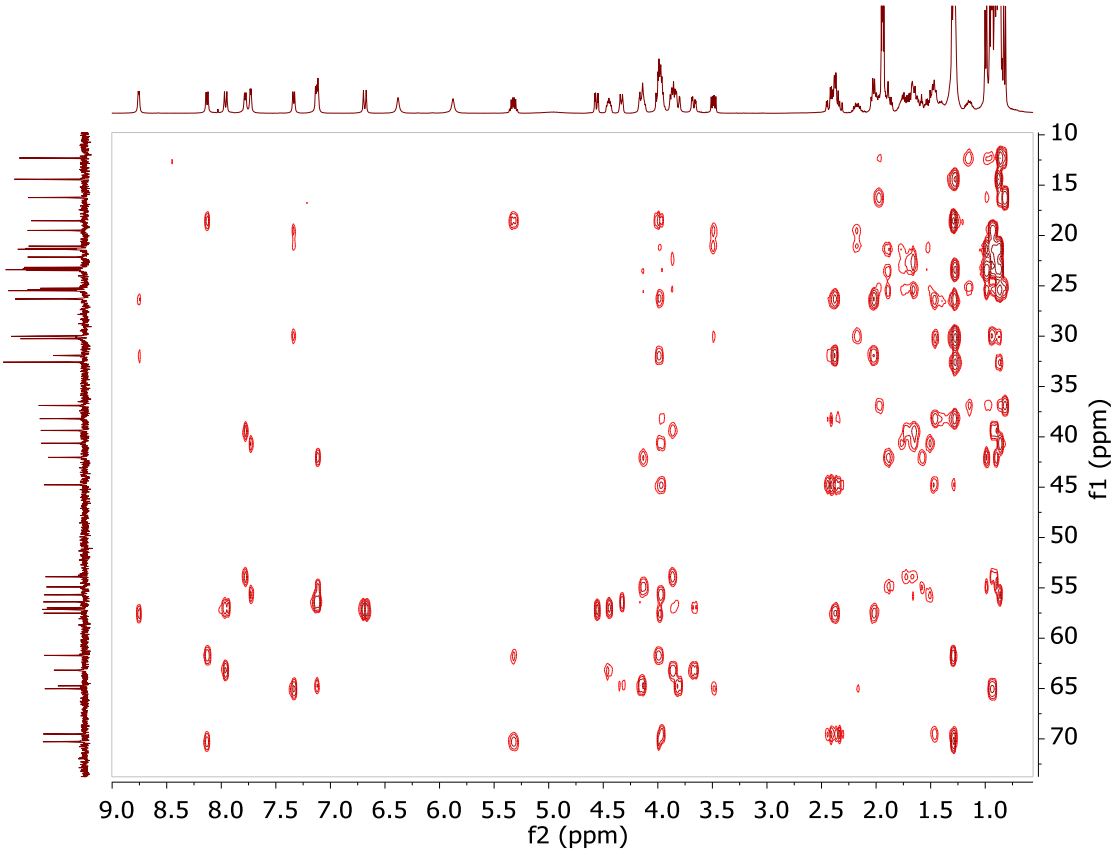

Figure A5: NMR spectra of pseudodesmin A (solvent: d_3-methanol, 400 MHz)

a. ^{1}H-NMR

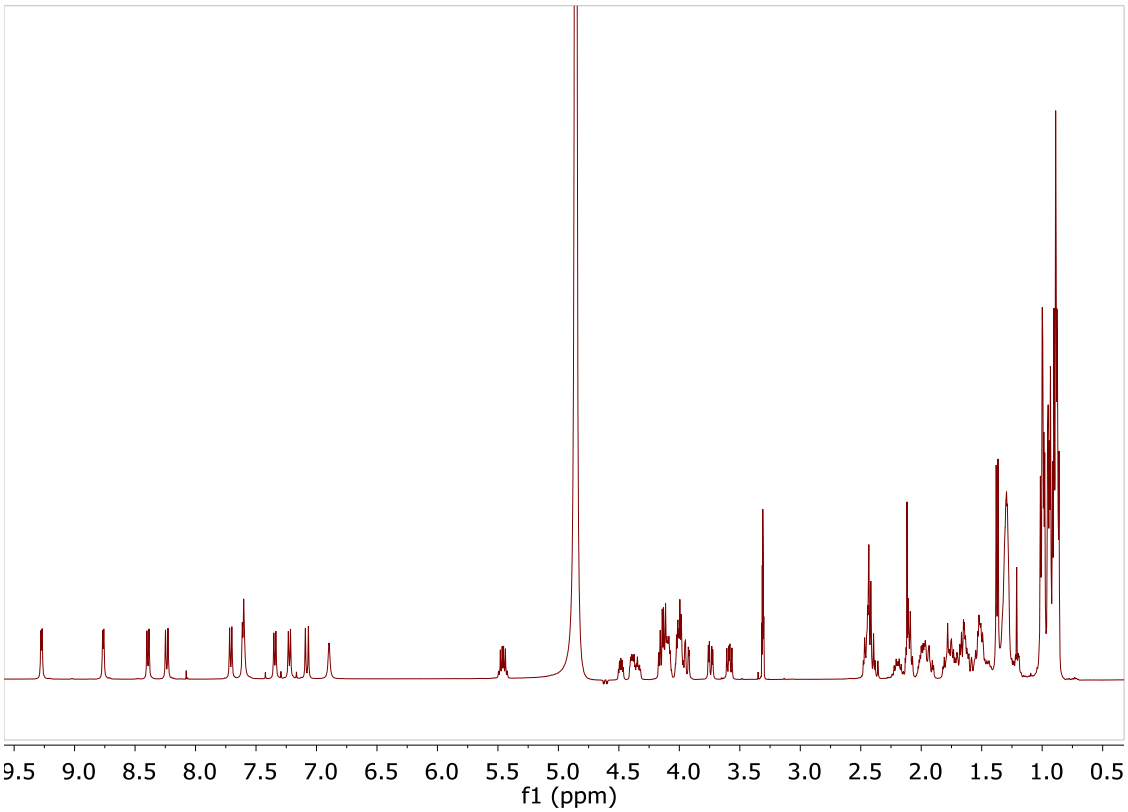

b. ^{13}C-NMR (100 MHz)

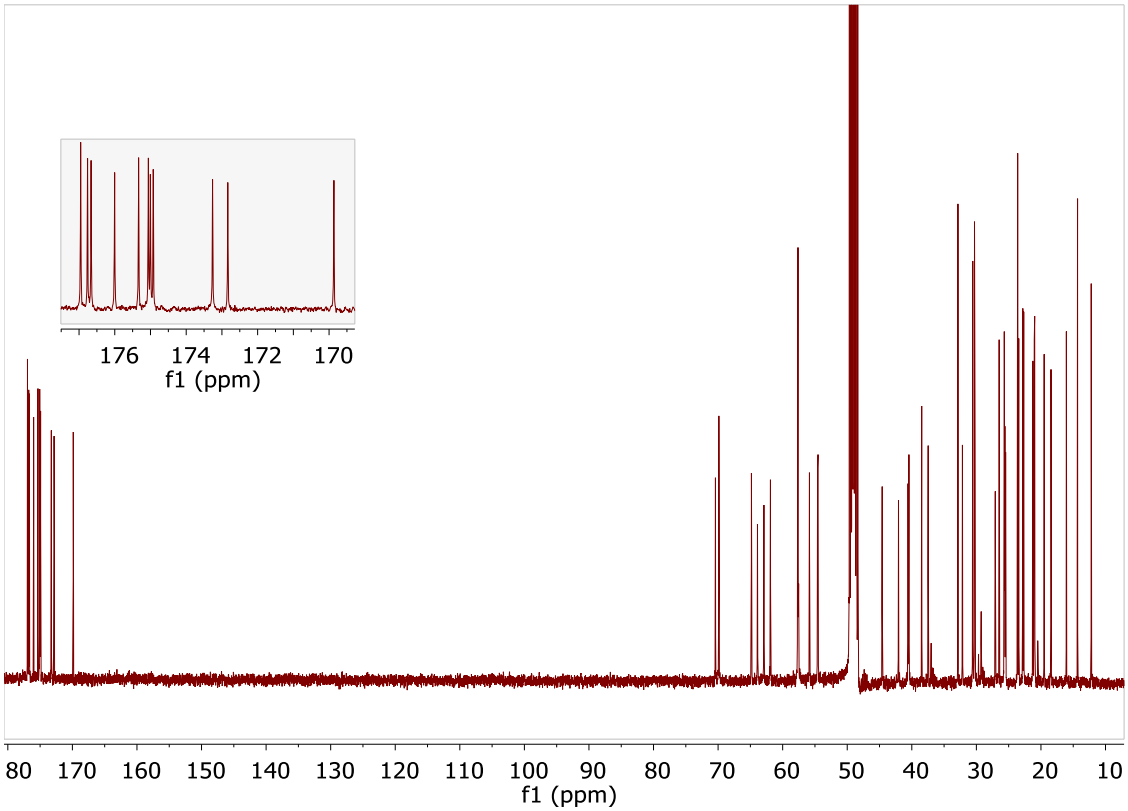

c. ^{13}C-DEPT-135 (100 MHz)

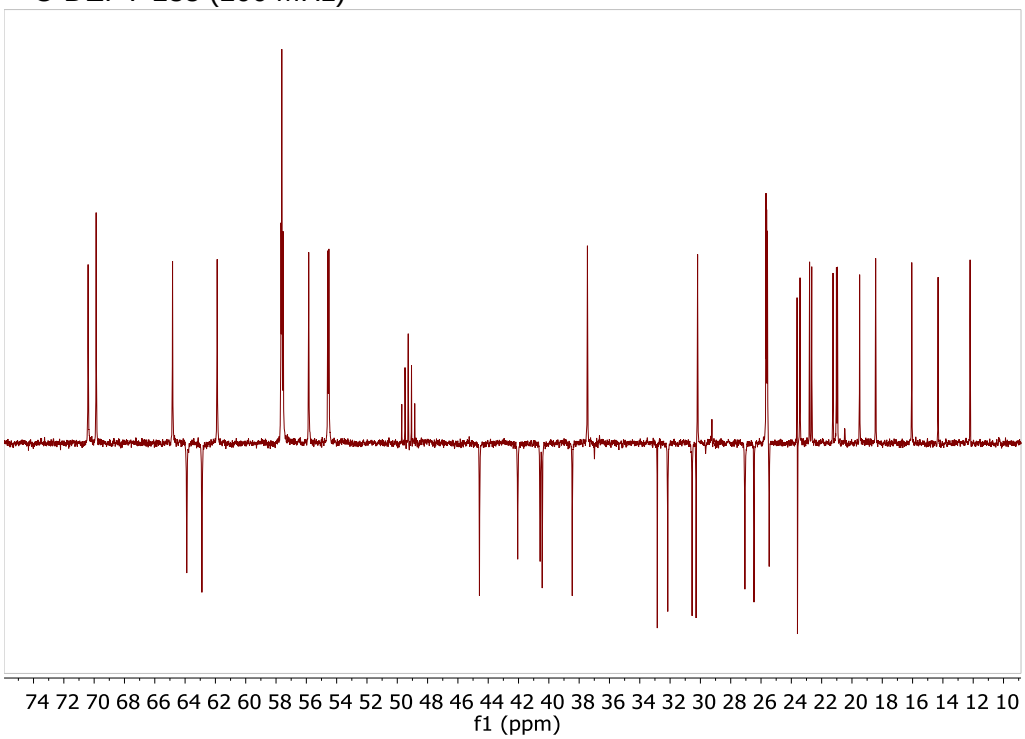

d. ^{1}H-^{1}H-COSY

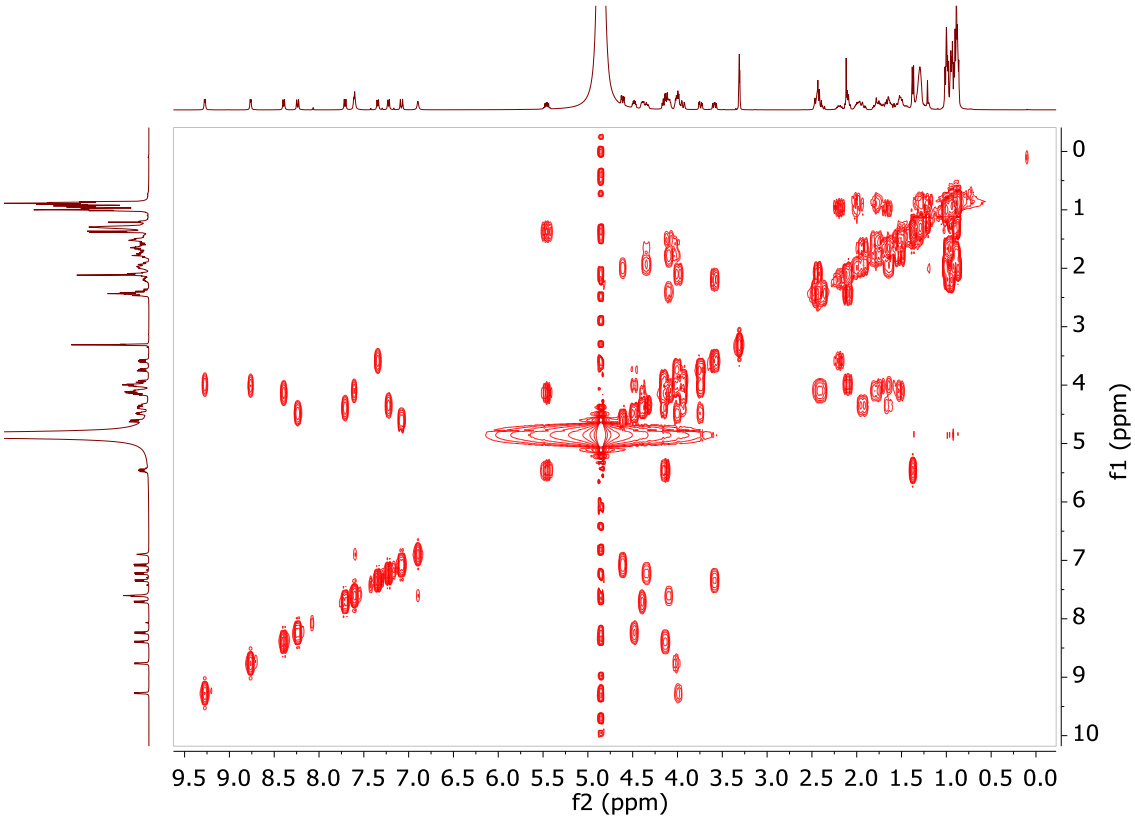

e. ^{1}H-^{13}C-HSQC

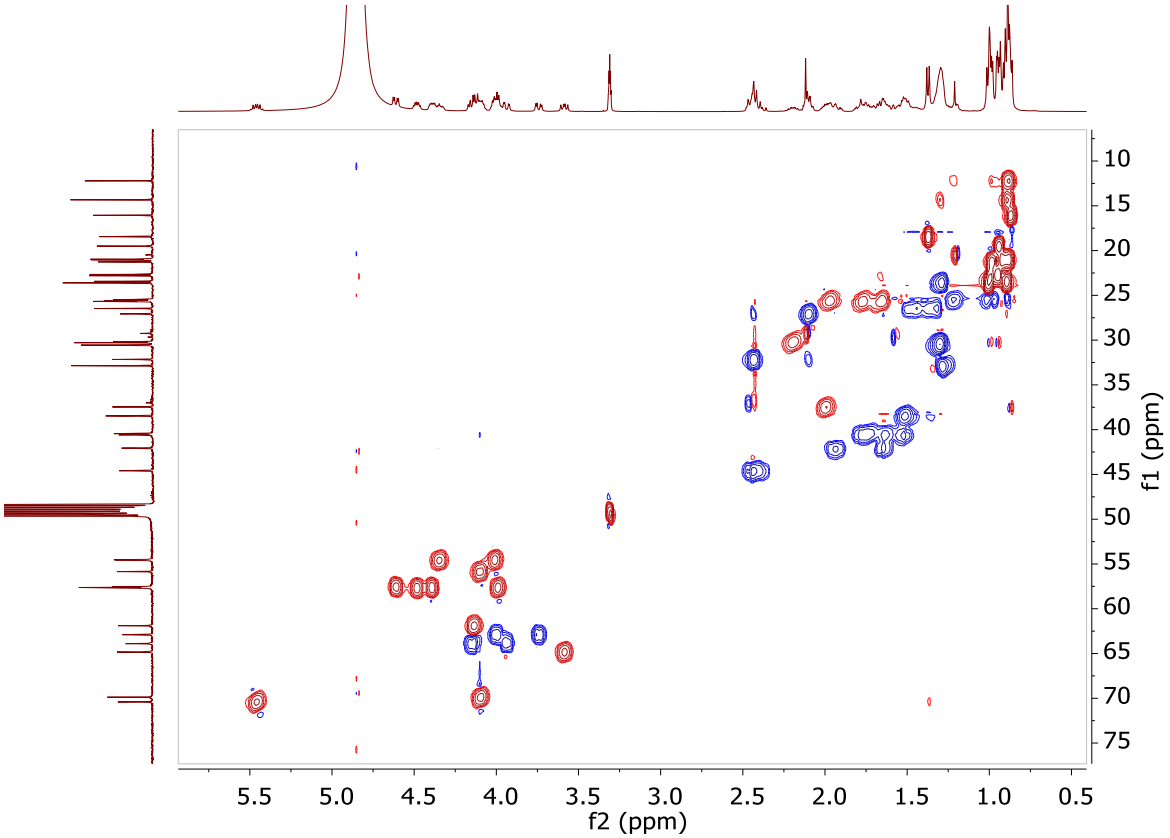

f. ^{1}H-^{13}C-HMBC

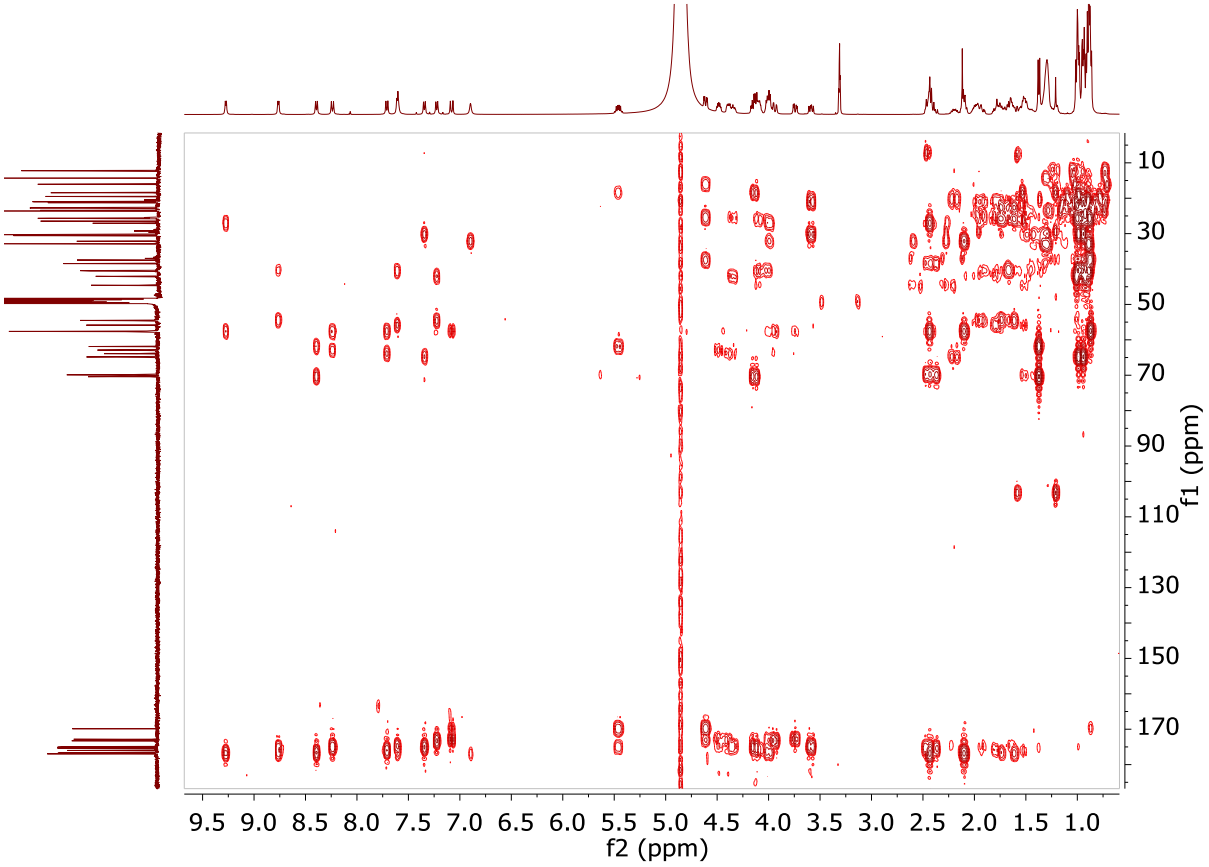

g. ^{1}H-^{13}C-HMBC-band selective

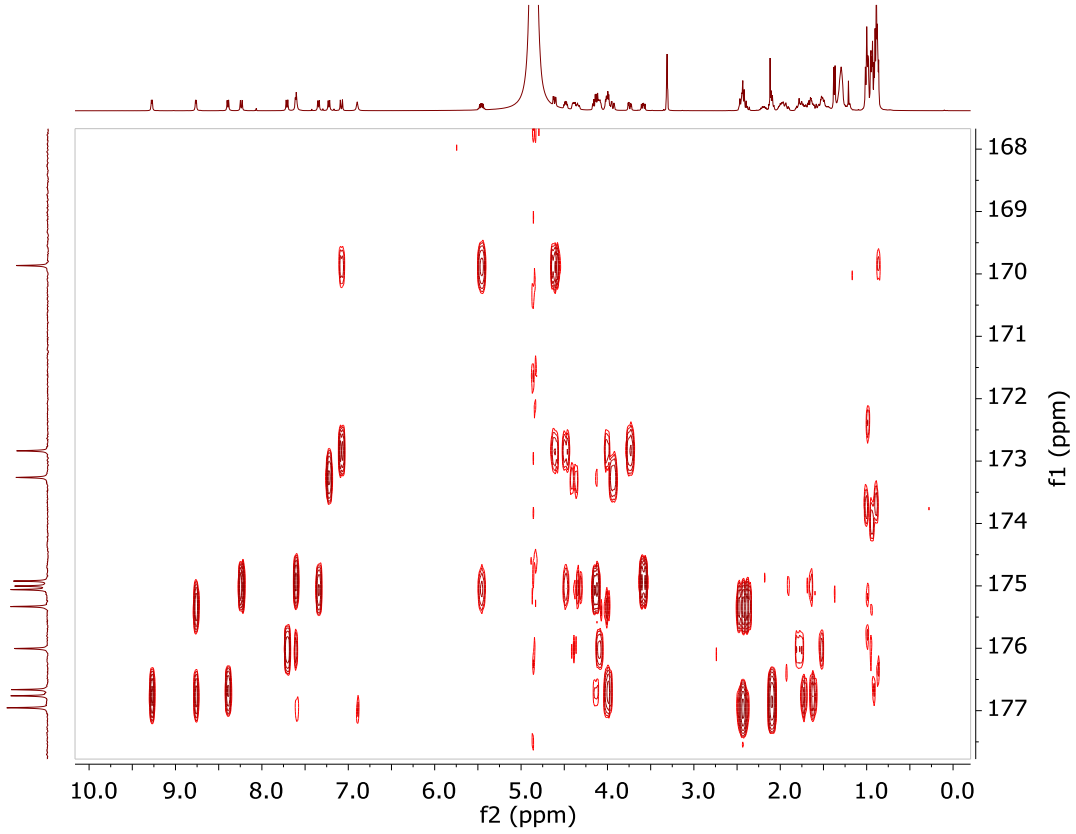

h. ^{1}H-^{13}C-HSQC-TOCSY

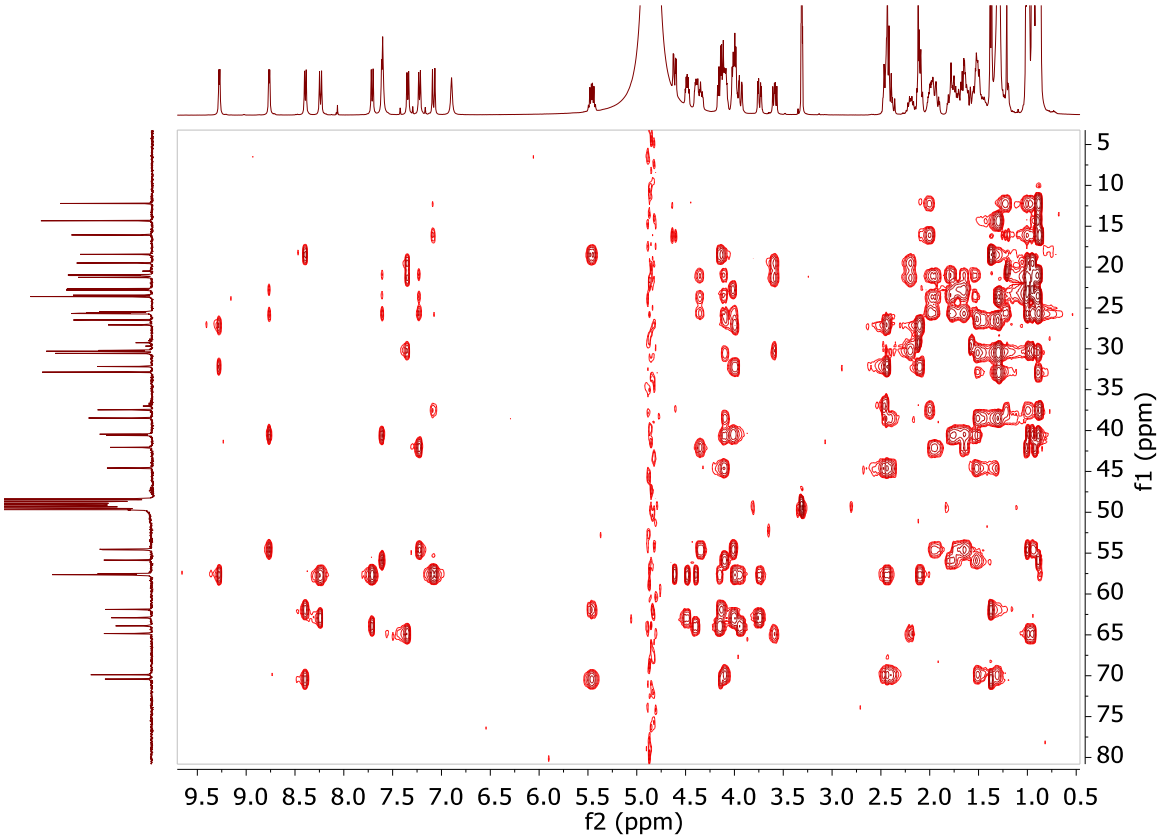

i. ^{1}H-^{1}H-TOCSY

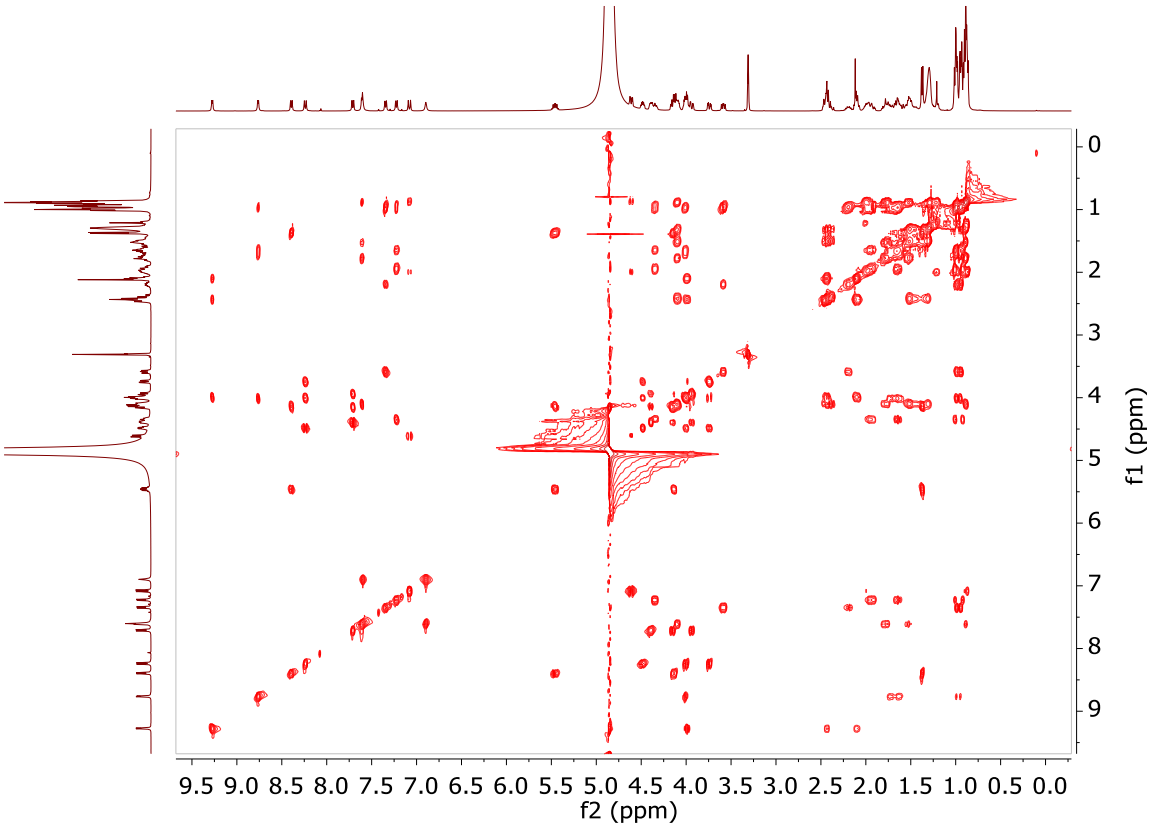

j. ^{1}H-^{1}H-NOESY

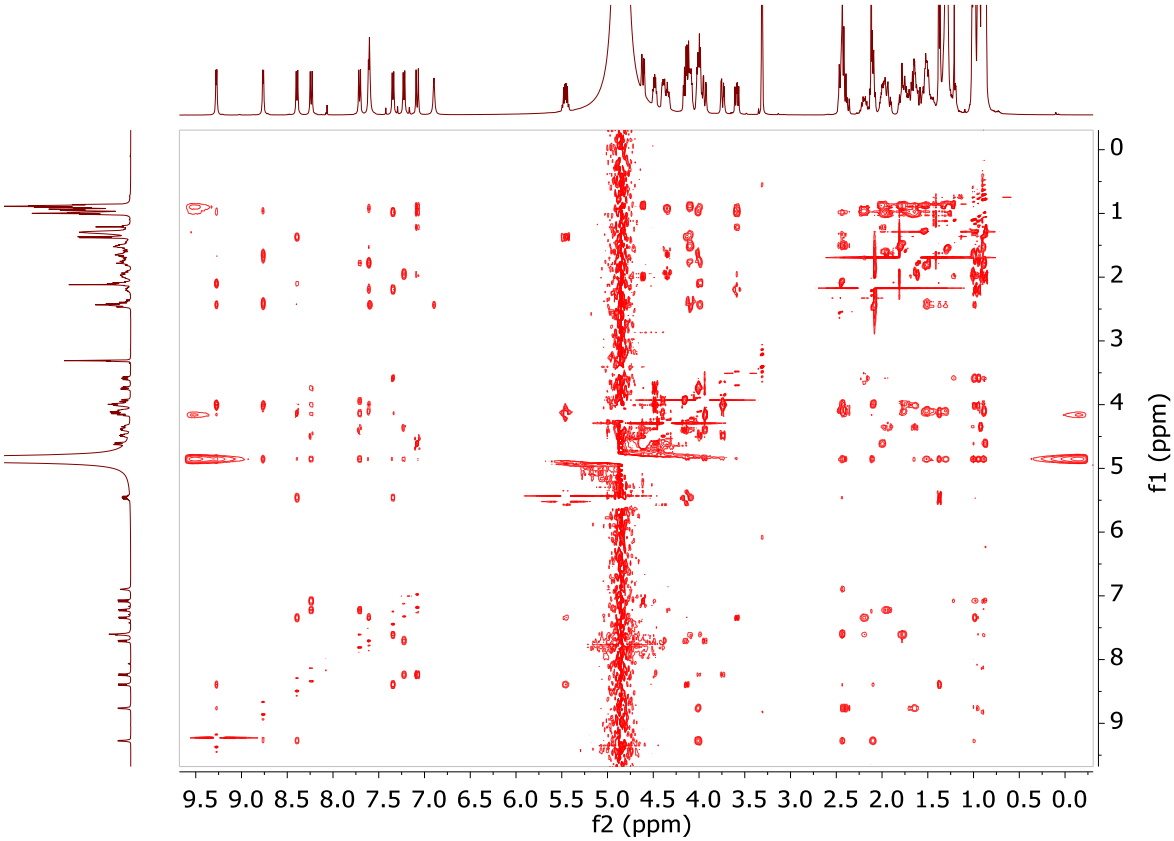

k. ^{1}H-^{15}N-HSQC

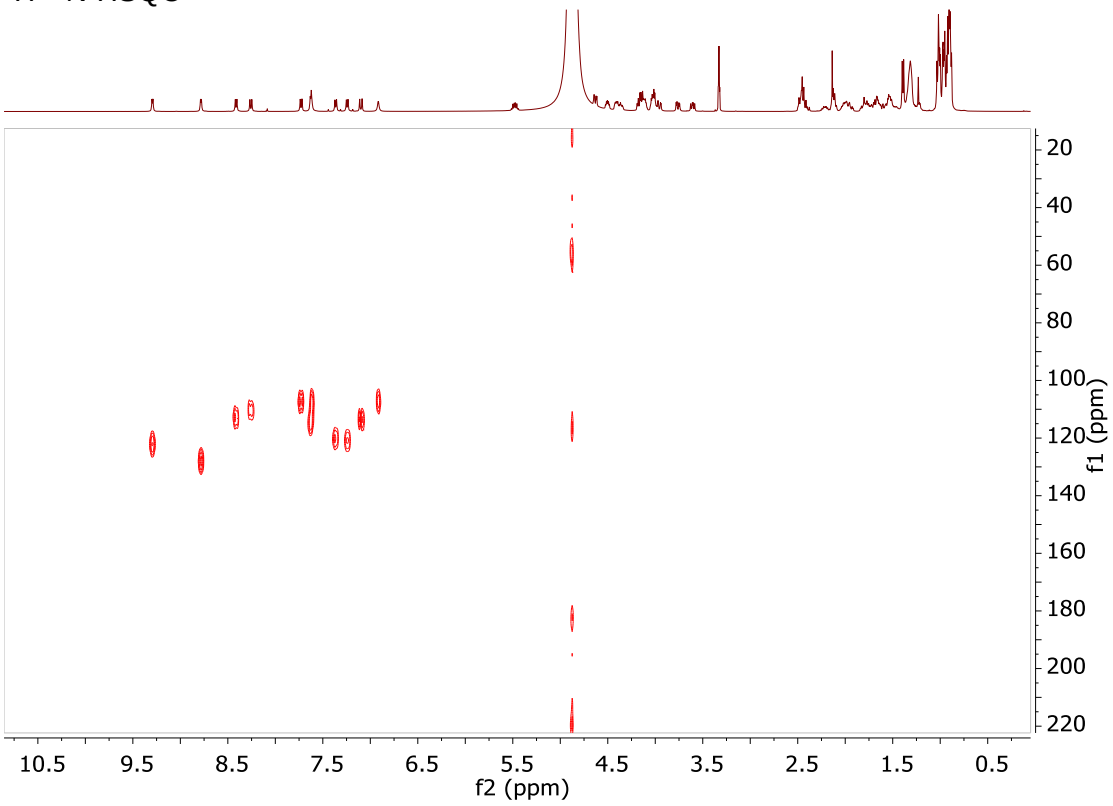

l. ^{1}H-^{15}N-HMBC

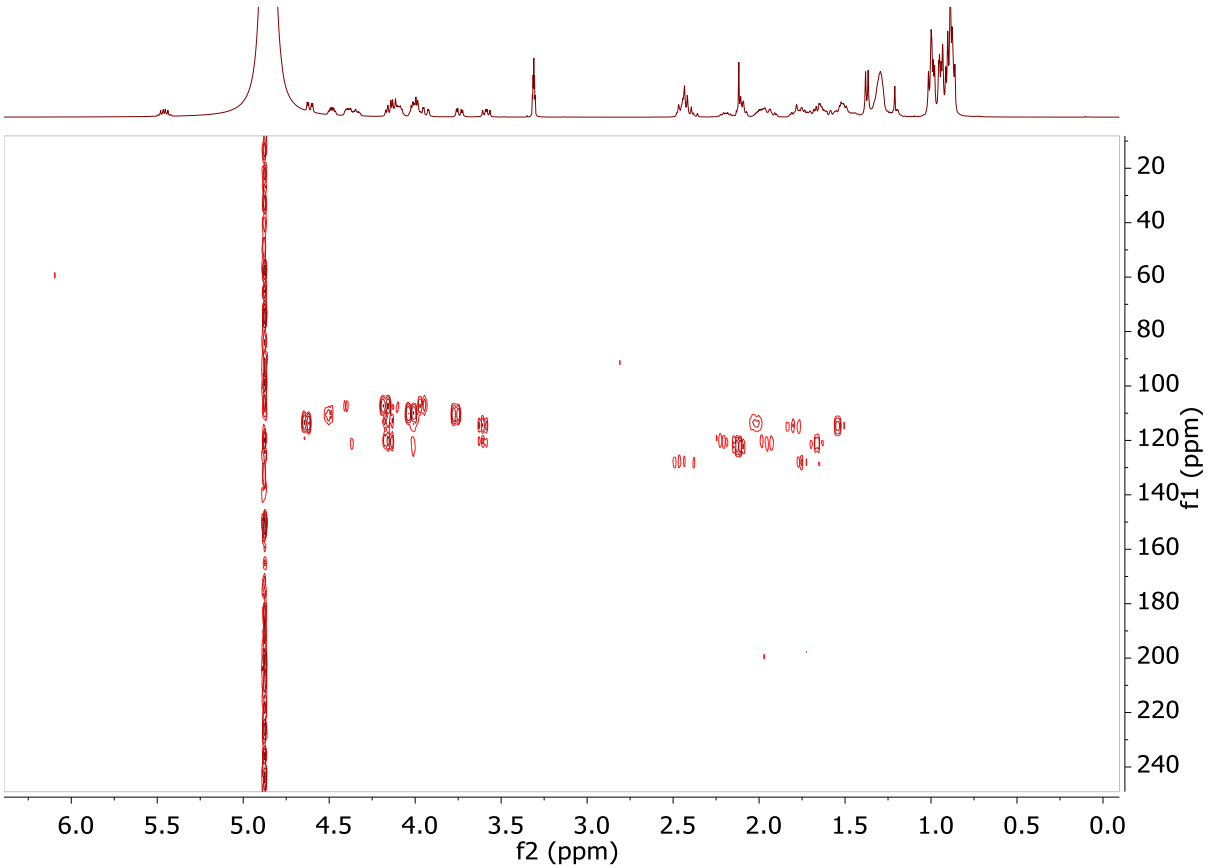

Figure A6: NMR spectra of compound **1** (d_3-MeOH, 400 MHz)

a. ^{1}H-NMR

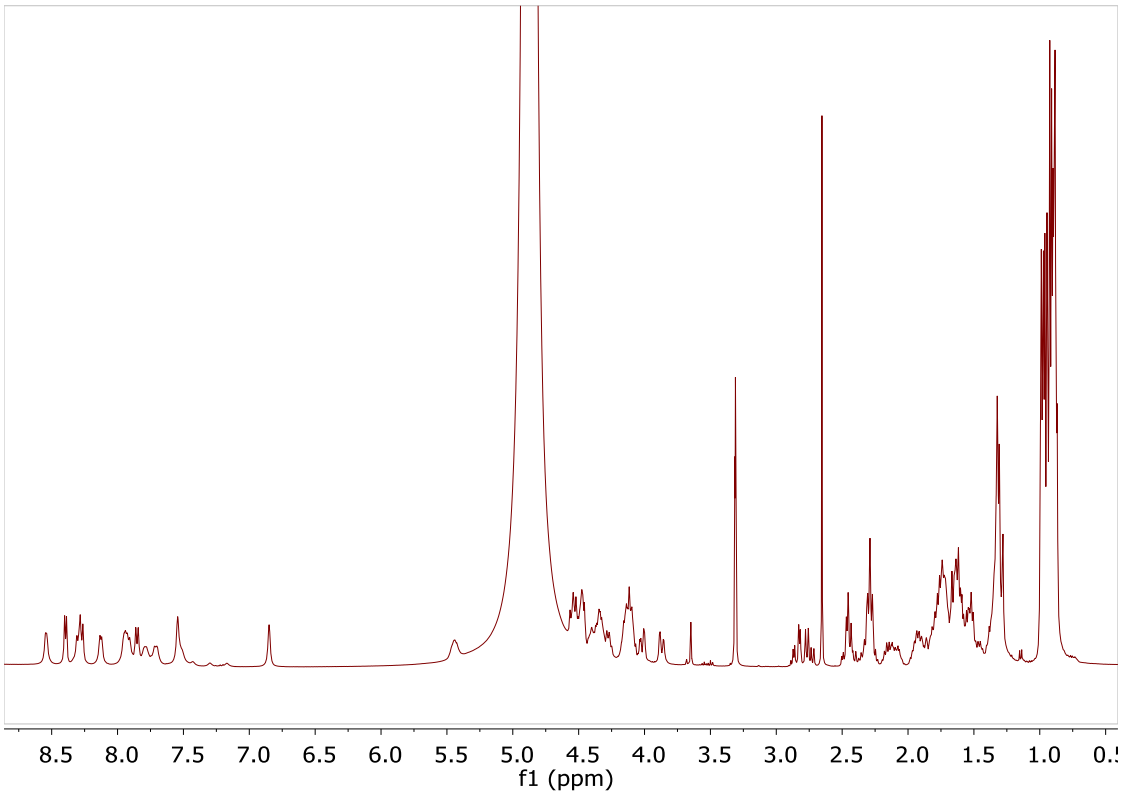

b. ^{13}C-NMR (100MHz)

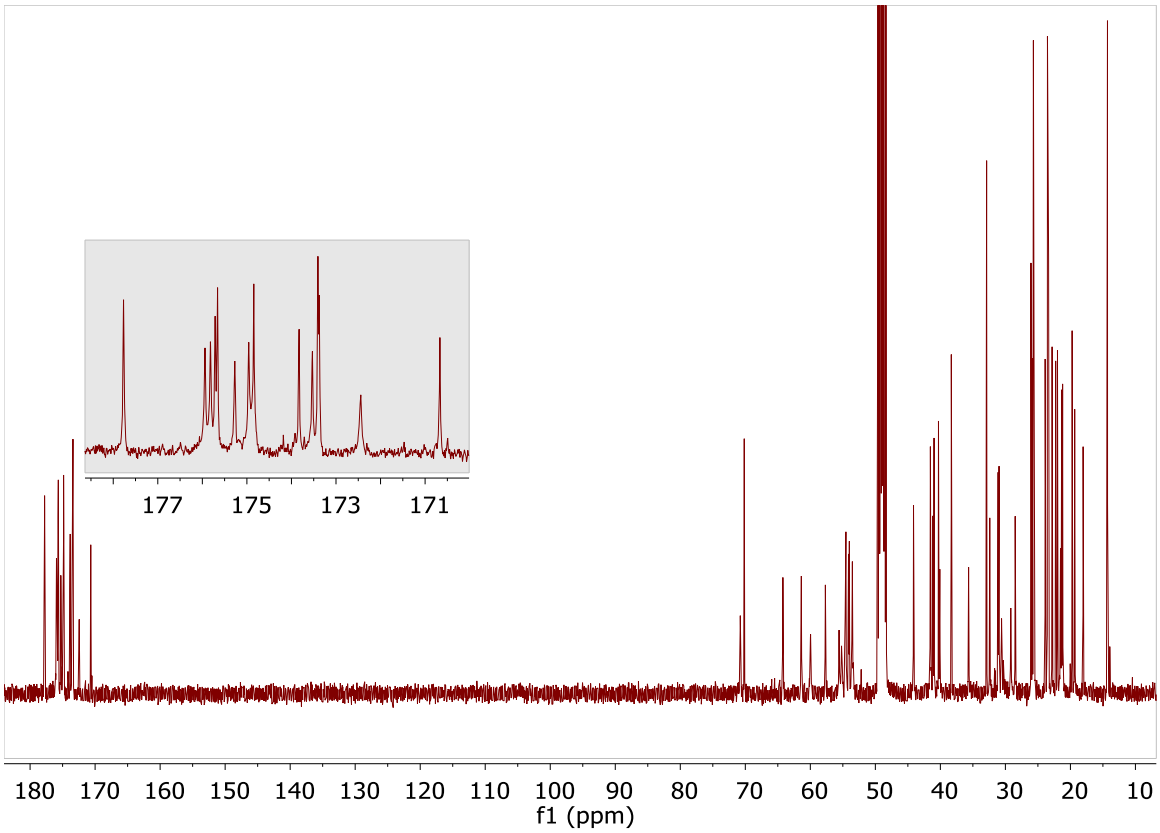

c. ^{13}C-DEPT-135

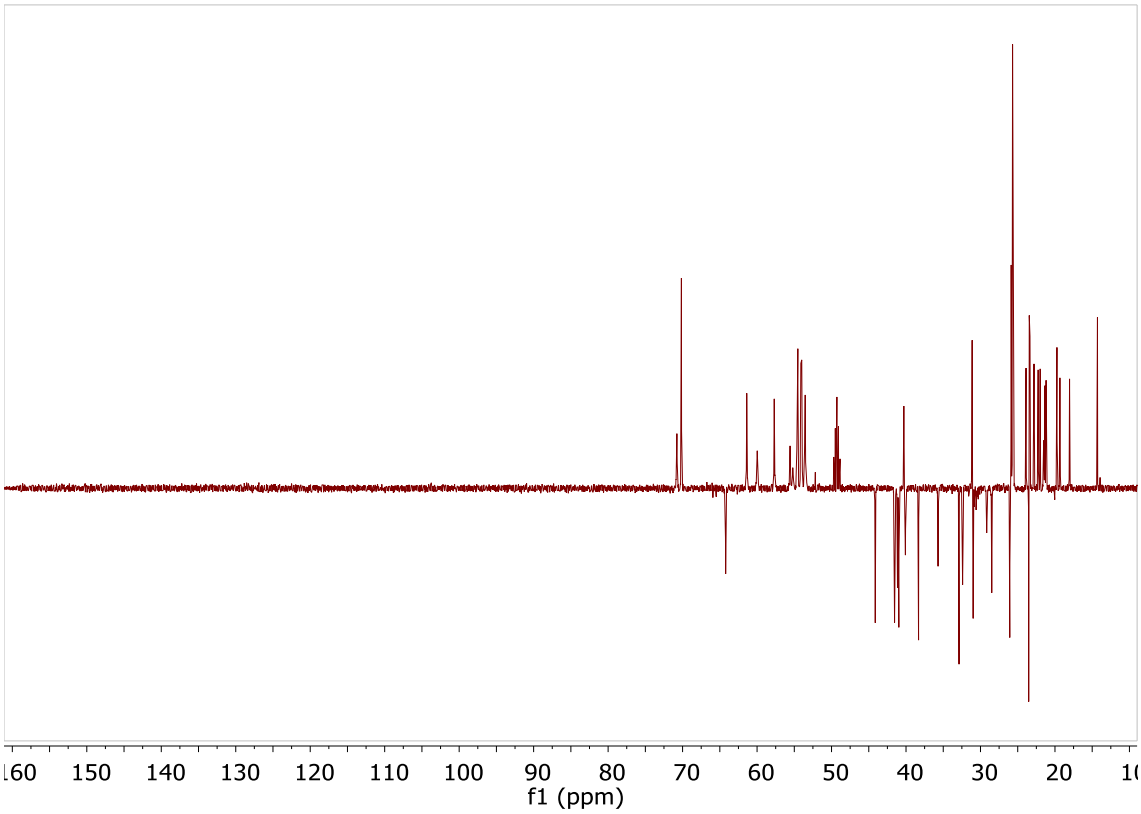

d. ^{13}C-J-mode NMR

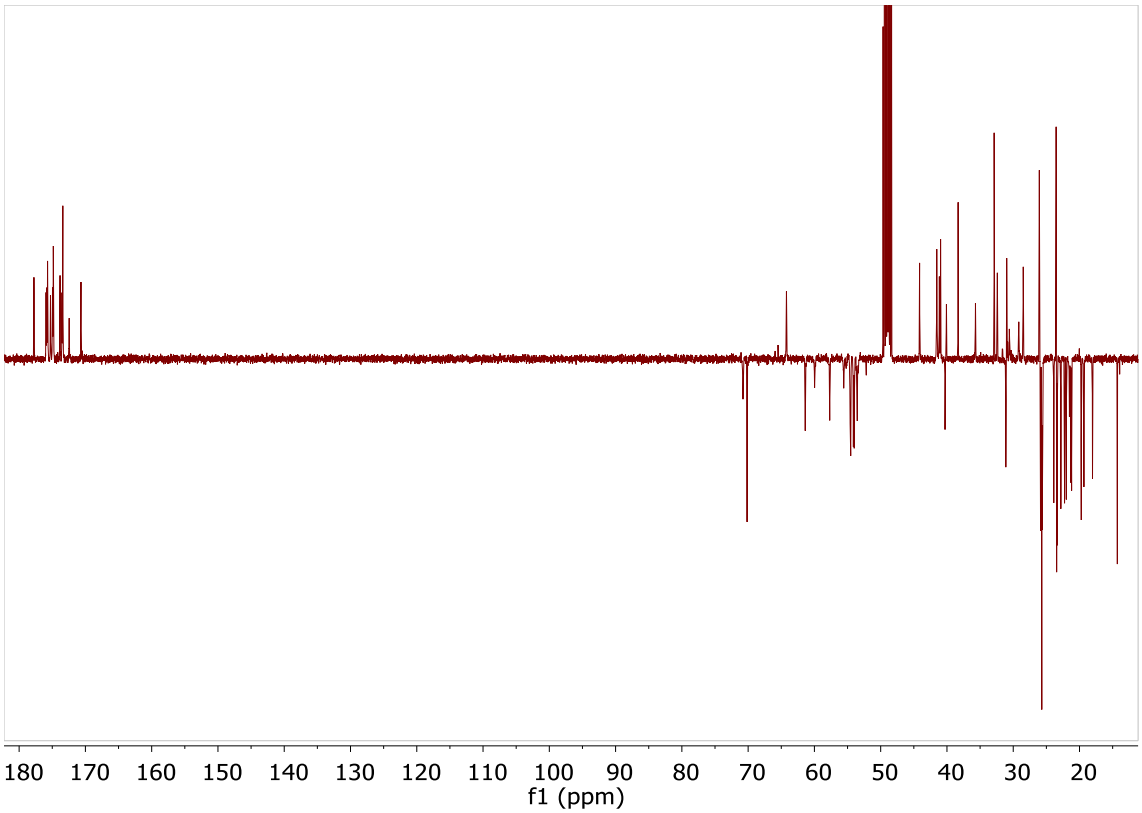

e. ^{1}H-^{1}H-COSY

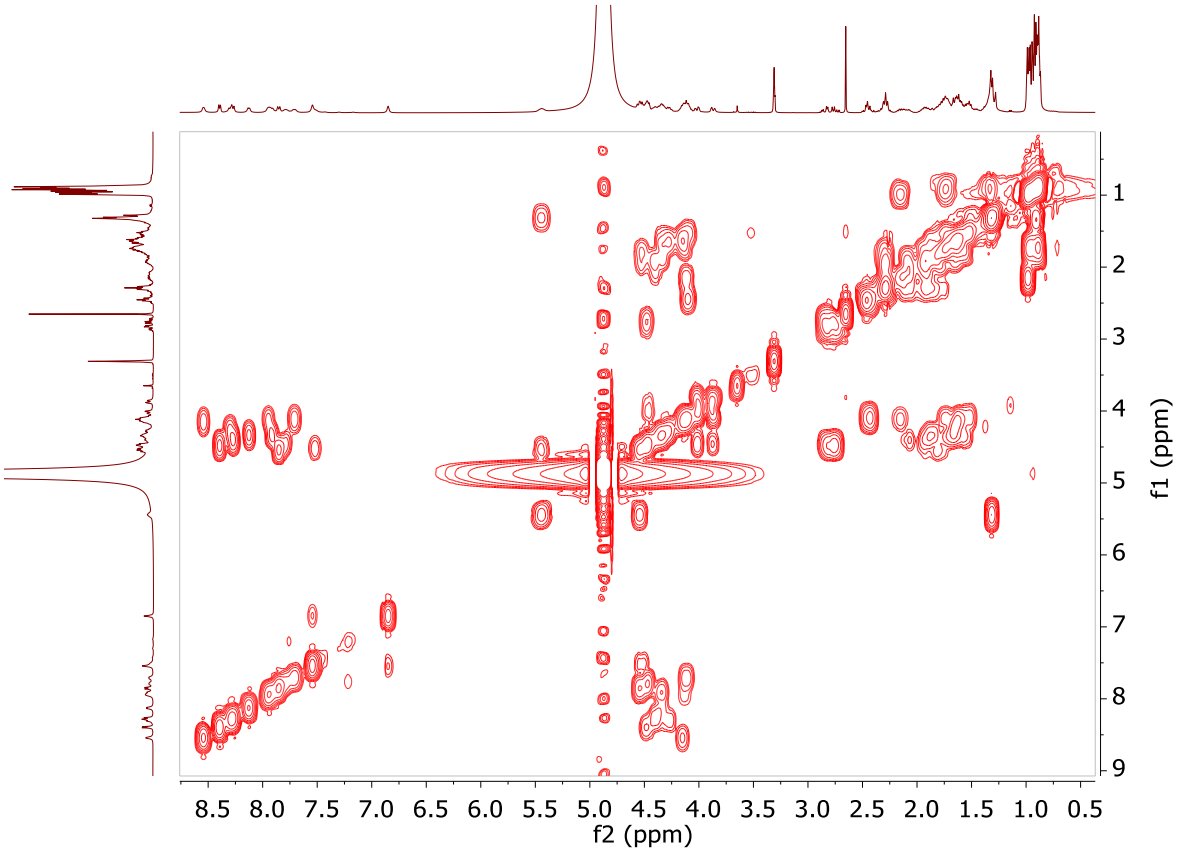

f. ^{1}H-^{13}C-HSQC

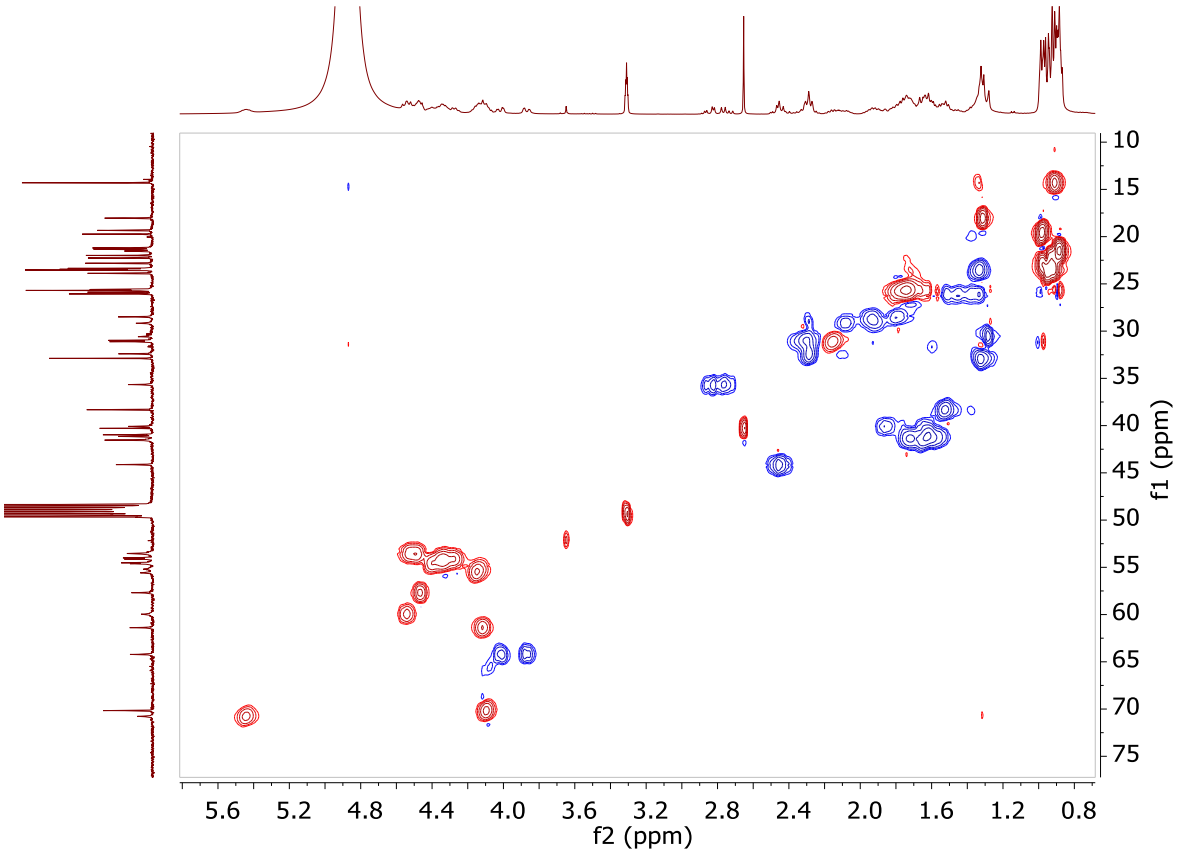

g. ^{1}H-^{1}H-TOCSY

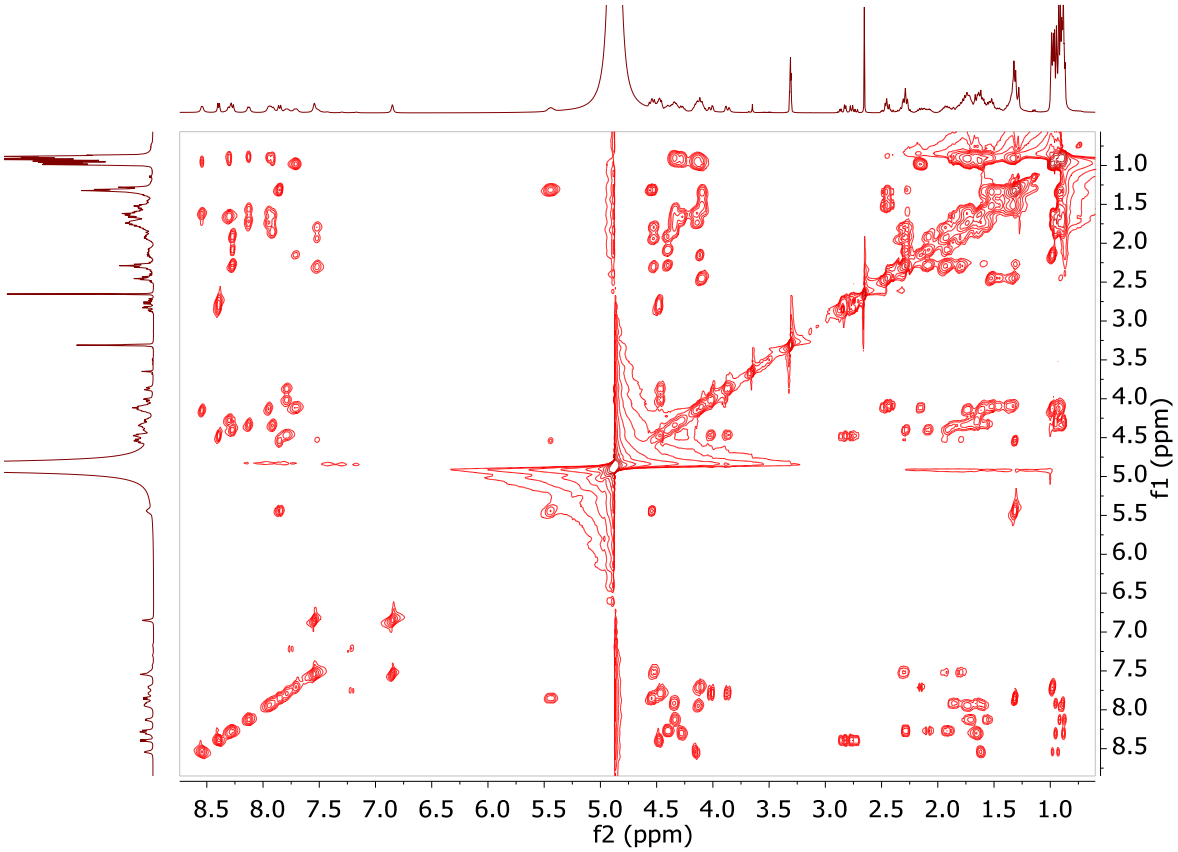

h. ^{1}H-^{13}C-HSQC-TOCSY

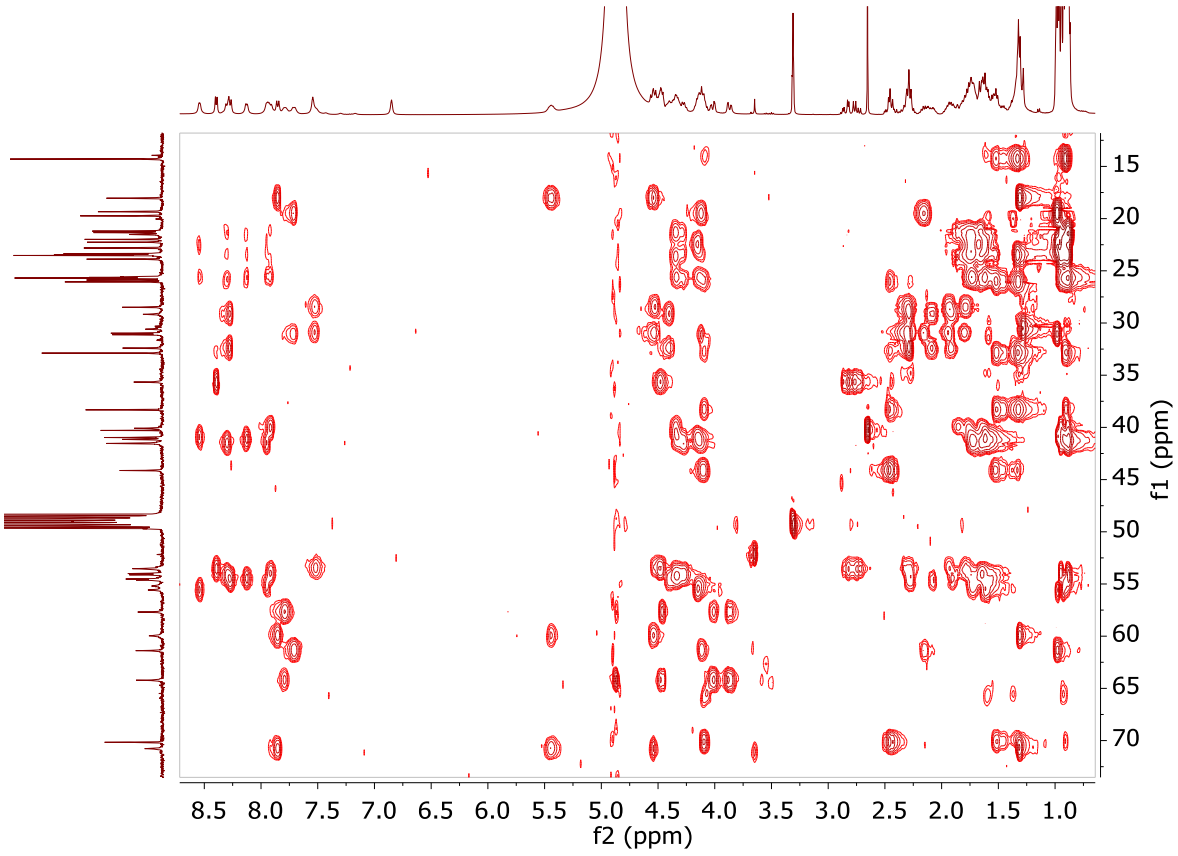

i. ^{1}H-^{13}C-HMBC

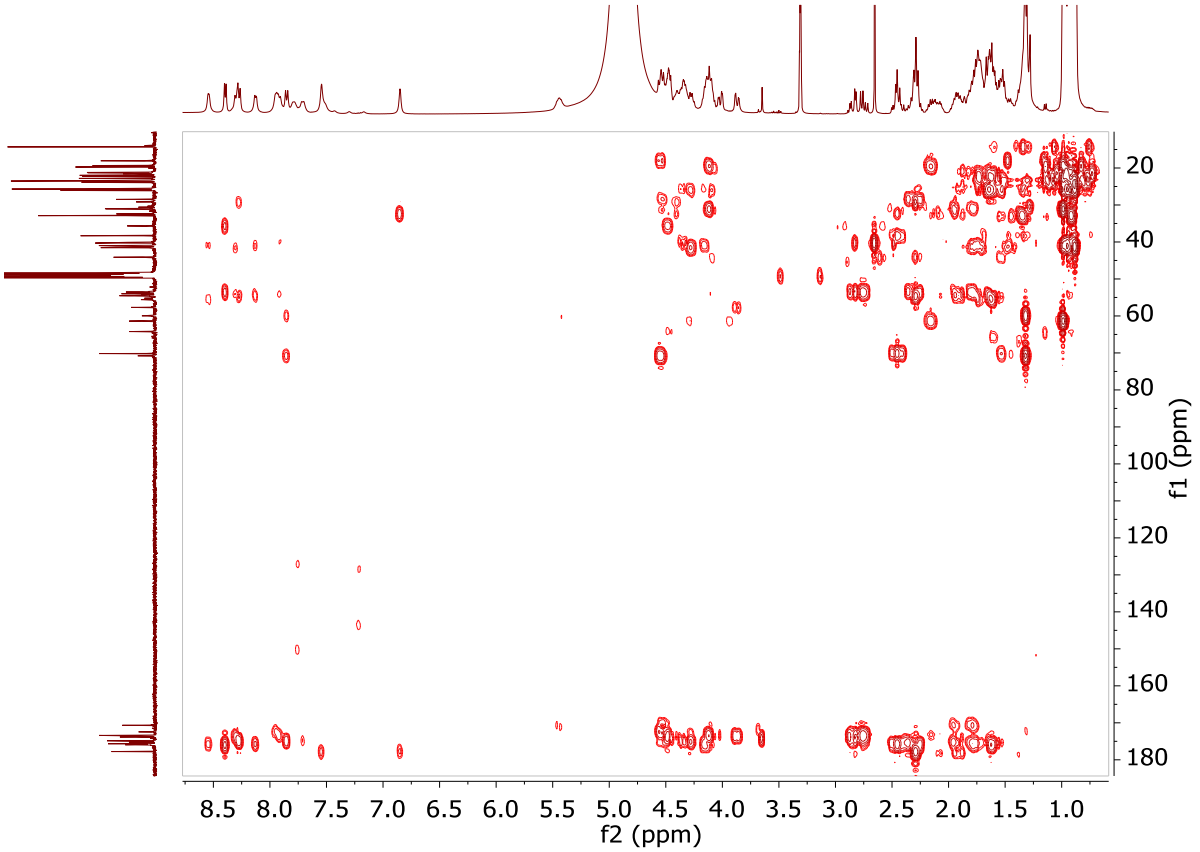

j. ^{1}H-^{1}H-NOESY

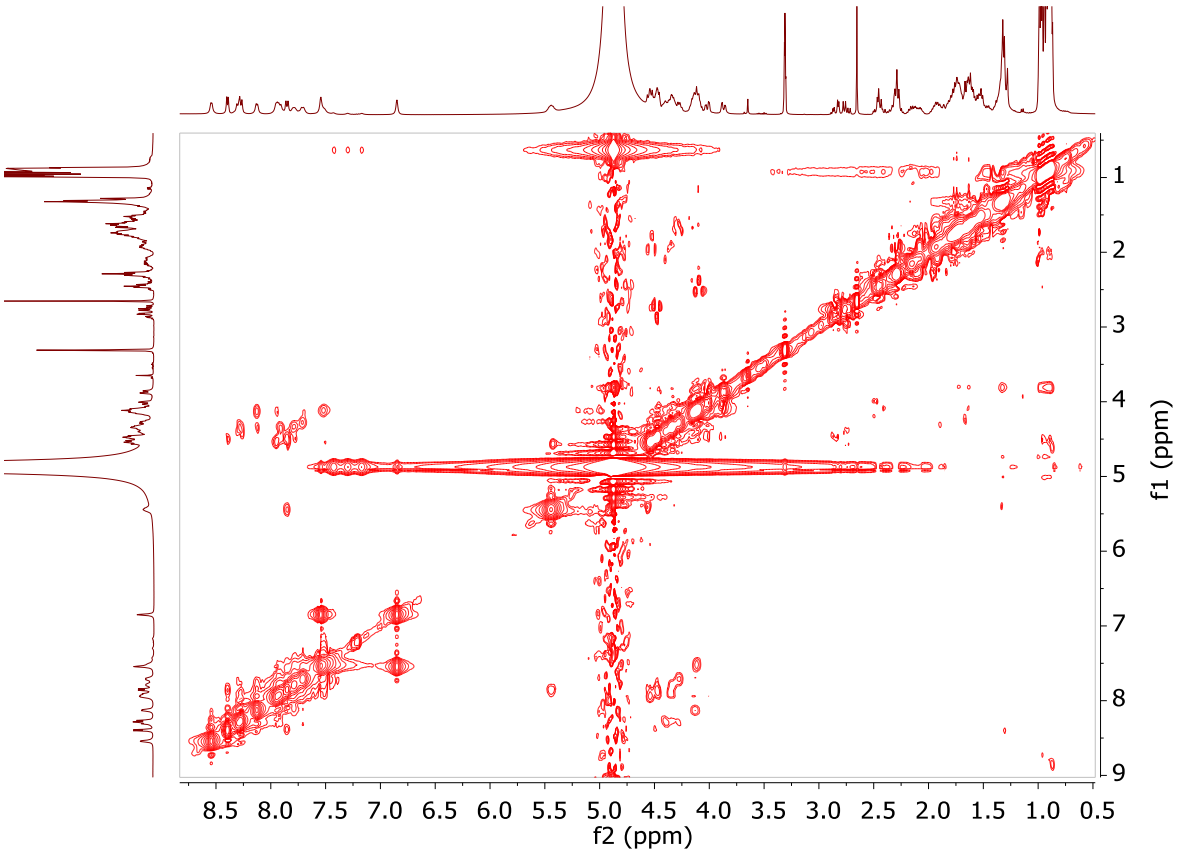

k. ^{1}H-^{15}N-HSQC

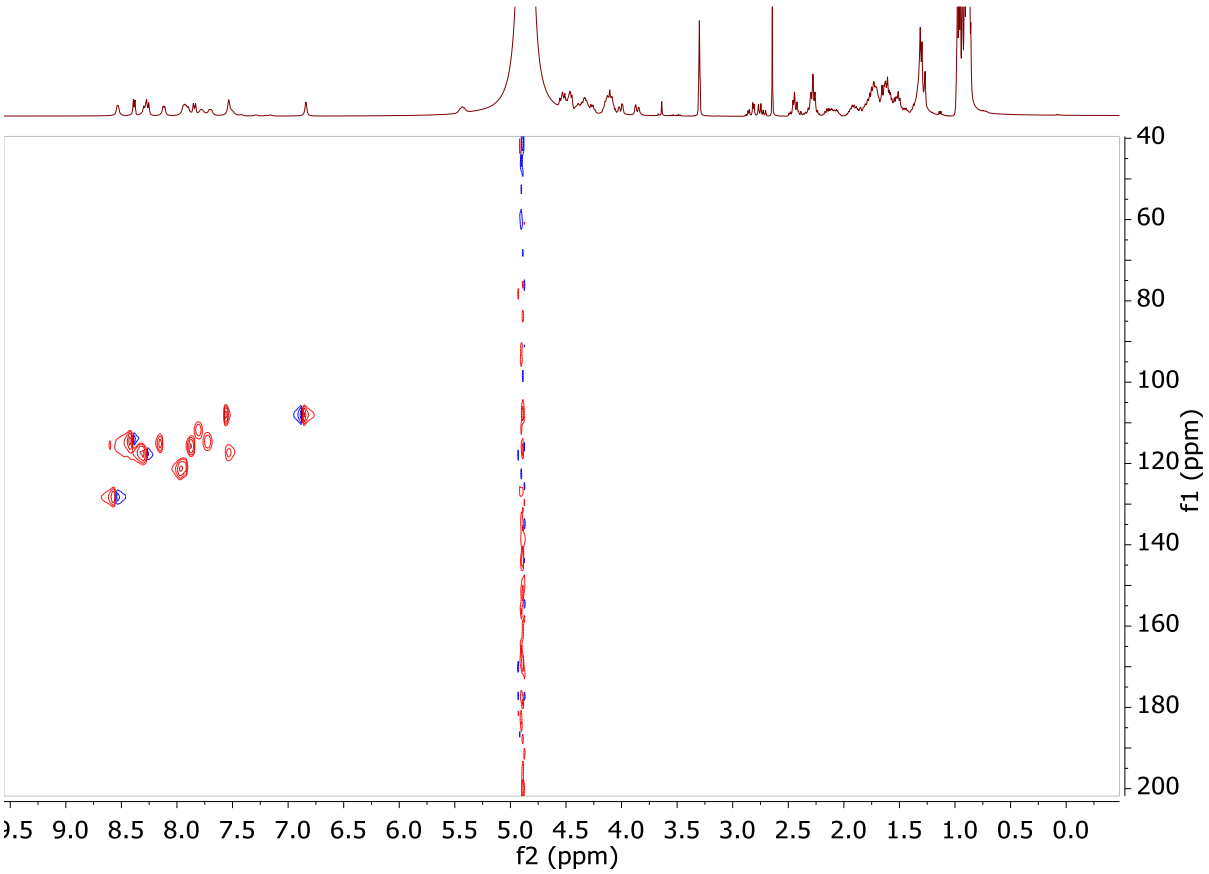

l. ^{1}H-^{15}N-HMBC

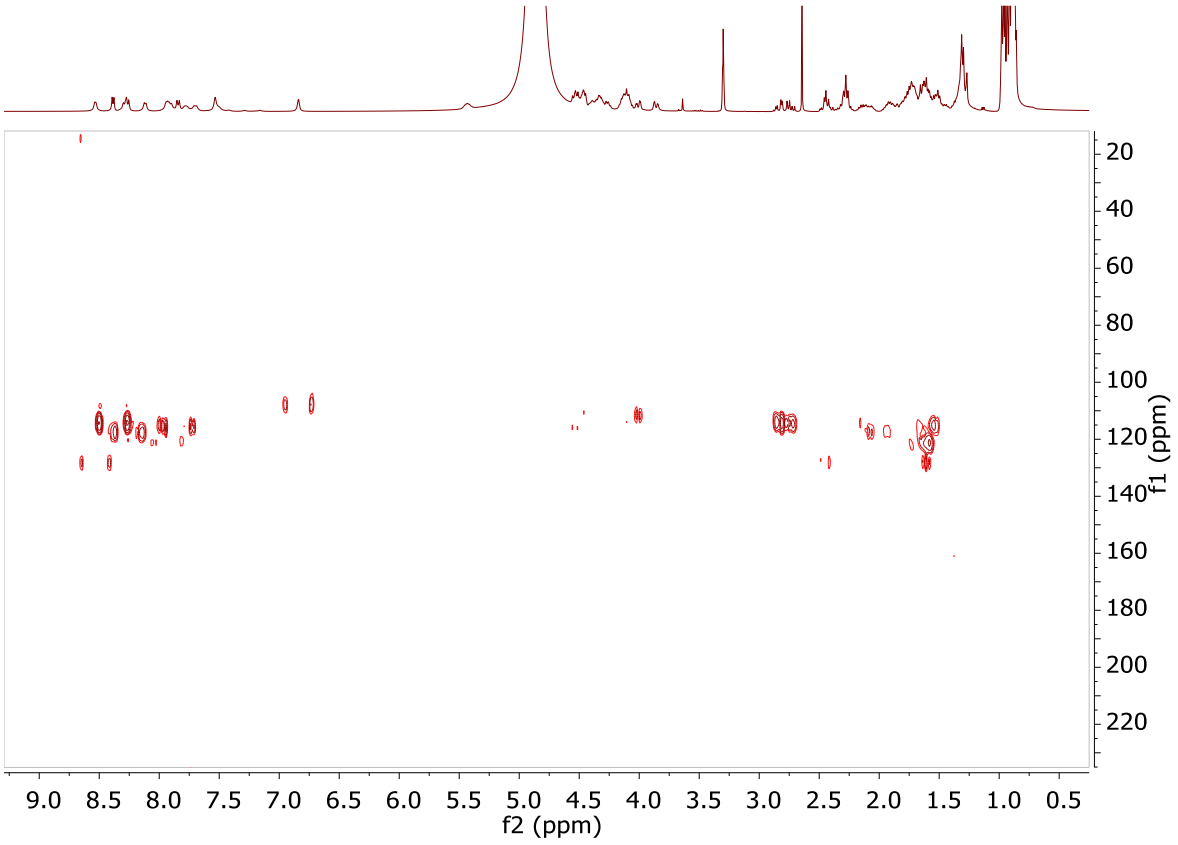

m. ^{1}H-^{13}C-HMBC-Band Selective

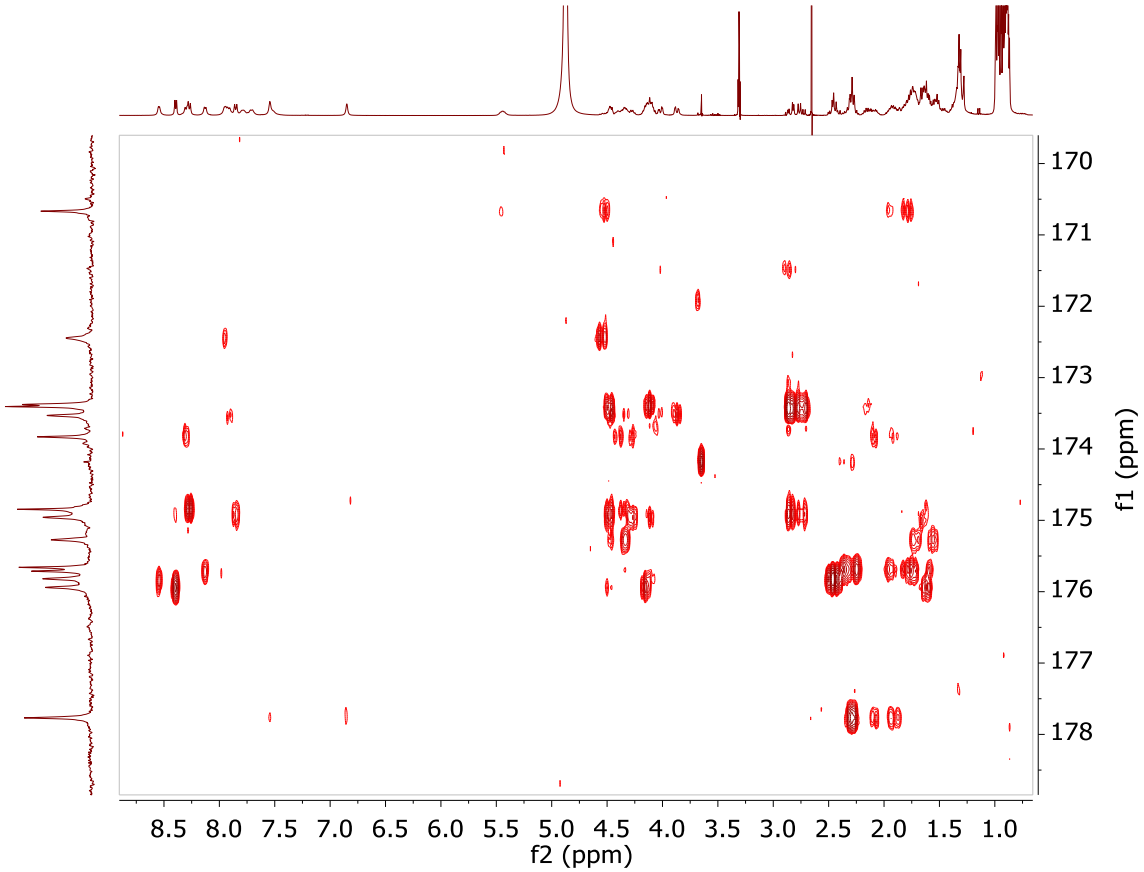

n. ^{1}H-^{13}C-HMBC-Band Selective

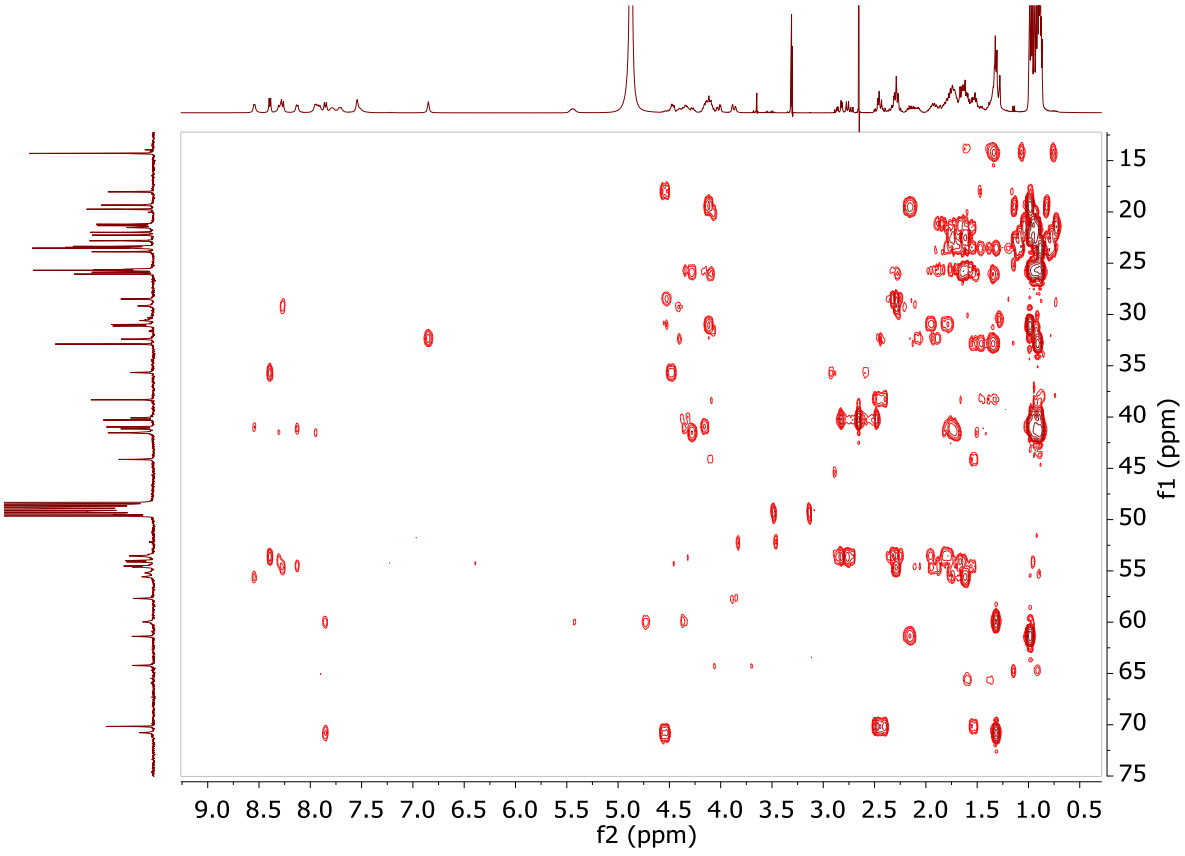

o. ^{1}H-^{13}C-HSQC-Band Selective

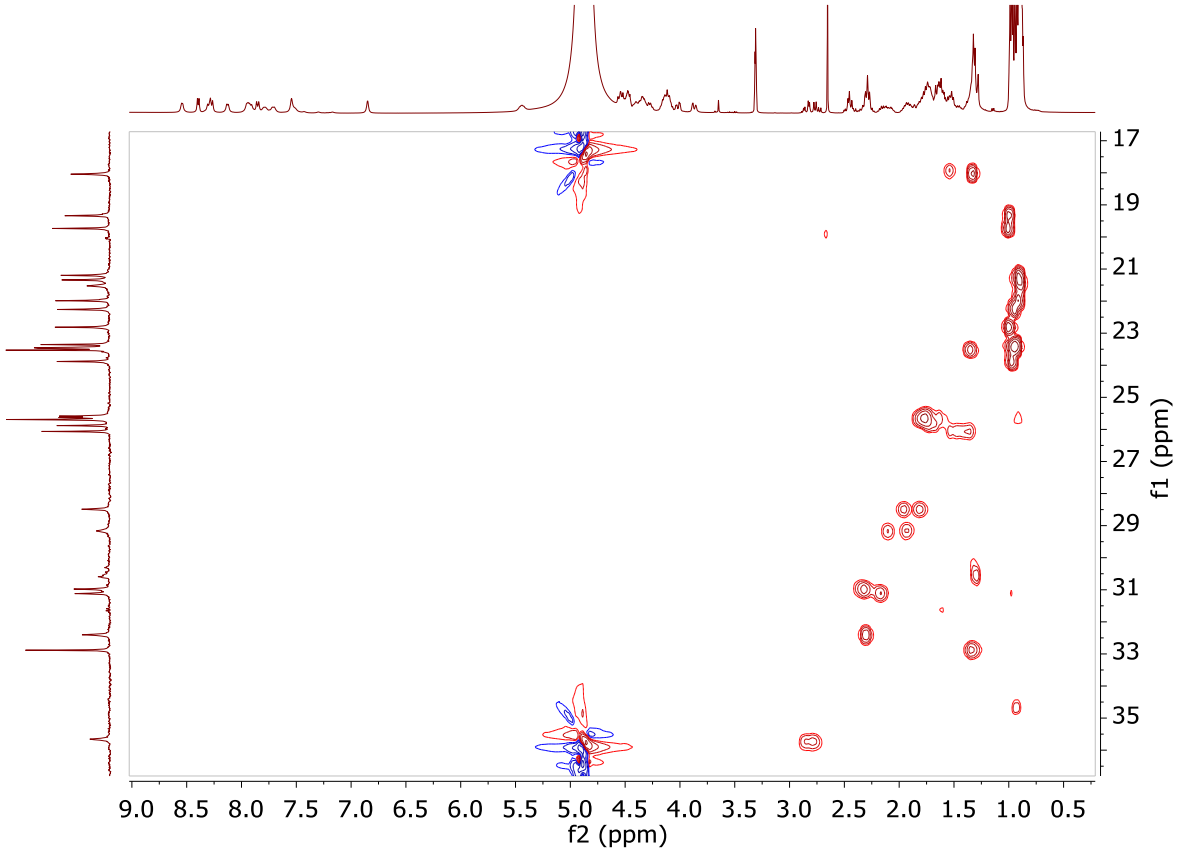

p. ^{1}H-^{13}C-HSQC-Band Selective

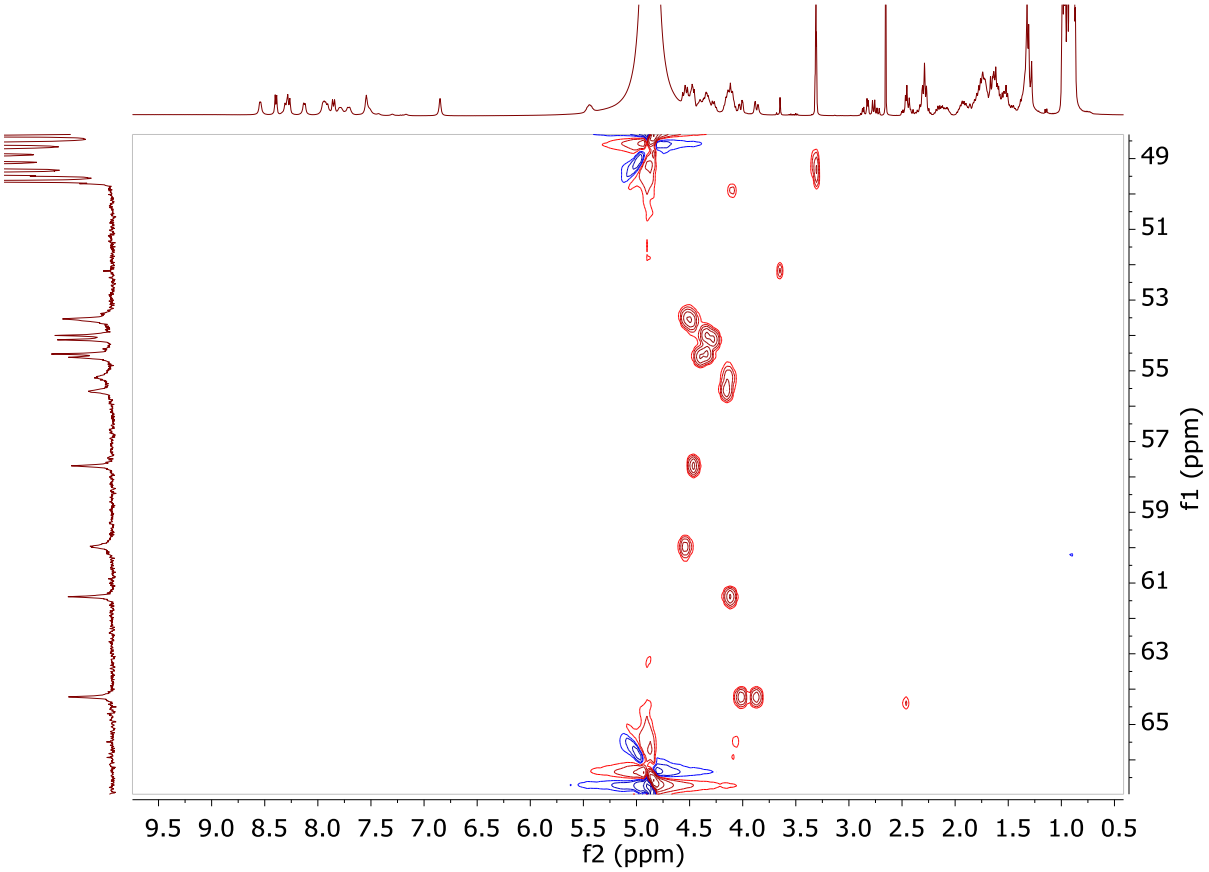

Figure A7: NMR spectra of compound **1** (d_3-MeOH, 700 MHz)

a. ^{1}H-NMR

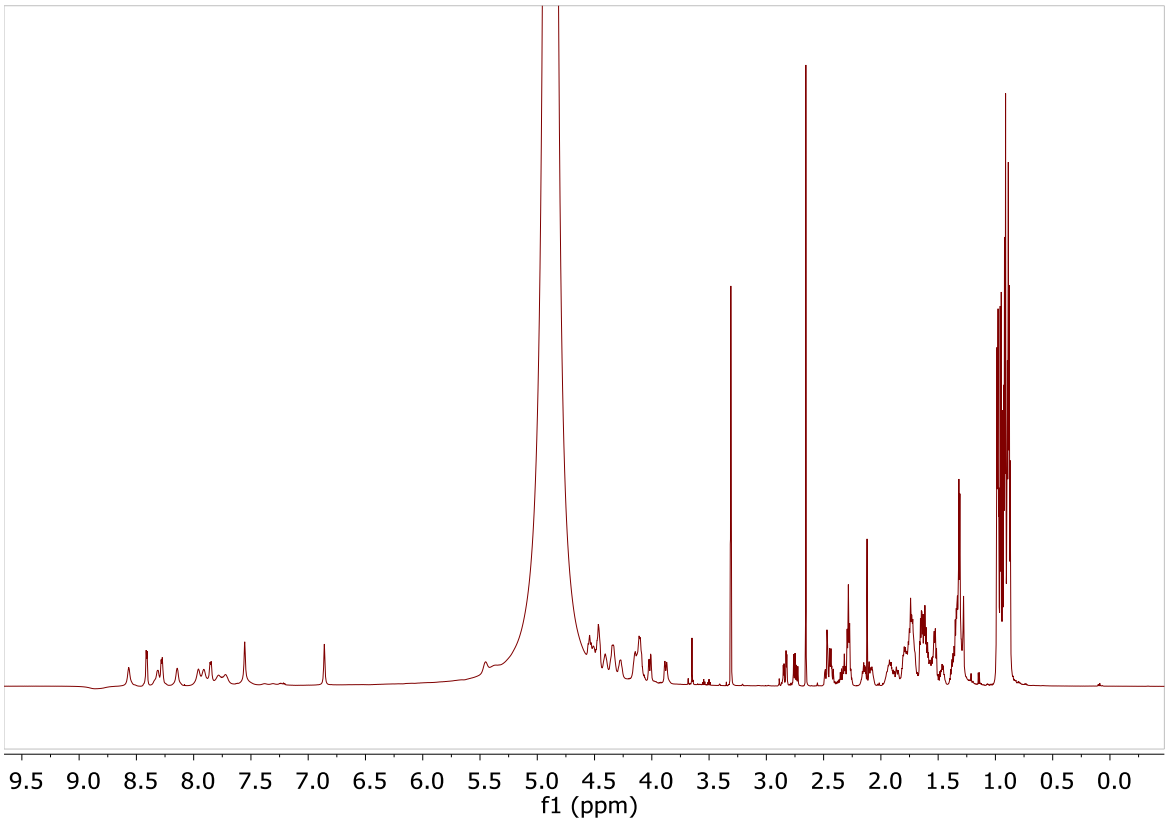

b. ^{13}C-NMR (176 MHz)

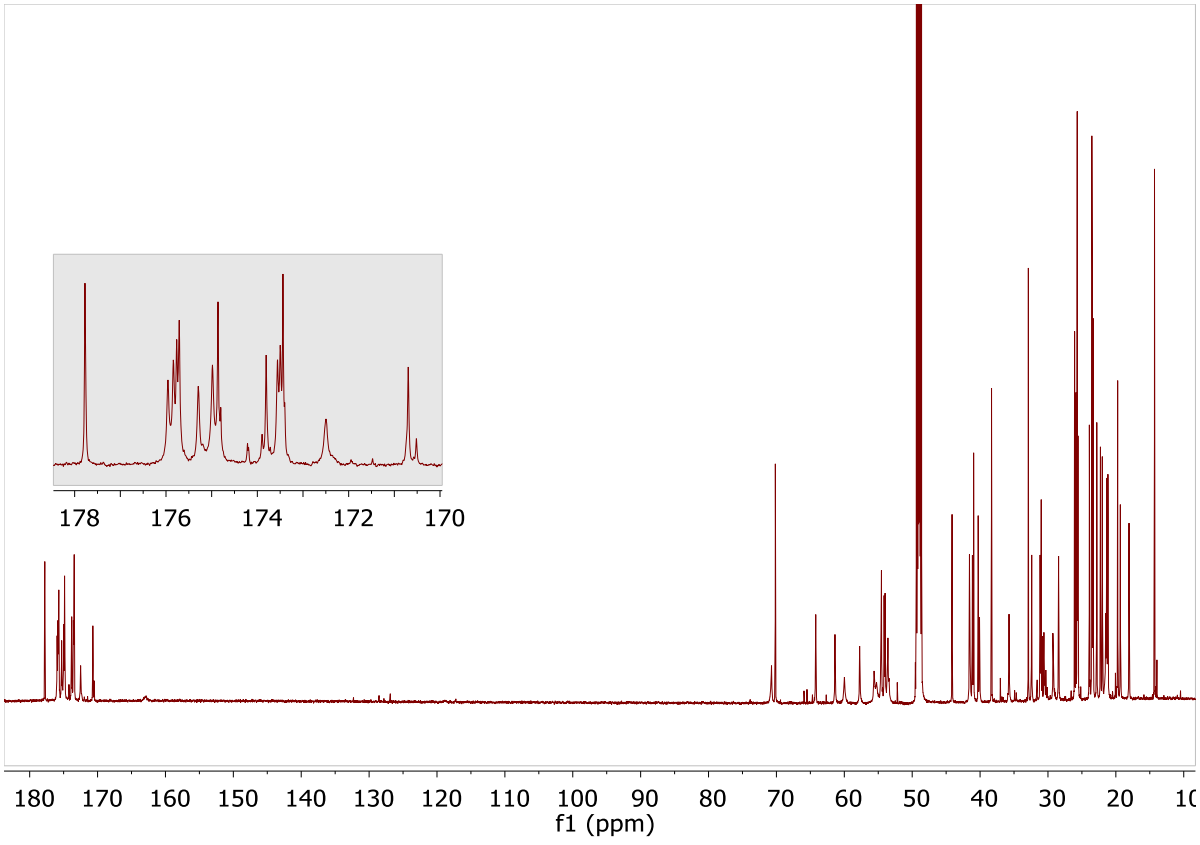

c. ^{1}H-^{13}C-HSQC

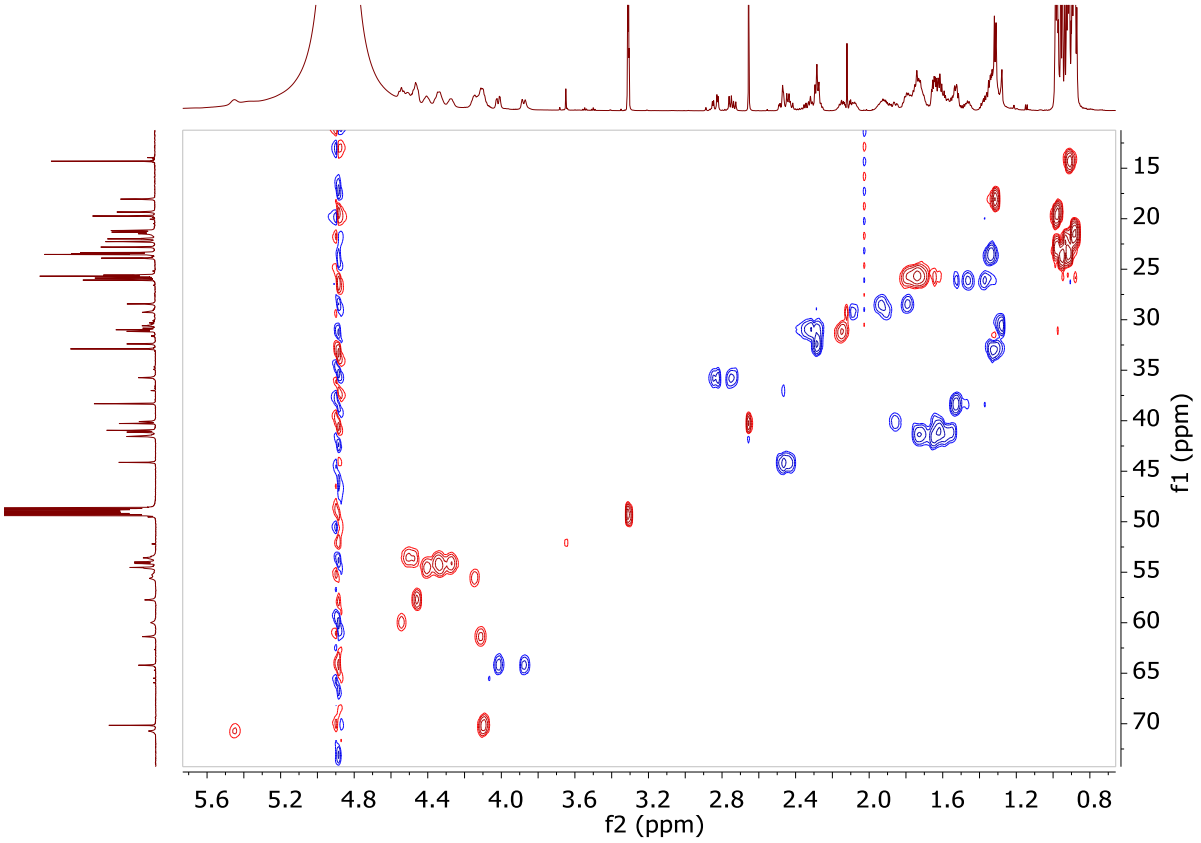

d. ^{1}H-^{1}H-COSY

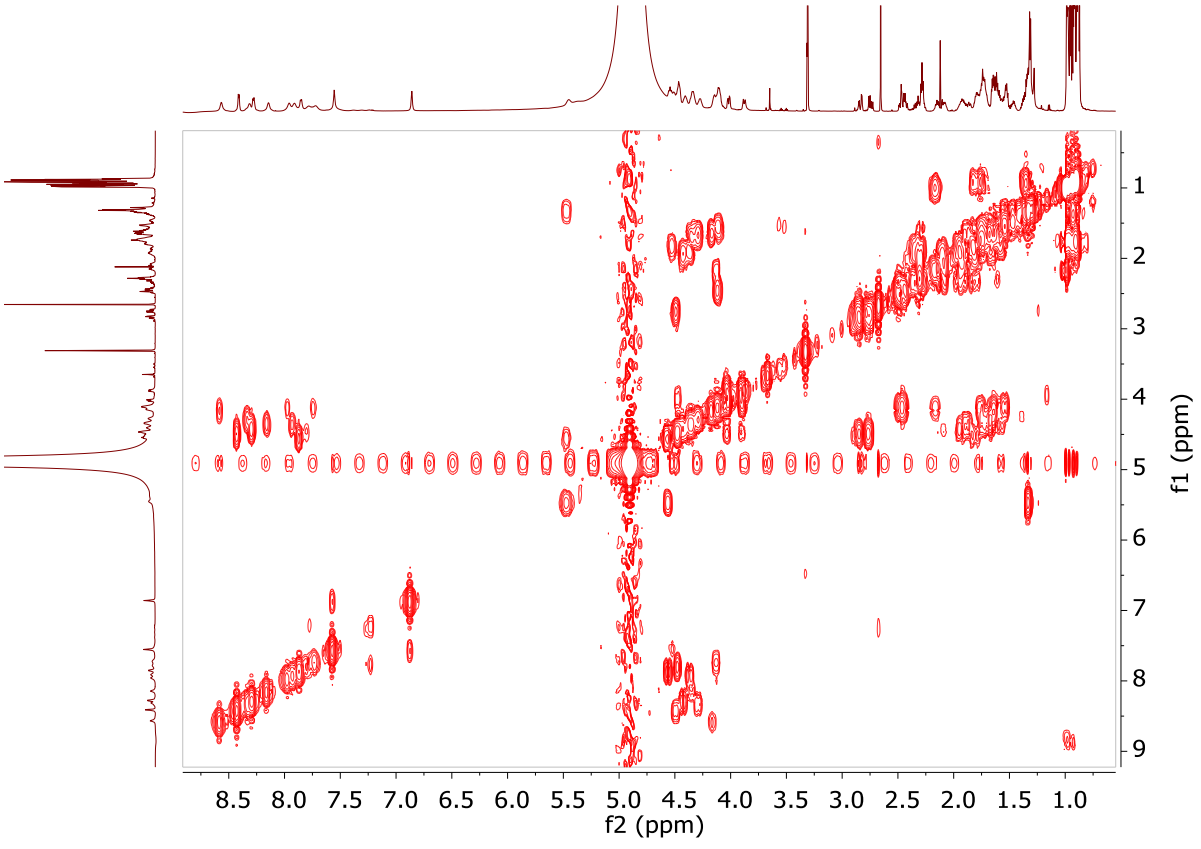

e. ^{1}H-^{13}C-HSQC-TOCSY

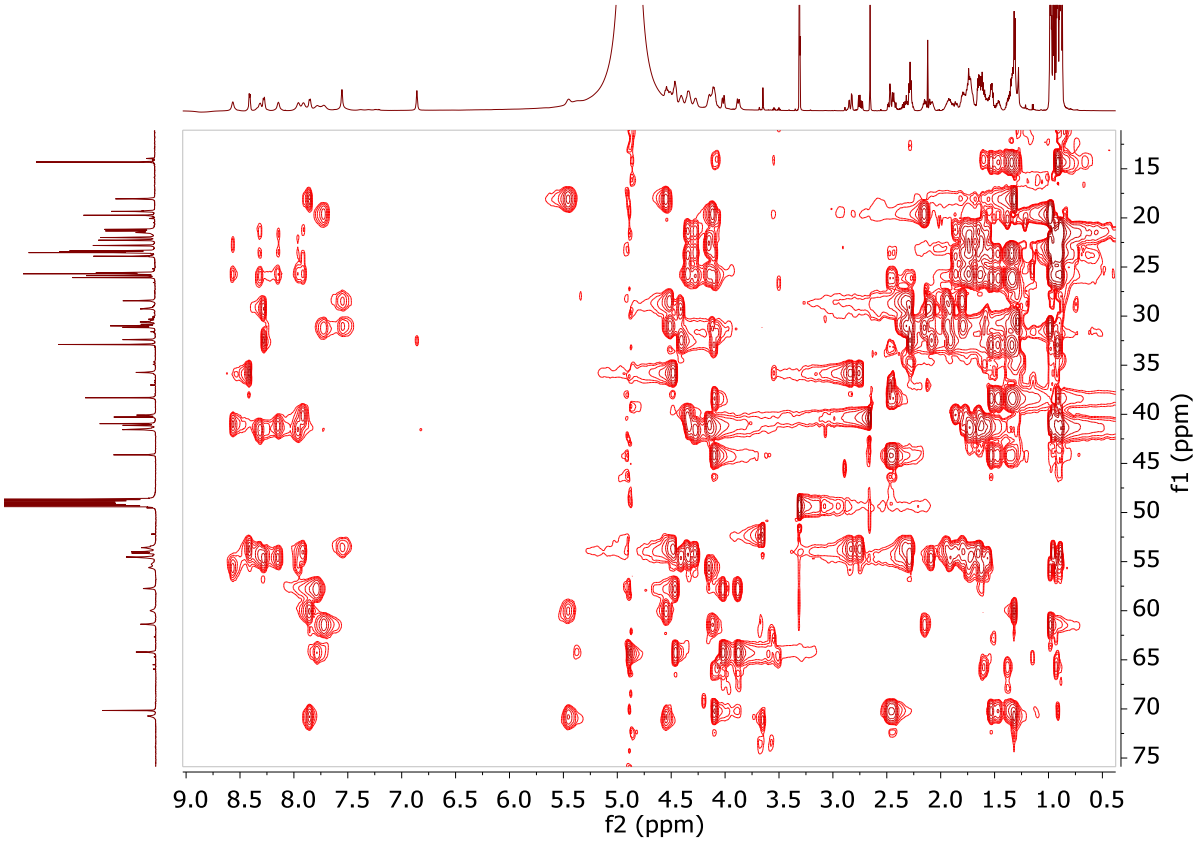

f. ^{1}H-^{13}C-HMBC-Band Selective

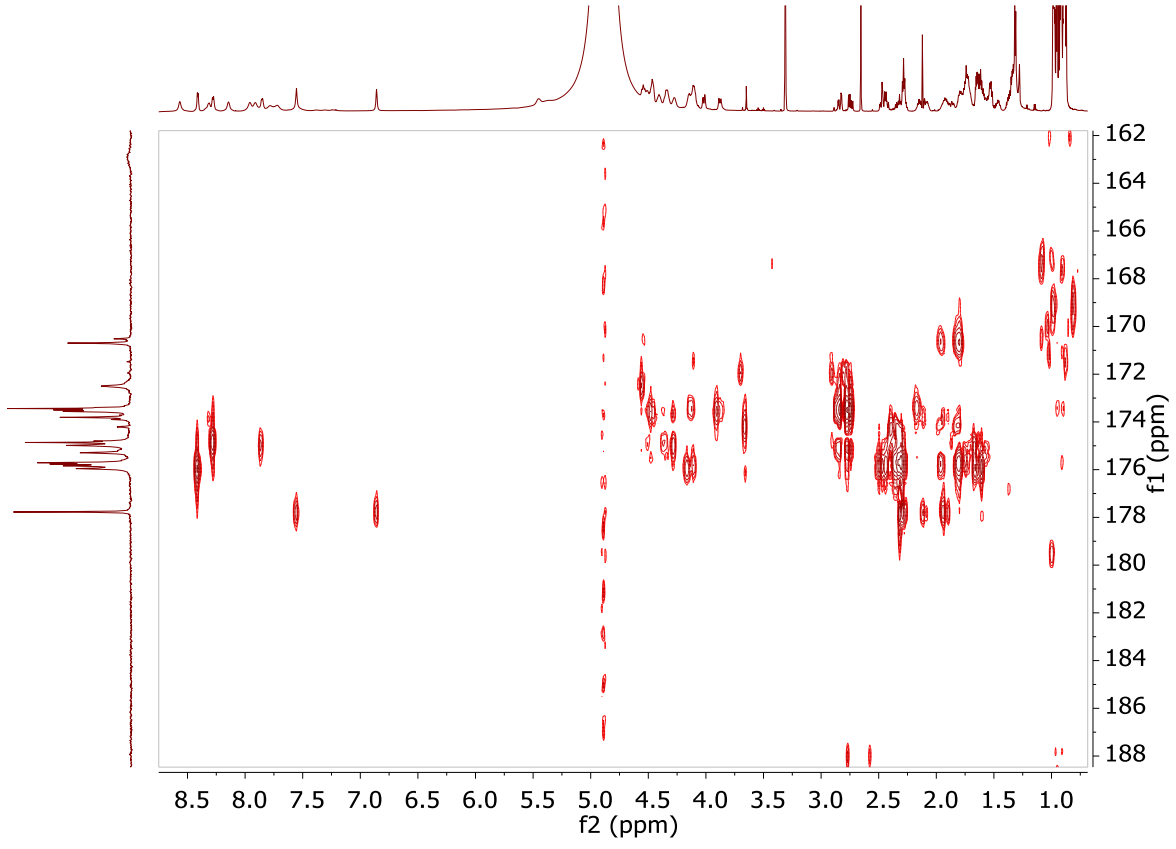

Figure A8: NMR Spectra of compound **2** (d_3-MeOH, 400 MHz)

a. ^{1}H-NMR

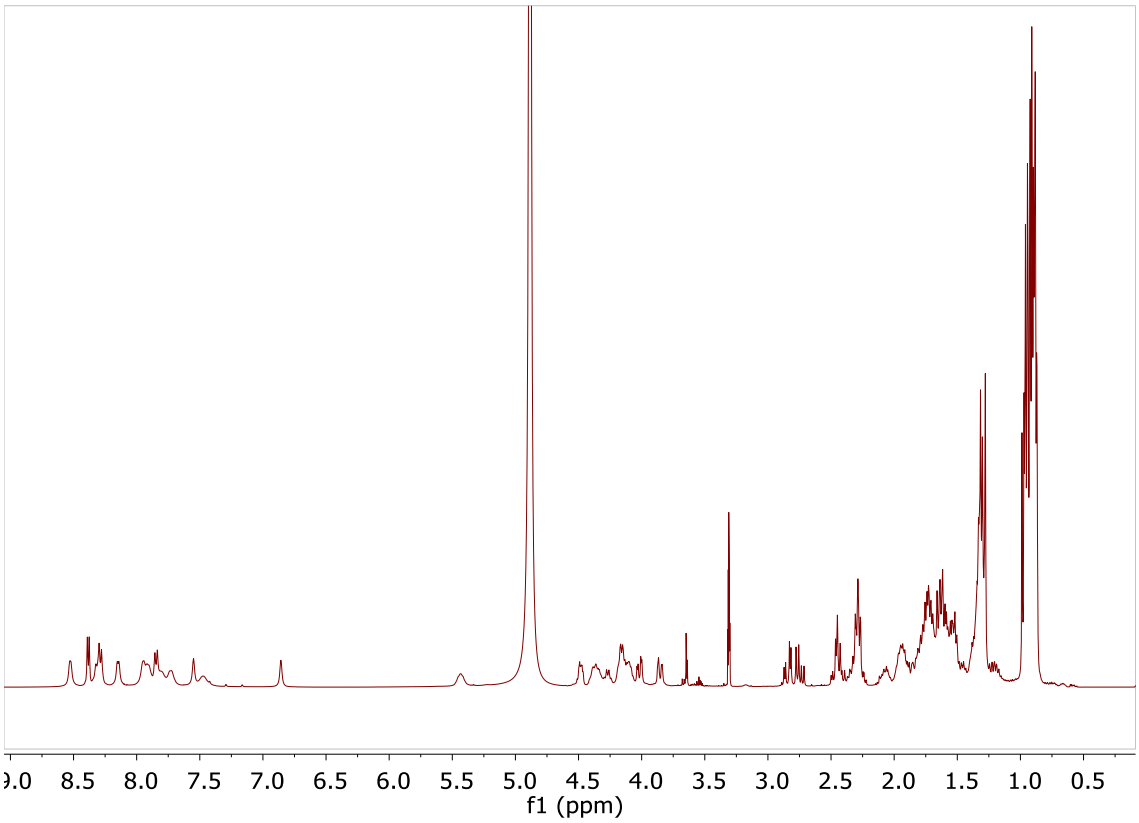

b. ^{13}C-NMR (100 MHz)

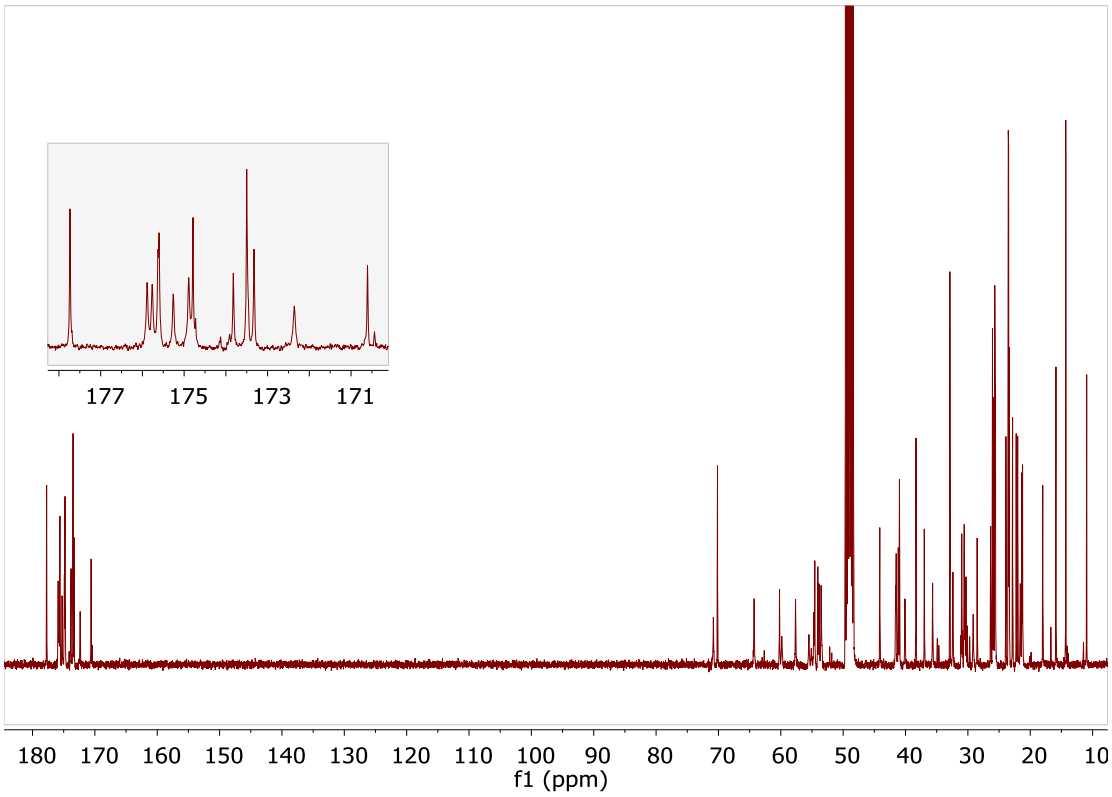

c. ^{13}C-DEPT-135

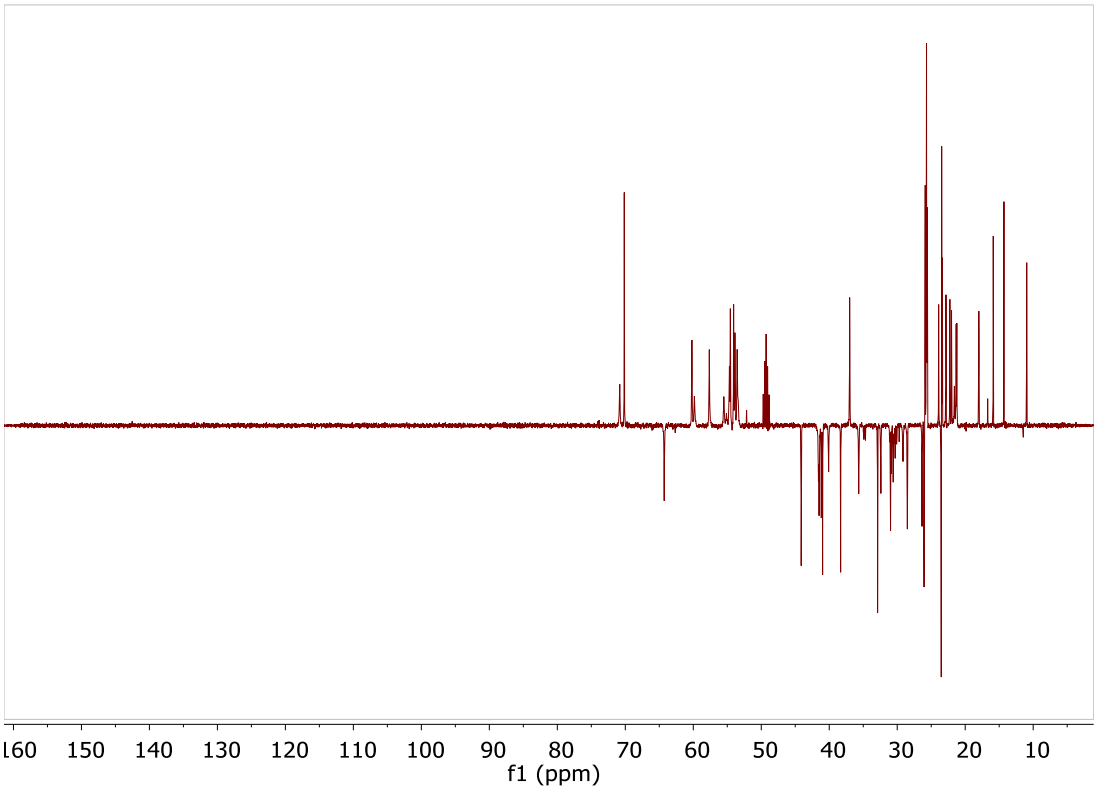

d. ^{1}H-^{1}H-COSY

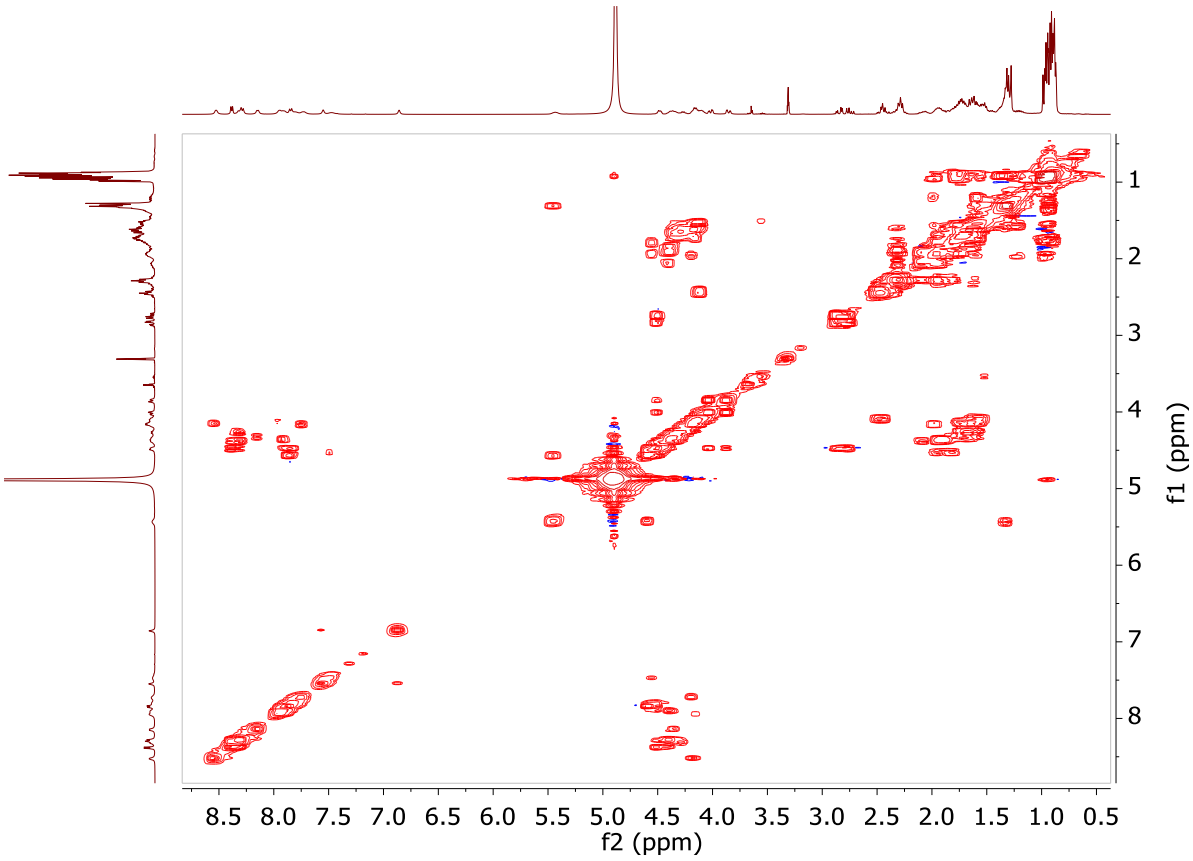

e. ^{1}H-^{13}C-HSQC

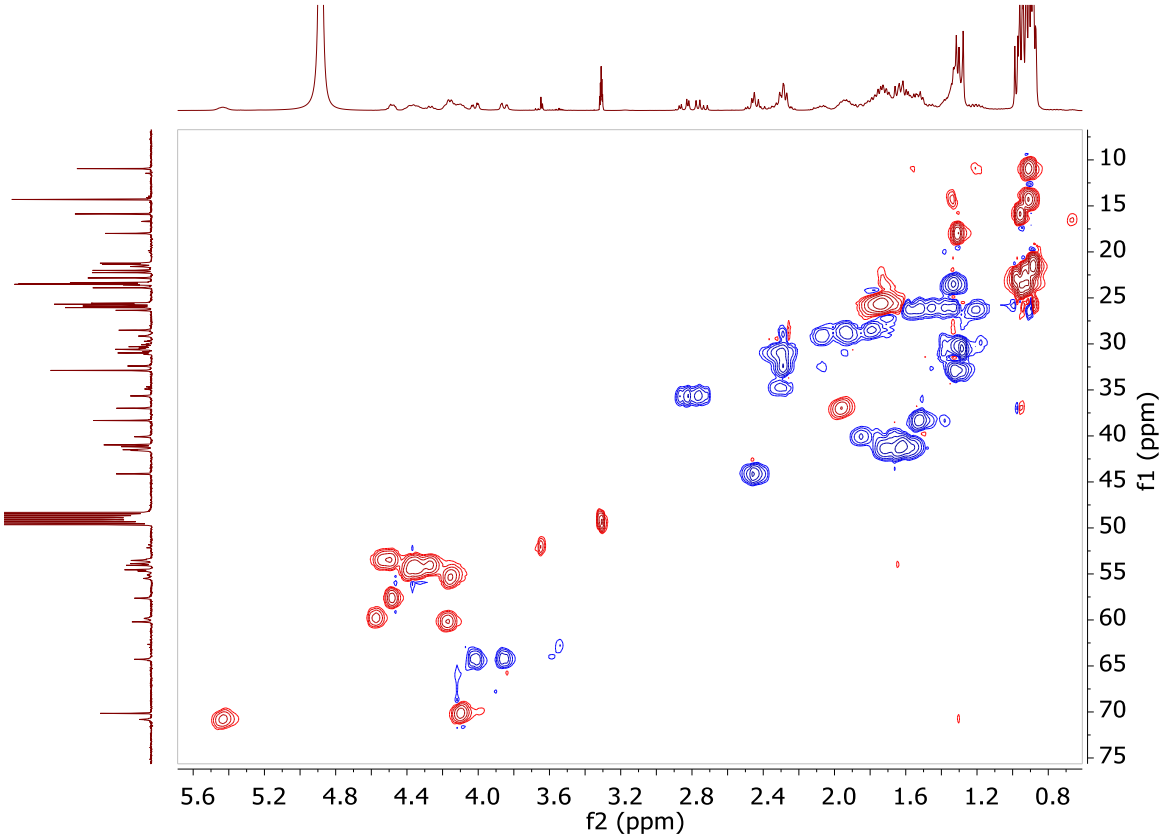

f. ^{1}H-^{1}H-TOCSY

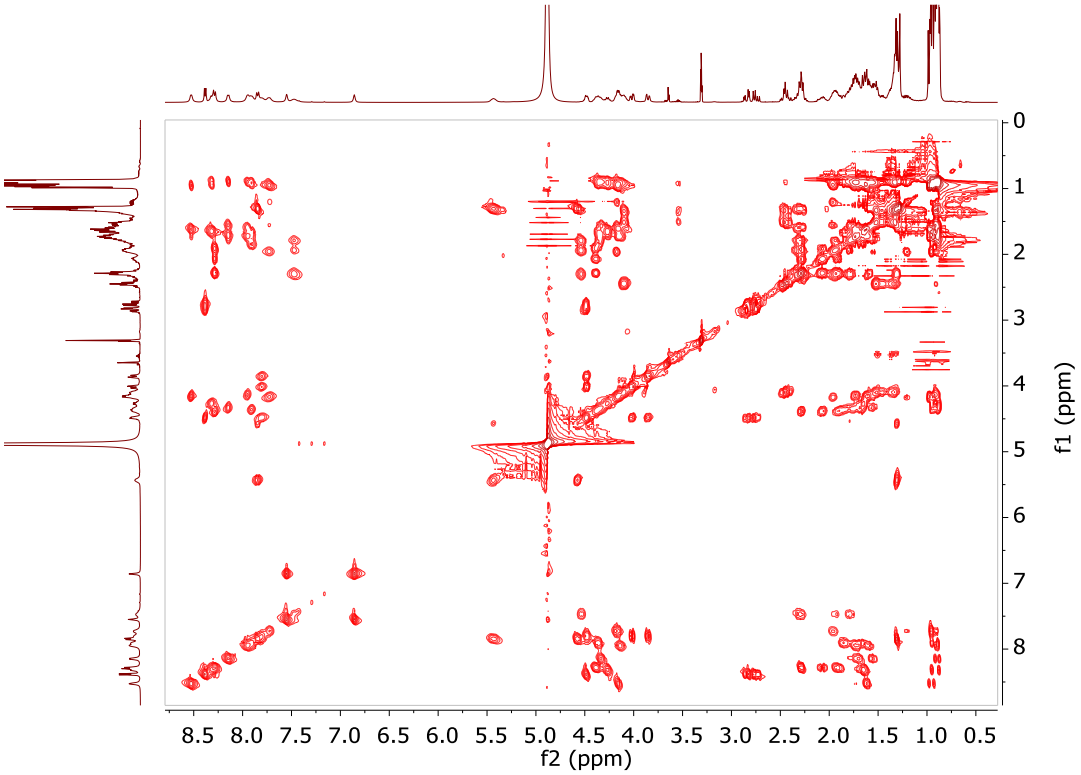

g. ^{1}H-^{13}C-HSQC-TOCSY

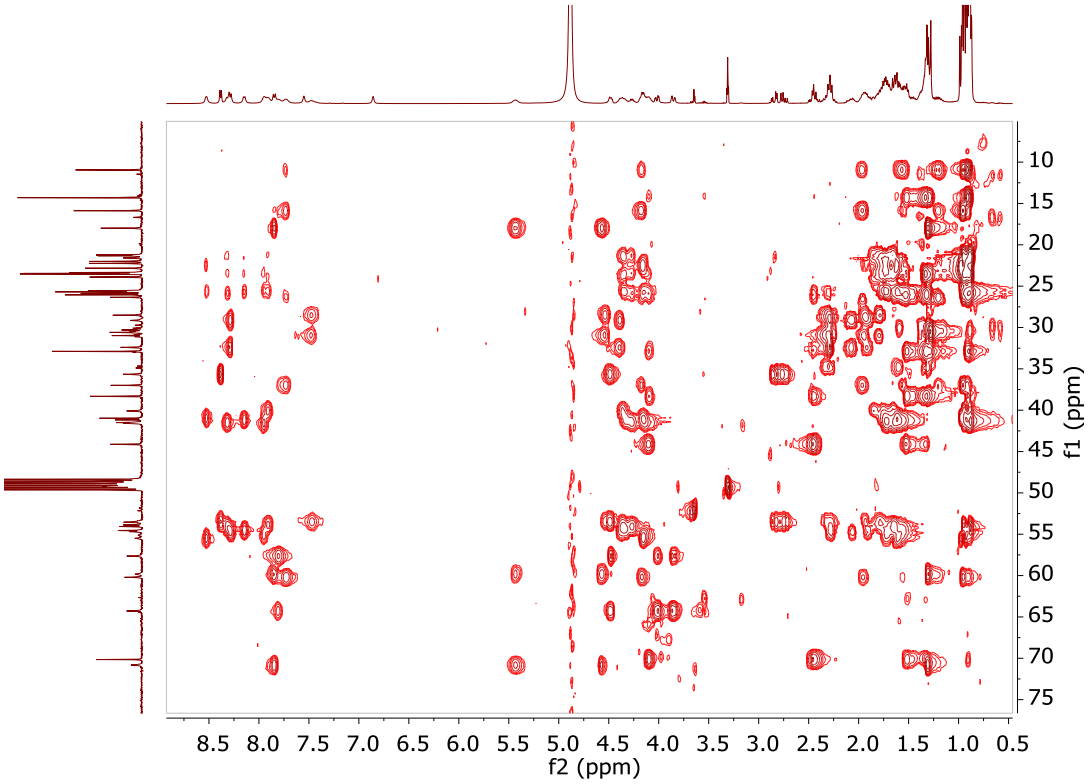

h. ^{1}H-^{13}C-HMBC

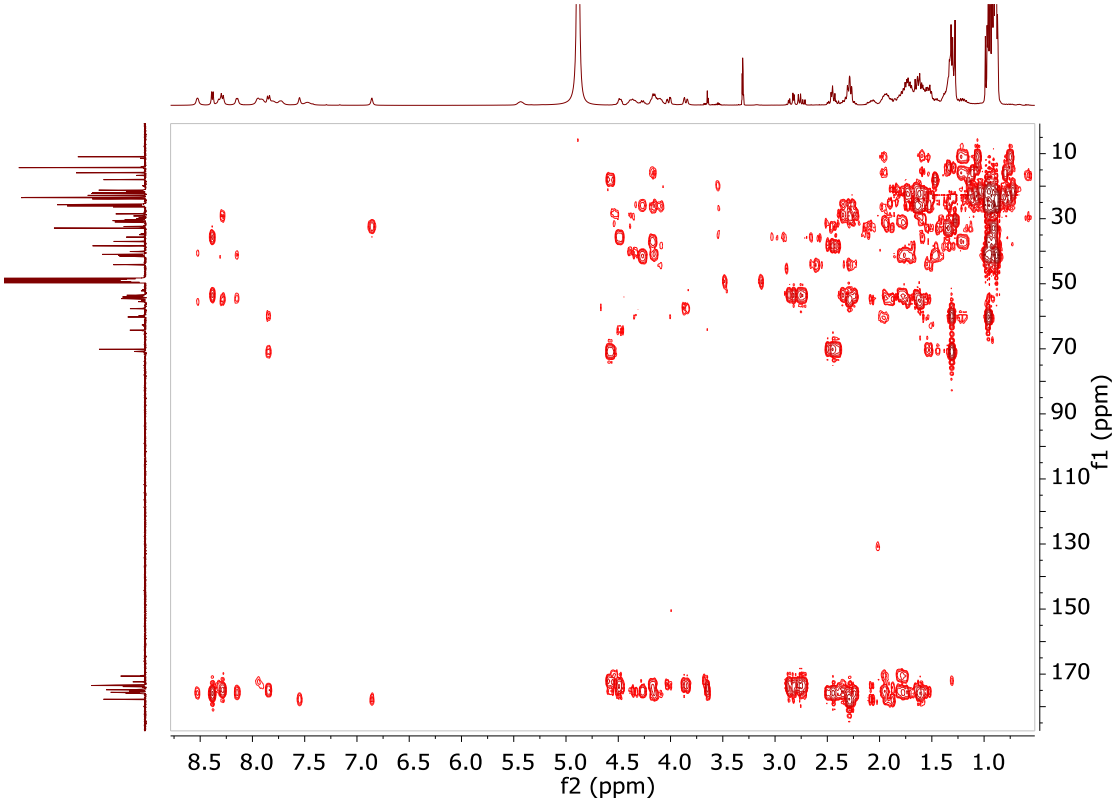

i. ^{1}H-^{13}C-HMBC-Band Selective

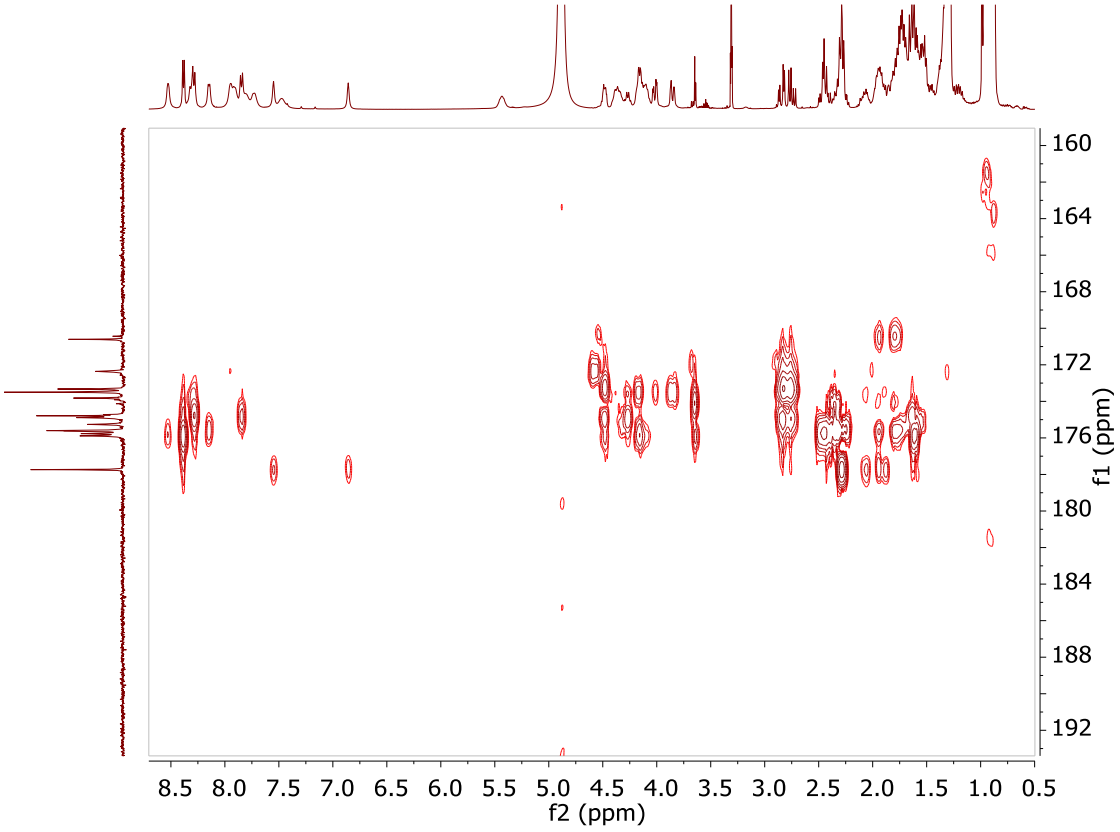

j. ^{1}H-^{15}N-HSQC (40.6 MHz)

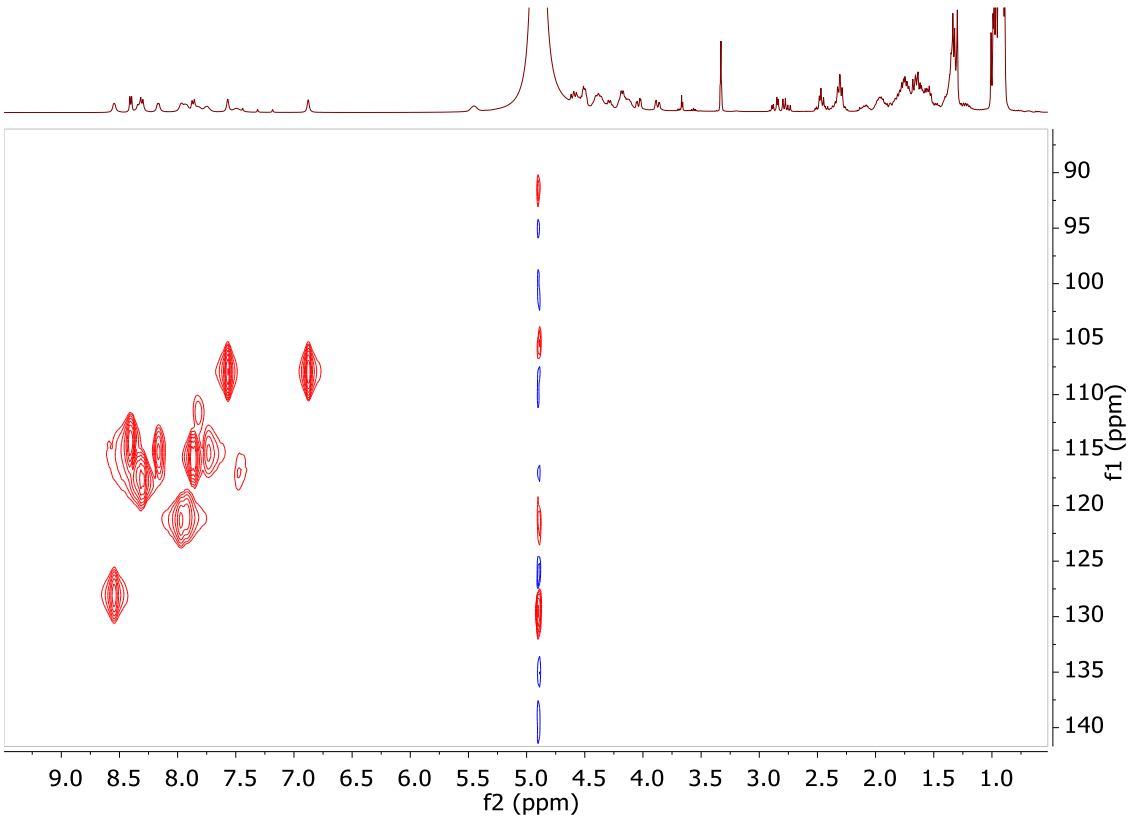

k. ^{1}H-^{15}N-HMBC

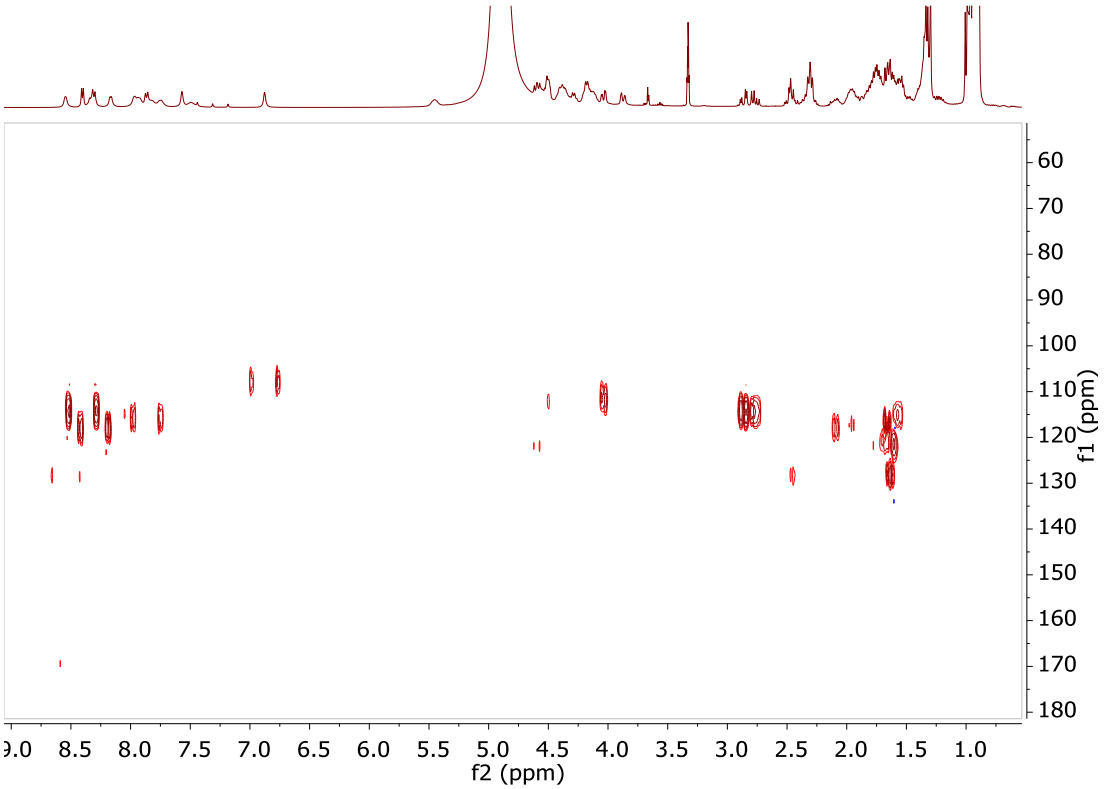

l. ^{1}H-^{1}H-NOESY

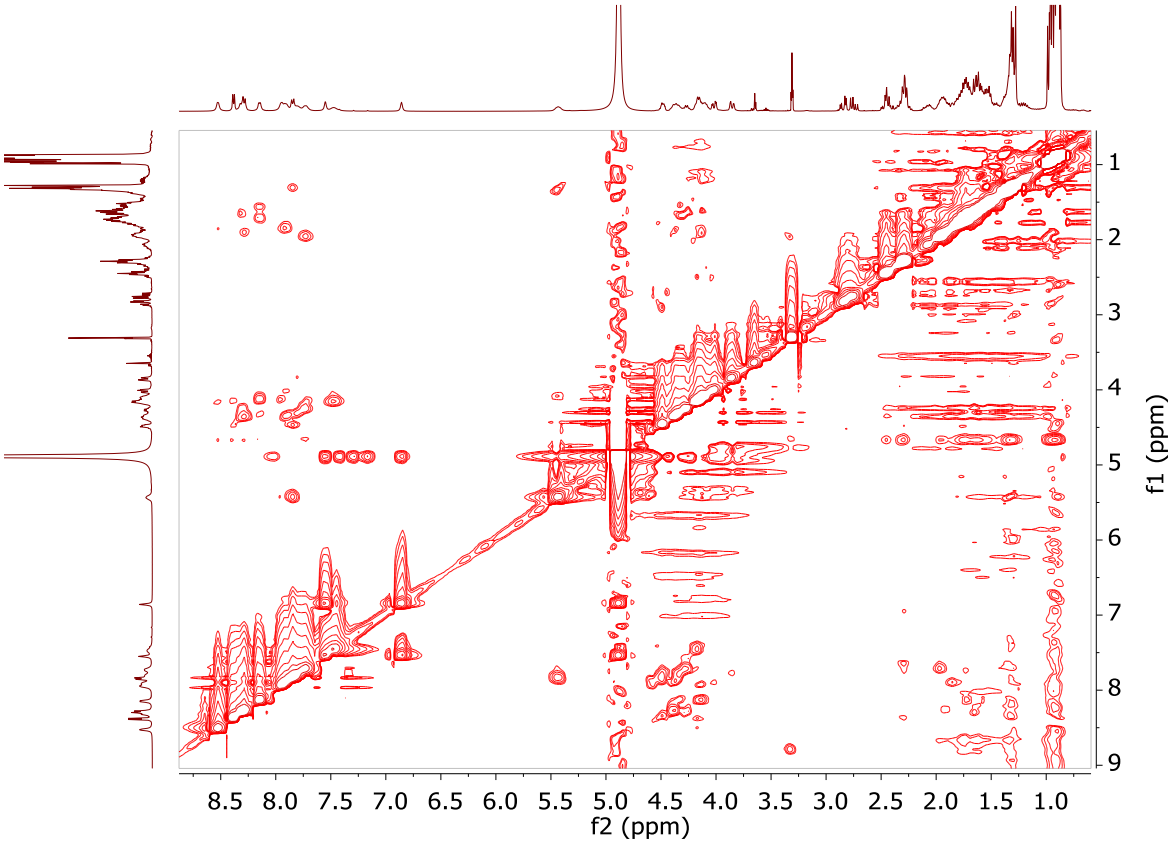

Figure A9: NMR spectra of compound **2** (d_3-MeOH, 700 MHz)

a. ^{1}H-NMR

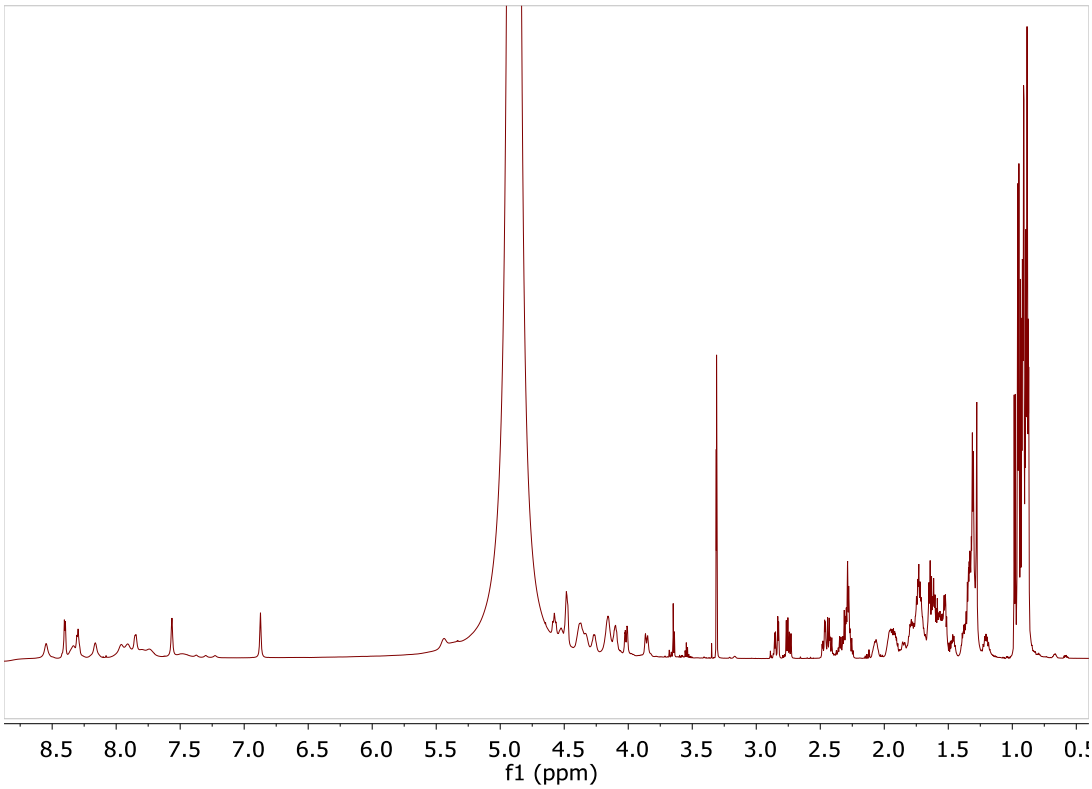

b. ^{13}C-NMR

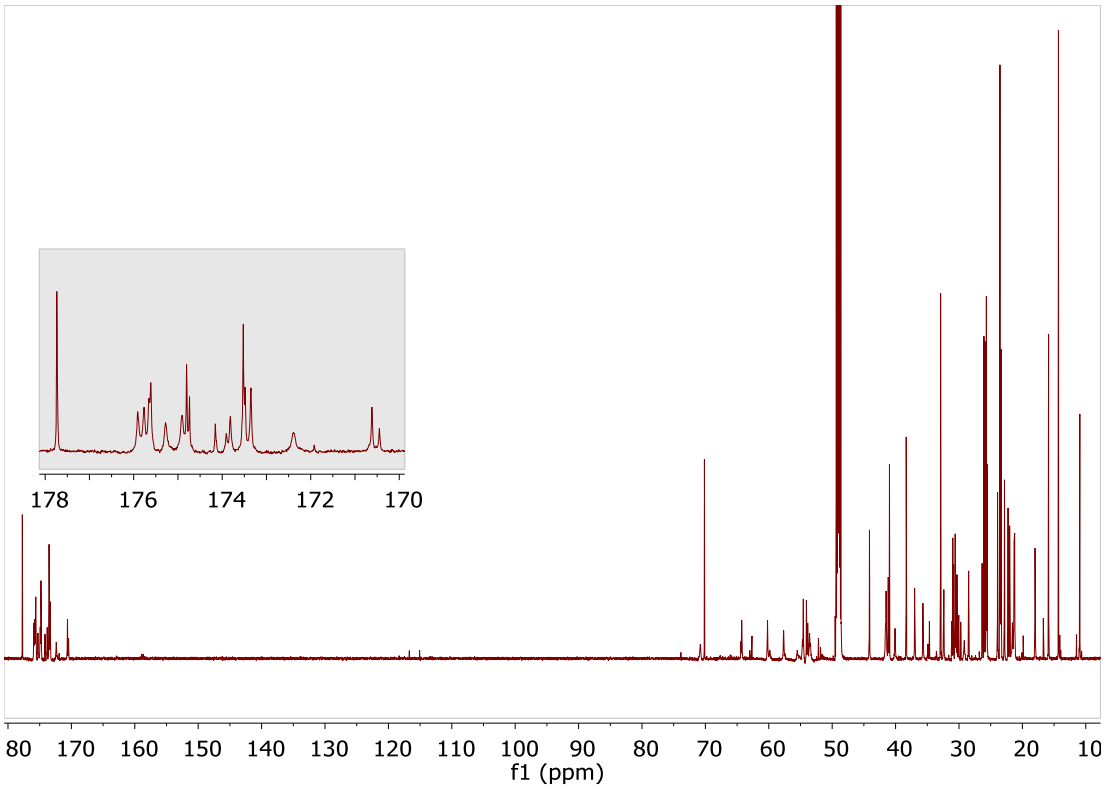

c. ^{1}H-^{13}C-HSQC

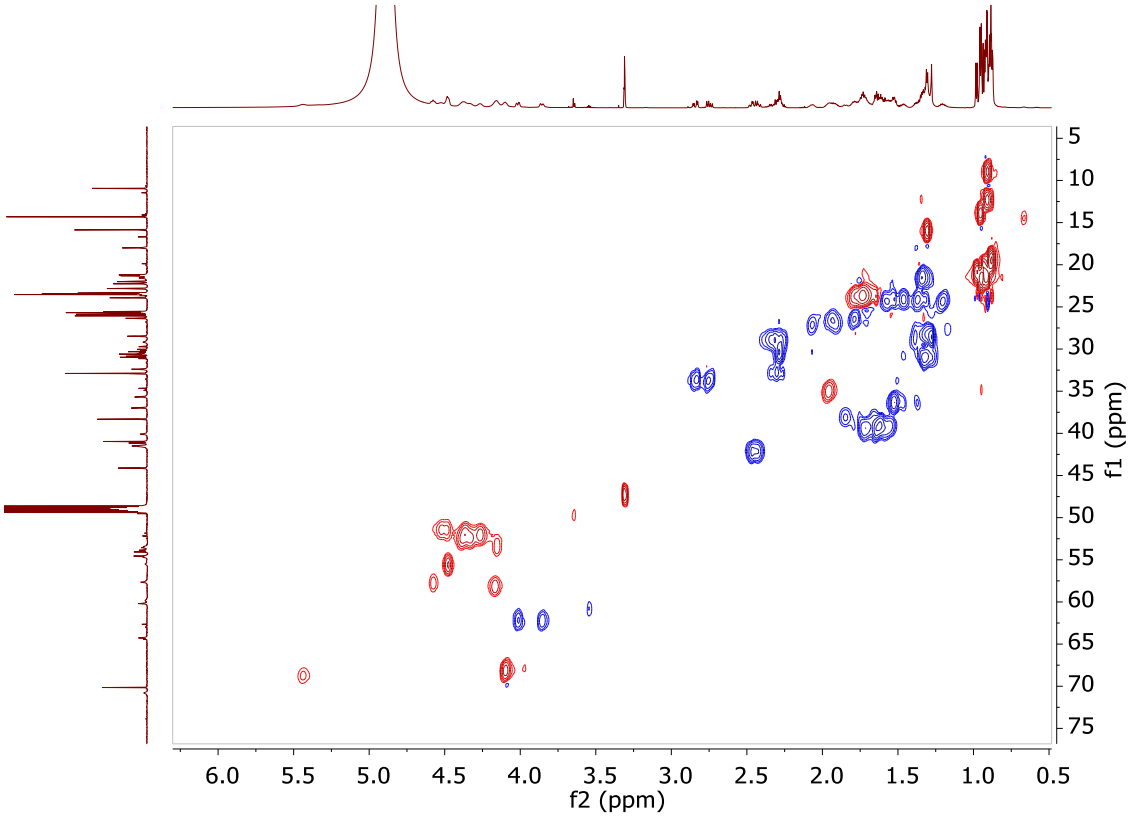

d. ^{1}H-^{1}H-TOCSY

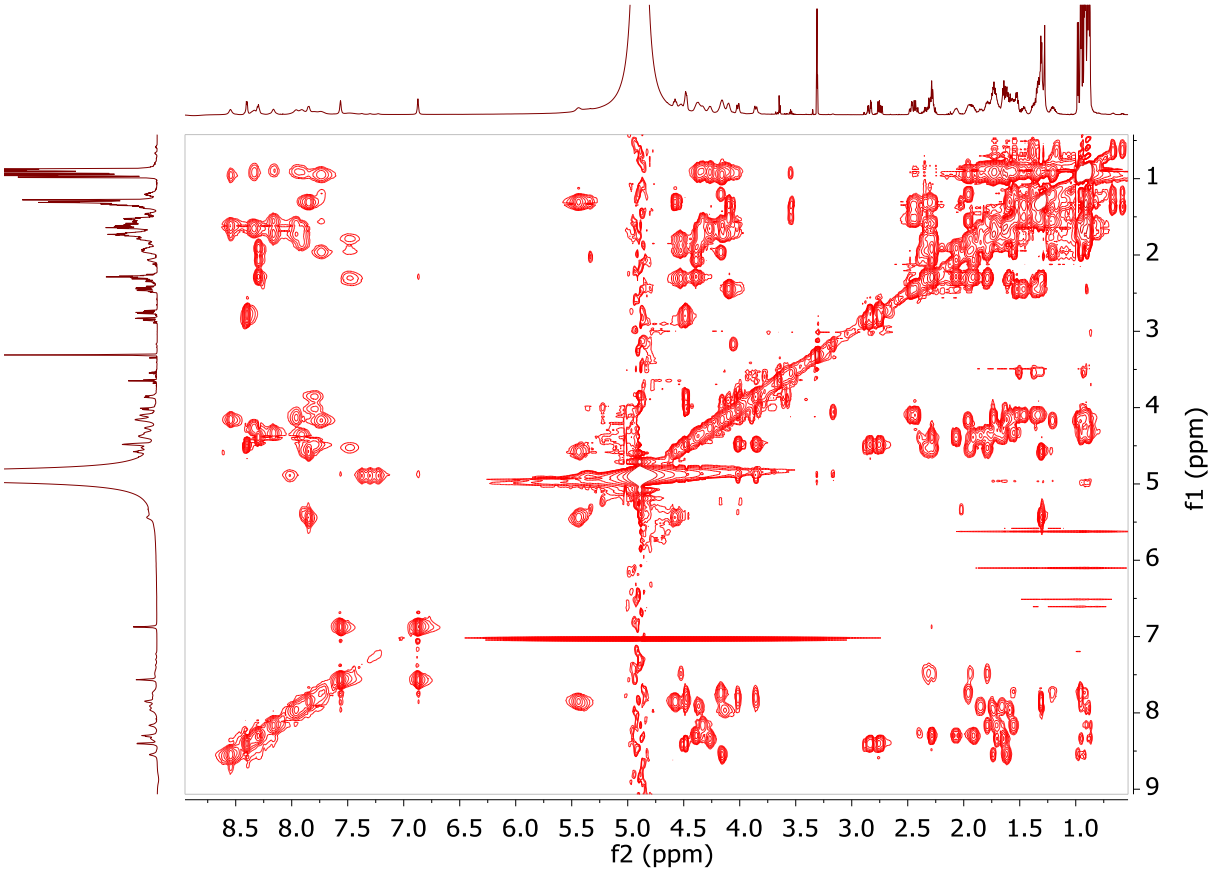

e. ^{1}H-^{13}C-HSQC-TOCSY

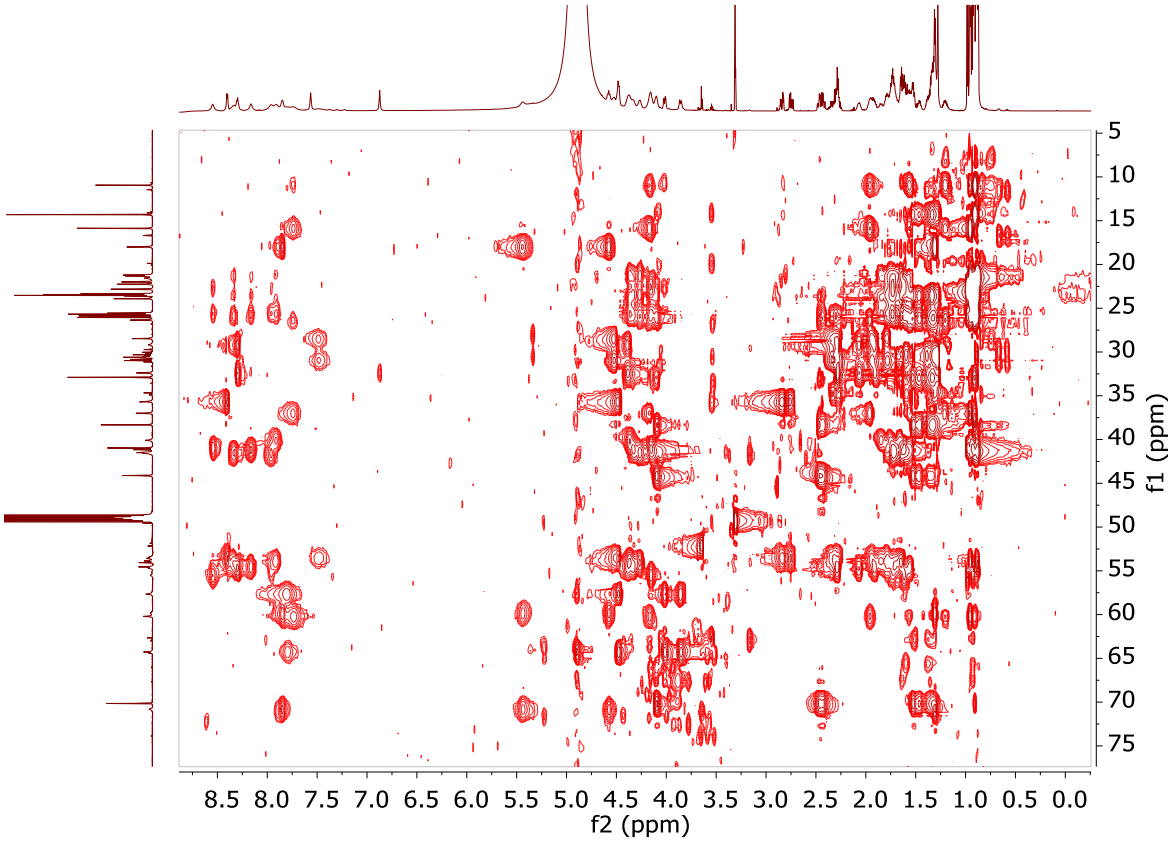

f. ^{1}H-^{13}C-HMBC-Band Selective

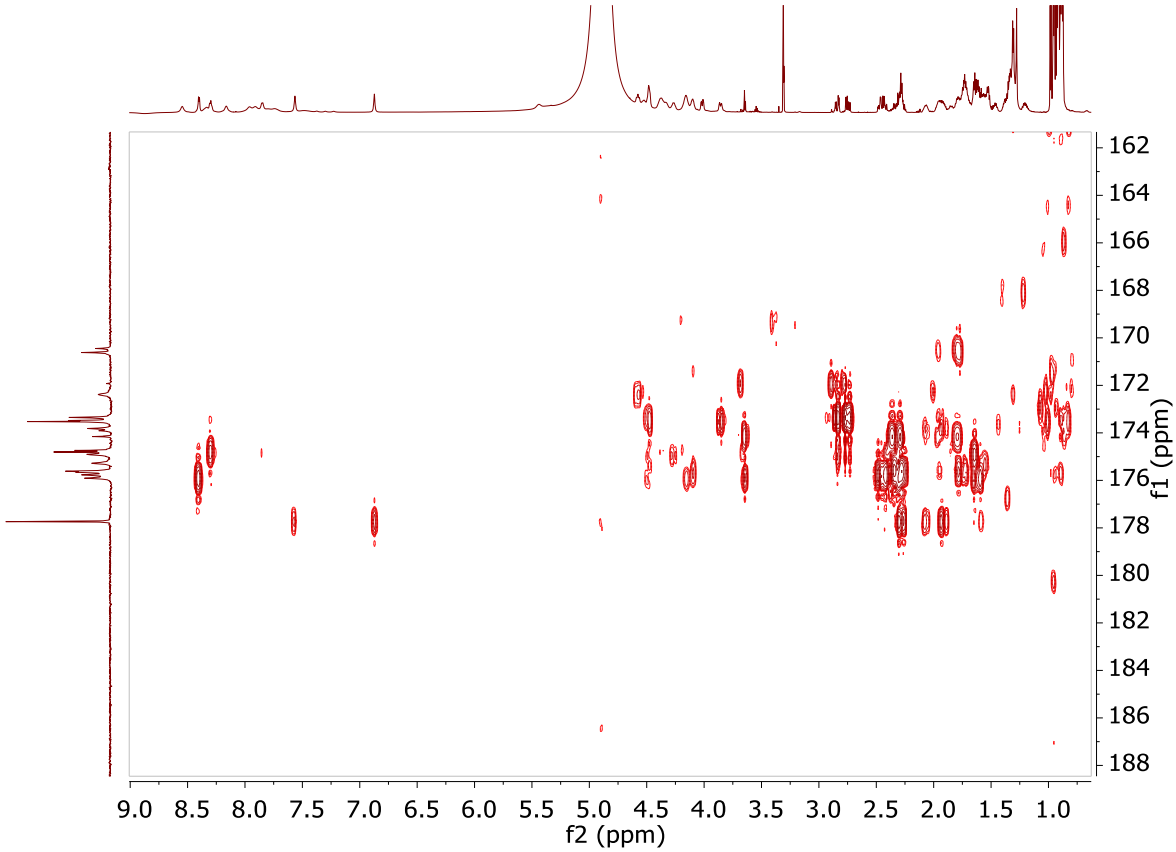

Figure A10: NMR spectra of compound **3** (d_3-MeOH, 400 MHz)

a. ^{1}H-NMR

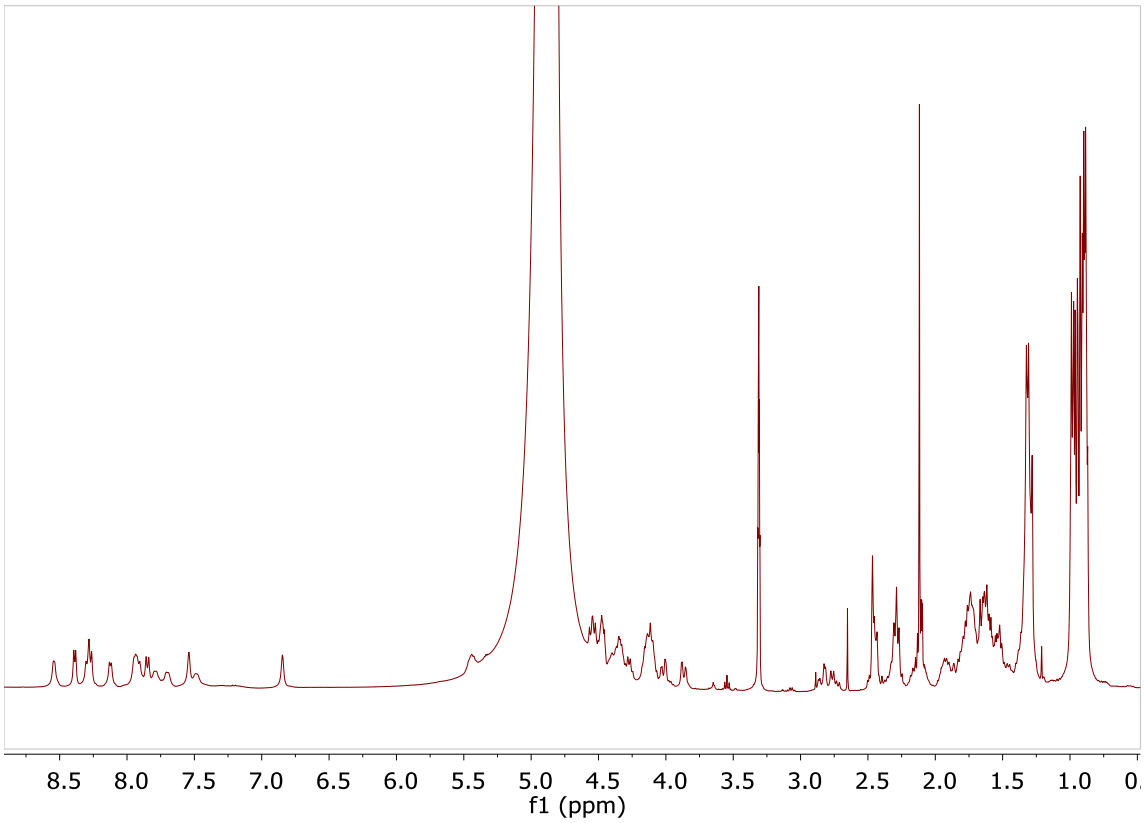

b. ^{13}C-NMR

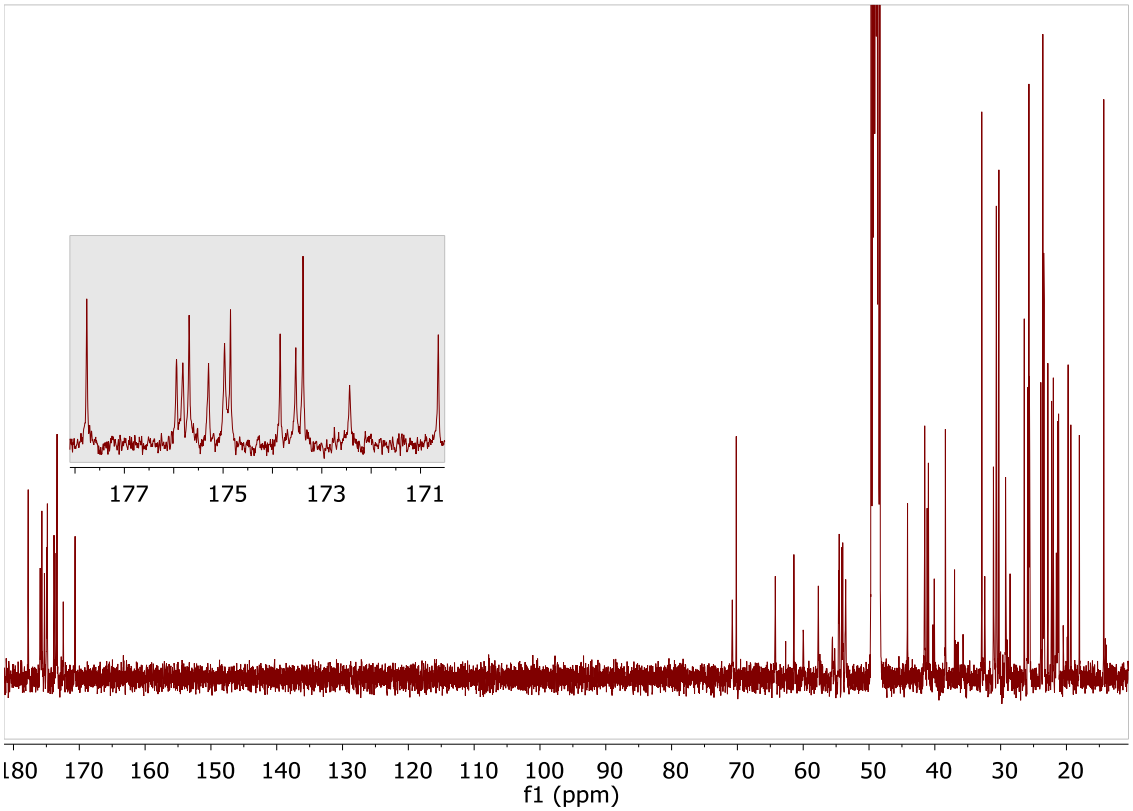

c. ^{13}C-DEPT-135

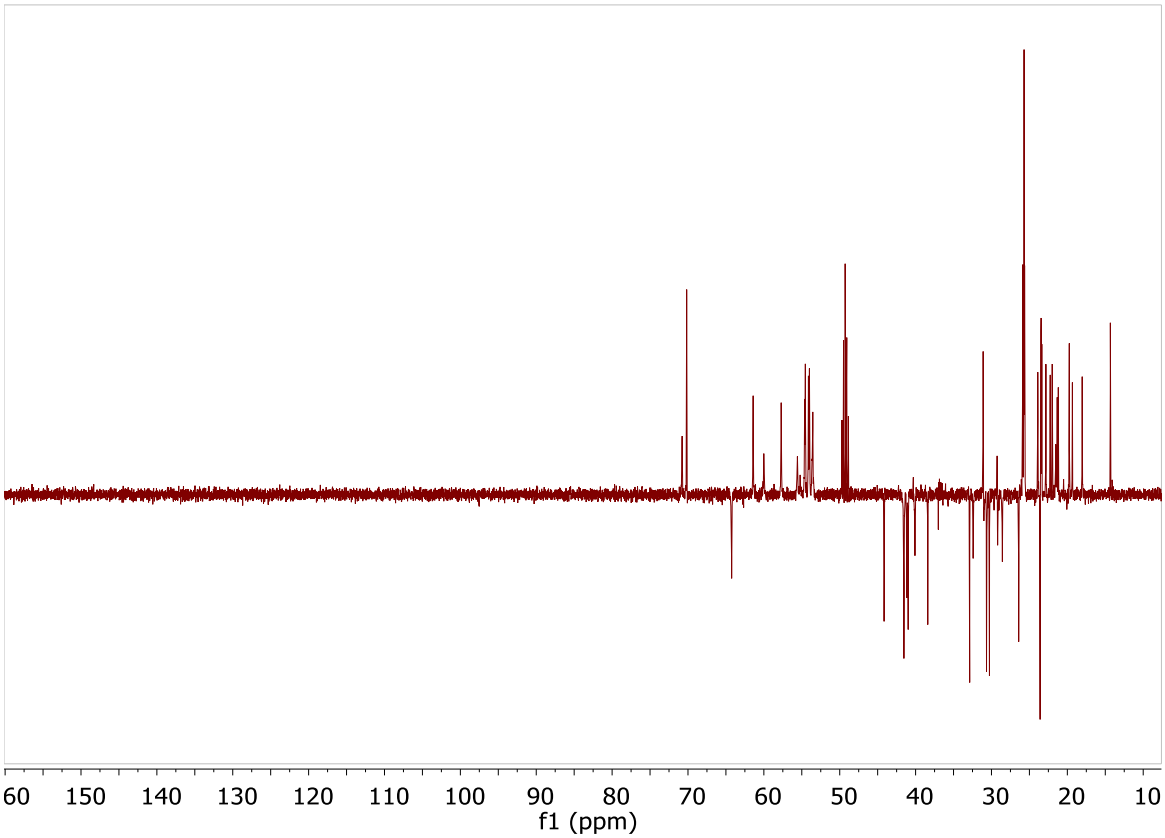

d. ^{1}H-^{1}H-COSY

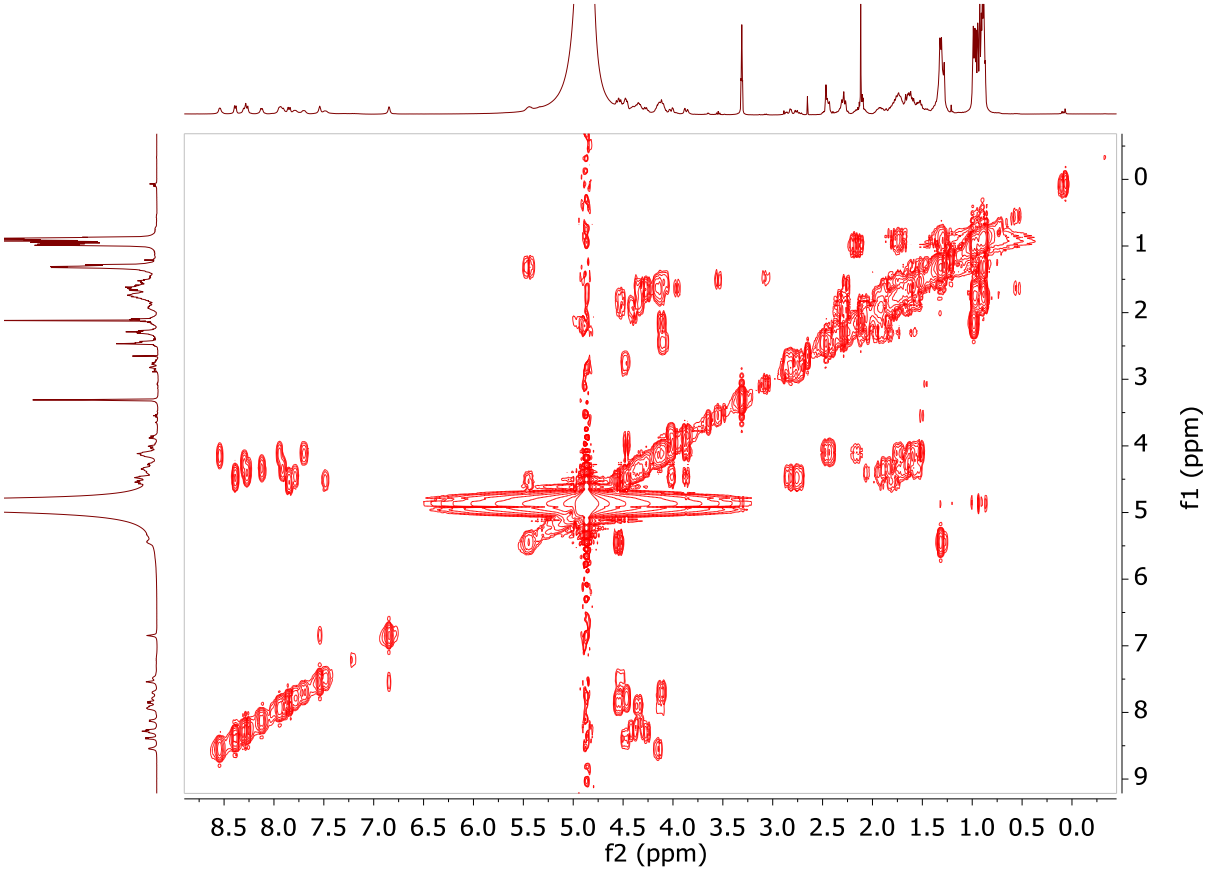

e. ^{1}H-^{13}C-HSQC

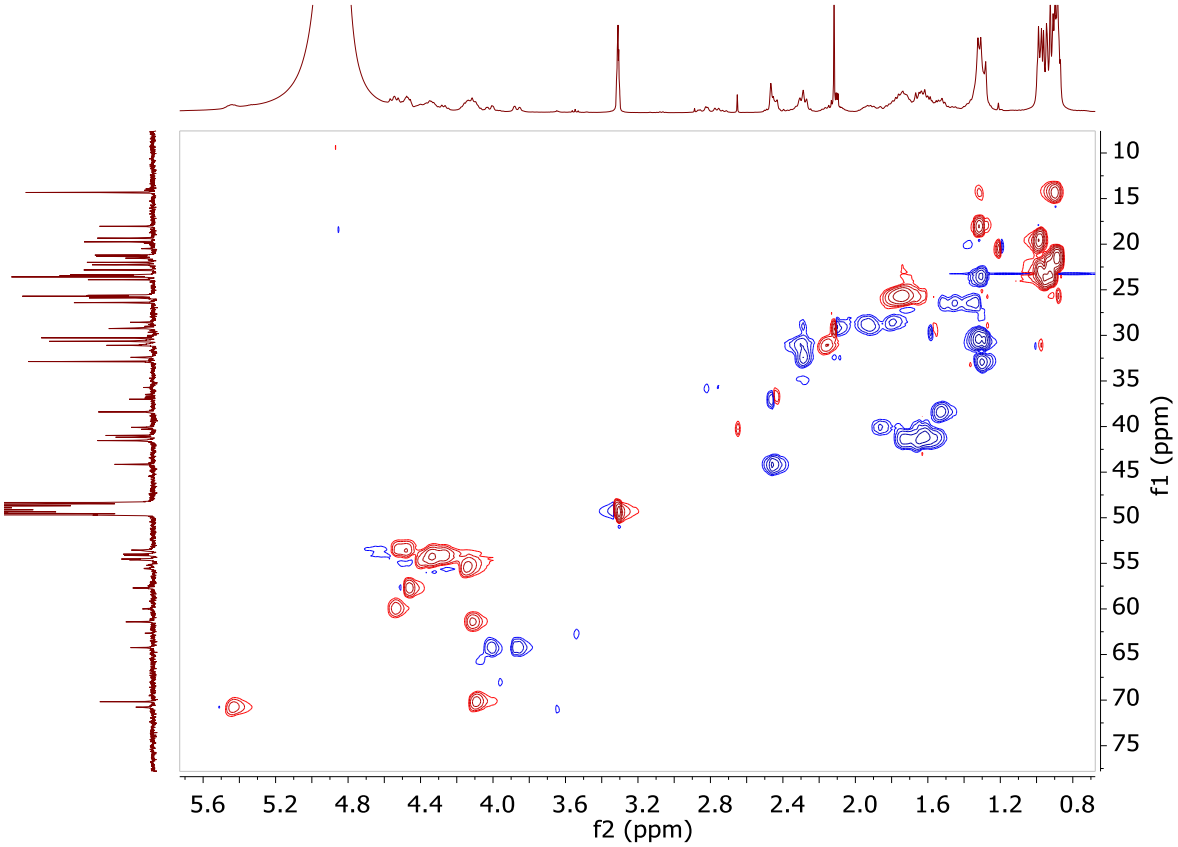

f. ^{1}H-^{13}C-HMBC

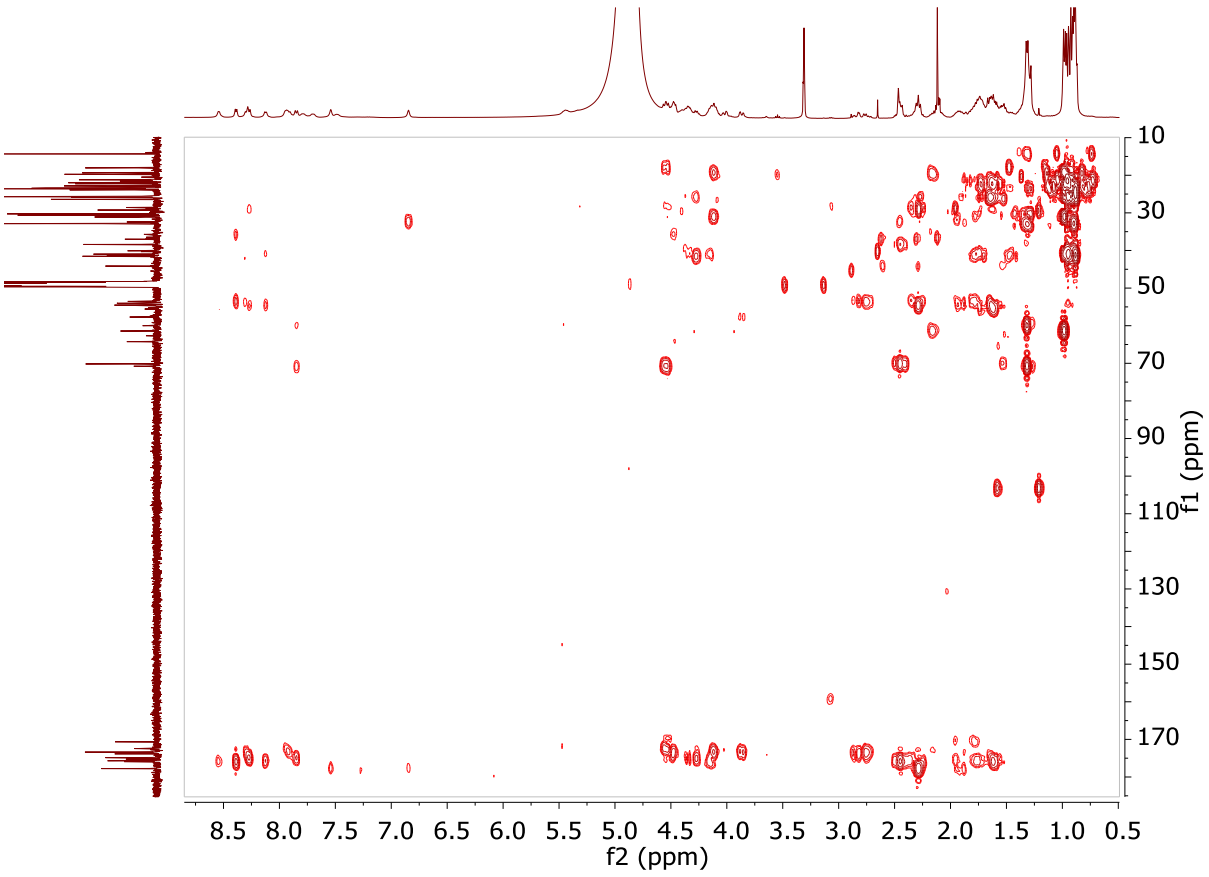

g. ^{1}H-^{1}H-TOCSY

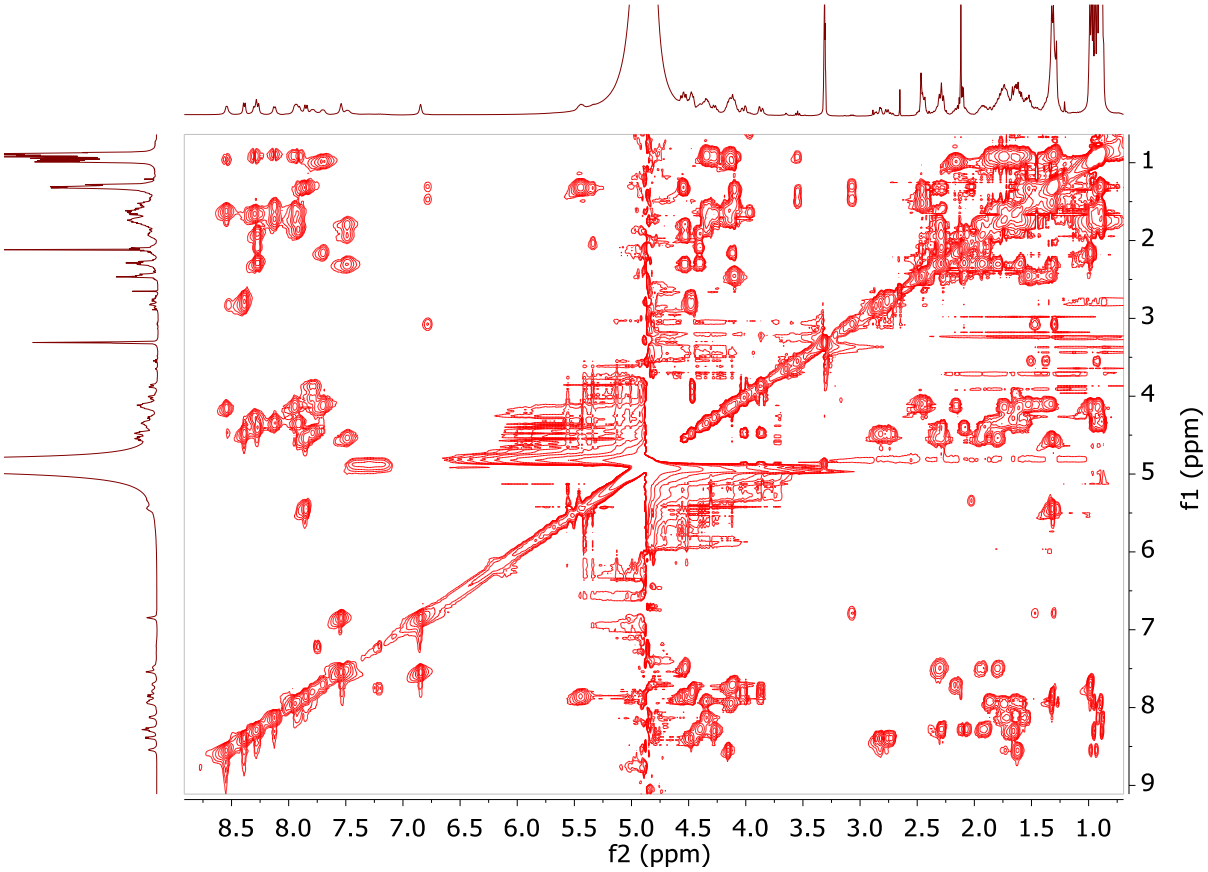

h. ^{1}H-^{13}C-HSQC-TOCSY

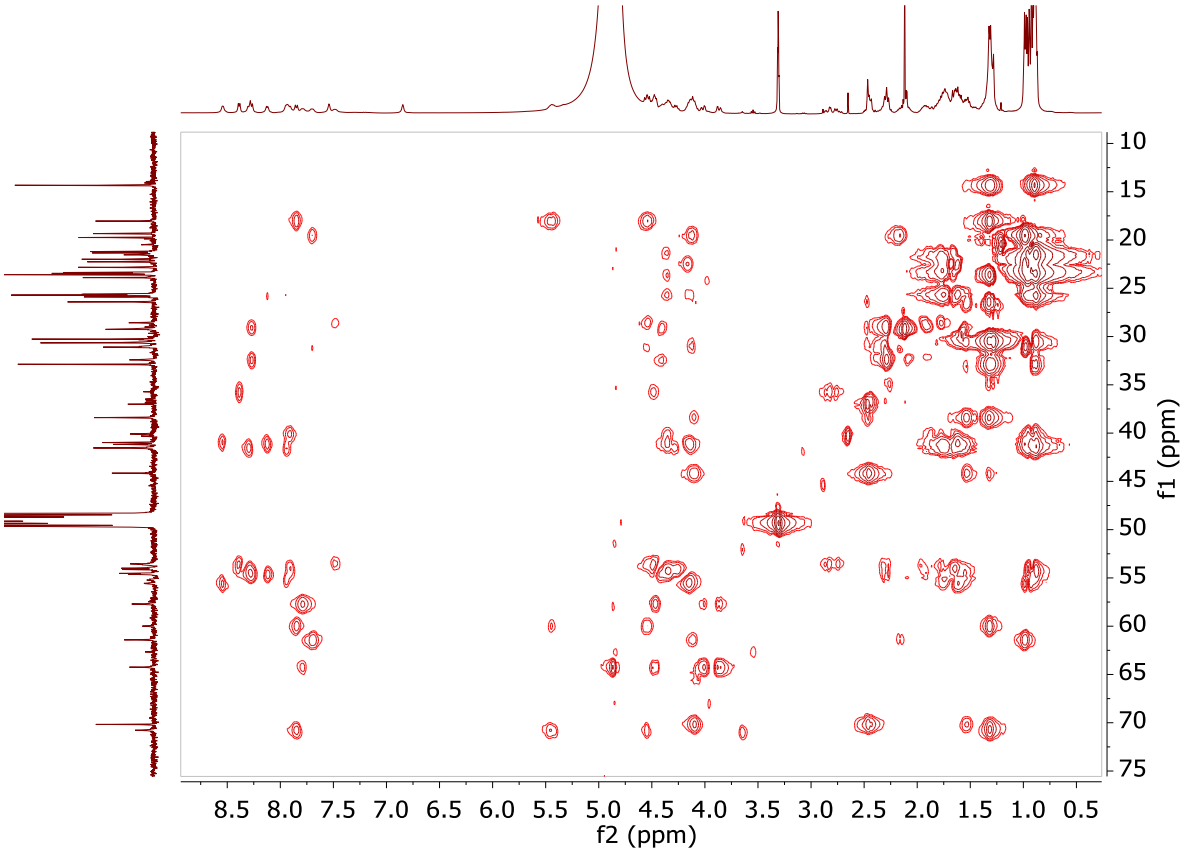

i. ^{1}H-^{1}H-NOESY

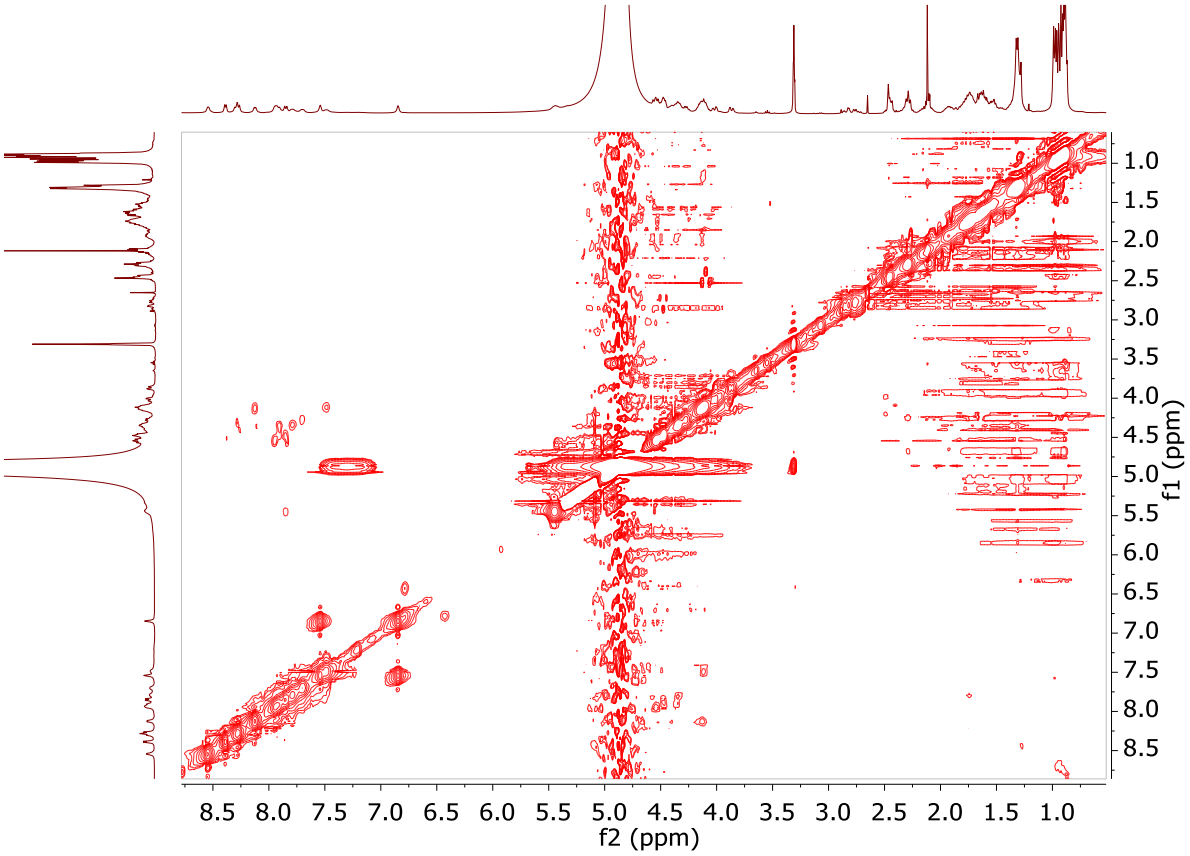

j. ^{1}H-^{15}N-HSQC

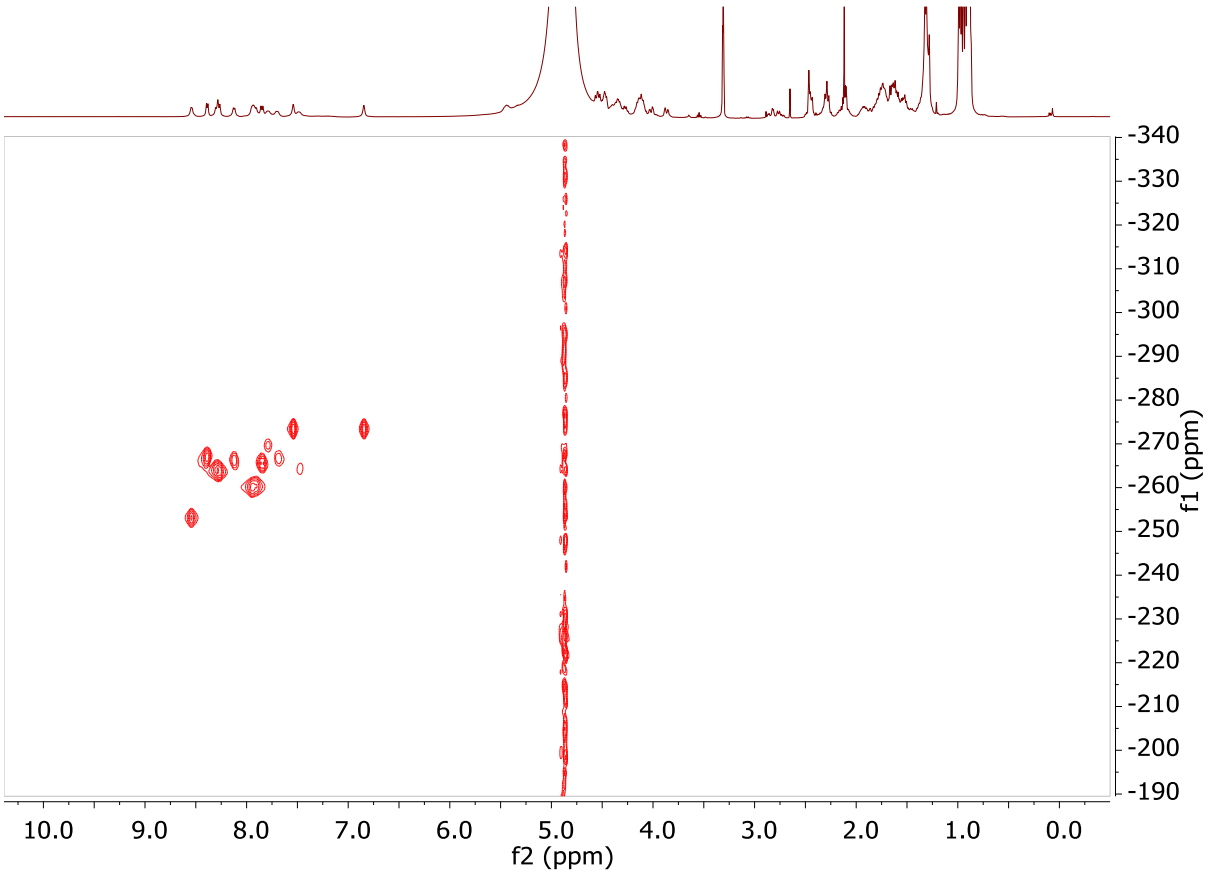

Figure A11: NMR spectra of compound **3** (d_3-MeOH, 700 MHz)

a. ^{1}H-NMR

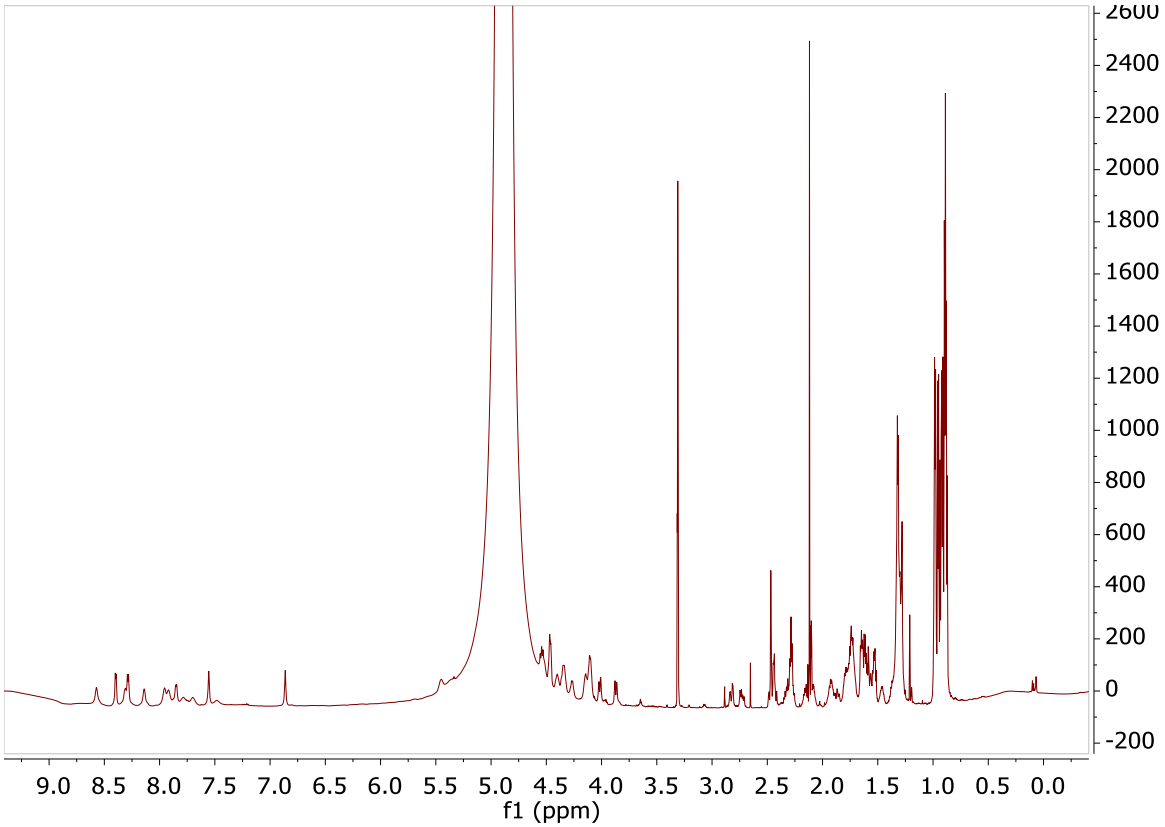

b. ^{13}C-NMR

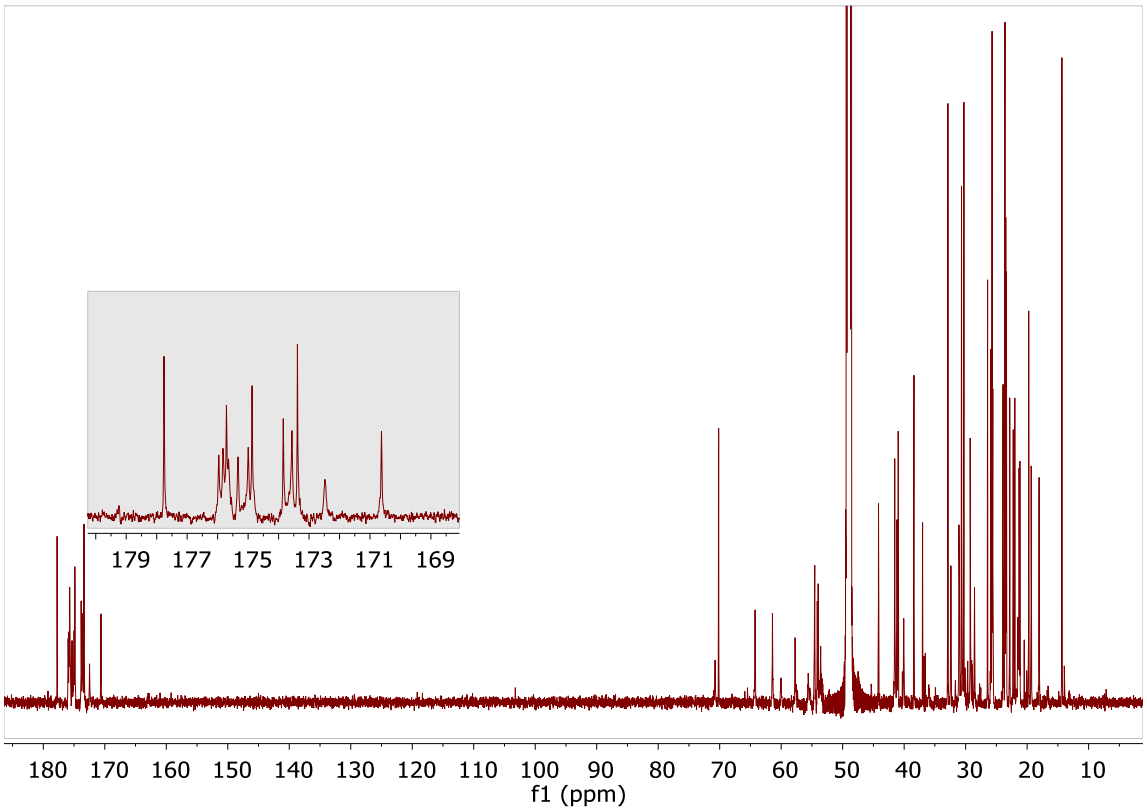

c. ^{13}C-DEPT-135

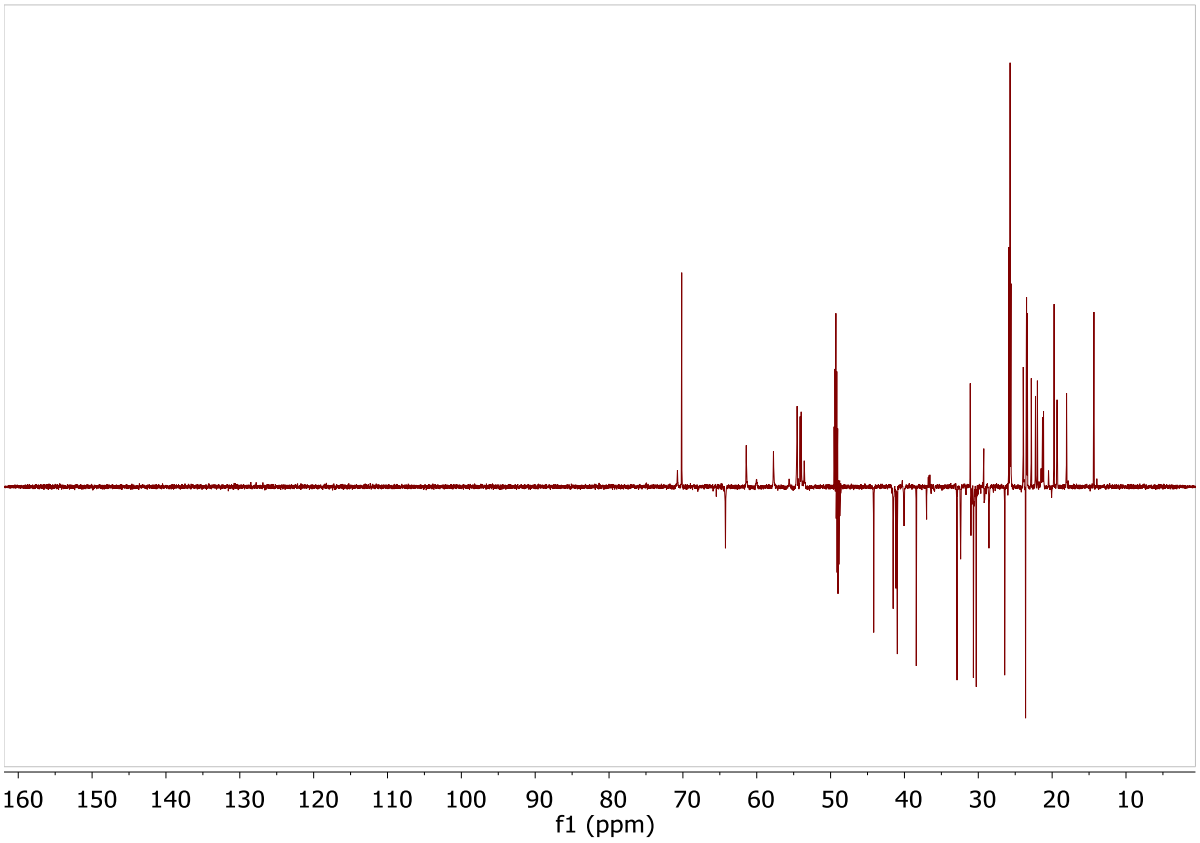

d. ^{1}H-^{13}C-HSQC

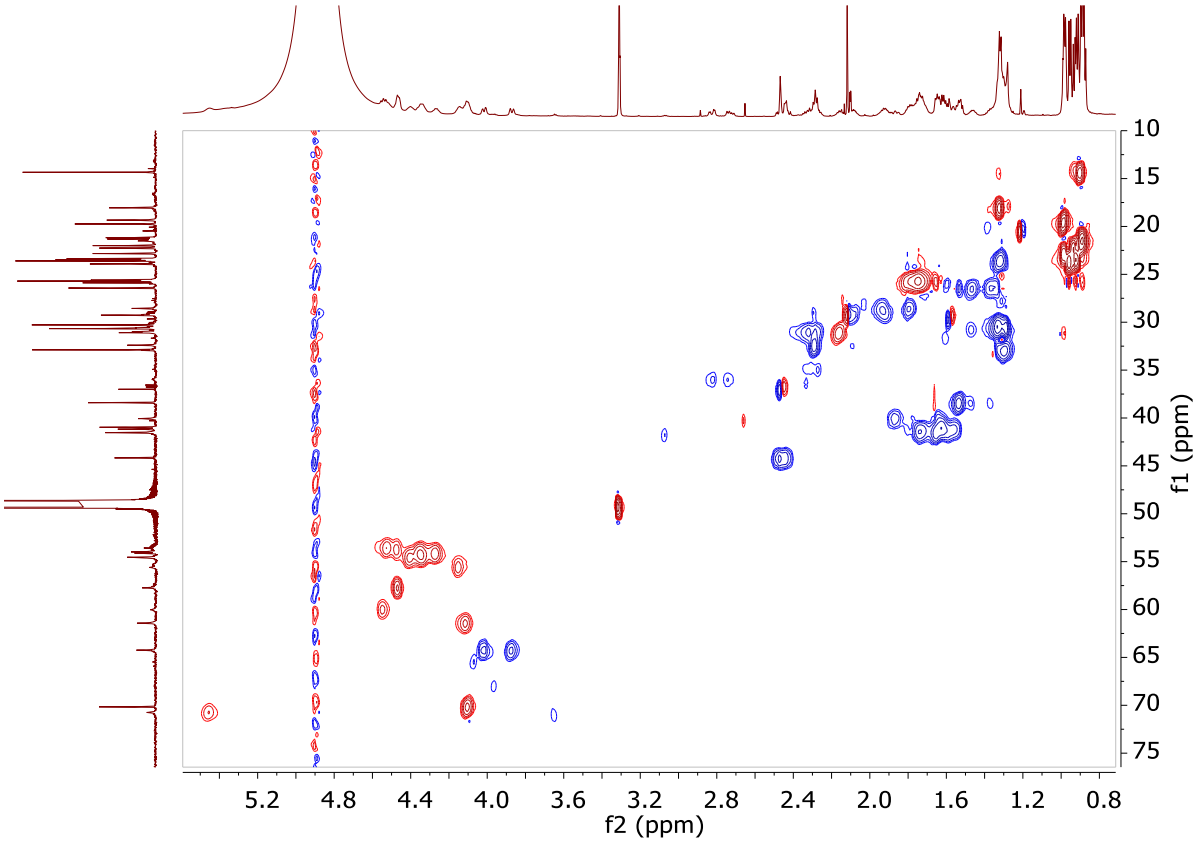

e. ^{1}H-^{1}H-TOCSY

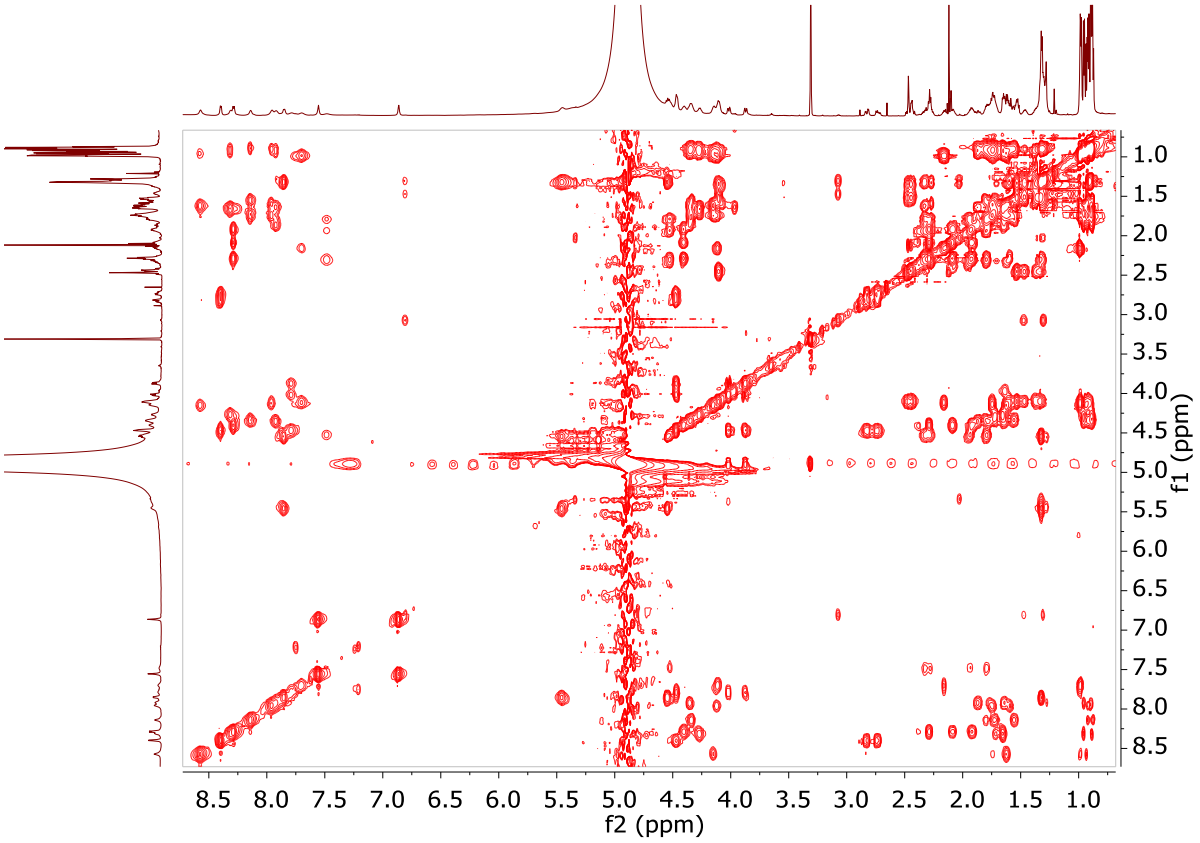

f. ^{1}H-^{13}C-HSQC-TOCSY

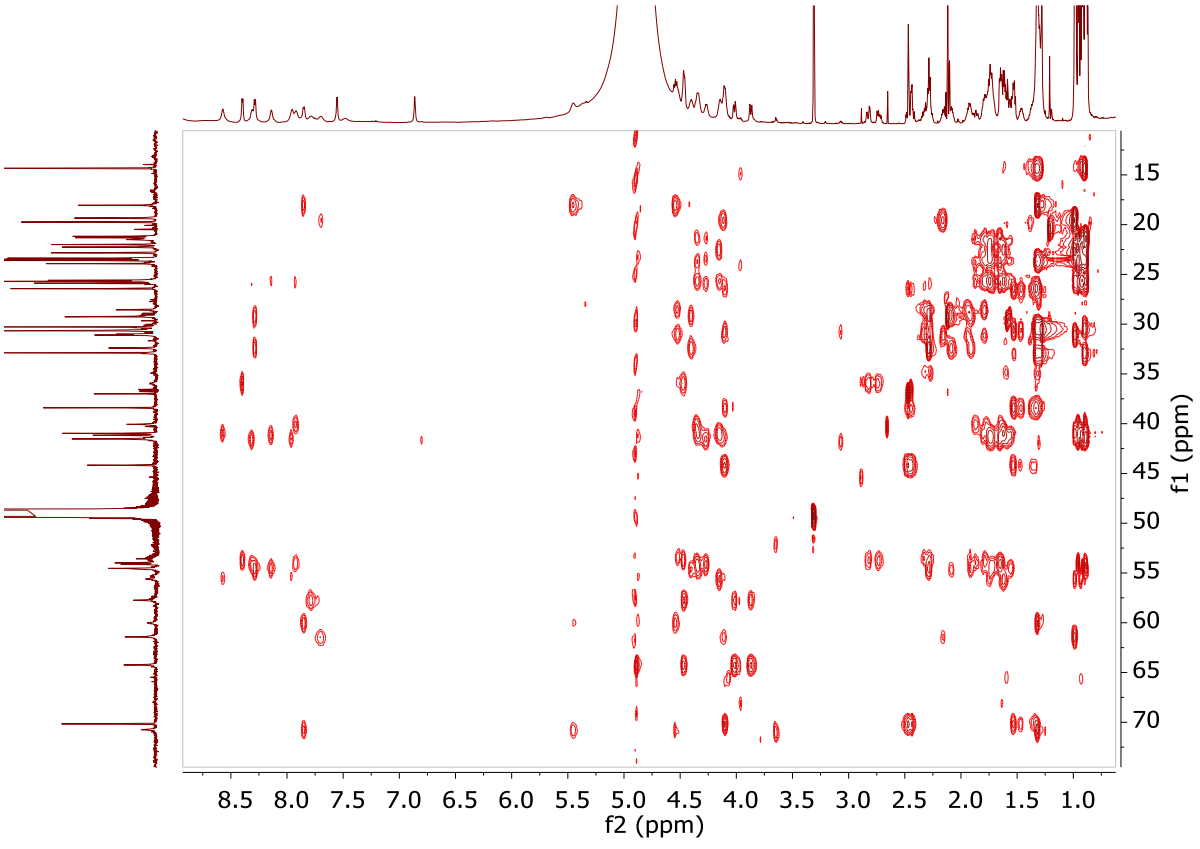

g. ^{1}H-^{1}H-COSY

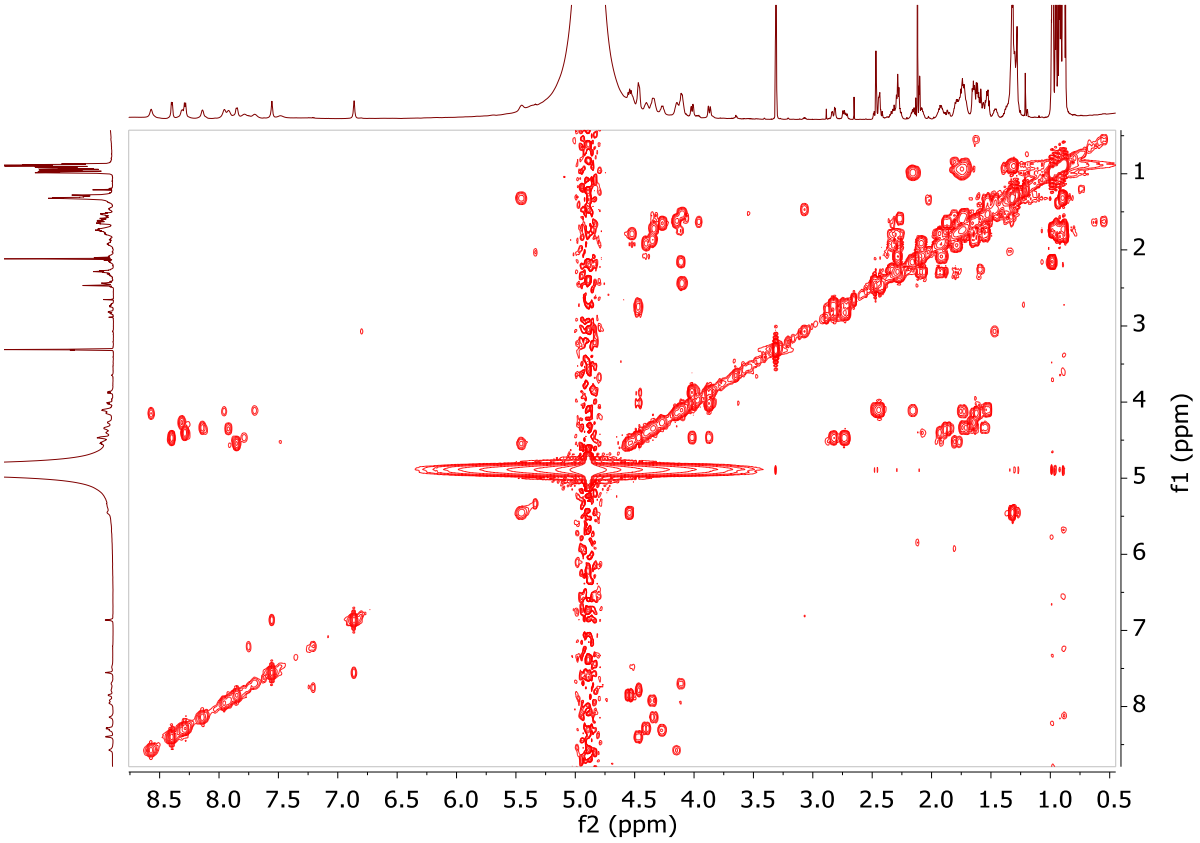

h. ^{1}H-^{13}C-HMBC

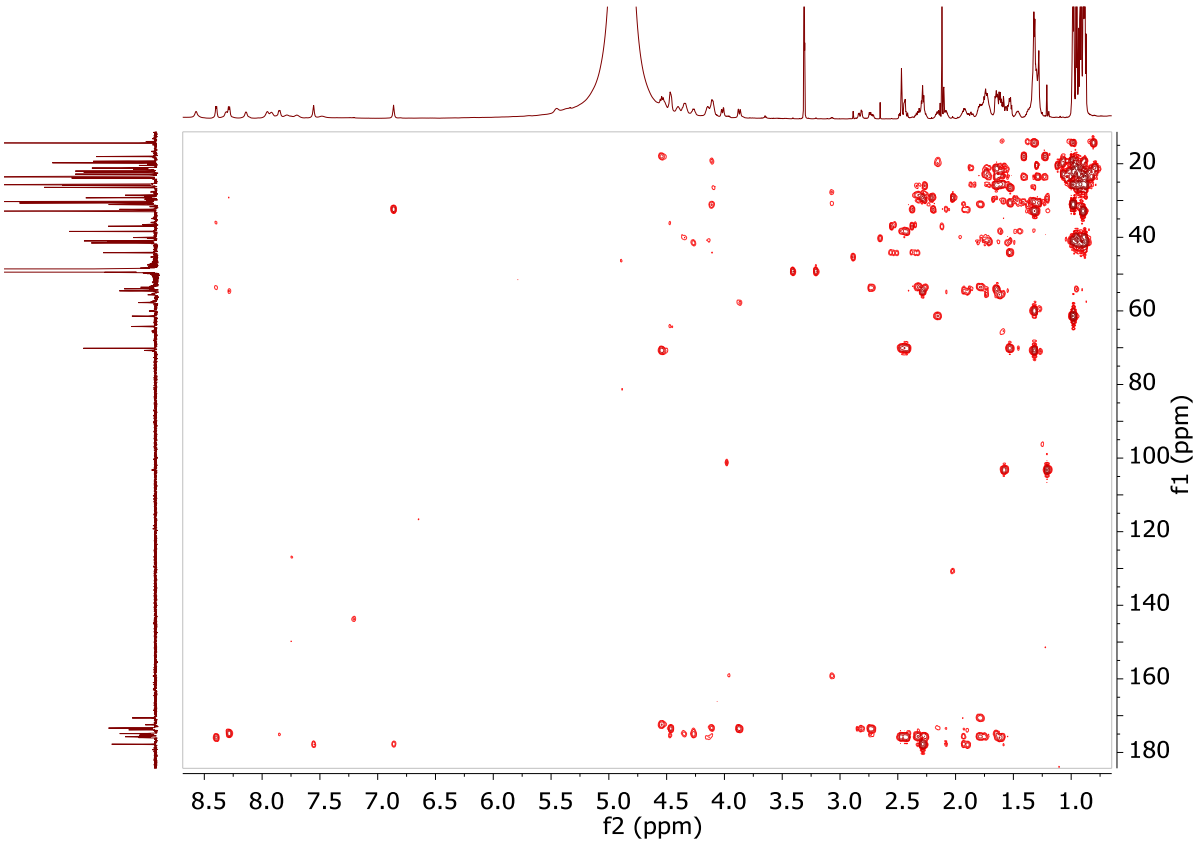

Figure A12: NMR spectra of compound **4** (d_6-Acetone, 400 MHz)

a. ^{1}H-NMR

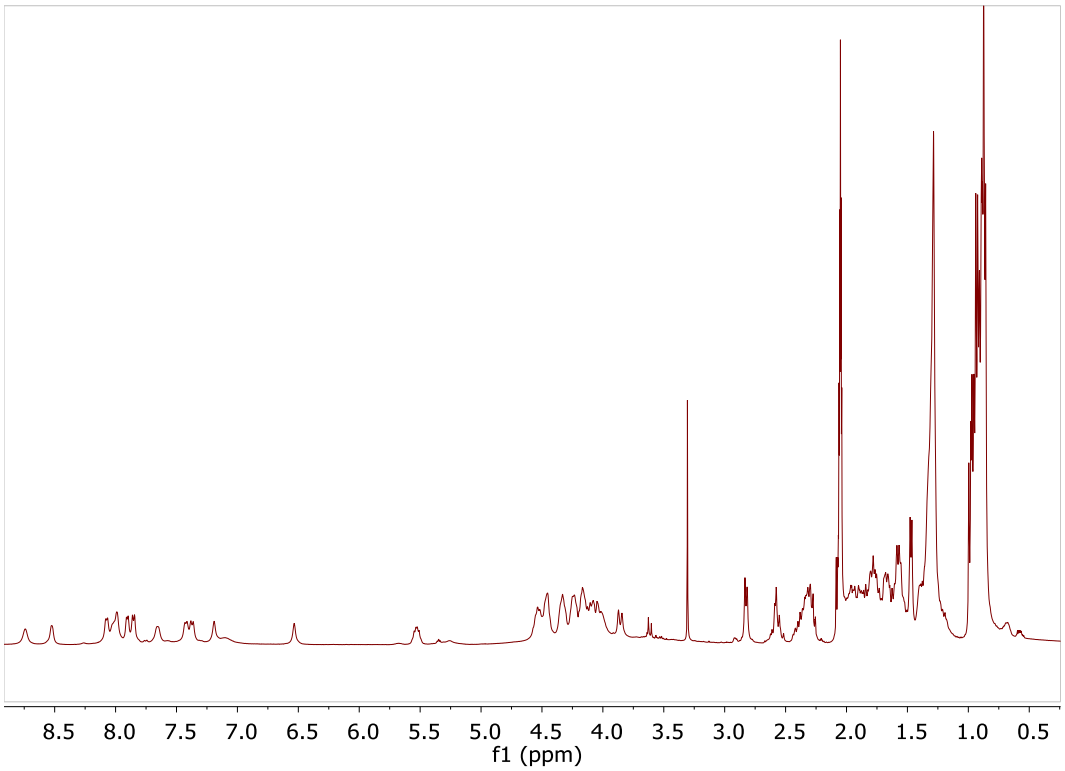

b. ^{13}C-NMR

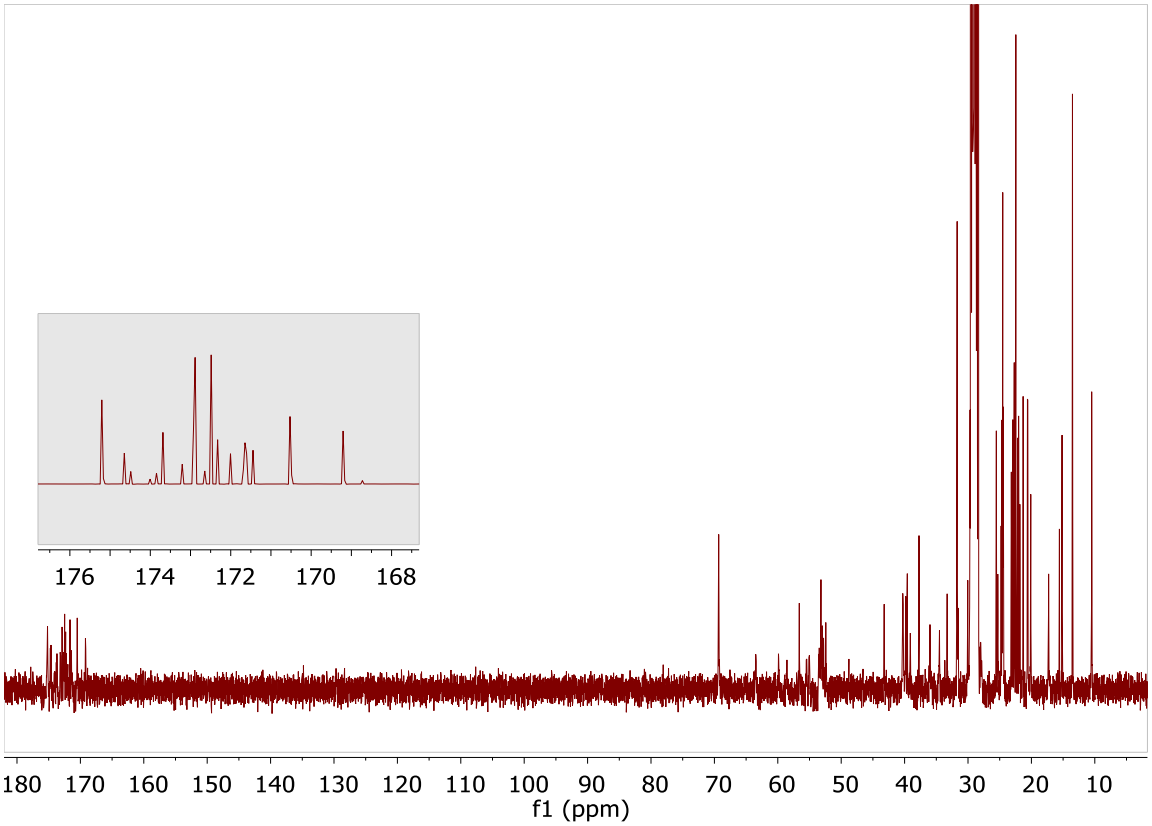

Figure A13: NMR spectra of virginiafactin A (d_3-MeOH, 400 MHz)

a. ^{1}H-NMR

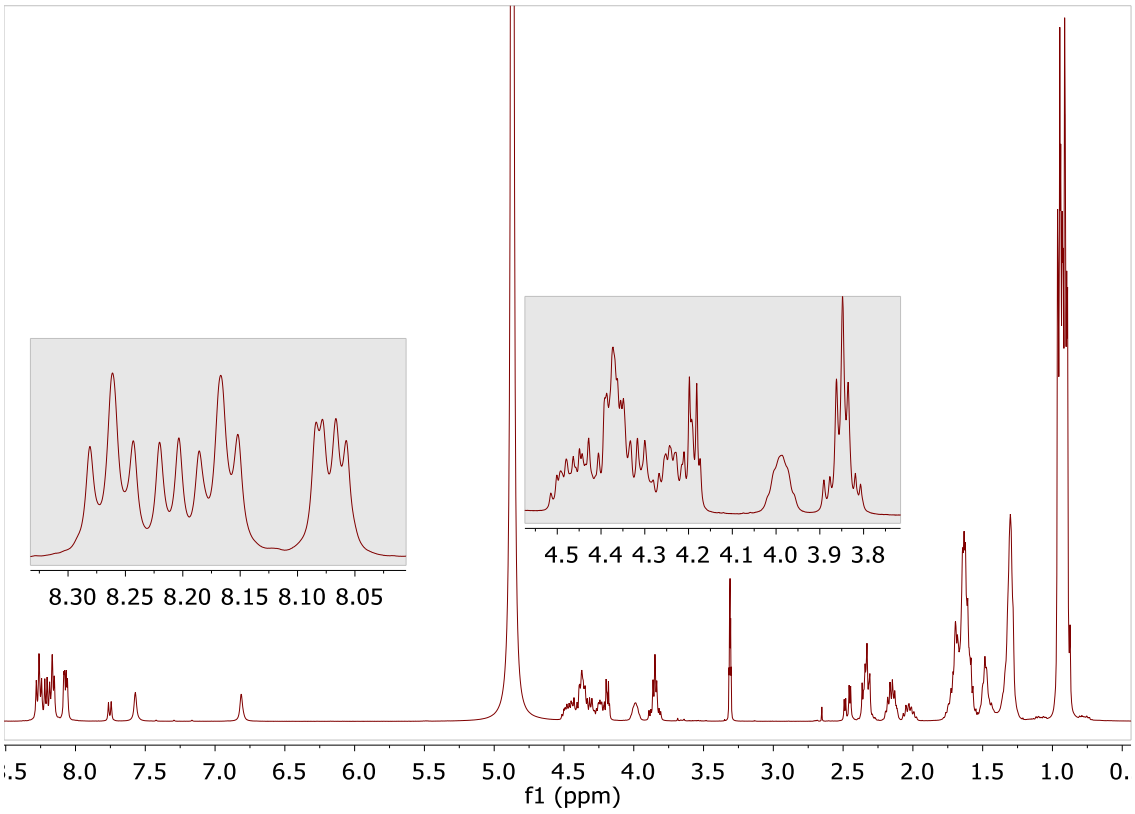

b. ^{13}C-NMR

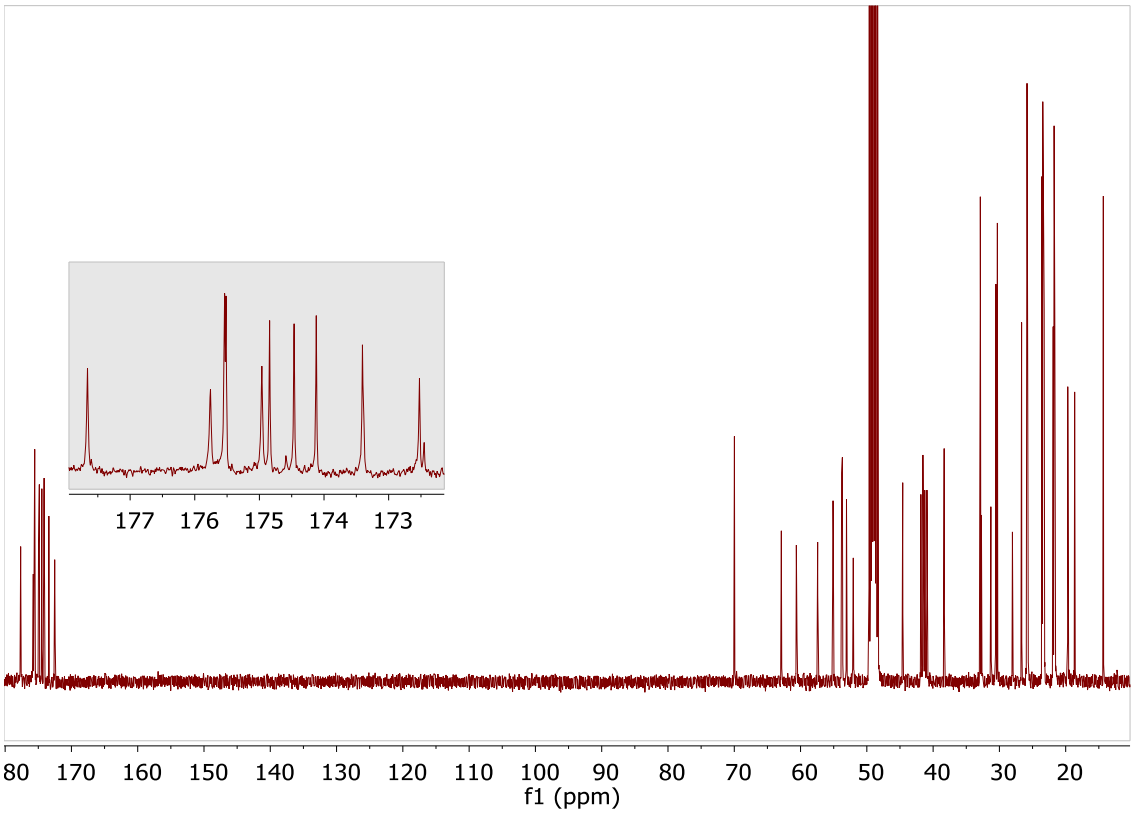

c. ^{1}H-^{13}H-COSY

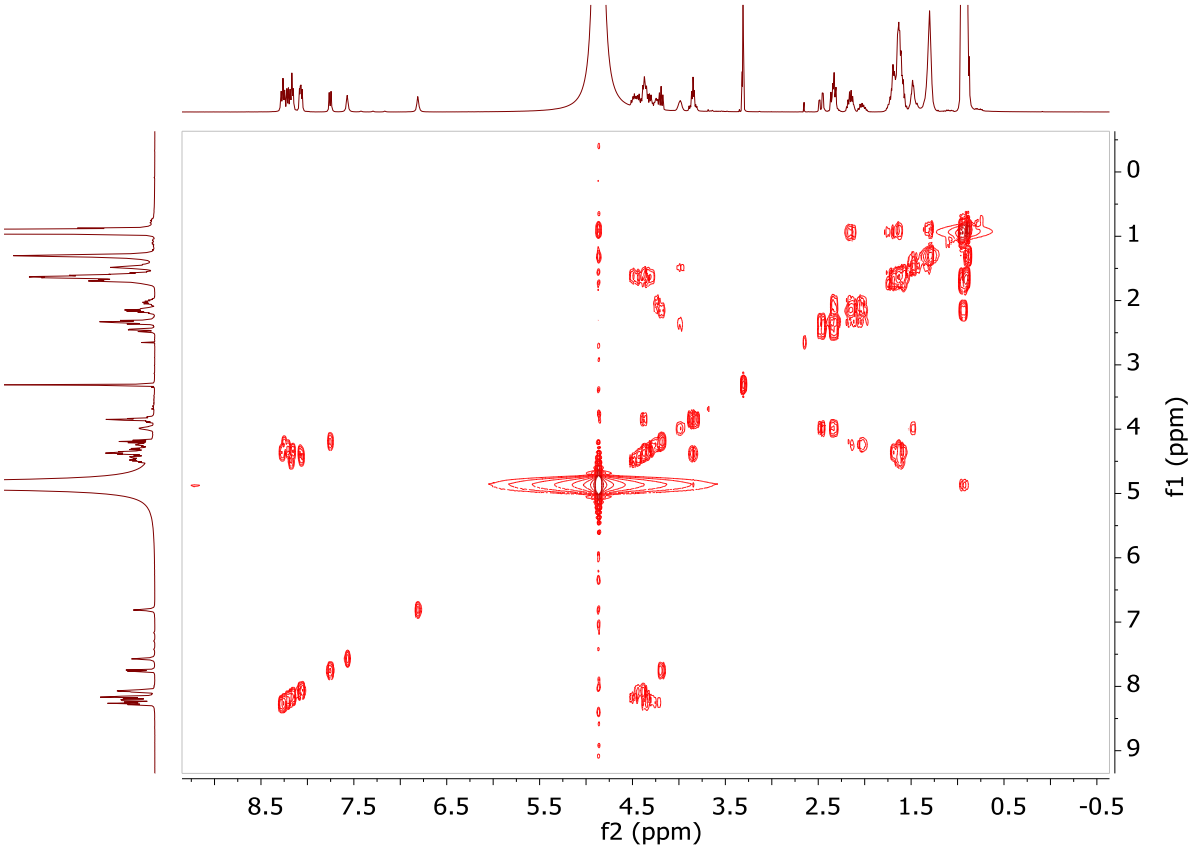

d. ^{1}H-^{13}C-HSQC

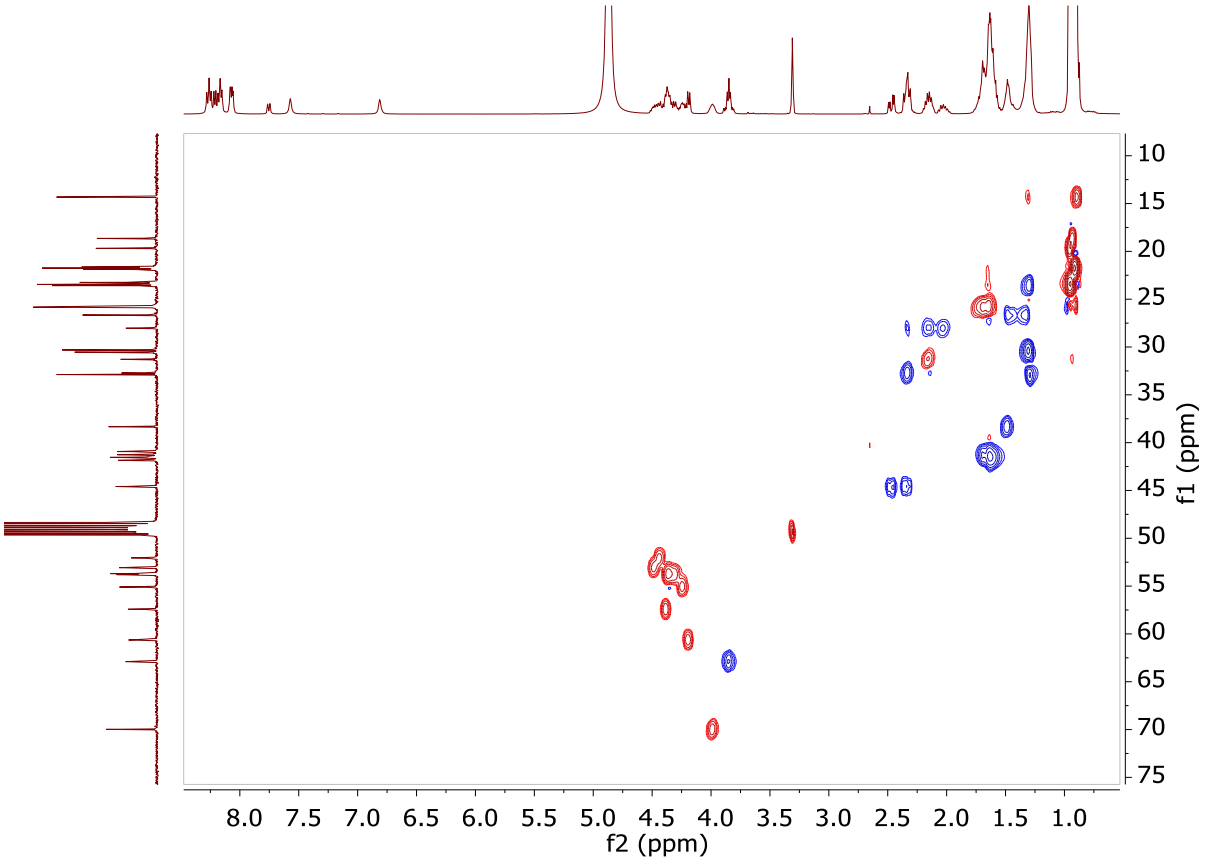

e. ^{1}H-^{13}C-HMBC

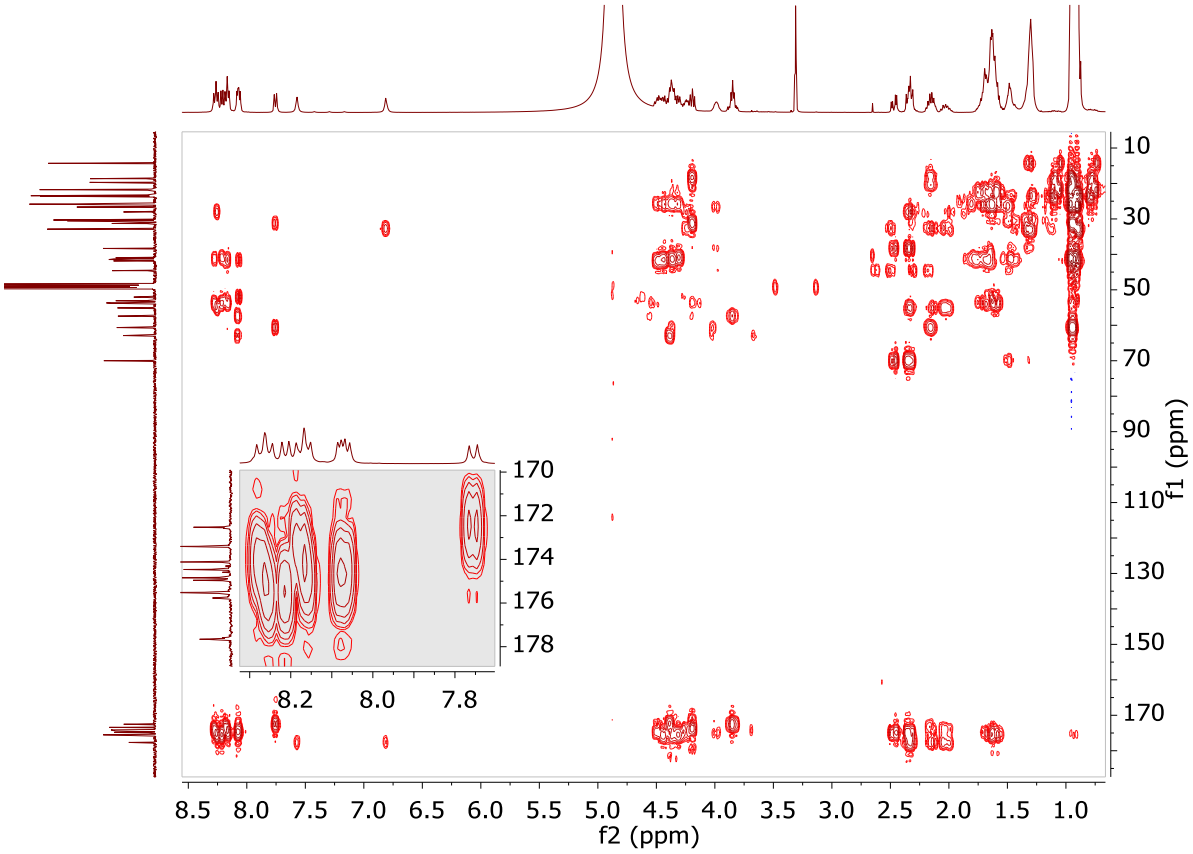

f. ^{1}H-^{1}H-TOCSY

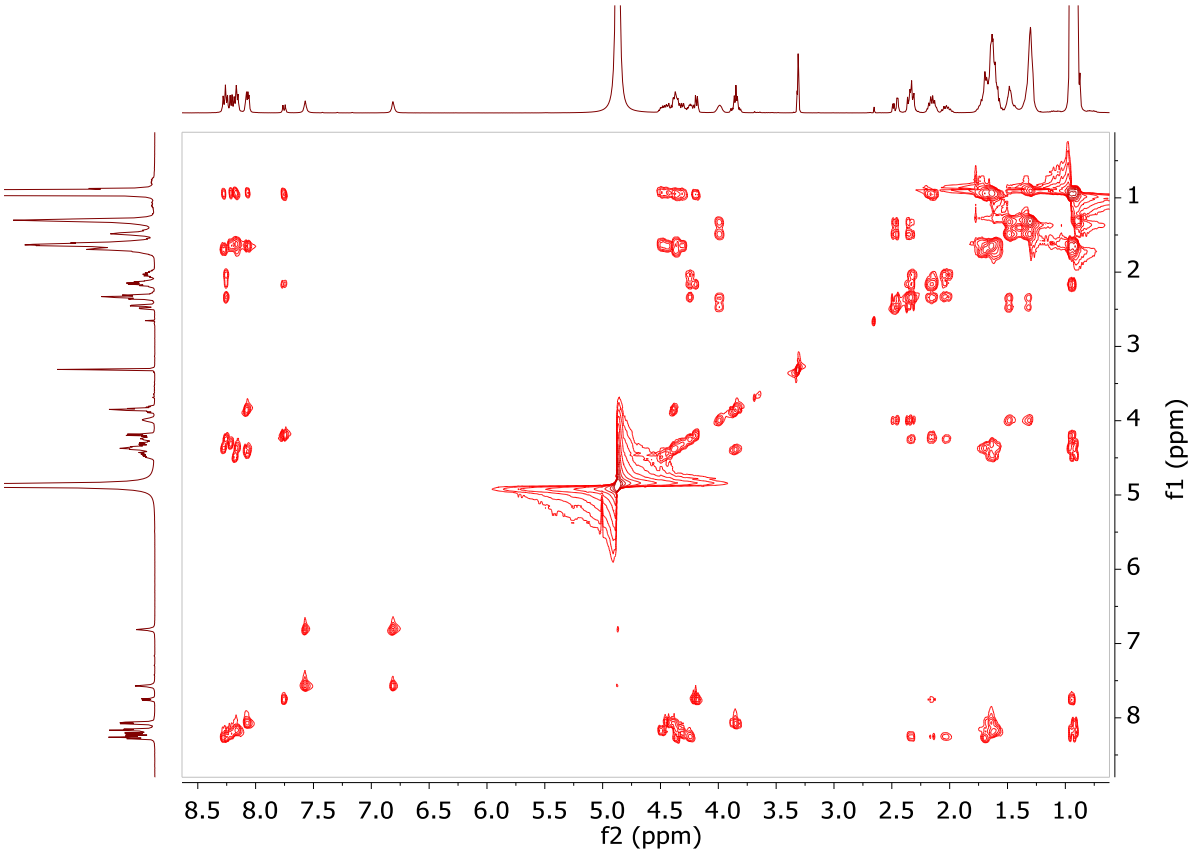

g. ^{1}H-^{13}C-HSQC-TOCSY

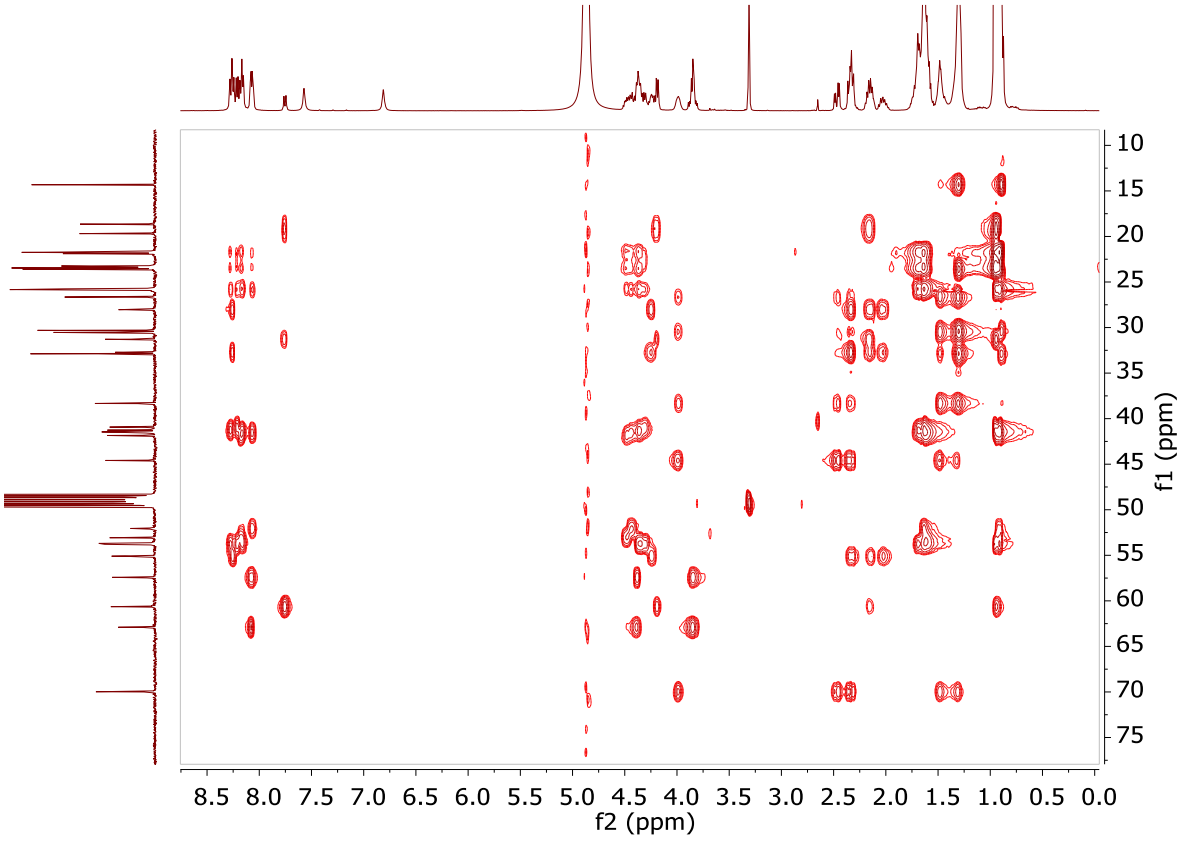

h. ^{1}H-^{1}H-NOESY

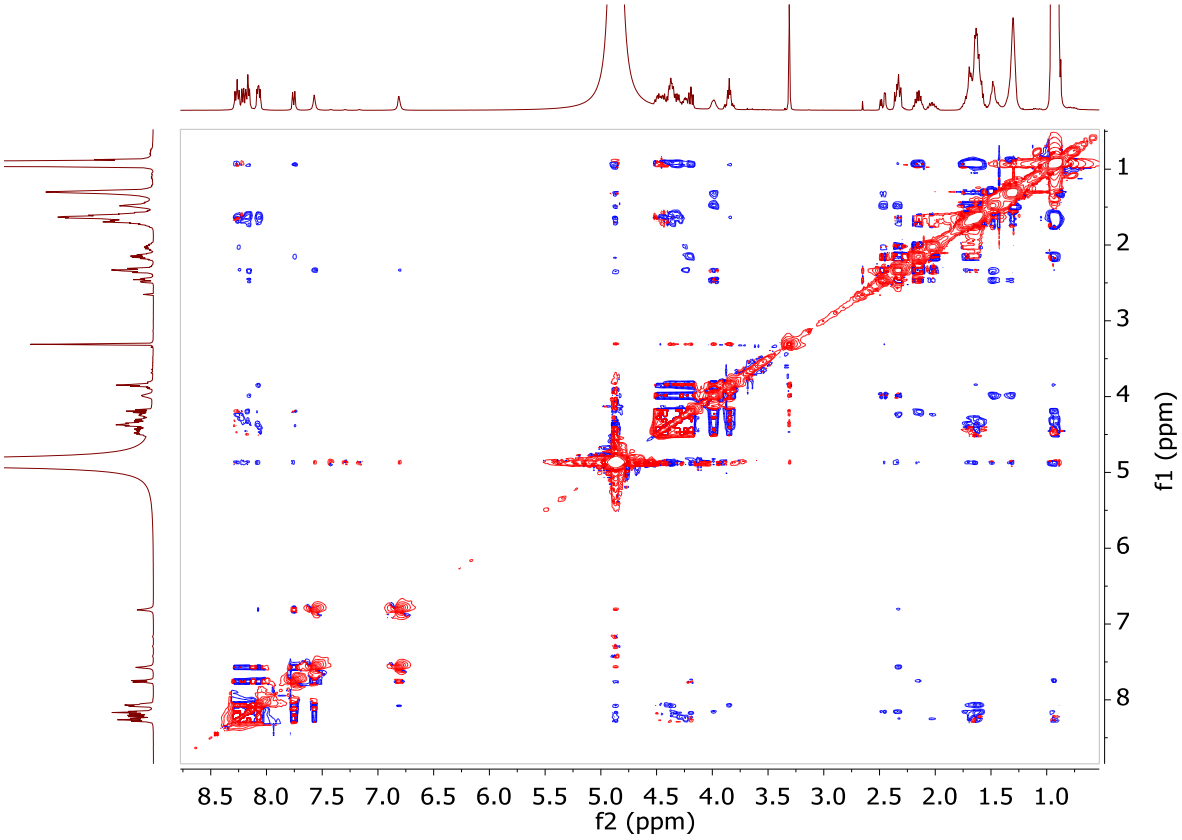

i. ^{1}H-^{15}N-HSQC

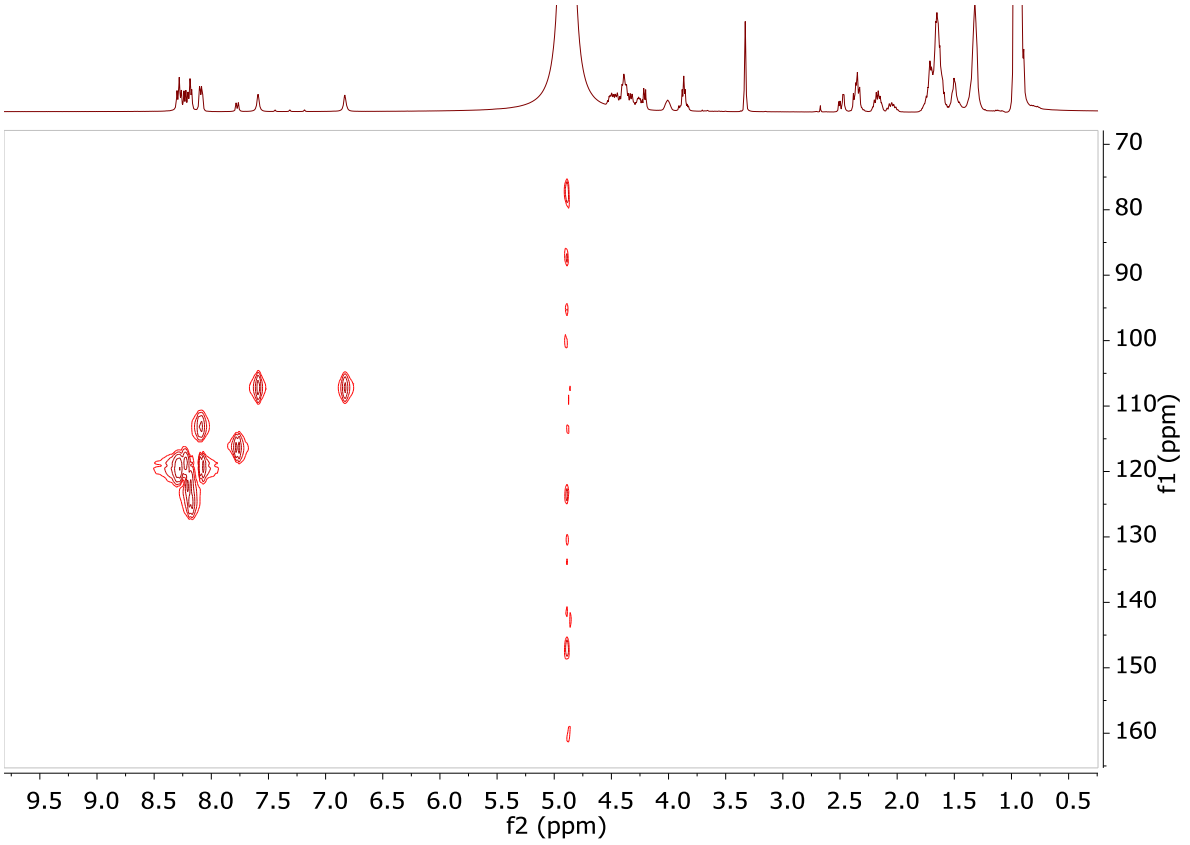

j. ^{1}H-^{15}N-HMBC

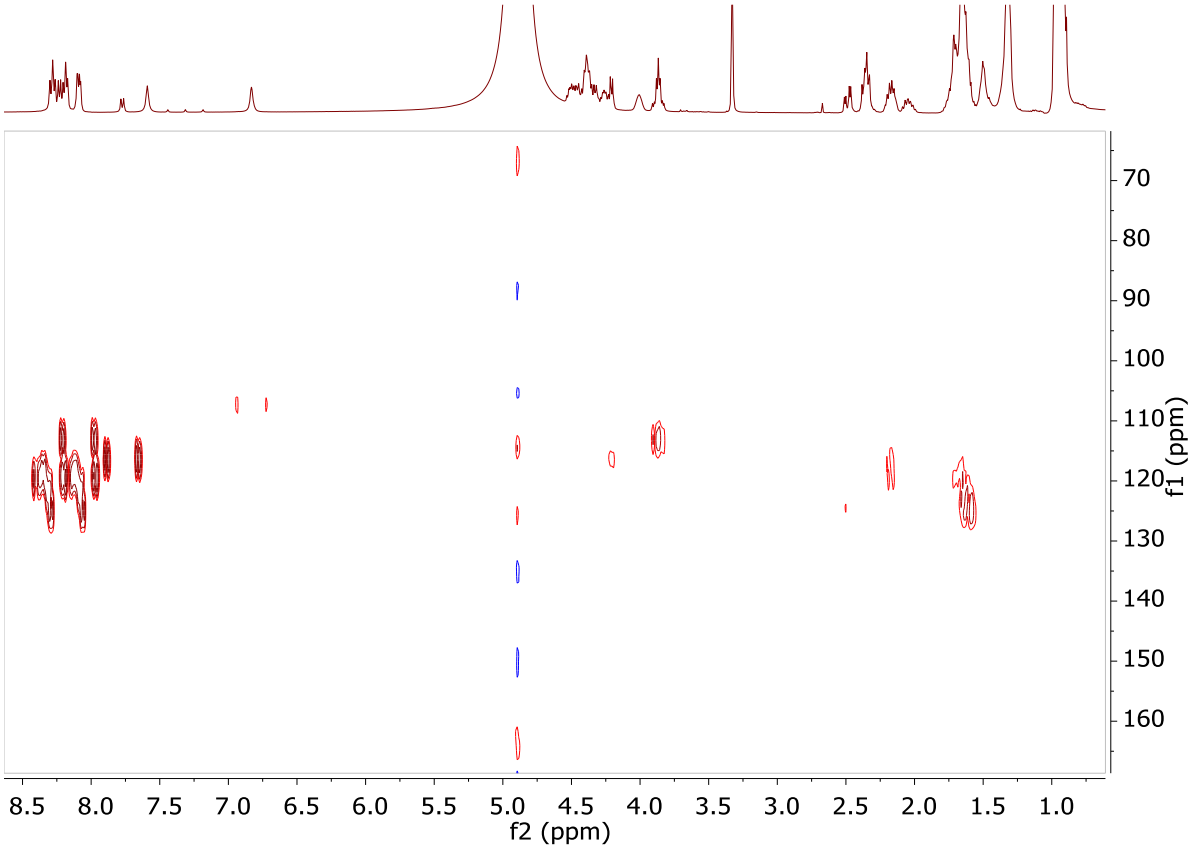

k. ^{1}H-^{13}C-HMBC-Band Selective

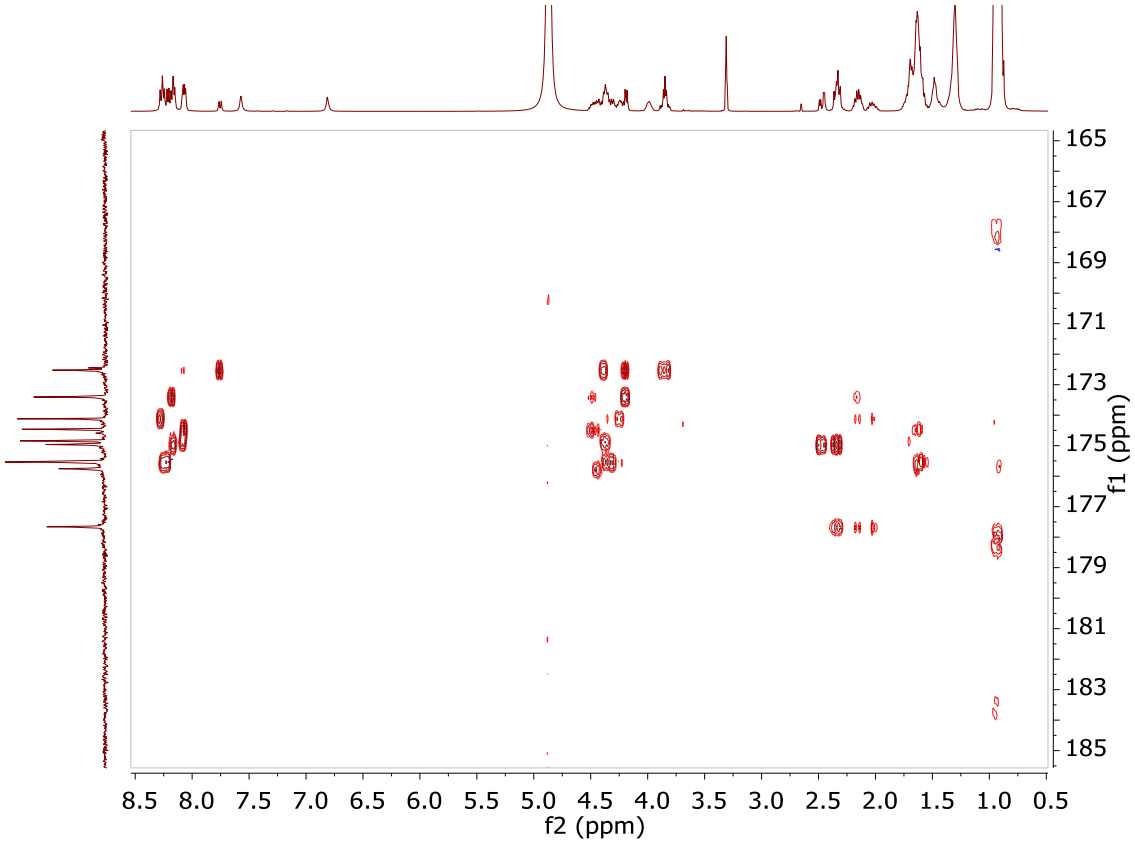

l. ^{1}H-^{13}C-HMBC-Band Selective

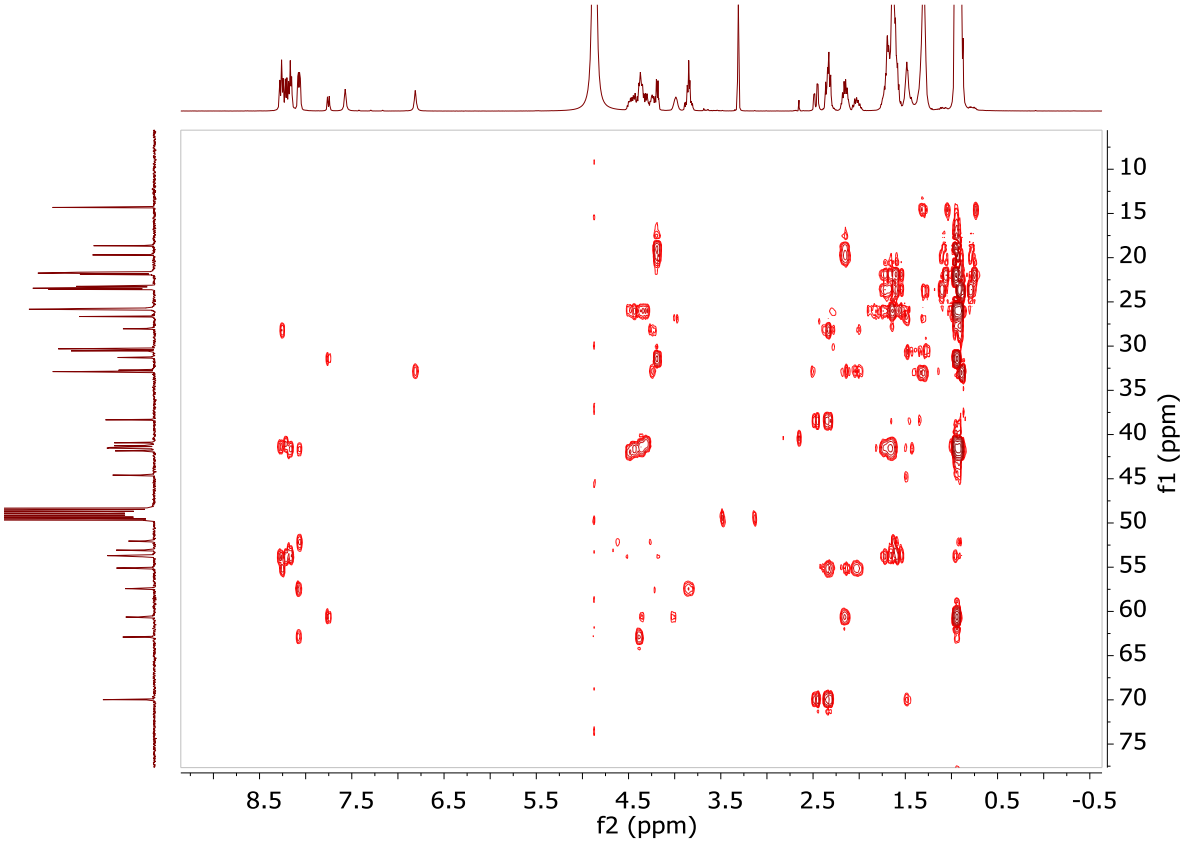

Figure A14: NMR spectra of virginiafactin B (d_4-MeOD, 400 MHz)

a. 1H-NMR

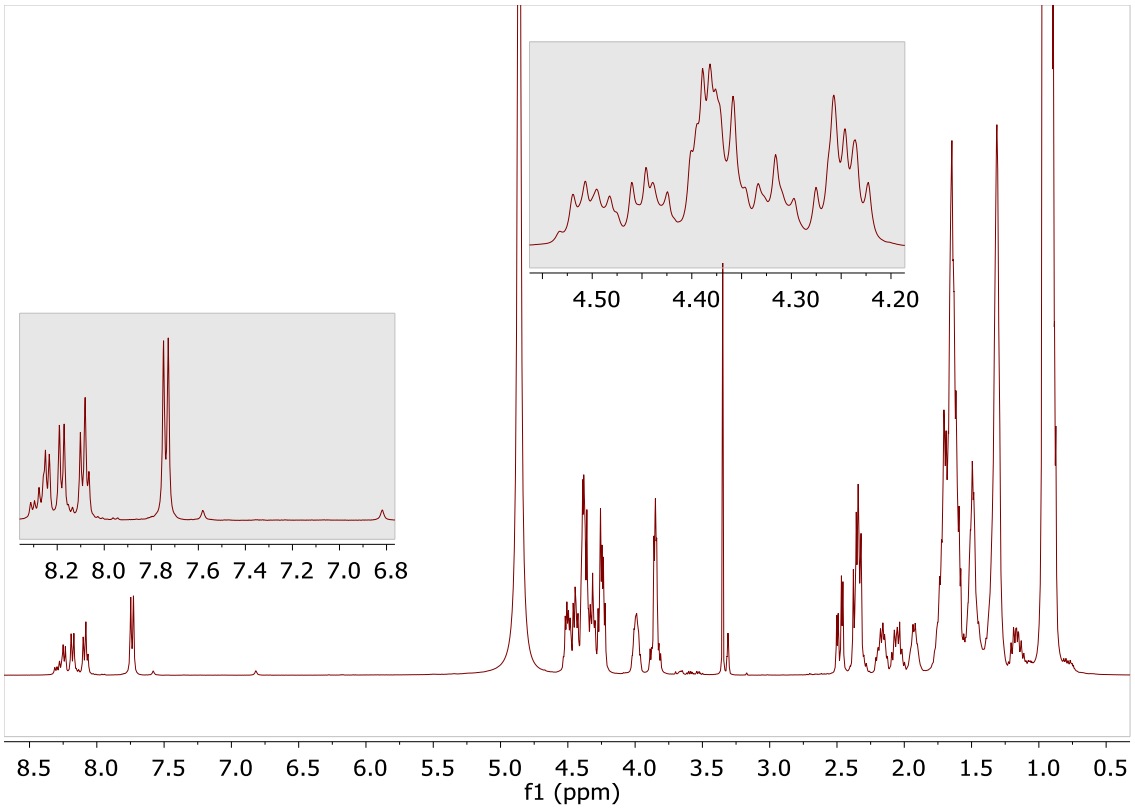

b. ^{13}C-NMR

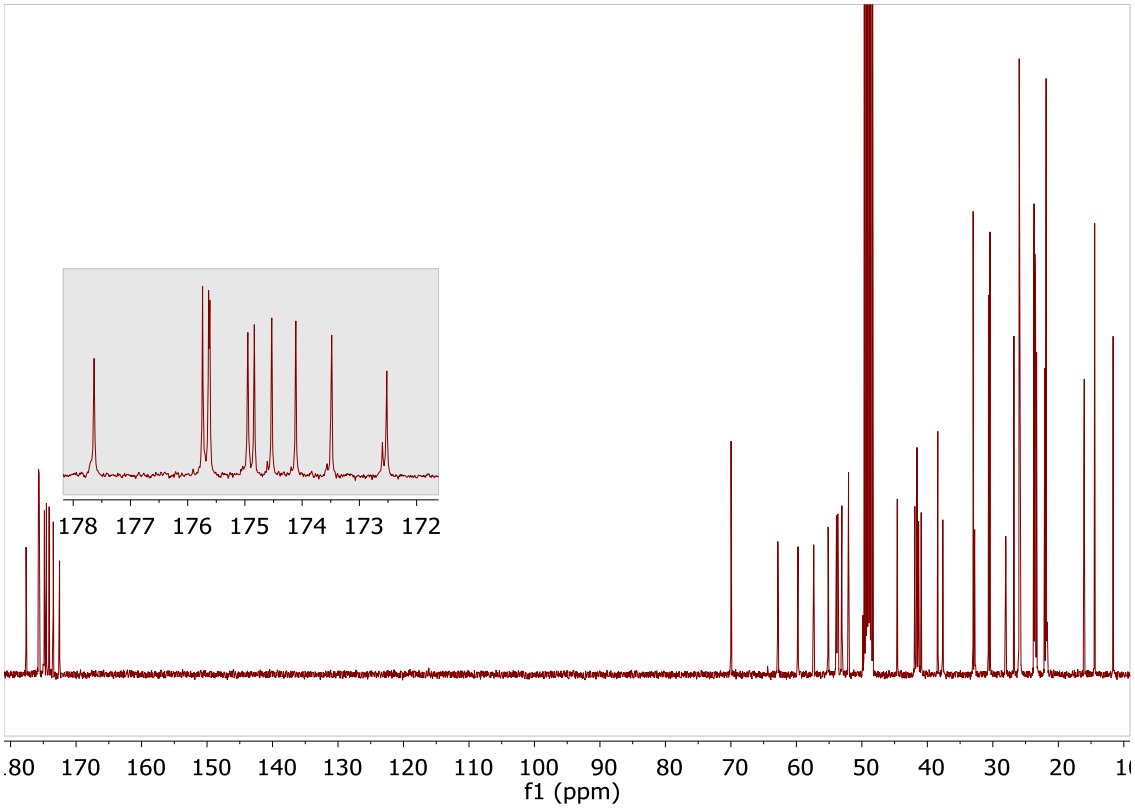

c. ^{13}C-DEPT-135

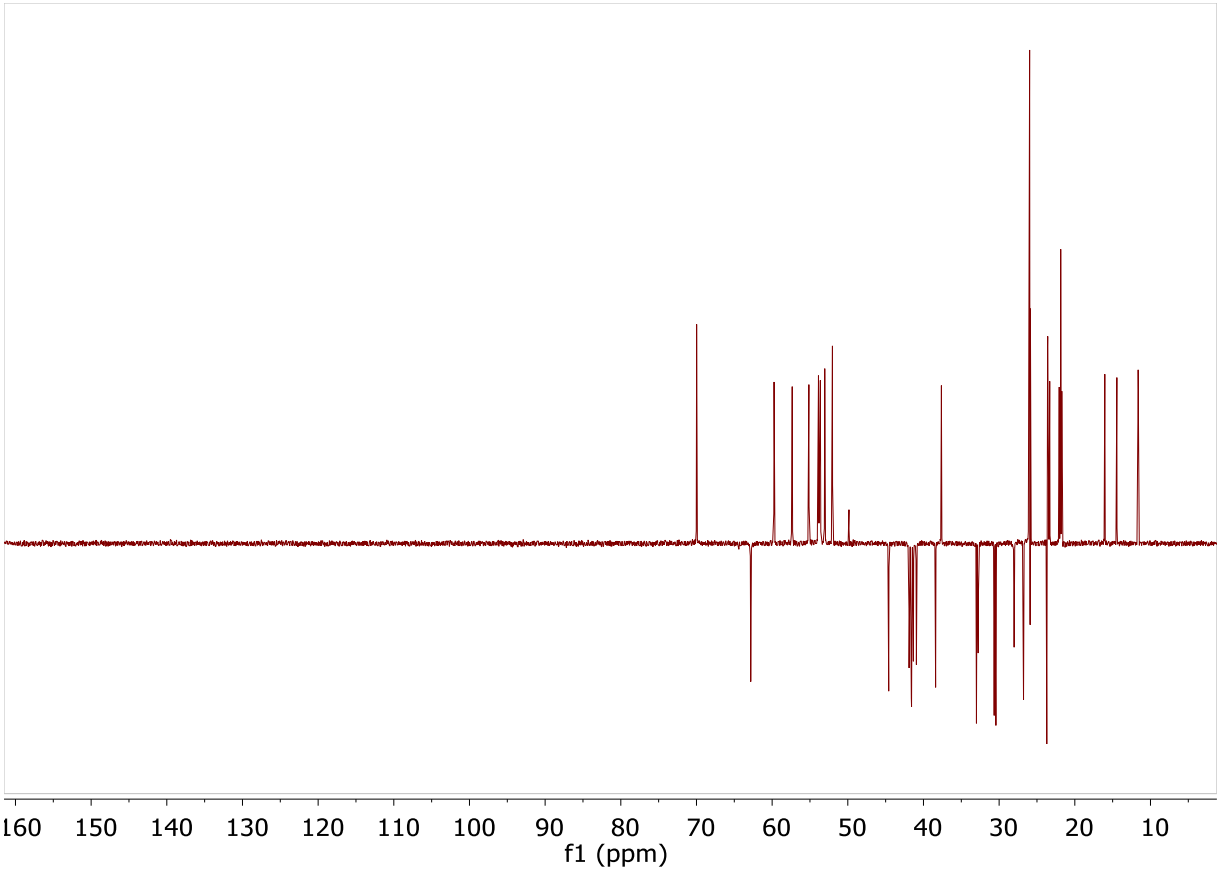

d. ^{1}H-^{1}H-COSY

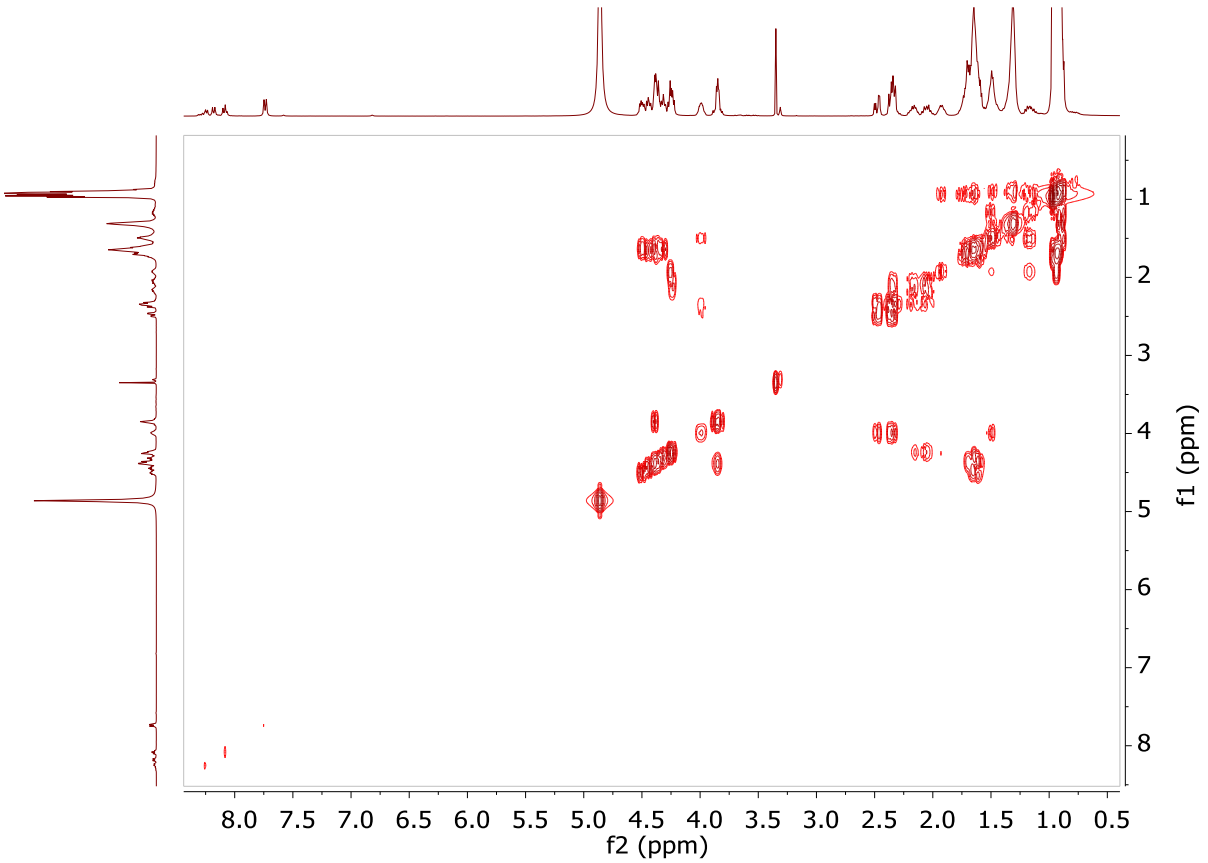

e. ^{1}H-^{13}C-HSQC

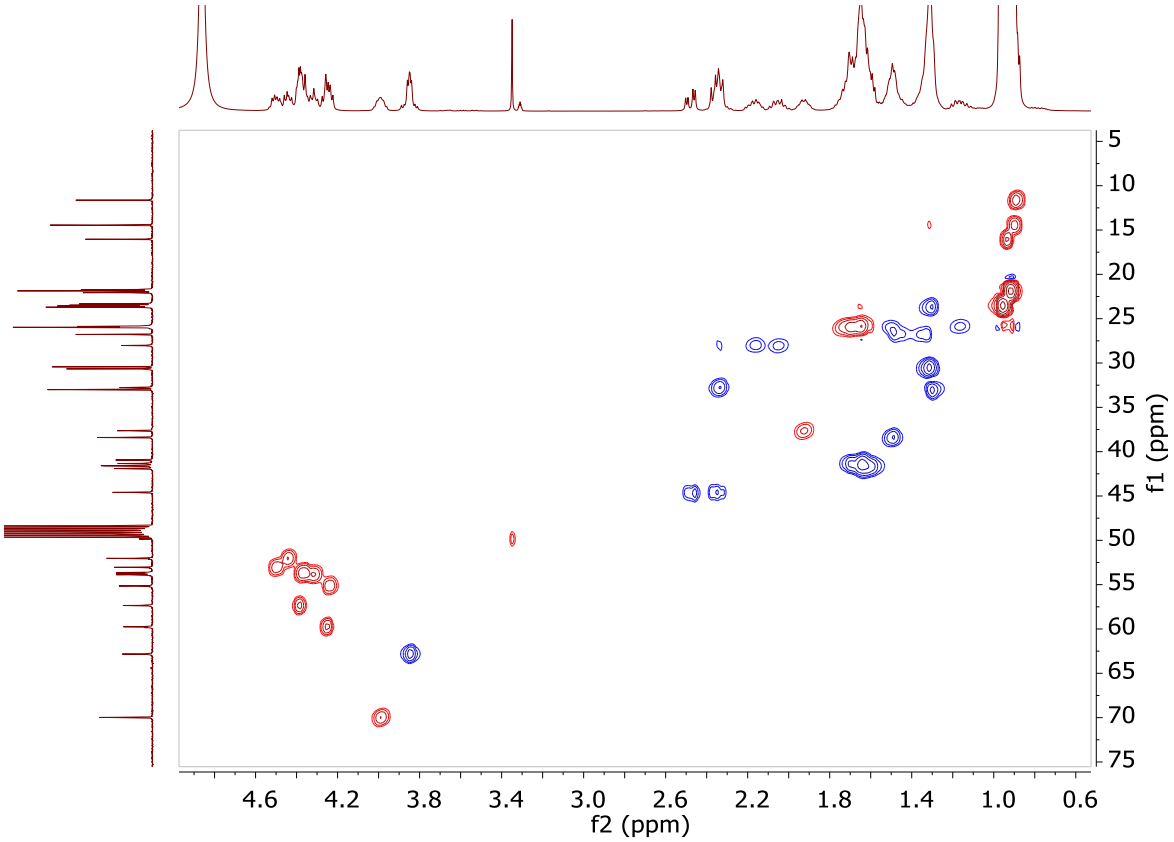

f. ^{1}H-^{13}C-HMBC

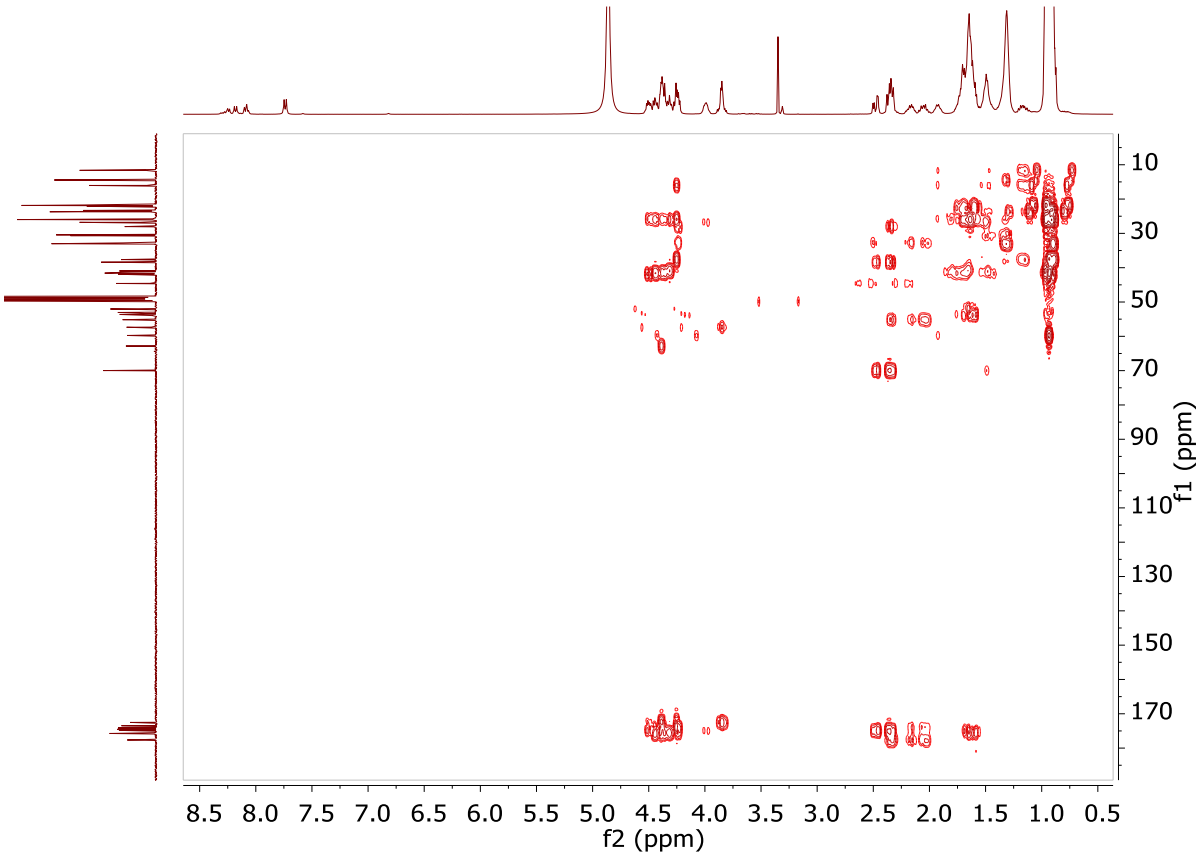

g. ^{1}H-^{1}H-TOCSY

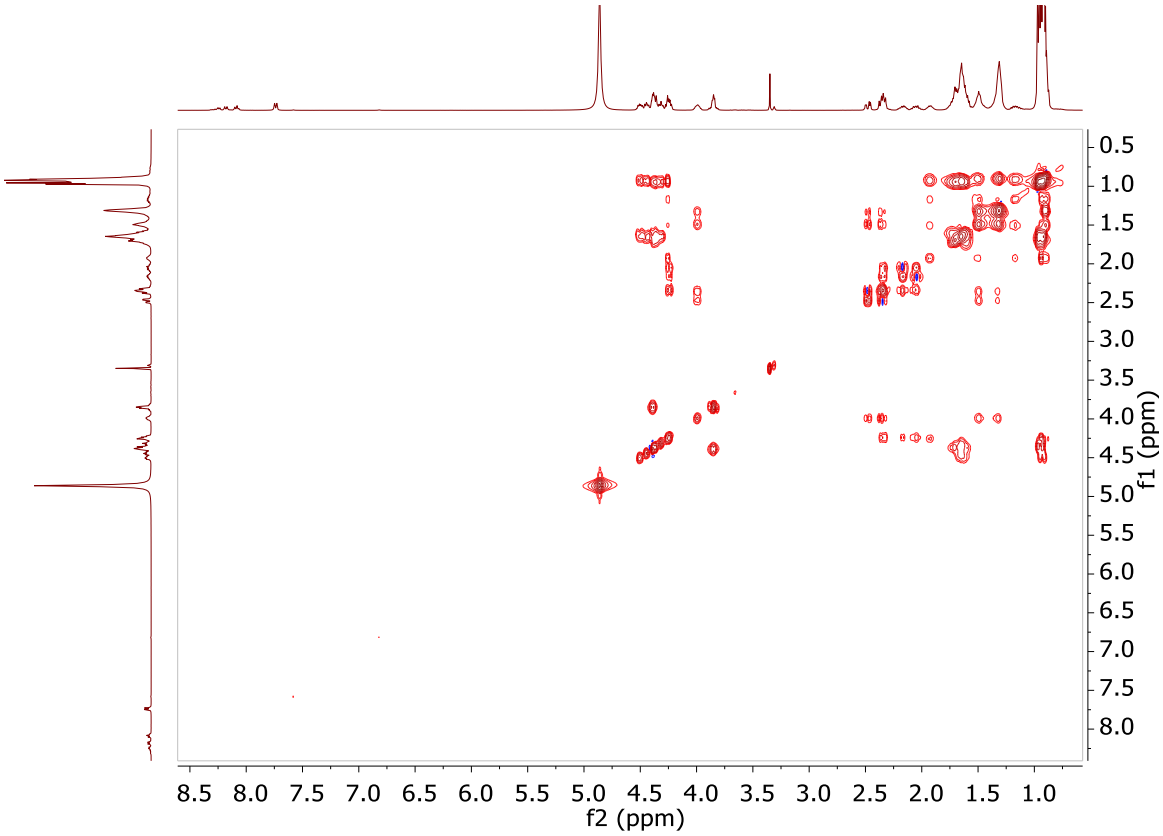

h. ^{1}H-^{13}C-HMBC

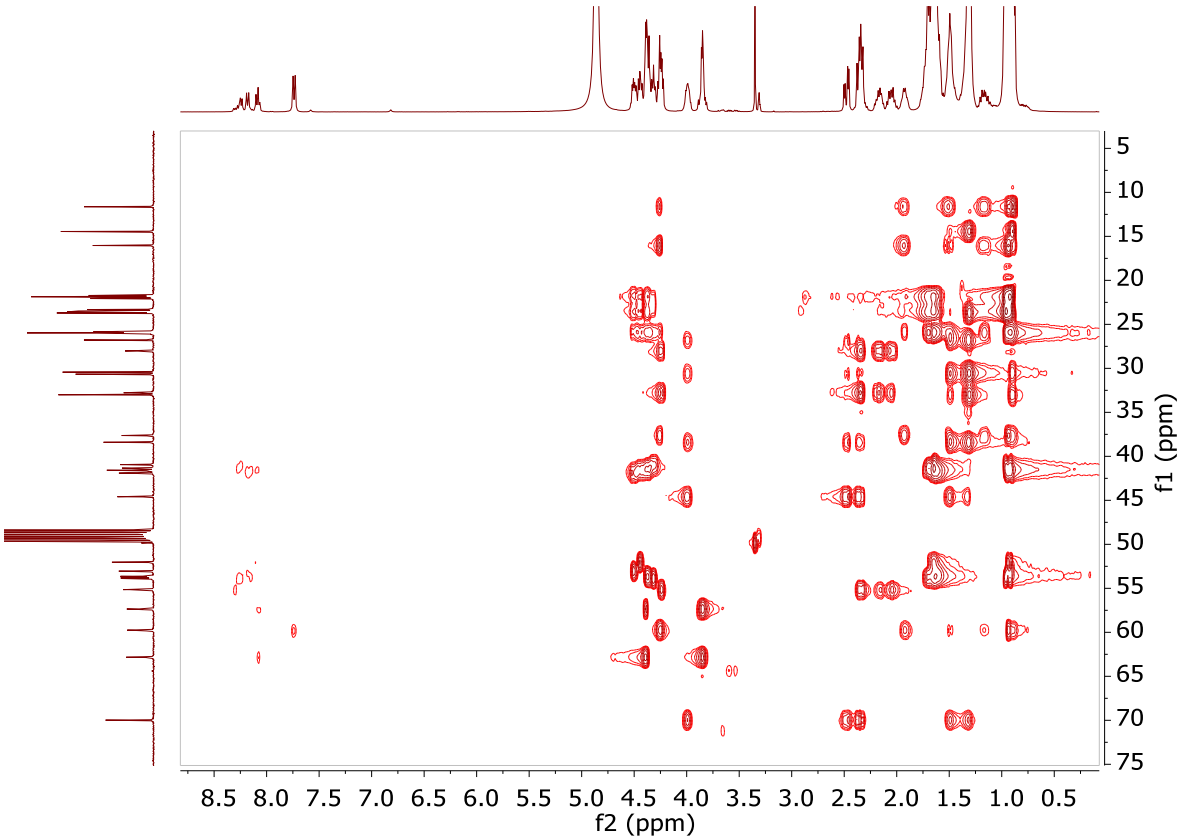

Figure A15: NMR spectra of compound **9** (d_3-MeOH, 400 MHz)

Appendix

a. ^{1}H-NMR

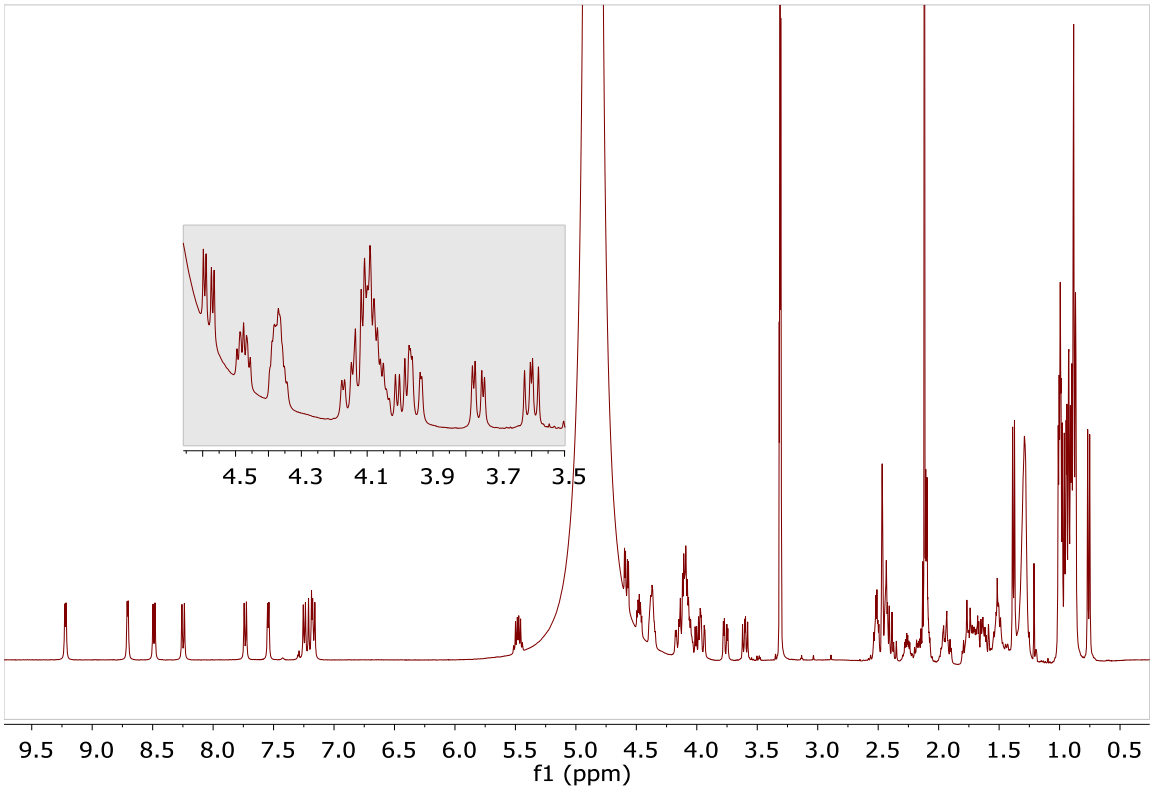

b. ^{13}C-NMR

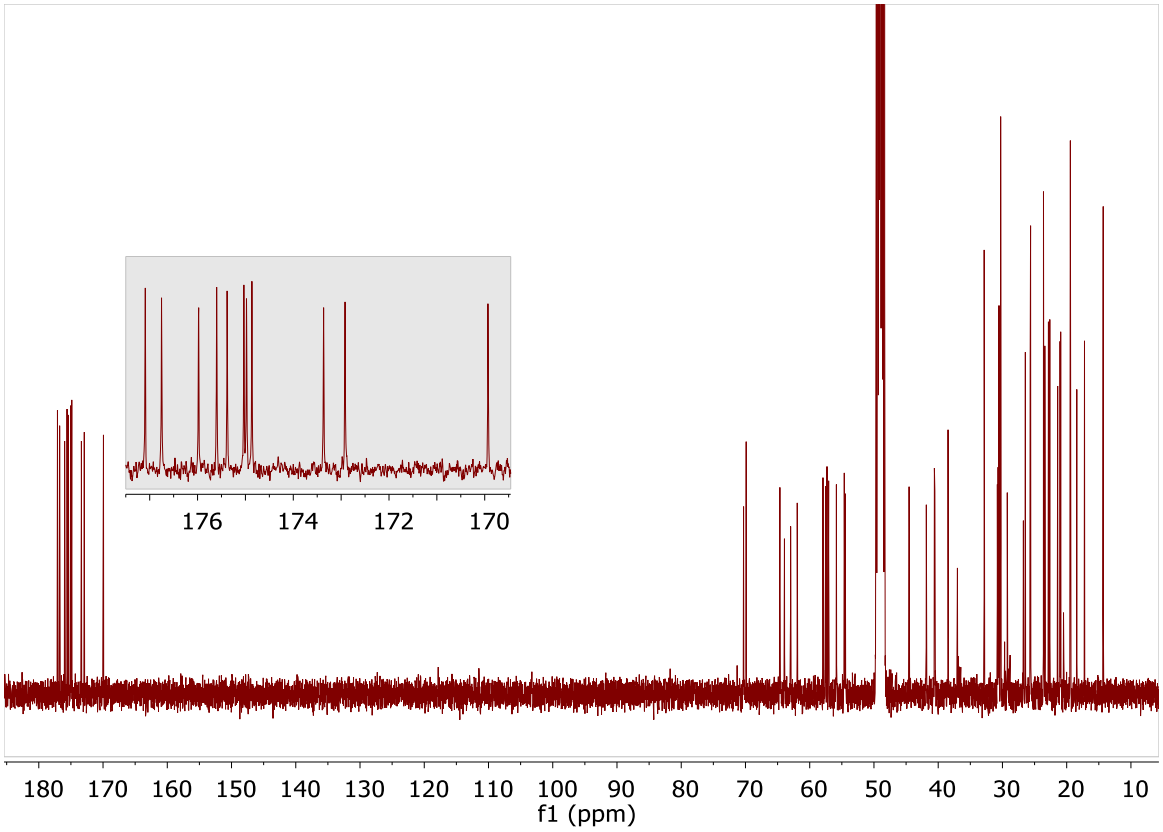

c. ^{1}H-^{1}H-COSY

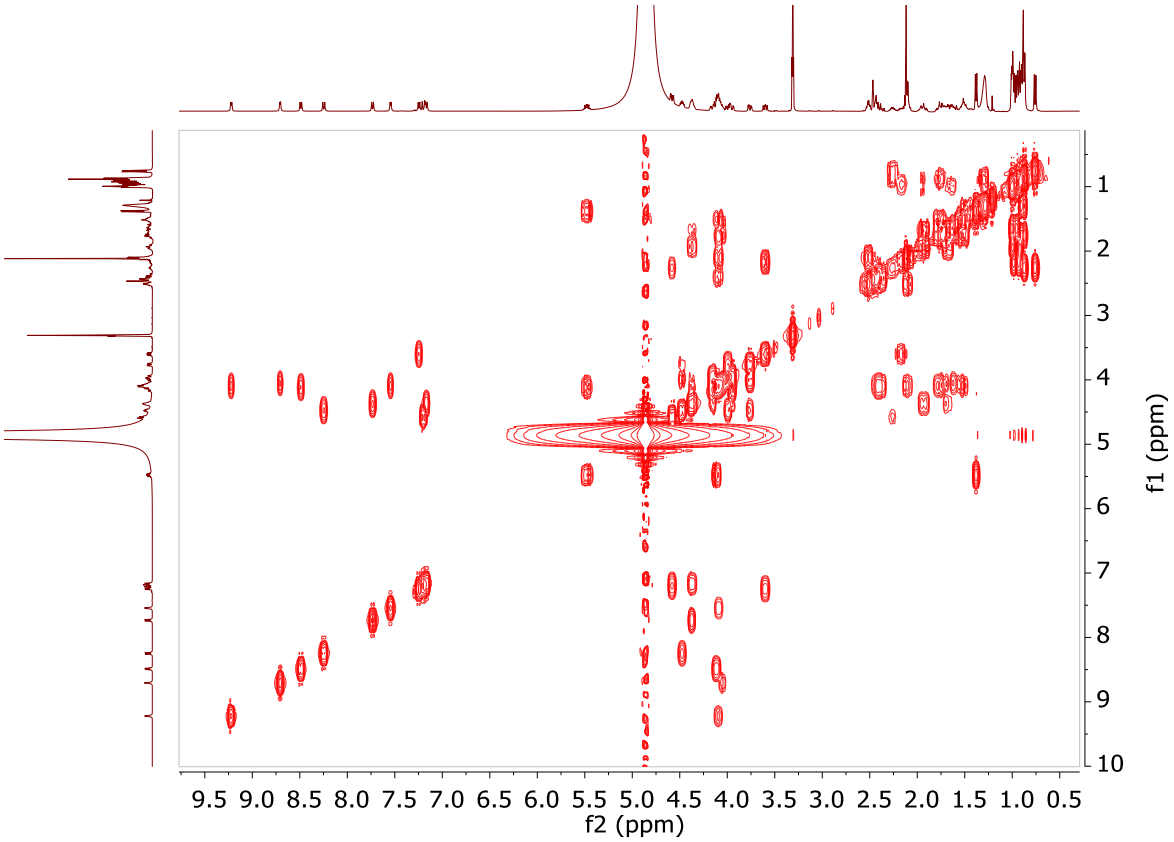

d. ^{1}H-^{13}C-HSQC

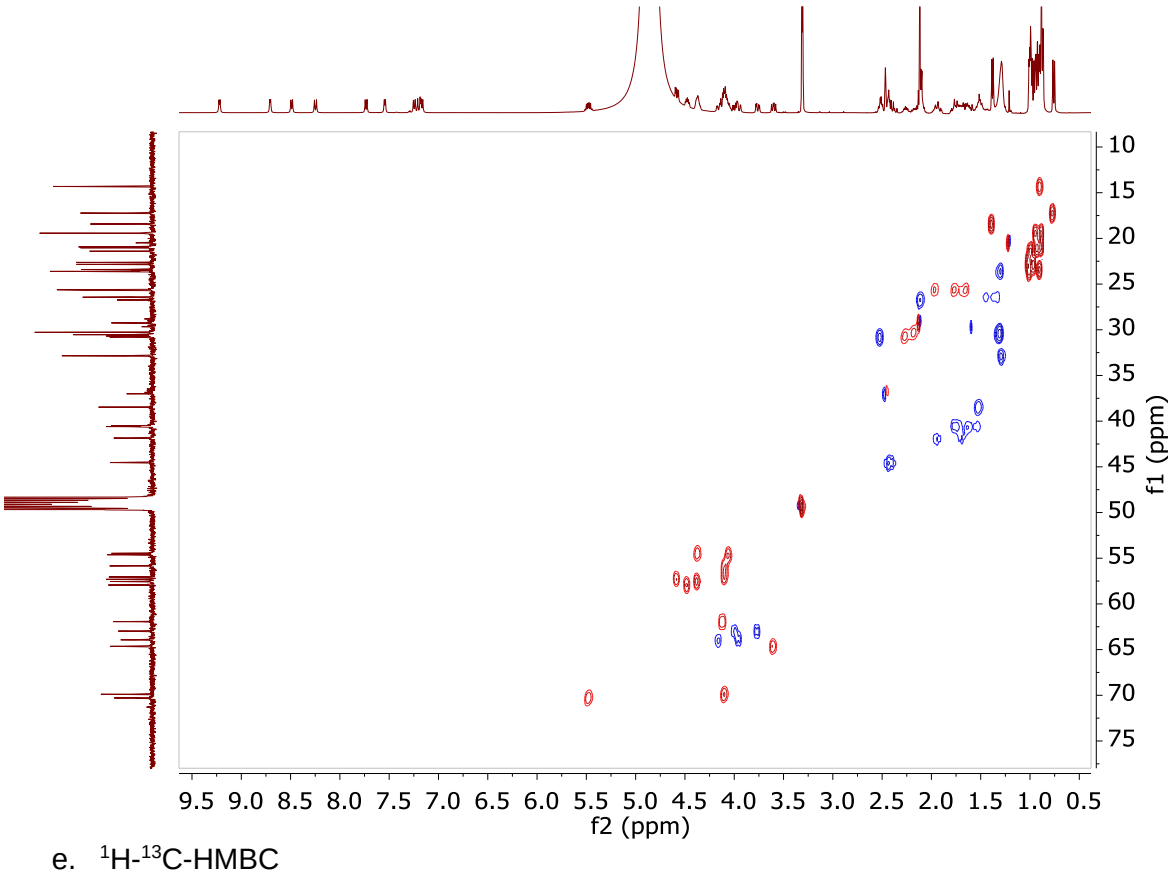

e. ^{1}H-^{13}C-HMBC

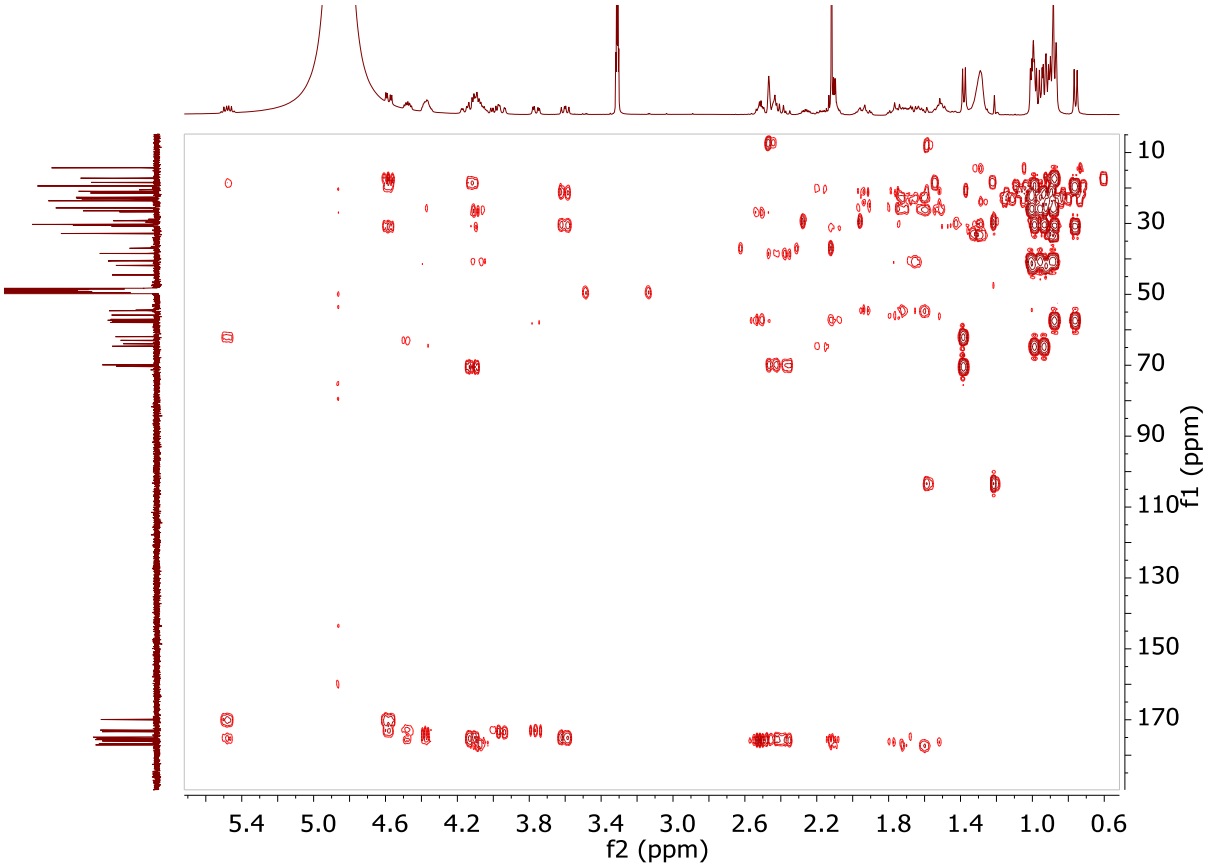

f. ^{1}H-^{1}H-TOCSY

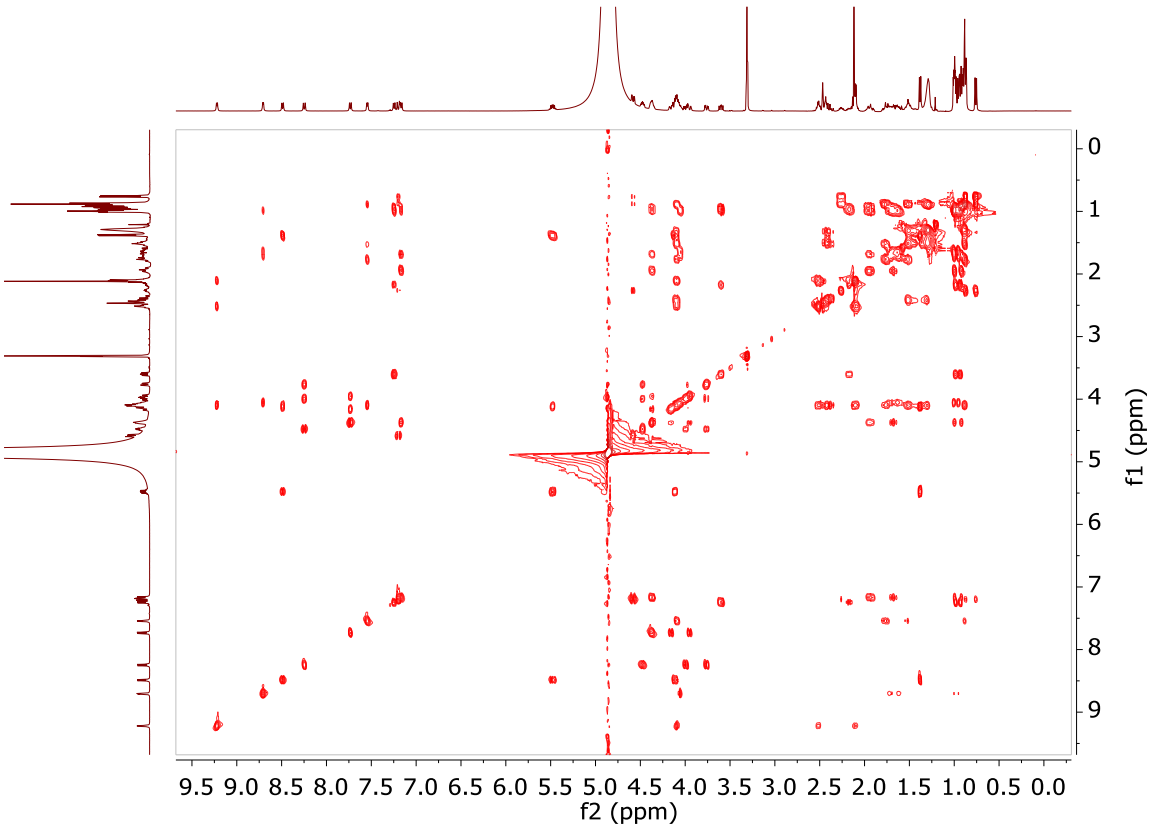

g. ^{1}H-^{13}C-HSQC-TOCSY

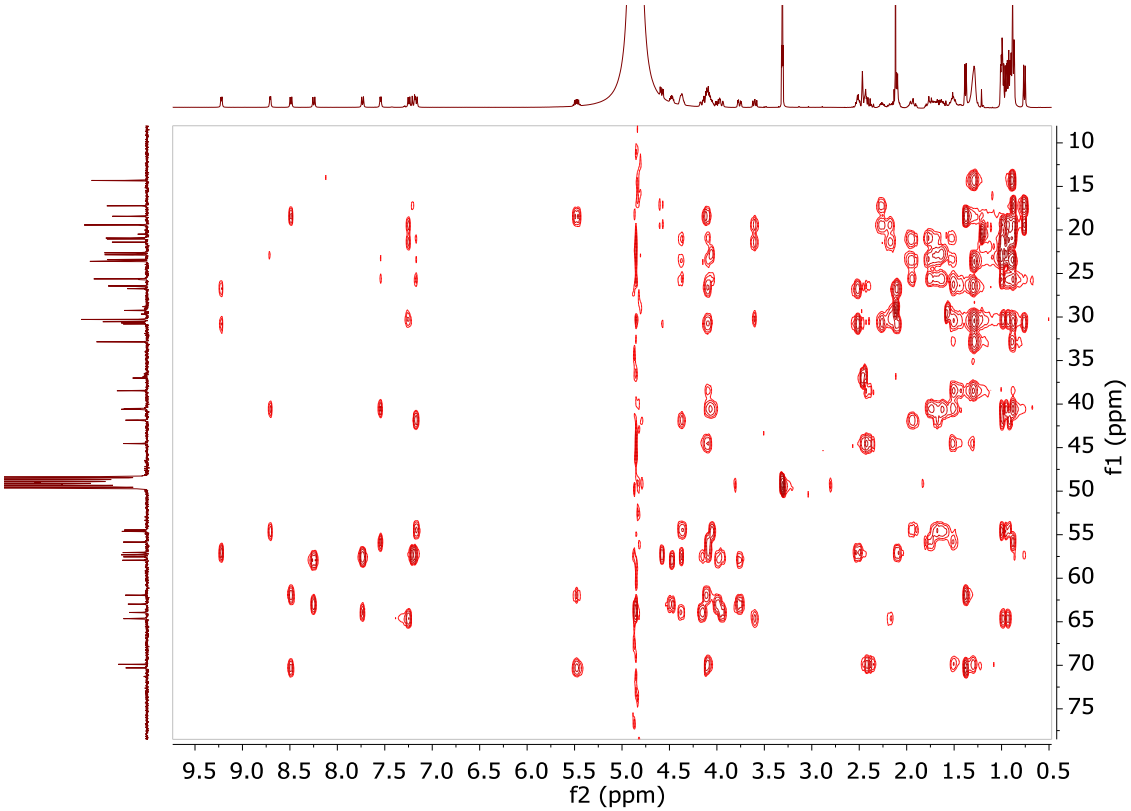

h. ^{1}H-^{15}N-HSQC

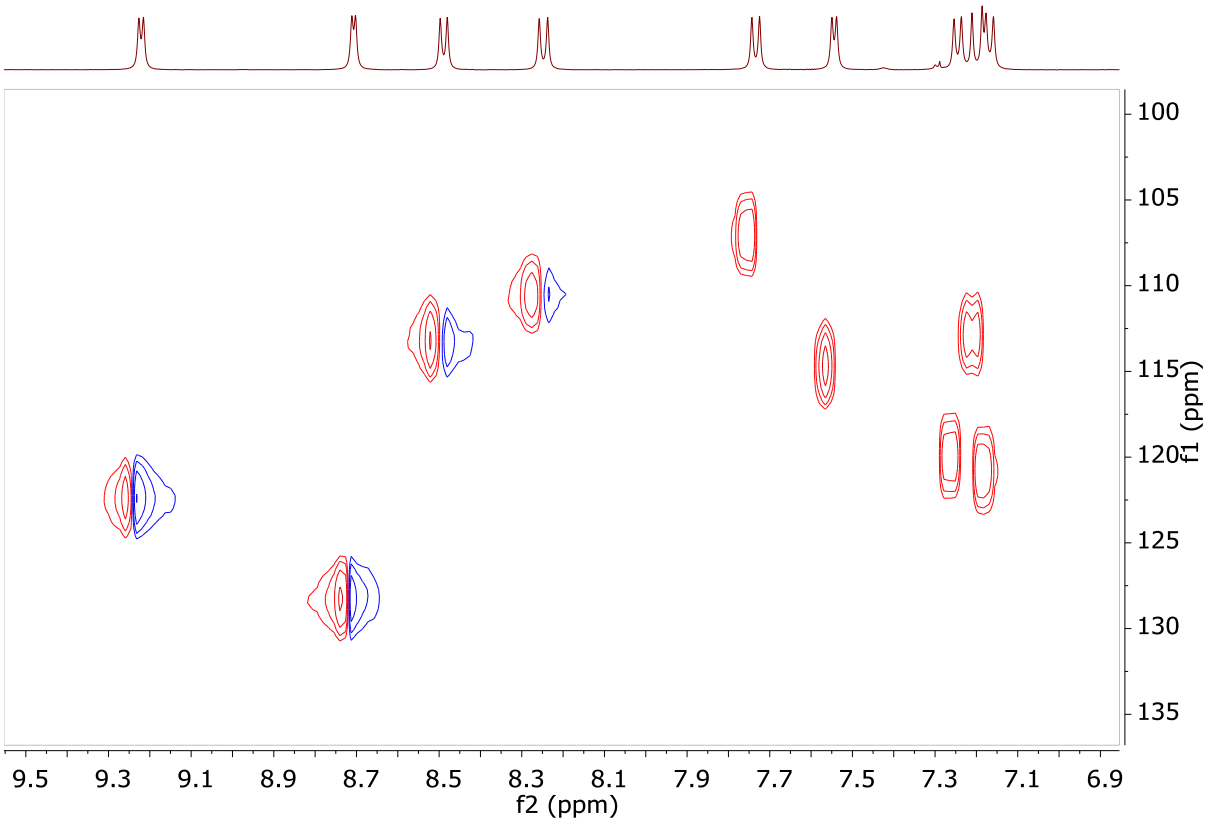

Figure A16: NMR spectra of compound **10** (d_3-MeOH, 400 MHz)

a. ^{1}H-NMR

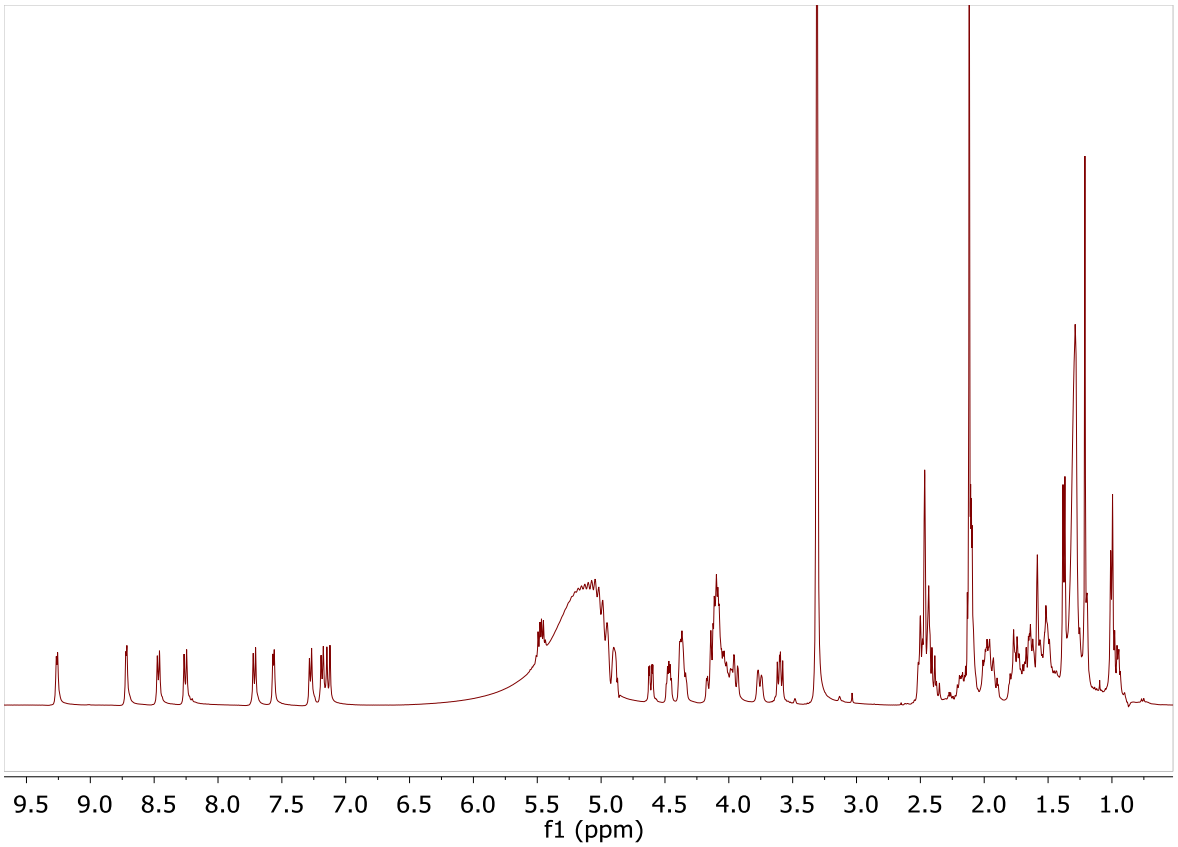

b. ^{13}C-NMR

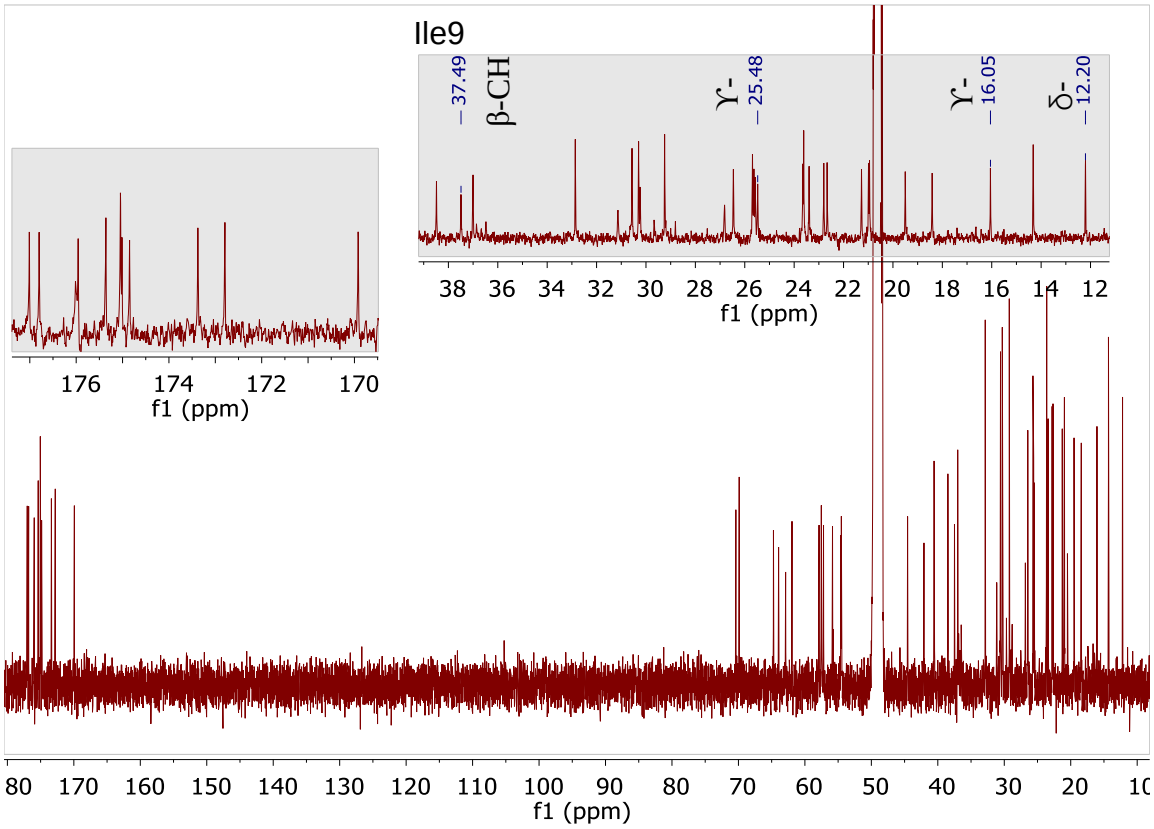

c. ^{13}C-DEPT-135

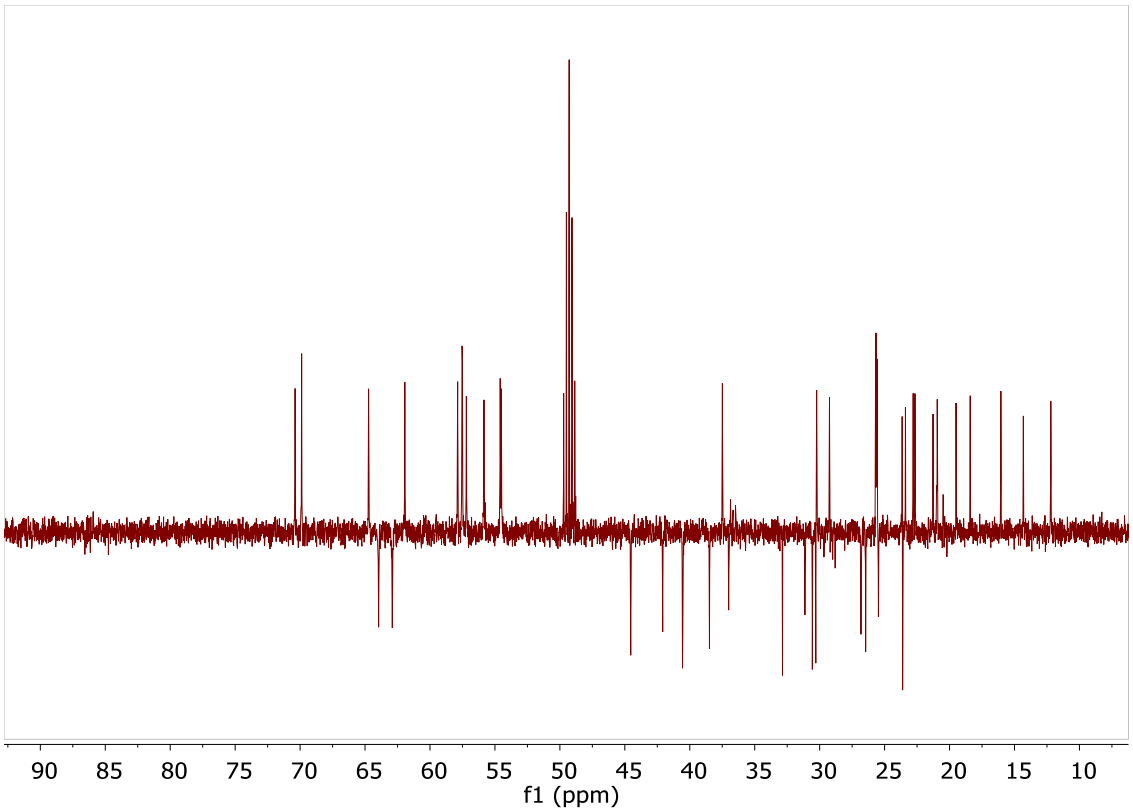

d. ^{1}H-^{13}C-HSQC

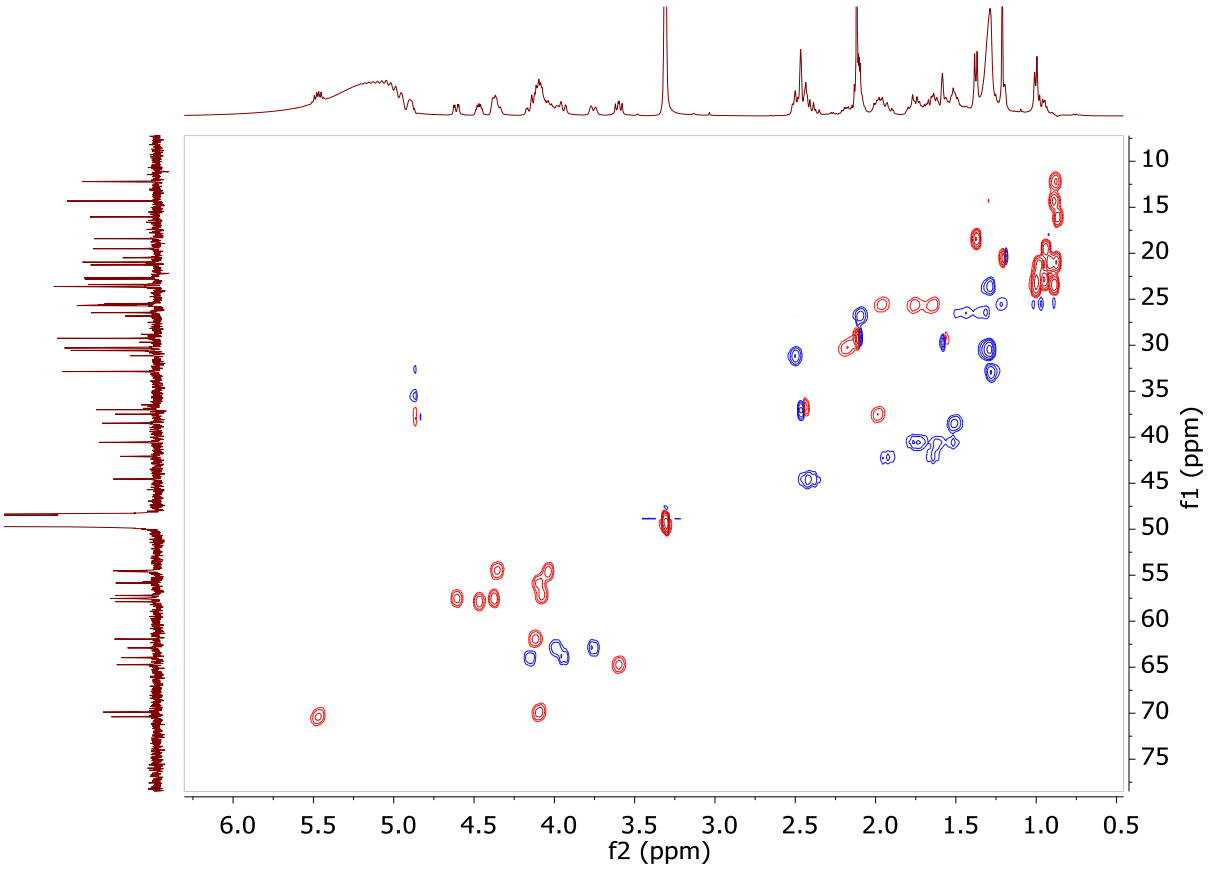

e. ^{1}H-^{1}H-TOCSY

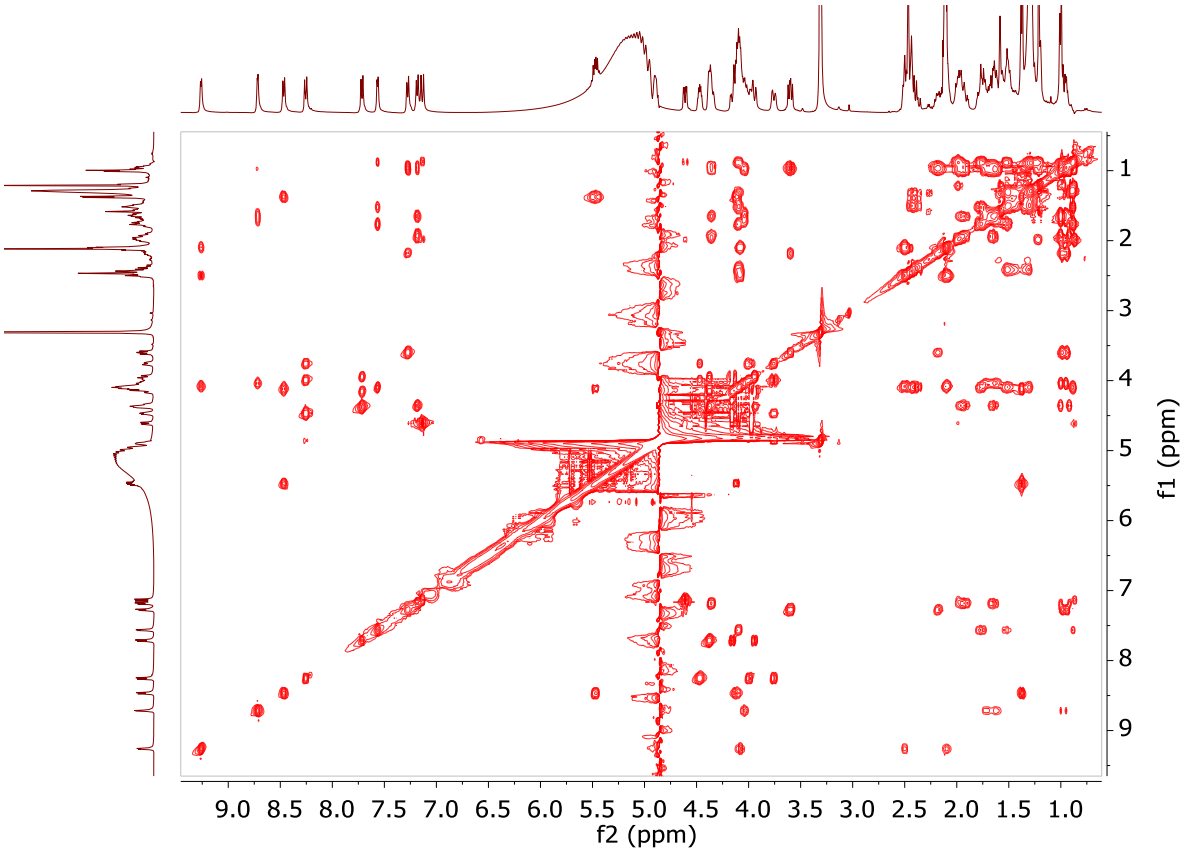

f. ^{1}H-^{13}C-HSQC-TOCSY

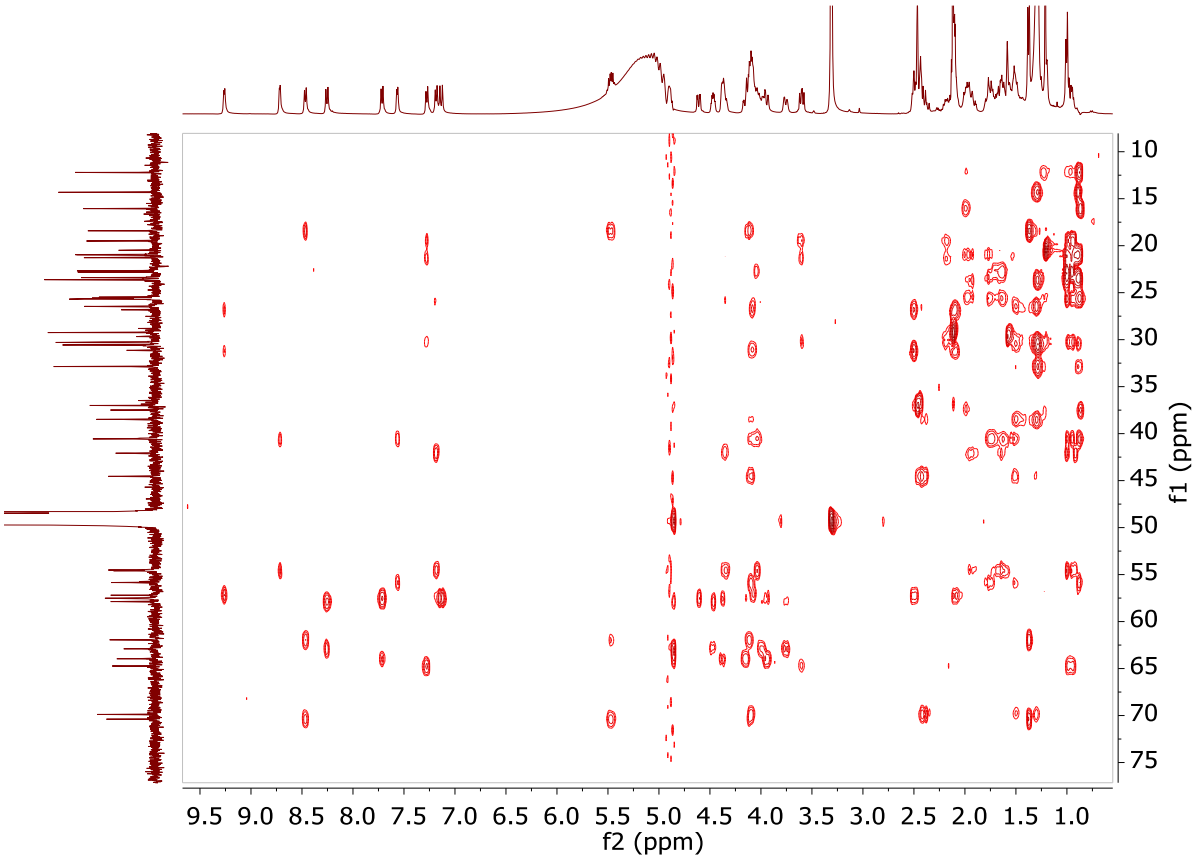

g. ^{1}H-^{15}N-HSQC

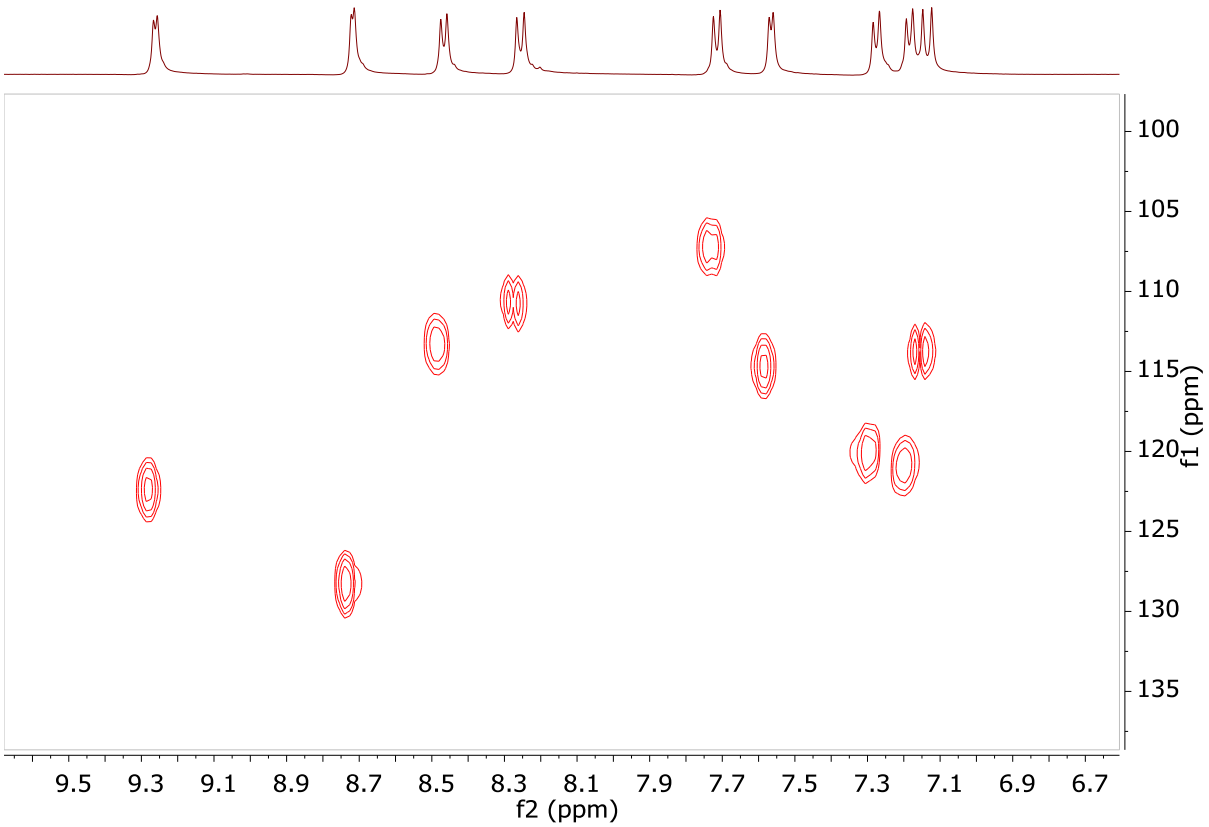
100
105
110
115
120
125
130
135
f1 (ppm)
9.5
9.3
9.1
8.9
8.7
8.5
8.3
8.1
7.9
7.7
7.5
7.3
7.1
6.9
6.7
f2 (ppm)

Figure A17: Images showing spores growth of ***B. salamandrivorans*** after 9 days in antifungal assays of the isolated compounds.

a. Lipo-dipeptide

200 µgmL^{-1} 100 µgmL^{-1} 50 µgmL^{-1}

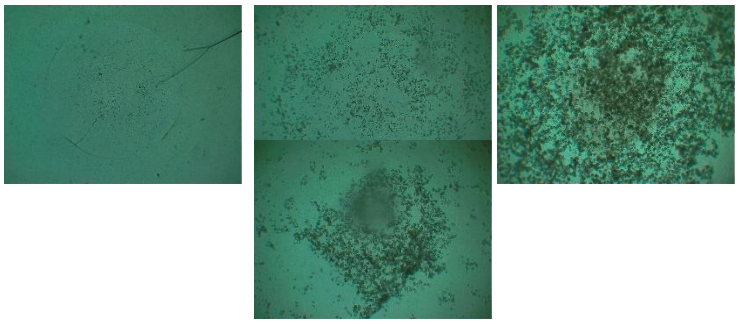

b. Pseudodesmin A

200 µgmL^{-1} 25 µgmL^{-1} 12.5 µgmL^{-1} 6.25 µgmL^{-1} 3.12

c. Virginiafactin A

200 µgmL^{-1} 100 µgmL^{-1} 50 µgmL^{-1} 25 µgmL^{-1}

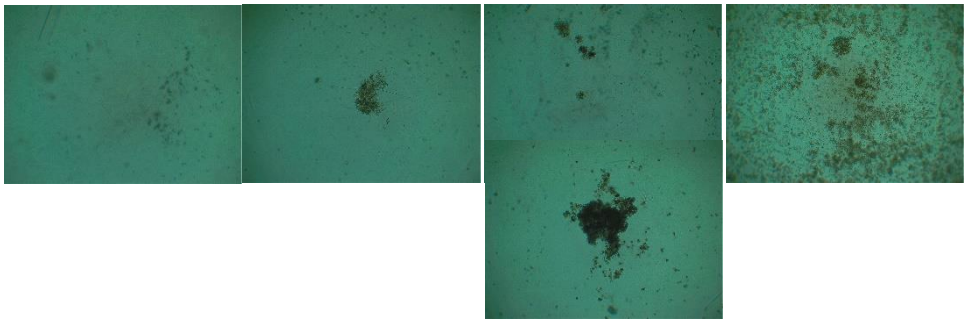

d. Virginiafactin B

200 µgmL^{-1} 25 µgmL^{-1} 12.5 µgmL^{-1} 6.25 µgmL^{-1}

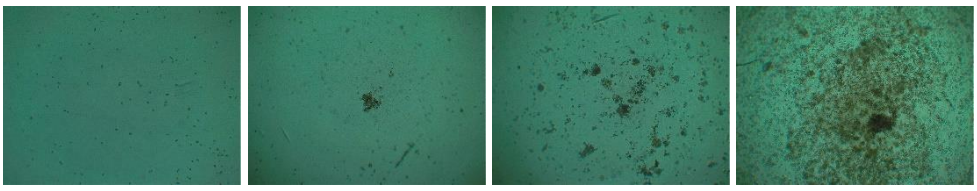

e. Compound 1 (1367 Da)

200 μgmL^{-1} 100 μgmL^{-1} 50 μgmL^{-1}

f. Compound 2 (1381 Da)

200 μgmL^{-1} 100 μgmL^{-1} 50 μgmL^{-1} 25 μgmL^{-1}

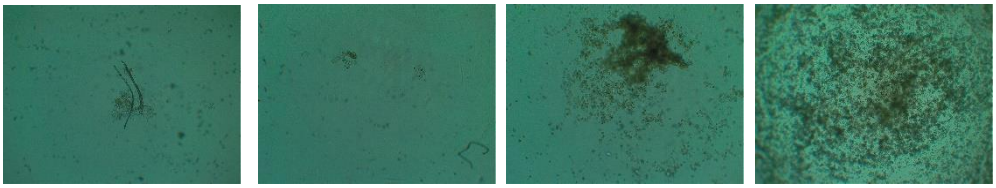

g. Compouns 3 (1395 Da)

200 μgmL^{-1} 100 μgmL^{-1} 50 μgmL^{-1} 25 μgmL^{-1}

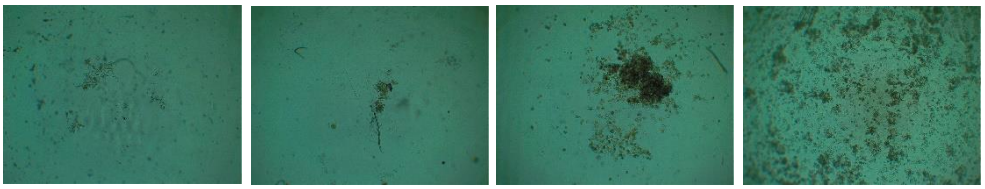

h. Compound 4 (1409 Da)

200 μgmL^{-1} 50 μgmL^{-1} 25 μgmL^{-1} 12.5 μgmL^{-1}

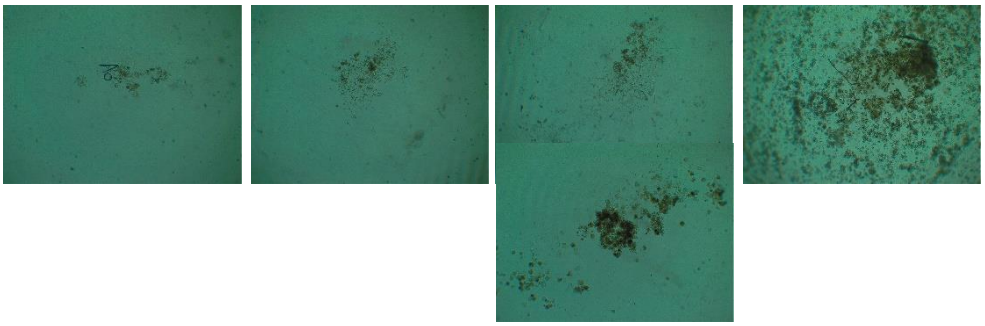

i. Compound 9 (1112 Da)

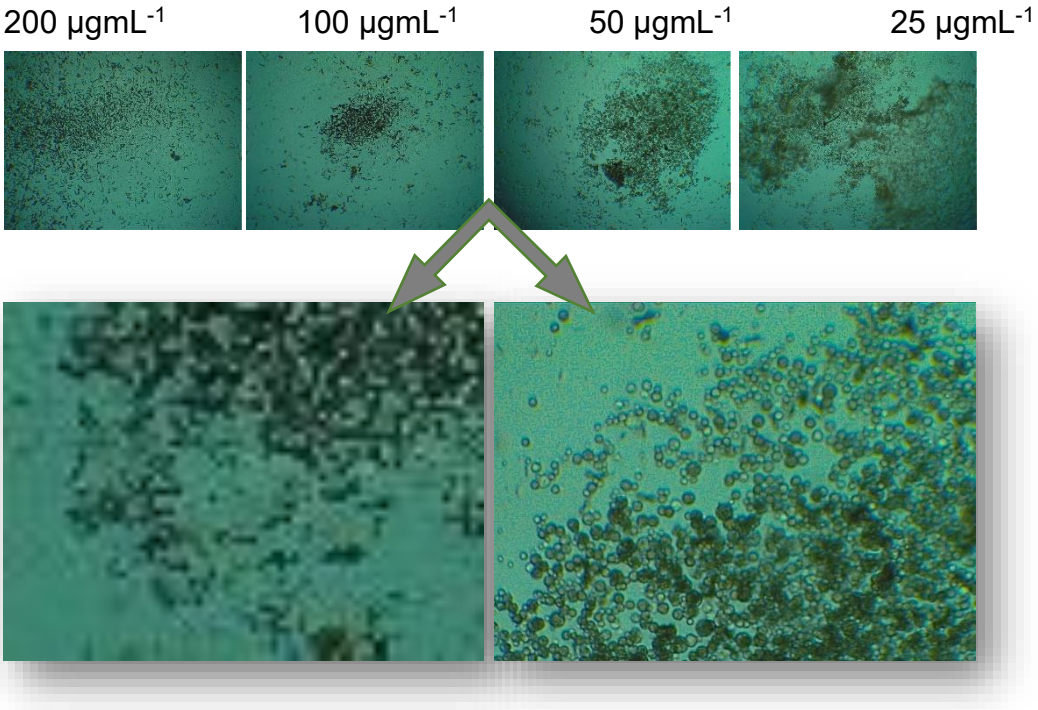

j. Compound 10 (1126 Da)

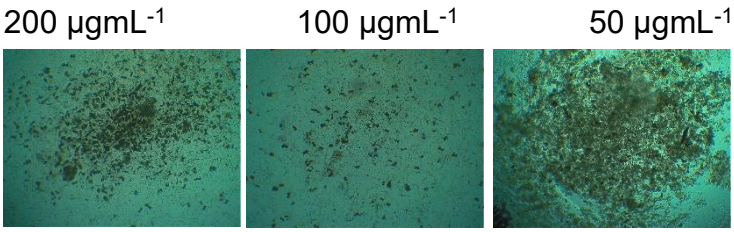

k. Cycloheximide (positive control)

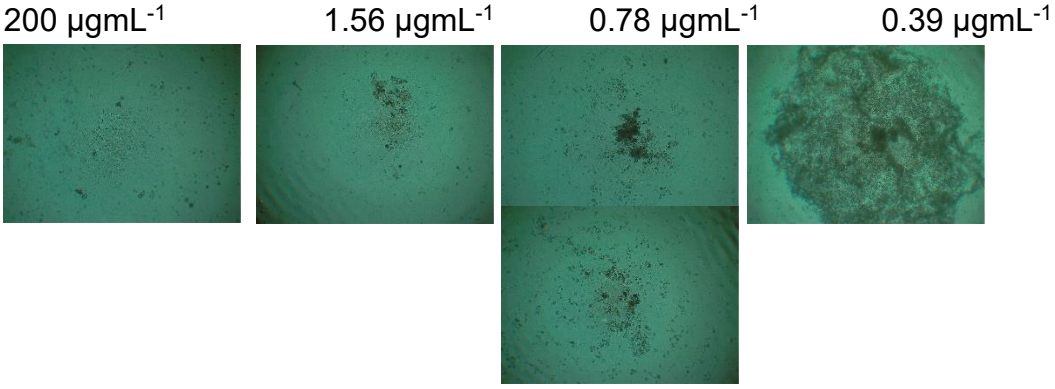

Figure A18: Images showing spores growth of ***B. dendrobatidis*** after 9 days in antifungal assays of the isolated compounds.

a. Lipo-dipeptide

200 µgmL^{-1} 100 µgmL^{-1} 50 µgmL^{-1}

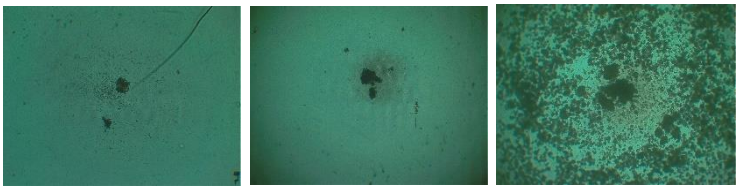

b. Pseudodesmin A

200 µgmL^{-1} 12.5 µgmL^{-1} 6.25 µgmL^{-1} 3.12 µgmL^{-1}

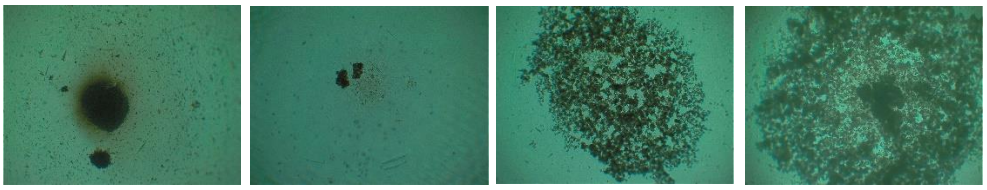

c. Virginiafactin A

200 µgmL^{-1} 50 µgmL^{-1} 25 µgmL^{-1}

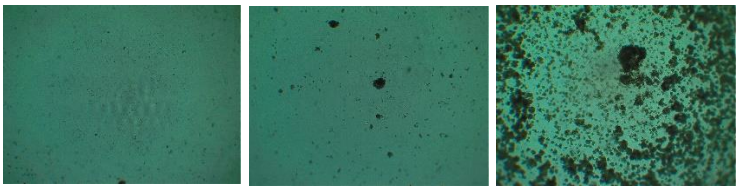

d. Virginiafactin B

200 µgmL^{-1} 25 µgmL^{-1} 12.5 µgmL^{-1} 6.25 µgmL^{-1}

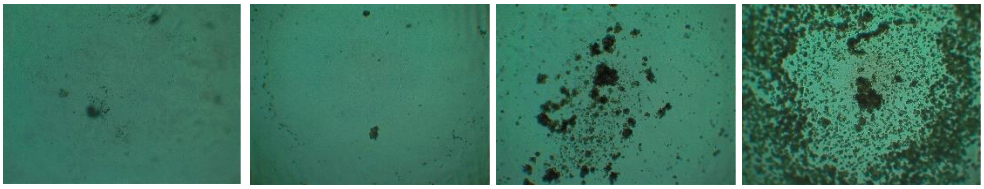

e. **Compound 1 (1367 Da)**

200 μgmL^{-1} 100 μgmL^{-1}

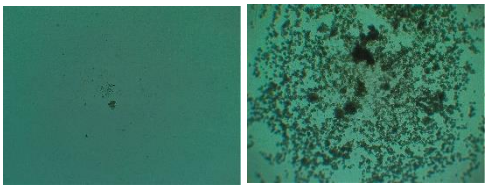

f. Compound 2 (1381 Da)

200 μgmL^{-1} 100 μgmL^{-1} 50 μgmL^{-1}

g. Compound 3 (1395 Da)

200 μgmL^{-1} 100 μgmL^{-1} 50 μgmL^{-1}

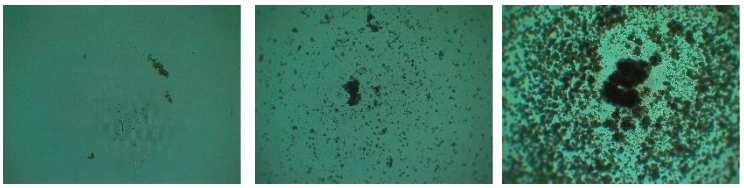

h. Compound 4 (1409 Da)

200 μgmL^{-1} 50 μgmL^{-1} 25 μgmL^{-1} 12.5 μgmL^{-1}

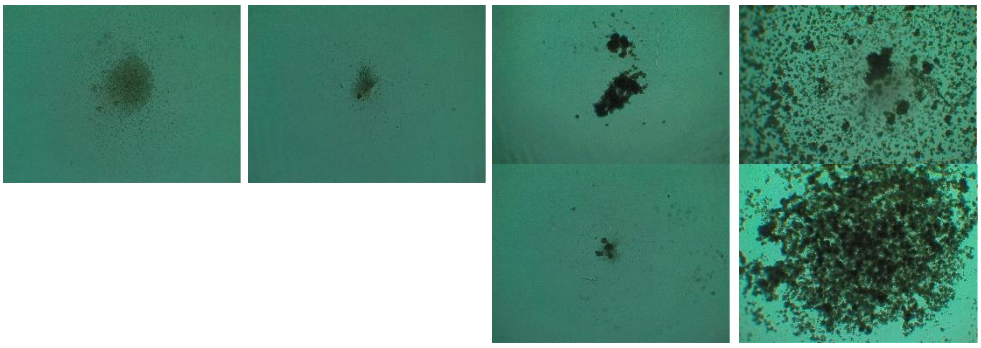

i. Compound 9 (1112 Da)

200 μgmL^{-1} 100 μgmL^{-1} 50 μgmL^{-1}

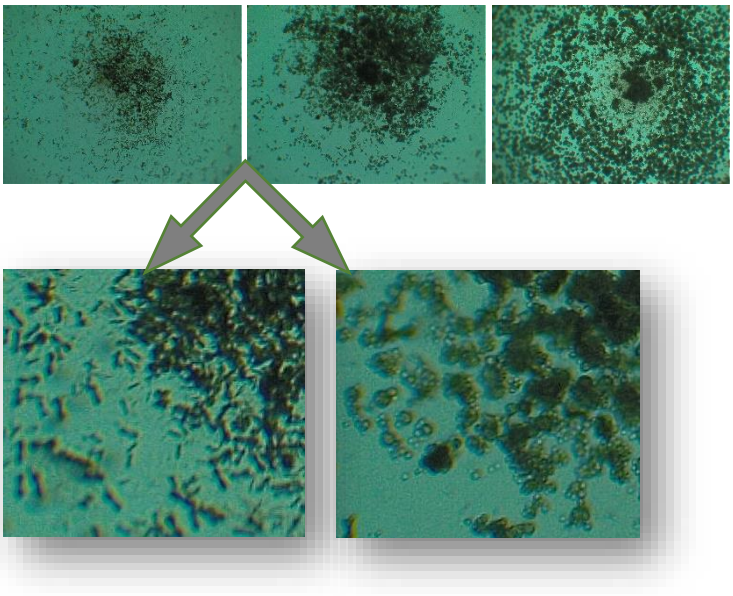

j. Compound 10 (1126 Da)

200 μgmL^{-1} 100 μgmL^{-1} 50 μgmL^{-1}

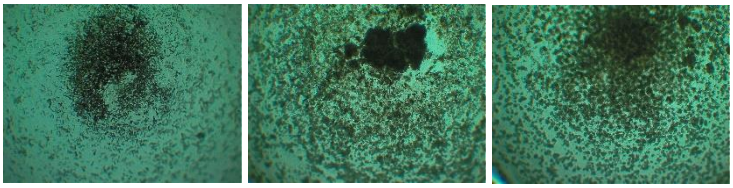

k. **Cycloheximide** (positive control)

200 μgmL^{-1} 0.39 μgmL^{-1} 0.19 μgmL^{-1} 0.09 μgmL^{-1}